Deepmoni Deka
Subrata Kumar Majumder
Mihir Kumar Purkait   *Editors*

Sustainable Environment

Proceedings of NERC 2022

Springer

Sustainable Environment

Deepmoni Deka · Subrata Kumar Majumder ·
Mihir Kumar Purkait
Editors

Sustainable Environment

Proceedings of NERC 2022

Springer

Editors
Deepmoni Deka
Centre for the Environment
Indian Institute of Technology Guwahati
Guwahati, India

Subrata Kumar Majumder
Department of Chemical Engineering
Indian Institute of Technology Guwahati
Guwahati, India

Mihir Kumar Purkait
Department of Chemical Engineering
Indian Institute of Technology Guwahati
Guwahati, India

Foreword

It is a matter of great satisfaction for me that Indian Institute of Technology Guwahati successfully hosted North-East Research Conclave (NERC) 2022 during 20–22 May 2022. The NERC 2022 was conducted on the theme "Sustainable Science and Technology". Concurrently, Assam Biotech Conclave (ABC) was also organized on 21–22 May 2022. Both the events attracted huge participation from policy-makers, researchers, industrialist, army and students. Even the participation of school children was overwhelming.

NERC and ABC had many events including panel discussions, exhibitions, keynote lectures, competitions and paper presentations. Presentation of technical papers forms the core of any research conference. NERC attracted 879 research papers on various themes covering science, technology and humanities. Out of these, some select papers have been published by Springer Nature in the form of 15 volumes. These papers have been peer reviewed and thoroughly edited by IIT Guwahati faculty members. I am sure that these volumes will prove to be excellent resource material for research. Most of the papers presented in these volumes highlight the special needs and aspiration of eight states of North-East India. I congratulate and thank authors, reviewers, editors and publisher for bring out proceedings.

Motivation for organizing NERC came from none other than Honourable Minister of Education, Government of India, Shri Dharmendra Pradhan Ji. It helped to bring policy-makers, researchers, industrialists, academicians, students and children in one forum. It is perhaps the rarest conclave covering almost all possible research themes. For better readability, the proceedings has been divided into 15 volumes, but each volume reflects diversity in terms of topics and researchers. Only common thread is sustainable development of North-East India. Invariably, Sustainable North-East India is a prerequisite for sustainable India and the whole world. In that sense, these

15 volumes will serve guiding and stimulating light for all the stakeholders of the development. I am pleased to dedicate these volumes to nation as a part of Azadi ka Amrit Mahotsav.

T. G. Sitharam
Director
Indian Institute of Technology Guwahati
Guwahati, India

Preface

Over decades of innovations and technological advances in pursuit of economic growth, humans have caused irreversible effects on the earth ecosystem. Anthropogenic activities along with urbanization are causing a detrimental effect on the environment. Therefore, the responsibility to conserve natural resources and to protect global ecosystems demands commitment toward sustainable environment. Sustainable environment is the practice where we ensure responsibly managing natural resources and protect overall ecosystem to meet the needs of present and future generations. To achieve this social reorientation are required from the mainstream development paradigm that is inclined toward economic growth to socio-ecologically sustainable and climate-resilient development models. Also, significant lifestyle changes along with conservation of natural resources is necessary for a better living.

Some of the major environmental issues across the globe are scarcity in drinking water, hazardous waste generation, environmental pollution, deforestation, desertification, food shortage, greenhouse gas emission, etc., which have triggered global warming, climate change, soil erosion, biodiversity loss, and depletion of fossil fuels. Environment sustainability measures which involve use of renewable sources of energy such as solar, wind, hydroelectric, and biomass are to be encouraged which will reduce environmental pollution and resource misuse. At the same time, crop rotation, solid waste management, water, wastewater treatment, rainwater harvesting, green technologies, recycling, and organic farming are some of the sustainable practices we must carry out for a sustainable environment. To achieve this goal, cleaner and energy-efficient technologies need to be developed and transferred for a holistic sustainable development.

The book is designed to cover topics that will address some of the issues challenging environment sustainability and measures that can be taken to ensure sustainability. Water contamination and scarcity of drinking water is one of the major problems across the globe causing health hazards. Sources of such contamination mostly occur during mining where interaction among minerals causes leaching which comes in contact with nearby water bodies thereby contaminating the groundwater table. Moreover, anthropogenic sources mainly pesticides and industrial wastes

released into water bodies cause surface water pollution which are not fit for drinking purpose. Reports of presence of micropollutants like arsenic, fluoride, lead, chromium, pharmaceuticals, etc., are documented causing several diseases. Therefore, sustainable wastewater treatment methods which will improve the quality of water and make it appropriate for a specific end-use will be elaborated. The book also discusses all types of waste, its segregation, and management. Improper dumping of waste and its management causes all types of pollution in air, soil, and water contaminating surface and groundwater. These practices have led to rapid degradation of environment and significant health hazard for the population. Therefore, scientific management of wastes and sustainable waste-to-wealth recycling technologies will be elaborated in the chapters. The book will also cover air pollutants and its effect on environmental health. Study of air pollutant concentration and its monitoring for weather forecasting and climate analysis will be discussed in the chapters.

The content of the book was designed to give an overview of recent developments, knowledge gaps related to new research areas, their implications, and future prospects. Apart from undergraduate and postgraduate students, this book is strongly recommended for people concerned in the chemical, biomedical, material science, biotechnology, and pharmaceuticals field of research.

We are very grateful to all the contributors for sharing with us their technical knowledge and expertise. We are also grateful to all the authors and owners of copyright who have kindly allowed us to reproduce diagrams and tables from their publications.

Finally, we continue to acknowledge our families, who provided patience, understanding, and encouragement throughout. We believe that the book is the right blend of both experimental and theoretical studies providing tremendous potential for knowledge and helps researchers and academicians contribute to a healthy and prosperous community.

Guwahati, India   Prof. Mihir Kumar Purkait

About This Book

The book will cover topics that address the global environmental issues, their challenges, and mitigation strategies for sustainable development. Some of the major challenges global environment is facing currently are global warming-induced climate change because of which various extreme weather events such as flood, drought, cyclone, and forest fires have increased. Industrialization with urbanization and human anthropogenic activities have caused a detrimental effect on the environment resulting in environmental pollution (air and water pollution), deforestation, degradation of ecosystems, soil erosion, groundwater depletion, drinking water scarcity, biodiversity loss, depletion of fossil fuels, etc. Therefore, it has become utmost necessary to switch to significant lifestyle stages along with conservation of natural resources for a sustainable environment. Sustainable environment may be defined as the practice of responsibly managing natural resources and protect overall ecosystem to support health and well-being of present and future generations. One of the major environment sustainability is the use of renewable sources of energy such as solar, wind, hydroelectric, and biomass which will reduce environmental pollution and also minimize resource misuse. At the same time, crop rotation, solid waste management, water treatment, and wastewater treatment are some of the sustainable practices we must carry out for a sustainable environment. Hope, the content of the book will give an overview of recent developments, knowledge gaps related to new research areas related to environment and their future prospects.

About IIT Guwahati

Indian Institute of Technology (IIT) Guwahati established in 1994 has completed 25 years of glorious existence in 2019. At present, the Institute has eleven departments, seven interdisciplinary academic centres and five academic schools covering all the major engineering, science, health care, management and humanities disciplines, offering B.Tech., B.Des., M.A., M.Des., M.Tech., M.Sc. and Ph.D. programmes. The institute presently offers a residential campus to 435 faculty members and more than 7500 students at present. Besides its laurels in teaching and research, IIT Guwahati has been able to fulfil the aspirations of people of the North-East region to a great extent since its inception in 1994. The picturesque campus is on a sprawling 285 hectares plot on the north bank of the Brahmaputra, around 20 km from the heart of the Guwahati city.

IIT Guwahati is the only academic institution in India that occupied a place among the top 100 world universities—under 50 years of age—ranked by the London-based Times Higher Education (THE) in the year 2014 and continues to maintain its superior position even today in various International Rankings. IIT Guwahati gained rank 37 globally in the "Research Citations per Faculty" category and overall 384 rank in the QS World University Rankings 2023 released recently. IIT Guwahati has retained the 7th position among the best engineering institutions of the country in the "India Rankings 2021" declared by the National Institutional Ranking Framework (NIRF) of the Union Ministry of Education. IIT Guwahati has been also ranked 2nd in the "Swachhata Ranking" conducted by the Government of India. Recently, IIT Guwahati has been ranked as the top-ranked University in 2019 for IT developers by HackerRank in the Asia-Pacific region.

Among other frontier areas of research and innovation, IIT Guwahati is working towards augmenting critical science research initiatives in genomics, developmental biology, health care and bioinformatics, flexible electronics, advanced functional materials, sustainable polymers, rural technologies, renewable energy, artificial intelligence, disaster resilience and risk reduction and water resources and management. In its silver jubilee year, IIT Guwahati is poised to scale newer heights through all-round growth and development.

Indian Institute of Technology Guwahati has dedicated itself to the cause of improving and empowering Northeast India through cutting-edge research, region relevant projects, innovations, individual and multilateral collaborations and special initiatives. Being the only IIT in the entire Northeastern region, IIT Guwahati has an immense amount of responsibility to develop the region and empower the people of the region.

While the entire country is celebrating the "Azadi ka Amrit Mahotsav"—75 glorious years of Independence, and the great pride with which our nation of more than a billion people has been steadily growing today, IIT Guwahati is strongly committed to support that pace of growth for the entire NE so that we can keep pace along with the rest of the country. The specific areas of focus where IIT Guwahati has been contributing immensely to the region are:

(a) Infrastructure development across multiple sectors
(b) Providing solutions for multiple natural disasters such as recurring floods, landslides, earthquakes, cyclones, hailstorms and other natural calamities
(c) Improving the education sector and creating opportunities for employment
(d) Internet, telecommunication and cultural integration
(e) Technological intervention in interdisciplinary areas
(f) Healthcare services and education
(g) Renewable energy generation (solar, wind, biomass, hydro, geothermal)
(h) Overall industrialization, refining fossil fuels and setting up biorefineries.

Besides bringing in the state-of-the-art technical knowhow for most of the above sectors, the institute has been partnering with the local governments and enhancing the technological and educational interactions such that the next-generation youth are empowered with knowledge, skills and necessary entrepreneurial ability. These measures in Assam as well as all other northeast states will usher in a new era of growth, and the opportunities it will provide for interaction with the ASEAN countries as part of the Act East Policy of the Government of India will bring prosperity to this region.

Prof. Parameswar K. Iyer
Dean, Public Relations, Branding and Ranking
Indian Institute of Technology Guwahati

From the Desk of Chairman of Technical Committee of NERC 2022

North-East Research Conclave 2022 was successfully organized during 20–22 May 2022 with the participation of thousands of delegates. A total of 879 oral and poster papers were presented in the conference on 16 different tracks. The theme of the conclave was Sustainable Science and Technology, which is very pertinent in the modern era of globalization. Science and technology has to address economic, environmental and social problems of the world. Technology and sustainability are not incompatible. In fact, technology can achieve the goal of sustainability, which also includes preserving our rich cultural heritage. Concurrently with North-East Research Conclave (NERC), Assam Biotech Conclave 2022 was also organized on 21–22 May 2022. These mega events were organized at Indian Institute of Technology Guwahati (IITG) in physical mode after two years of pandemic period. Along with IITG, Science, Technology and Climate Change Department and Department of Education, Government of Assam were also organizers of these events under the patronage of Shri Dharmendra Pradhan Ji, Honourable Minister of Education and Minister of Skill Development and Entrepreneurship in the Government of India, and Shri Himanta Biswa Sarma Ji, Honourable Chief Minister of Assam.

It is a matter of great pleasure that Springer Nature is publishing the select papers from the conclave in 15 volumes. These are Advanced Functional Materials, Low Cost Manufacturing Technologies, Agro and Food Processing Technologies, Artificial Intelligence and Data Science based R&D interventions, Conservation of Biodiversity in the North Eastern States of India, Disaster Management, Healthcare Research and Related Technologies, Innovative Design for Societal Needs, Policies for Research and Innovation, Research and Innovation for Sustainable Development Goals, Sustainable Environment, Sustainable Energy Generation and Storage, Sustainable Transportation and Urban Development, Teaching and Learning Technologies, Technologies for Rural Development. These volumes are useful archival and reference materials for policy-makers, researchers and students.

As Chairman of Technical Committee, I am thankful to all Editors of all volumes, reviewers and student volunteers who have put tireless efforts to review, select and edit the papers of respective divisions, overcoming the time-constraint. Support provided by Convener, Prof. Vimal Katiyar, Dean R&D, IITG, and Co-conveners

Prof. Subhendu Sekhar Bag, Associate Dean R&D, IITG, and Shri Kailash Karthik N., IAS, is commendable. It is difficult to express words of gratitude for the Director, IITG, Prof. T. G. Sitharam, who has been motivating and guiding all the teams of NERC 2022 and ABC 2022.

Uday Shanker Dixit
Professor, Department of Mechanical Engineering, and
Head, Center for Indian Knowledge Systems

North East Research Conclave-2022: Toward Sustainable Science and Technology

It is extremely important and imperative to have knowledge-driven growth based on innovation in the case of academic higher education institutes of high repute. The North-Eastern region endowed with rich biodiversity comprises eight states. However, the climatic conditions, limited connectivity, lack of research infrastructure/institutes, territorial conflicts and the mountainous terrain of these regions are major impediments to the research ecosystem in the North-East. Quality higher education focusing on industry–academia collaboration and translational research is extremely beneficial for society. It has also been rightly pointed out by the Hon'ble Prime Minister Sh. Narendra Modi that, "*India cannot develop till Eastern India develops*".

With this idea and as India marks 75 years of Independence, Indian Institute of Technology Guwahati organized "The North-Eastern Research Conclave" from 20

to 22 May 2022. This grand event was jointly conducted with Science, Technology and Climate Change Department and the Department of Education, Govt. of Assam, at IIT Guwahati Campus.

The mission behind the conclave was to showcase the best R&D activities from educational and research institutions across North-East India and to create an environment, conducive to development of local indigenous technologies and innovations, creating the scope and laying the foundation for entrepreneurship.

In order to attract people and spread awareness about the event, a roadshow was initiated from IIT Guwahati on 7 May 2022 in order to reach all the partnering academic institutes and make them an integral part of the mega event. The Director, IITG, waved the NERC 2022 flag and sent off the road show vehicle from the institute. More than 400 students, staff and faculty participated actively in the roadshow.

A huge response was received by participants from throughout the country. The total no. of participating institutions in this conclave included 7 IITs, 10 NITs, 5 IIITs and other CFTIs, 23 research laboratories, 17 central-funded universities, 47

other universities/institutes along with about 100 schools. Eminent personalities from industries, start-ups, research councils and PSUs also joined in.

The presence of dignitaries from important Ministries was observed such as Shri Dharmendra Pradhan, Hon'ble Union Minister of Education and Minister of Skill Development and Entrepreneurship, Government of India; Dr. Himanta Biswa Sarma, Hon'ble Chief Minister of Assam State; Dr. Ranoj Pegu, Hon'ble Minister of Education, Government of Assam; Dr. Rajkumar Ranjan Singh, Hon'ble Minister of State for Education, Government of India; Dr. Subhas Sarkar, Hon'ble Minister of State for Education, Government of India; Shri Keshab Mahanta, Hon'ble Minister of Science Technology and Climate Change, Government of Assam and many more.

The inauguration ceremony of the conclave was followed by the signing of an MoU between IIT Guwahati and the Government of Assam to establish "The Assam Advanced Health Innovation Institute (AAHII)". This MoU would prove to be a unique partnership between the Government of Assam and IIT Guwahati in order to set up a research institution to leverage advanced technologies to transform medical science. This joint venture company will be able to invite participation from intending parties including corporates/businesses/research institutions and philanthropic organizations.

The third edition of Assam Biotech Conclave 2022 was also held as part of NERC 2022. It brought together the Biotech Entrepreneurs, industry leaders, researchers, academicians, government representatives, policy-makers, innovators and investors together on one platform to explore the possibilities of biotechnology in North-East India and to discuss the new opportunities in the transition.

Officers from the Indian Army also actively participated in the conclave. A talk on "Atmanirbhar Bharat—Indian Army Initiatives towards Self Reliance" was delivered by Lt. Gen. D. S. Rana AVSM, YSM, SM General Officer Commanding, Gajraj Corps on 21 May 2022. The talk was aligned with the vision of the apex leadership of the Government of India and initiatives undertaken by the Indian Armed Forces with a focus on the integration of civil–military establishment in the field of self-reliance. He also elucidated that institutions such as IIT Guwahati which has many running research projects and elaborate student exchange and joint collaboration setup with a large number of countries have the wherewithal to take up defence-related R&D and also facilitate delivery with industry partners. He also invited IIT Guwahati to participate in EAST TECH Symposium planned at Kolkata in July 2022. This led to the signing of an MoU between Indian Army Eastern Command and IIT Guwahati on 7 July 2022 during East Tech 2022. This would further impetus to Indigenisation and Raksha Atmanirbharta.

Royal Society of Chemistry, Global battery experiment was performed by more than 1300 students in three sessions starting from 20 May to 22 May at IIT Guwahati. Along with the global battery experiment, creating skilful educators (teacher training programme) was also conducted in parallel sessions. Students had arrived from various schools across Assam and other North-Eastern states.

The Guwahati Declaration was launched at the valedictory ceremony of the conclave by Shri Lok Ranjan, Secretary, Ministry of Development of North Eastern Region (DoNER), in the presence of Shri Kailash Karthik, Deputy Commissioner, Kamrup. The declaration is intended to create a set of guidelines, through which individual as well as a collective responsibility to promote and encourage innovation at the grass-root level and strive to stimulate and execute indigenization and entrepreneurship can be taken up.
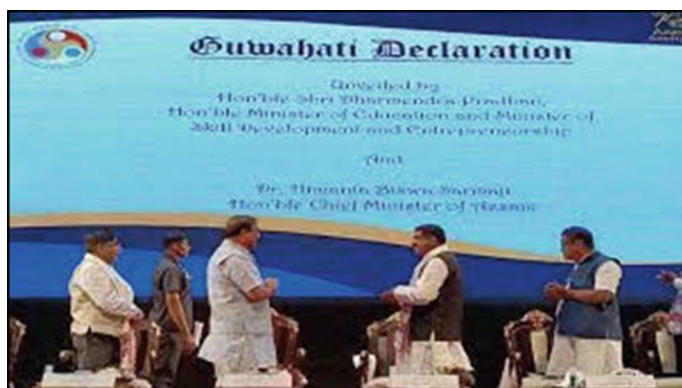
Science, education, research and innovation are the four pillars on which the development, as well as the work culture of a nation, rests. This was well articulated by the promising number of exhibitors being seen participating from all across the NE states in the NERC 2022. All the NITs, CFTIs and CFIs were allocated two stalls each, where the delegates showcased the working models of their inventions. Distinctive pavilions were arranged for IIT, NIT, CFIs and CFTIs. Excellent response was obtained from the start-ups all across the NE states. Federation of Industry Commerce of North Eastern Region (FINER) had partnered with NERC 2022 as an

industry partner, and they showcased 50 start-ups as a part of the exhibition under the FINER Pavilion. Other significant organizations that came forward to showcase their allied R&D start-ups were the Oil and Natural Gas (Oil and Natural Gas Pavilion), Indian Army (Defense Pavilion) and NE-Railway (NE-Railway Pavilion).

Multifarious research work on topics of societal relevance was presented by researchers from different organizations/institutes. The presentations were conducted in oral and poster presentation modes. The thematic areas for these presentations were part of some of the Sustainable Development Goals (SDGs) such as SDG-3: Good Health and Wellbeing; SDG-7: Affordable and Clean Energy; SDG-9: Industry, Innovation and Infrastructure; SDG-11: Sustainable Cities and Communities and SDG-12: Responsible Consumption and Production. Some of the papers highlighted environmental sustainability, efficiency and management issues, which are important to be presented in the case of North-East regions. Two awards were given under each technical category for these presentations. Overall, the technical sessions were

a grand success due to the active cooperation from editors, chairpersons of all the sessions and student volunteers of IITG.

The Government of India has taken various steps to encourage women in the field of science and technology. In this line, the IIT Guwahati Woman Researcher Award was approved to recognize the contribution of women Faculty members of IIT Guwahati fraternity. This prestigious award was conferred to Dr. Latha Rangan who is Senior Professor in the Department of Biosciences and Bioengineering, Indian Institute of Technology Guwahati, India. Prof. Rangan has played a key role in plant biotechnology and sustainable development and especially in the areas of energy security, food security and medicinal crops.

The conclave paved the way for creating mass awareness of Research and Innovation for developing a sustainable society. There was knowledge exchange and dissemination that led to the establishment of Centres of Excellence in Translational Collaborative Research and Innovation. This mega event led to the bridging of the gap between industry–academia and creating handholding pathways for setting up long-term collaboration for R&D innovations towards the goal of establishing sustainable NE India. The conclave brought together over 8000 participants including Hon'ble Ministers, Official Bureaucrats, Eminent Professors, Scientists, Renowned Industrialist, School Children/Teachers and Others delegates. This revolutionized the R&D road map of all the NE states through various dissemination of policies which will benefit the sustainable development of all NE states in near future.

It is an honour and a moment of extreme pride for getting the NERC proceedings published in the prestigious Springer volumes. We would like to thank and acknowledge the globally active publisher Springer for helping us being able to publish the

articles on 15 broad areas. We would also like to thank all the authors for their contribution to the grand success of NERC 2022 and wish them great success in all of their future endeavours.

Prof. Vimal Katiyar
Dean, R&D
Department of Chemical Engineering
Centre for the Sustainable polymer
Indian Institute of Technology Guwahati
Guwahati, India
vkatiyar@iitg.ac.in

Prof. Subhendu Sekhar Bag
Associate Dean, R&D
Department of Chemistry
Centre for the Environment
Indian Institute of Technology Guwahati
Guwahati, India
ssbag75@iitg.ac.in

Contents

Environment Pollution and Remediation

Environmental Issues: Problems and Sustainable Solutions

About the Editors

Dr. Deepmoni Deka is working as Technical Officer Gr-I in Centre for the Environment at Indian Institute of Technology Guwahati, India. She completed her postgraduation in Molecular Biology and Biotechnology from Tezpur University and Ph.D. in Environment from Indian Institute of Technology Guwahati. Her research interests include bioremediation of environmental pollutants from soil and water, monitoring of ground and surface water quality, nutrient quality, determination of NPK content in soil, purification and characterization of industrial microbial enzymes, bioethanol production using waste biomass, resource recovery, waste valorization, biopolymer based hydrogel. She has 15 research publications in peer reviewed journals, 1 book chapter and more than 25 conference papers. Presently, she is working in the field of biobased plastic production using waste, wastewater treatment specifically pharmaceuticals, dye and heavy metal removal, biopolymer based hydrogel for sensing of pollutants and drugs.

Dr. Subrata Kumar Majumder is a Professor in Chemical Engineering Department at Indian Institute of Technology Guwahati, India. He completed his Ph.D. in Chemical Engineering from Indian Institute of Technology Kharagpur. His research interests include Process Intensification in Chemical Processes, Intensification in environmental process system, Micro-nano bubble science and technology and its applications, Microchannel-based and Jet driven gas-aided extraction, Mineral Beneficiation, Enhanced Oil Recovery by Micro-nanobubble, Multiphase Flow and Reactor Development. He is a Life Fellow of Council of Engineering and Technology (India), Life Fellow of Indian Institute of Chemical Engineers and Fellow of the International Society for Research and Development, London. He is a recipient of various honours and awards like: Editor, *Journal of Chemical Engineering Research Studies*, Guest editor, *American Journal of Fluid Dynamics*, published by Scientific and Academic Publishing Co., USA, Editorial board member of *Scientific Journal of Materials Science*, IIME Award on beneficiation from Indian Institute of Mineral Engineers (IIME), Editorial board Member of the *Journal of Science and Technology*, Scientific and Academic Publishing, USA, Advisory board member of Excelling Tech Publishers (ETP), London, UK., life member of Indian Institute of Mineral

Engineers, member of Institute of Engineers (India), Member of Asia-Pacific Chemical, Biological and Environmental Engineering Society (PCBEE), senior member of International Association of Engineers (IAE), Japan. He authored four books, five book chapters, has 76 conference papers and has more than 100 publications in several reputed international journals. He has completed several sponsored and consultancy projects. He has a collaboration with the Aalborg University, Denmark and University of Los Andes, Colombia, Curtin University, Australia, Edith Cowan University, Australia. Presently he is working in the field of Microbubble science and technology and its applications in mineral beneficiation, industrial effluent treatment, and arsenic, ammonia and dye removal and process intensifications in chemical and mineral processing.

Dr. Mihir Kumar Purkait is a Professor in the Department of Chemical Engineering at Indian Institute of Technology Guwahati (IITG). Prior to joining as faculty in IITG (2004), he has received his Ph.D. and M.Tech. in Chemical Engineering from Indian Institute of Technology, Kharagpur (IITKGP) after completing his B.Tech. and B.Sc. (Hons.) in Chemistry from University of Calcutta. His current research activities are focused in four distinct areas viz. (i) advanced separation technologies, (ii) waste to energy, (iii) smart materials for various applications and (iv) process intensification. In each of the area, his goal is to synthesis stimuli responsive materials and to develop a more fundamental understanding of the factors governing the performance of the (c^12,500, h-index = 64, 10 index = 150). He has authored 10 books in CRC press and Elsevier in last 5 years.

Water Quality and Wastewater Treatment

Multi-metal Adsorption and Cyclic Desorption Characteristics of Zn^{+2} and Cu^{+2} Constituting Multi-component Synthetic Wastewater System Using Commercial Resins

Prabhat Kumar Patel [iD] **, Lalit Mohan Pandey** [iD] **, and Ramagopal Uppaluri** [iD]

1 Introduction

The incessant release of household, industrial, and agriculture wastes into water-bodies translates into irreversible pollution of water bodies. Among them, heavy metals constitute a substantial class and have a potential role to jeopardize human health (due to their carcinogenic status and bio-accumulating proclivity) through the human food chain. Unlike most organic pollutants, heavy metals cannot be eliminated through biological decay. Thereby, their non-biodegradable status in the environment accounts for greater toxicity for the living beings and catalyzes critical need to remove them from the ecosystem and sustain human and biological species health and harmonious co-existence [17]. Further, good quality water is becoming scarce on a day-to-day basis, and henceforth, it is important to reuse wastewater bodies being generated through mining and industrial operations and colonized municipalities.

The removal of hazardous heavy metals (iron, copper, lead, chromium, zinc, etc.) from effluents is very difficult owing to the many obstacles. Both conventional and novel separation schemes exist for the resolution of such stiff prepositions. Notable processes among these are membrane separators, ion exchangers, electro-chemical reducers, leaching and adsorption processes [21], chemical precipitators,

P. K. Patel
Centre for the Environment, Indian Institute of Technology Guwahati, Guwahati, Assam, India
e-mail: prabhat18@iitg.ac.in

L. M. Pandey
Department of Biosciences and Bioengineering, Indian Institute of Technology Guwahati, Guwahati, Assam, India
e-mail: lalitpandey@iitg.ac.in

R. Uppaluri (✉)
Department of Chemical Engineering, Indian Institute of Technology Guwahati, Guwahati, Assam, India
e-mail: ramgopalu@iitg.ac.in

coagulators and flocculators, biosorbers, electro-kinetic processes, nanoparticle-assisted processes, and foam fractionators. These can be formally classified into three categories, namely schemes involving greater usage of chemical media, sorptive approaches, and biomaterials and processes [24]. Environmental sustainability, cost-effectiveness, long-term adsorbent performance by withstanding cyclic adsorption–desorption processes, and acceptable recovery are few targets being targeted for the identification of potential separation schemes for industrial-scale operations [14]. Multiple heavy metal containing wastewater streams (with Cu, Zn, Pb, and Fe) can be characterized to be with lower metal concentrations. For such systems, chelating and ion exchange resins that follow the combined principles of physisorption and chemisorption are highly promising. With alternate ligands made of either hydroxyl or sulfonic acid or aminomethyl phosphonic acid or nitrogen, many commercial ions exchange resins possess greater affinity to reversibly bind multiple metal ions and thereby pave the way for the mitigation of heavy metal content in the water bodies. Till date, numerous investigations affirmed the promising performance of many such resins having sulfonic acid functional group (Amberlite IR 120H [7], Dowex 50 W [18], Purolite C100 [1], Dowex HCR S/S [2], Lewatit SP 112 [8], Dowex marathon C [22], Amberjet 1200H, Amberlite IRN97H [20]), iminodiacetic acid functional group (Amberlite IRC748, Amberlite NDC 702 [11], styrene DVB copolymer [12], GMA/DVB magnetic resin [4], Lewatit TP208 [15], Lewatit TP 207 [8]), aminomethyl phosphonic acid functional group (Lewatit TP 260 [15, 8]), carboxylic functional group (Amberlite IRA 400 [3], Lewatit CNP 80 [23], Carboxyphenyl resorcinarene-impregnated Amberlite XAD-4 [26]), phenolic functional group (Modified quebracho tannin resin [25]), tetrazolyl functional group (Polyvinyltetrazole grafted PS resins [6], N-methyl glucamine functional group (Amberlite IRA 743 [15]), and amine functional group (Aminated resin via SI-ATRP [16]).

In the above-cited investigations, most researchers targeted simple aqueous solutions being prepared with either one or two heavy metals. Very few prior art targeted about and more than 4 heavy metal containing solutions [6, 10–12]. Thus, it is apparent that for simpler solutions, close to 100% desorption efficiency may have been reported which is bound to reduce significantly for complex solutions containing 4–6 heavy metal ions along with other ions and additives. Indicating such reduction in the desorption efficiency, [12] considered Styrene–DVB copolymer ion exchange resin (having Iminodiacetic acid functional group) and four heavy metal ion containing solutions but inferred lower desorption efficiencies of 0%, 45%, 70%, and 65% for Cd, Pb, Ni, and Cr, respectively.

Thus, it is important to identify a complex simulation wastewater system that possesses 4–6 heavy metals along with other precursors [5]. Thereby, depending upon the solution complexity, HSAB theory needs to be considered for the identification of relevant commercial ion exchange resins and thereby carry out adsorption and desorption studies. Considering such conceptual methodology, two solutions have been identified based on the available wastewater stream data in the available prior art and refer to Cu^{+2} and Zn^{+2} dominating solutions being generated from agricultural waste and mining industry [13]. Thereby, according to HSAB theory, Amberlite IR

120H (containing sulfonic acid functional group) and Lewatit TP 260 (containing aminomethyl phosphonic acid functional group) commercial ion exchange resins have been identified to gain useful insights into the competence of the resins to address cyclic adsorption–desorption characteristics using simple acid and base eluents.

Thus, the associated lacunae in the field of multi-heavy metal containing solutions and commercial resins-based adsorption–desorption can be briefly summarized as follows. Firstly, prior arts considered 4 or more heavy metal containing solutions for investigated commercial resins. Such solutions will be closer in their constitution to the real-world industrial effluents and thereby provide useful insights to consider pre-treatment processes prior to adsorption. For example, if a metal ion concentration is jeopardizing the cyclic desorptive efficiency of a resin, the metal ion removal shall be targeted prior to the adsorption process. Secondly, cyclic adsorption–desorption studies were considered by very few authors and hence the competence of the resin cannot be evaluated. Thirdly, for all cases that involved significant single-cycle desorption efficiencies, complex and expensive eluents have been deployed which are impractical for industrial and commercial usage. Fourthly, while scanty literature referred to cyclic desorption efficiencies, the data does not provide efficiency of each cycle and thereby useful insights with respect to growing trends of irreversible adsorption with cycle number could not be gained. Thus, considering all these, a useful methodology shall be outlined by considering all bottlenecks associated with the commercial resin-based multi-heavy metal cyclic adsorption and desorption characteristics and efficacy. Such investigations can provide useful understanding into the complex issues that detriment the promising performance of the adsorbent. This work targets the Zn^{+2} and Cu^{+2}-based multi-heavy metal adsorption and desorption characteristics of Amberlite IR 120H and Lewatit TP 260 resins. Inferential comprehension of the optimality of resin dosage, contact period, and metal concentration range of simulated effluent was made possible as a result of this adsorption research. In this study, we employed FTIR, FESEM, and EDX to examine the surface and morphology of the resin. Thereafter, equilibrium and kinetic models were utilized for their fitness. Finally, various basic (KOH, NaOH) and acidic (HCl, HNO_3, and H_2SO_4) eluents were deployed in variant concentration range to potentially evaluate adsorption–desorption characteristics of 3 cycles. A comparative assessment of obtained findings is also targeted with respect to the best available literature.

2 Methodology and Materials

2.1 Chemicals and Reagents

Millipore water (Make: milliQ), magnesium sulfate ($MgSO_4$), zinc sulfate ($ZnSO_4 \cdot 7H_2O$), potassium sulfate (K_2SO_4), lead nitrate ($Pb(NO_3)_2$), aluminum sulfate ($Al_2(SO_4)_3 \cdot 18H_2O$), sodium sulfate ($Na_2SO_4$), potassium sulfate ($K_2SO_4$), ferrous sulfate ($FeSO_4 \cdot xH_2O$), and copper sulfate ($CuSO_4 \cdot 5H_2O$) were received from

Table 1 Salient characteristics of Amberlite IR 120H and Lewatit TP 260

Properties	Commercial resins used	
	Amberlite IR 120H	Lewatit TP 260
Active group	Sulfonic acid	Aminomethylphosphonic acid
Maximum operating range (°C)	150	80
Purchased form	As shipped H	As shipped Na
Particle size (mean) (mm)	0.5	0.5
Operation pH range	0–14	0–14
Total transferring capacity	1.9 meq/ml wet resin 4.50 mmol/ml	2.3 mmol/g

Sigma-Aldrich Corporation, Bangalore, India, and were deployed to prepare aqueous simulated effluent solutions with desirable metal concentrations. Amberlite IR 120H and Lewatit TP 260 commercial resins were received from Sigma-Aldrich Corporation. The solution pH was checked using pH meter (VSI-301). The chemical and physical characteristics of commercial resins (Amberlite IR 120H and Lewatit TP 260) are discussed in Table 1.

2.2 Characterizations and Analysis

Atomic absorption spectrophotometry (AAS; Varian; Netherland; Spectra AA 220FS) was conducted to measure the multiple heavy metal concentrations in the aqueous media. Corresponding wavelengths for Cu, Pb, Zn, and Fe refer to 324.8, 217.0, 213.9, and 248.3 nm, respectively. Mean value of triplicate experiment datasets was reported in this study. Fourier transform infrared spectrophotometry (FTIR; Shimadzu; Japan; IR Affinity1) (4000–400 cm^{-1} wavenumber range) was applied to reflect functional group's presence in untreated and exhausted resins. The compositions of elements present in the resins (prior to and after sorption) were observed with energy dispersive X-ray analyzer equipped field emission scanning electron microscope (FESEM EDX; Zeiss; Germany; Sigma).

2.3 Multi-heavy Metal Containing Synthetic Wastewater Solutions

Two alternate multiple heavy metal containing solutions were chosen from relevant prior art [13] and these refer to Cu^{+2} and Zn^{+2} dominant systems with other heavy and non-heavy metals. Table 2 summarizes the compositions of the synthetic wastewater solutions being prepared for adsorption and desorption investigations. These wastewater solution palettes have been conveyed to have originated from

Table 2 Concentration of metals in the solution with their maximum permissible limits

S.No	Metals	Solution		Max. permissible limit (mg L^{-1})
		Copper-based solution (Solution 1) (mg L^{-1})	Zinc-based solution (Solution 2) (mg L^{-1})	
1	Cu^{+2}	**375.4**	6.1	**0.5**
2	Zn^{+2}	3.5	**389.8**	**2**
3	Mg^{+2}	98.6	77.4	–
4	Al^{+3}	201.2	168.8	5
5	Na^{+}	497.6	366.9	200
6	K^{+}	49.8	10.4	–
7	Pb^{+2}	**10.4**	**5.3**	**0.05**
8	Fe^{+2}	**123.7**	**209.6**	**2.0**

Bold values signify the targeted metal ion concentrations

agricultural and mining waste streams in the mentioned prior art. Thus, the metal ions prevalent in the chosen composition refer to heavy metals (Cu, Zn, Fe, Pb, and Al) and non-heavy metals (Na, Mg, and K). Appropriate metal salt quantities have been measured and diluted in deionized water to achieve the mentioned simulated wastewater compositions.

2.4 Batch Adsorption Studies

Commercialized resins (0.2–2 g L^{-1}) were introduced into 50 mL of simulated solution in 100 mL conical flasks. Thereafter, batch adsorption experiments were conducted at 200 rpm and at 298 K. The simulated effluent system was studied to be highly sensitive to pH and tended to precipitate below and above a pH range of 3–4. Hence, pH optimality was not addressed in this work, and all experiments were conducted at the solution natural pH (3.82 and 3.64 for copper and zinc) dominant solutions 1 and 2, respectively. Other than the pH, among contact duration, adsorbent dosage and baseline metal ion concentration, only one parameter at a time was involved in consideration for optimality. Thereby, the processing variables have been altered and varied from 187.7 to 563.1 mg L^{-1} Cu^{+2} and 194.9 to 584.7 mg L^{-1} Zn^{+2} for an adsorption time of 12 h. After adsorption, the solution multi-heavy metal concentrations were determined using AAS for Pb, Fe, and Cu for solution 1 and Pb, Fe, and Zn for solution 2 due to their existence beyond permissible limit and hypothesis that others would exist only within the permissible limit as per the environmental legislations (Table 2). AAS equipment was utilized to investigate the concentrations of Cu^{+2}, Pb^{+2}, Fe^{+2}, and Zn^{+2} in the adsorbate. Based on mean values deduced from triplicate runs, adsorption capacity (AC) and percentage removal (%R) were evaluated applying the expressions:

$$Removal = \frac{C_o - C_e}{C_o} \times 100 \, (\%) \tag{1}$$

$$Adsorption \, capacity (q_e) = \frac{C_o - C_e}{W} \times V \, (mg \, g^{-1}) \tag{2}$$

where V, C_o, C_e, and W are vol. of solution (L), baseline and equilibrium concentration (mg L^{-1}), mass of adsorbent (g), respectively.

2.5 Batch Desorption Studies

Considering multi-heavy metal adsorbed Amberlite IR 120H and Lewatit TP 260 resins, NaOH, HCl, KOH, and H$_2$SO$_4$ eluents in wider concentration range (0.1–2 M) were utilized to investigate the desorption performance. The desorption experiments involved adding 50 mL of eluent to the resin at optimal adsorbent dosage (determined from adsorption studies) and subsequent mechanical shaking (at 200 rpm) and optimal contact time (chosen for adsorption studies) and at 25 °C. After completing this task, the final multi-heavy metal concentrations were determined using AAS and for mentioned metals for both solutions 1 and 2. Thereafter, mass balance expressions were deployed to evaluate metal transferred to the solution and subsequent recovery. To obtain useful insights into adsorption–desorption cycle efficacy, three consecutive cycles were considered for same feed concentration. Thereby, cycle efficacy was evaluated after each desorption cycle and represented in a schematic diagram for each measured heavy metal.

3 Results and Discussion

3.1 Batch Adsorption Characteristics

The batch adsorption characteristics have been evaluated in terms of adsorption capacity (AC) and removal efficiency (RE). According to adsorption studies being performed at fixed choice of solution pH 3.82 for Cu(II)-based solution (solution 1) and 3.61 for Zn(II)-based solution (solution 2), contact time (TC = 720 min), and initial metal ion concentration (C$_0$) (Cu^{+2} 375.4 mg L^{-1}, Pb^{+2} 10.4 mg L^{-1}, Fe^{+2} 123.7 mg L^{-1} for solution 1 and Zn^{+2} 389.8 mg L^{-1}, Pb^{+2} 5.3 mg L^{-1}, Fe^{+2} 209.6 mg L^{-1} for solution 2) and variant choice of adsorbent dosage (DA) (0.2–2 g L^{-1}), Fig. 1a, b, respectively, depicts the influence of DA on Fe^{+2}, Cu^{+2} and Pb^{+2} for Amberlite IR 120H. Thereby, the optimal DA has been inferred to be 1.6 g L^{-1} for all three heavy metal ions. Corresponding optimal RE and AC were 64.8% and 152.1 mg g^{-1} for Cu^{+2}, 87.4% and 5.7 mg g^{-1} for Pb^{+2} and 72.9% and 56.4 mg g^{-1} for Fe^{+2} in solution 1. Similarly, Fig. 1c, d shows DA optimality graph associated

to Fe^{+2}, Zn^{+2}, and Pb^{+2} adsorption on Amberlite IR 120H for solution 2. Thereby, the optimal DA has been referred to be 1.4 g L^{-1} for all three heavy metals on Amberlite IR 120H for solution 2. Corresponding batch adsorption data are 61.5%, 171.2 mg g^{-1} for Zn^{+2} and 73.2%, 2.8 mg g^{-1} for Pb^{+2}, and 64.6%, 96.7 mg g^{-1} for Fe^{+2}. Similarly, Fig. 2a, b shows DA optimality graph associated with Fe^{+2}, Cu^{+2}, and Pb^{+2} adsorption on Lewatit TP 260 for solution 1, respectively. Thereby, based on optimal RE and AC, the optimal DA has been evaluated as 1.4 g L^{-1} for Fe^{+2}, Cu^{+2}, and Pb^{+2} for Lewatit TP 260. Corresponding batch adsorption data are 79.1%, 247.2 mg g^{-1} for Cu^{+2}, 78.2%, 6.8 mg g^{-1} for Pb^{+2}, and 60.4%, 62.3 mg g^{-1} for Fe^{+2} in solution 1.

Similarly, Fig. 2c, d shows DA optimality graph associated to Fe^{+2}, Zn^{+2}, and Pb^{+2} adsorption on Lewatit TP 260 for solution 2. Corresponding batch adsorption data are 67.5%, 219.3 mg g^{-1} for Zn^{+2}, 62.1%, 2.7 mg g^{-1} for Pb^{+2}, and 72.7% and 126.9 mg g^{-1} for Fe^{+2} in solution 2. As predicted, the adsorbent capacity for larger dosages was increased as an outcome of the increased accessibility of active sites. The % removal of metals was reduced as a result of decreased adsorption of these metals. Based on adsorption studies conducted at fixed solution pH 3.82 for Cu^{+2}-based solution (solution 1) and 3.61 for Zn^{+2}-based solution (solution 2), initial metal ion concentration, agitation speed 200 rpm, DA (1.6 g L^{-1} for Amberlite IR 120H in solution 1, 1.4 g L^{-1} for Amberlite IR 120H in solution 2 and 1.2 g L^{-1} for Lewatit TP 260 in both the solution 1 and 2) and, Fig. 3a, b shows TC optimality graph associated to Fe^{+2}, Pb^{+2} and Cu^{+2} adsorptive behavior on Amberlite IR 120H
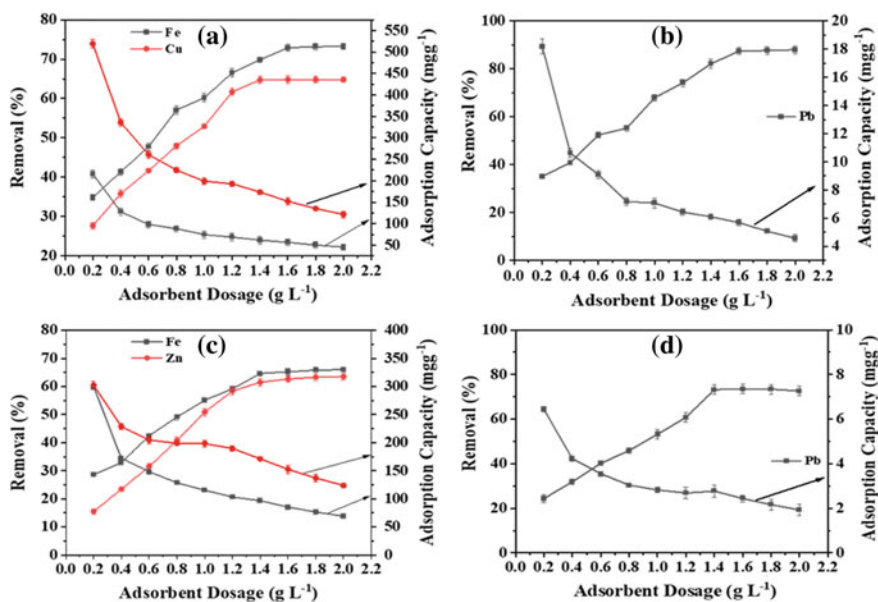
Fig. 1 Impact of adsorbent dosage on Fe^{+2}, Cu^{+2}/Zn^{+2}, and Pb^{+2} adsorption characteristics on Amberlite IR 120H **a**, **b** solution 1 and **c**, **d** solution 2
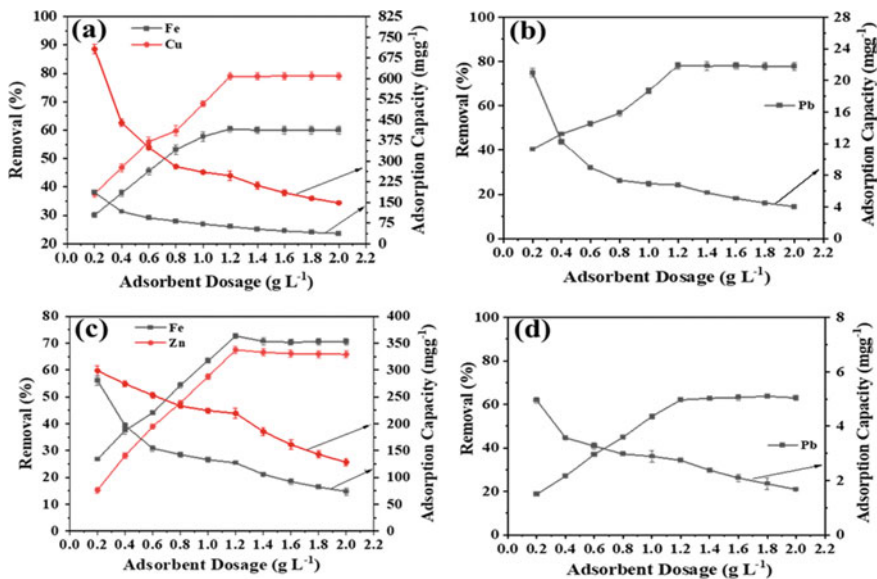
Fig. 2 Impact of adsorbent dosage on Fe^{+2}, Cu^{+2}/Zn^{+2}, and Pb^{+2} adsorption characteristics on Lewatit TP 260 **a**, **b** solution 1 and **c**, **d** solution 2

for solution 1. Thereby, based on optimal RE and AC, optimal TC has been evaluated as 420 min for solution 1 and 480 min for solution 2 with Amberlite IR 120H.

Corresponding batch adsorption data are 65.2%, 153.0 mg g^{-1} for Cu^{+2}, 82.02%, 5.5 mg g^{-1} for Pb^{+2}, and 71.5%, 55.3 mg g^{-1} for Fe^{+2} in solution 1. Similarly, From Fig. 3c, d, optimal batch adsorption data are 61.7%, 171.2 mg g^{-1} for Zn^{+2} and 69.8%, 2.6 mg g^{-1} for Pb^{+2}, and 62.2%, 93.1 mg g^{-1} for Fe^{+2} in solution 2.

Similarly, Fig. 4a, b shows TC optimality graph associated with Fe^{+2}, Cu^{+2}, and Pb^{+2} adsorption on Lewatit TP 260 for solution 1. Thereby, based on optimal RE and AC, optimal contact time has been evaluated as 300 min for Fe^{+2}, Cu^{+2}, and Pb^{+2} for Lewatit TP 260. Corresponding % removal and maximum adsorption capacities are 77.5%, 242.6 mg g^{-1} for Cu^{+2}, 78.5%, 6.8 mg g^{-1} for Pb^{+2}, and 58.7%, 60.5 mg g^{-1} for Fe^{+2} in solution 1. Similarly, Fig. 4c, d shows contact time optimality graph associated to Fe^{+2}, Zn^{+2}, and Pb^{+2} adsorption on Lewatit TP 260 for solution 2. Corresponding batch adsorption data are 67.0%, 217.8 mg g^{-1} for Zn^{+2} and 61.4%, 2.3 mg g^{-1} for Pb^{+2}, and 72.1%, 125.2 mg g^{-1} for Fe^{+2} in solution 2.

Speciation-based analysis of the solution indicated that heavy metals in (1–6) pH range have been exist in their ionic forms and as Pb^{++}, Fe^{++}, and Cu^{++} in solution 1 and Pb^{++}, Zn^{++}, and Fe^{++} in solution 2. Since experiments were conducted at natural solution pH (i.e., 3.82 for Cu^{+2} based solution and 3.61 for Zn^{+2} based solution), stronger interaction of all heavy metal ions with oxygen and nitrogen containing groups in the resin did occur. –NH$_2$ groups would get protonated at lower pH levels, and thereby facilitate resin to adsorb more metal ions. Also, therefore higher adsorption capabilities have been achieved. Thus, the speciation collaborated with the prevalent resins
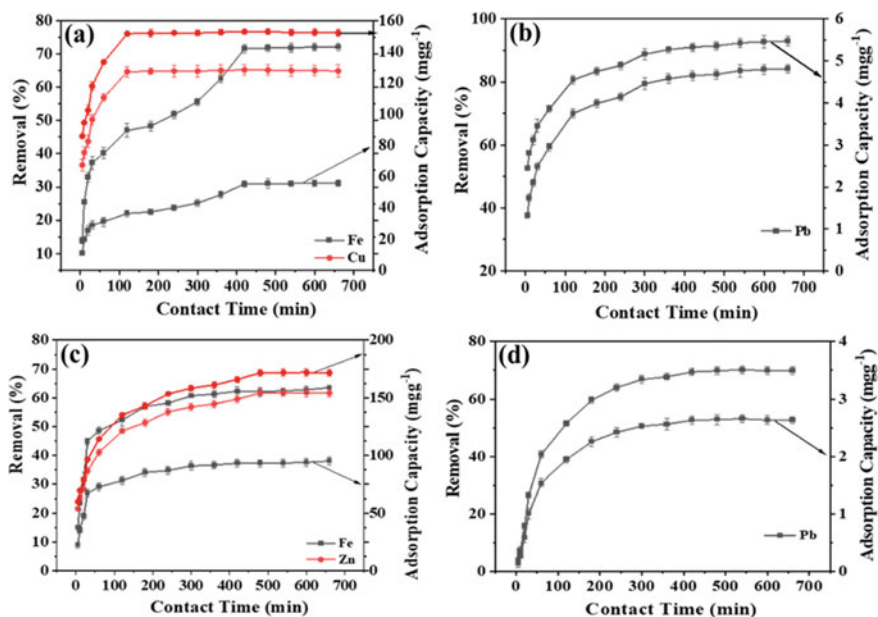
Fig. 3 Impact of adsorbent contact time on Fe^{+2}, Cu^{+2}/Zn^{+2}, and Pb^{+2} adsorption characteristics on Amberlite IR 120H **a, b** solution 1 and **c, d** solution 2
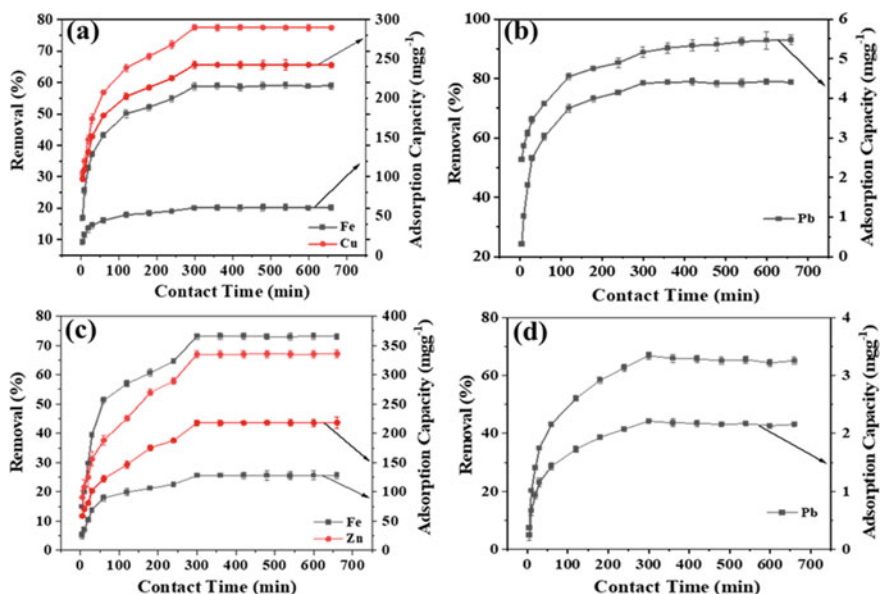
Fig. 4 Impact of adsorbent contact time on Fe^{+2}, Cu^{+2}/Zn^{+2}, and Pb^{+2} adsorption characteristics on Lewatit TP 260 **a**, **b** solution 1 and **c, d** solution 2
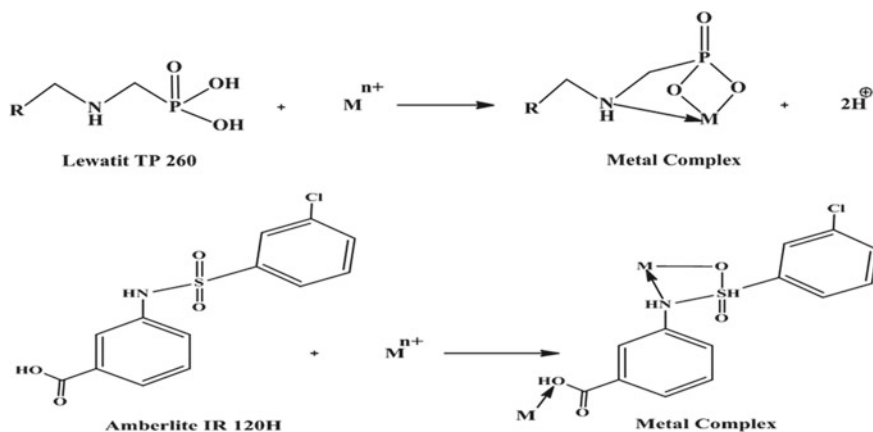
Fig. 5 Proposed mechanism of metal adsorption on commercial resins

functional groups and solution pH. Further, affirmation of this hypothesis would be possible through FESEM and EDX analysis. Relevant adsorption mechanisms for both resins have been depicted in Fig. 5.

3.2 Equilibrium and Kinetic Model Fitness

For the chosen solutions, Figs. 6 and 7 depict Langmuir fitness plots and Freundlich fitness plot for multi-heavy metal adsorption on Amberlite IR 120H and Lewatit TP 260. Figure 6a, c, respectively, illustrate Langmuir fitness plots for Cu^{+2} and Zn^{+2} solutions in Amberlite IR 120H, while Fig. 6b, d correspondingly depict for the Lewatit TP 260 resin. While, Fig. 7a, c, respectively, illustrate Freundlich fitness plots for Cu^{+2} and Zn^{+2} solutions in Amberlite IR 120H, while Fig. 7b, d correspondingly depict for the Lewatit TP 260 resin. Based on model parameter table (Table 3) and Figs. 6 and 7, the best fit model was Langmuir isotherm model for all the resins and solutions. The table also presented R_L value range of about 0–1 and thereby affirms favorable status of the resin for metal recovery from the chosen solutions. Trends have been found for Pb^{+2} and Fe^{+2} for Amberlite IR 120H and Lewatit TP 260 resins.

Figure 8 depicts pseudo-second-order fitness plots for Amberlite IR 120H… and Lewatit TP 260, in which Fig. 8a, c are for Cu^{+2} and Zn^{+2} solutions in Amberlite IR 120H and Fig. 8b, d are for Lewatit TP 260, respectively. Figure 9 depicts pseudo-first-order fitness plots for Amberlite IR 120H and Lewatit TP 260, in which Fig. 9a, c are for Cu^{+2} and Zn^{+2} solutions in Amberlite IR 120H and Fig. 9b, d are for Lewatit TP 260, respectively.

For better understanding, we have included relevant fitness variables in Table 4. The Figures and Table convey the best fitness of pseudo-second order for Amberlite IR 120H and Lewatit TP 260 with greater than 0.96 regression coefficient value.
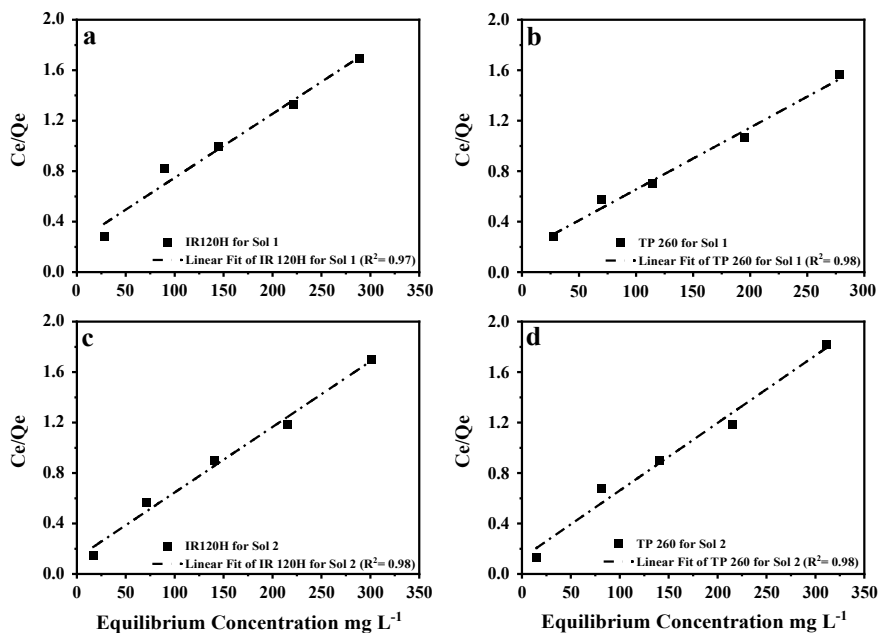
Fig. 6 Langmuir equilibrium fitness plots **a**, **b** for Cu^{+2} and **c**, **d** for Zn^{+2}
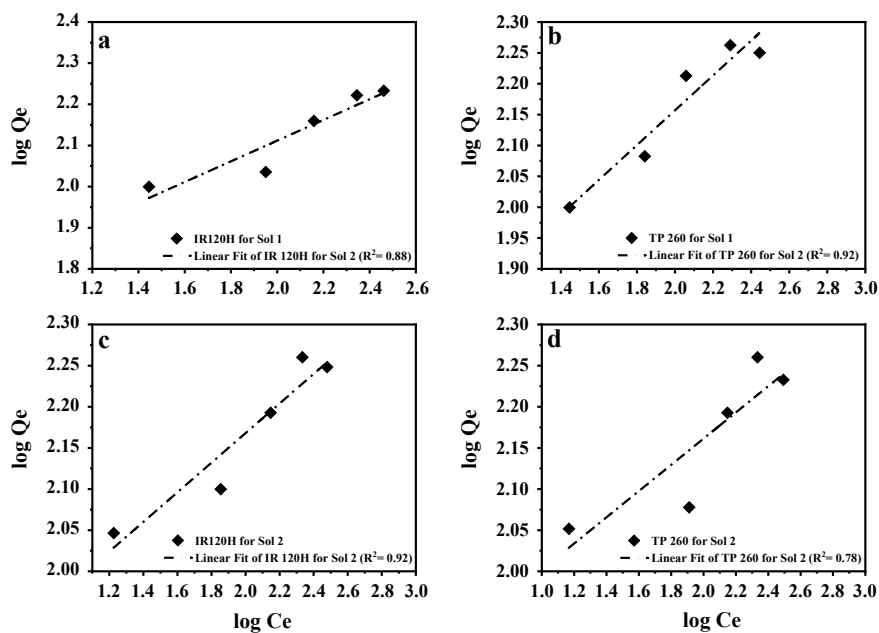
Fig. 7 Freundlich equilibrium fitness plots **a**, **b** for Cu^{+2} and **c**, **d** for Zn^{+2}

Table 3 Heavy metal adsorption equilibrium model data of commercial resin represented by design variables

Metals	Commercial resin	Solution	Parameters of Langmuir fitness plots				Parameters of Freundlich fitness plots		
			Q_o (mg g^{-1})	B (L mg^{-1})	R^2	R_L	K_f	n	R^2
Cu	Amberlite IR 120H	Solution 1	196.1	0.02	0.97	0.2–0.07	40.6	3.98	0.88
Fe			54.3	0.24	0.99	0.06–0.02	27.9	7.03	0.83
Pb			4.3	2.78	0.99	0.06–0.02	3.3	8.7	0.84
Zn		Solution 2	192.3	0.04	0.98	0.11–0.04	64.3	5.56	0.91
Fe			133.3	0.06	0.98	0.13–0.05	28.7	3.30	0.92
Pb			1.9	3.68	0.99	0.05–0.03	1.5	9.45	0.86
Cu	Lewatit TP 260	Solution 1	204.1	0.03	0.99	0.15–0.06	39.2	3.54	0.92
Fe			57.1	0.19	0.99	0.08–0.03	24.5	5.50	0.91
Pb			5.2	1.67	0.99	0.10–0.04	3.1	4.00	0.80
Zn		Solution 2	196.1	0.04	0.98	0.13–0.05	64.3	5.98	0.78
Fe			133.3	0.05	0.98	0.15–0.05	27.4	3.23	0.90
Pb			1.8	2.53	0.98	0.07–0.05	1.3	6.33	0.87
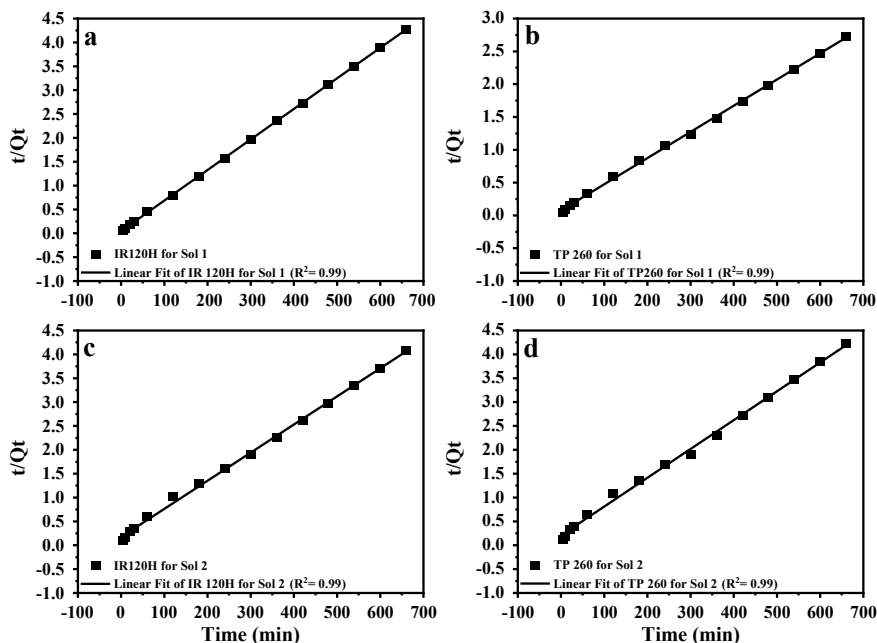
Fig. 8 Pseudo-second-order kinetic model fitness plots **a**, **b** for Cu^{+2} and **c**, **d** for Zn^{+2}
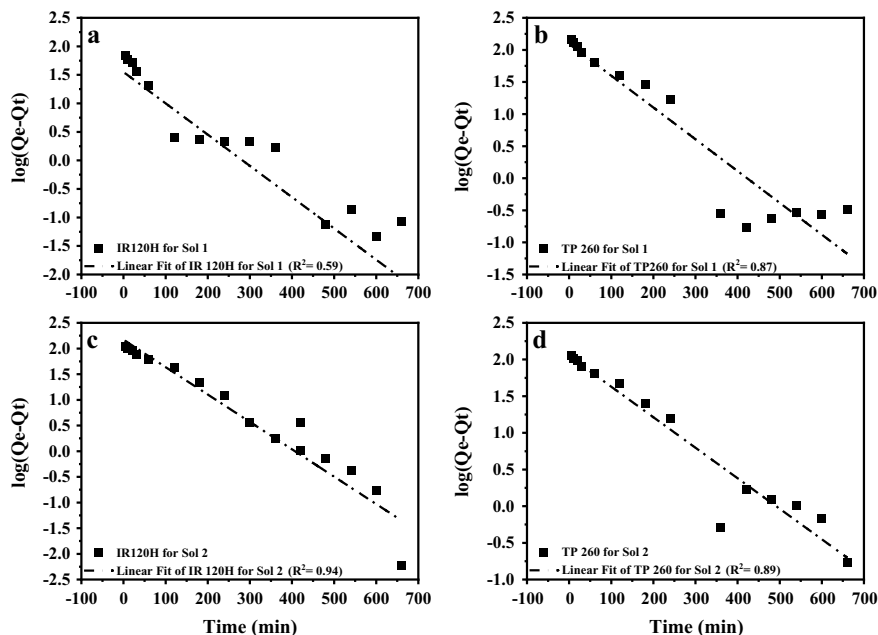
Fig. 9 Pseudo-first-order kinetic model fitness plots **a**, **b** for Cu^{+2} and **c**, **d** for Zn^{+2}

Similarly, the same trends are found for other metal ions like Pb^{+2} and Fe^{+2} for both commercial resins.

3.3 Commercialized Resin Characterization

FTIR spectra

Figure 10a, b conveys the FTIR spectra of Amberlite IR 120H and Lewatit TP 260 resins, respectively. At high frequencies (3400–3200 cm^{-1}), both anion exchanging resins indicate a wider –OH stretching vibration range. For Amberlite IR 120H, the peak at 2860–2930 cm^{-1} refers to C–H bond stretching through symmetric and asymmetric vibrations. Also, benzene ring vibrations were confirmed at 1630 cm^{-1} frequency band. Further, the bands at 1122 and 1413 cm^{-1} correspond to –SO$_2$ groups of sulfonic acid. In addition, several minor peaks at 1002 cm^{-1}, 1038 cm^{-1}, 1134 cm^{-1}, 1168 cm^{-1} do exist and confirm upon sulfonic acid groups [19]. After heavy metal adhered functional groups of Amberlite IR 120H adsorption, these peaks are shifted toward frequency bands of 999, 1029, 1156 cm^{-1} and thereby confirms heavy metal interaction.

For pure Lewatit TP 260, a strong band at 3420 cm^{-1} is observed which is assigned to amine groups present in the resin. The compounds with P–OH groups have a broad

Table 4 Heavy metal adsorption kinetic model data of commercial resin represented by design variables

Metals	Commercial resin	Experimental capacity (Q_{exp}, mg g^{-1})	Solution	Parameters of Pseudo-first-order model			Parameters of Pseudo-second-order model		
				Q_e (mg g^{-1})	K_1 (min^{-1})	R^2	Q_e (mg g^{-1})	K_2 (g mg^{-1} min^{-1})	R^2
Cu	Amberlite IR 120H	154.3	Solution 1	35.4	0.013	0.59	156.25	0.0009	0.99
Fe		55.7		56.0	0.009	0.77	59.17	0.0003	0.97
Pb		5.5		2.1	0.005	0.65	5.60	0.0086	0.99
Zn		161.6	Solution 2	148.2	0.012	0.94	169.49	0.0002	0.99
Fe		91.8		104.2	0.011	0.59	96.15	0.0003	0.99
Pb		2.6		1.8	0.006	0.69	2.97	0.0036	0.99
Cu	Lewatit TP 260	242.6	Solution 1	114.8	0.011	0.87	250.0	0.0002	0.99
Fe		60.8		21.1	0.008	0.66	62.89	0.0008	0.99
Pb		6.8		2.2	0.006	0.55	7.02	0.0090	0.99
Zn		156.6	Solution 2	100.4	0.009	0.89	166.67	0.0002	0.99
Fe		98.5		58.4	0.010	0.90	104.17	0.0003	0.99
Pb		2.2		1.2	0.006	0.74	2.28	0.0149	0.99
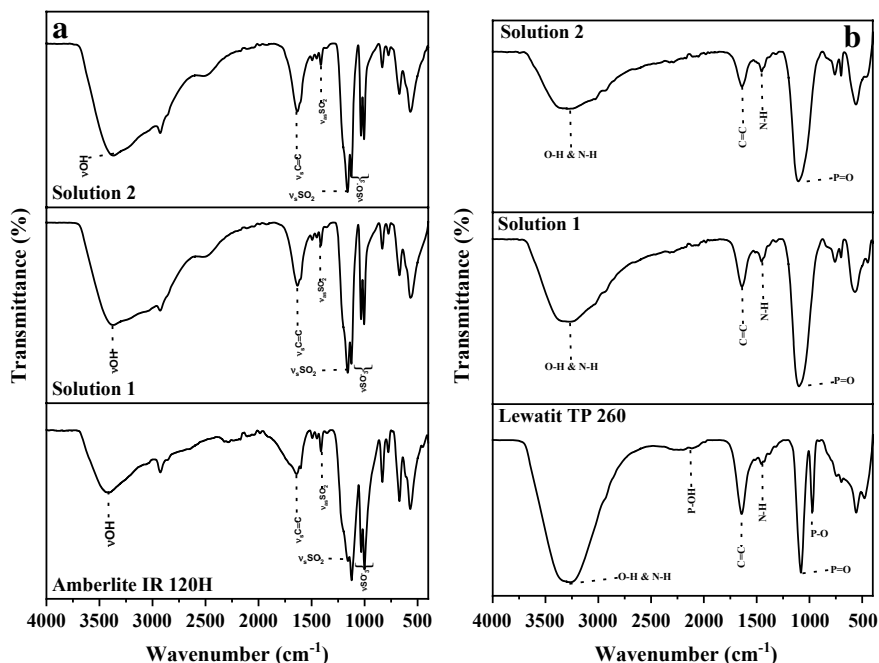
Fig. 10 FTIR spectra of raw and heavy metal loaded **a** Amberlite IR 120H and **b** Lewatit TP 260 resins

band of medium intensity at 2732 and 2323 cm^{-1} which are due to the O–H stretching vibrations, and a strong band is observed due to P–O stretching at 1220 cm^{-1} [9]. The bands at 1631 and 1723 cm^{-1} are assigned to the formation of the –NH bond. After metal adsorption, a strong band of 972 cm^{-1} is disappeared and is assigned to the meal interaction with the resin.

EDX spectra

EDX spectra obtained for pure Amberlite IR 120H and Lewatit TP 260 resins are depicted in Figs. 11 and 12. The EDX spectra of Amberlite IR 120H (Fig. 11) confirm the presence of C (68.8 atomic weight %), O (23.2 atomic weight %), and S (5.6 atomic weight %). For Lewatit TP 260 (Fig. 12) pure resin, the composition refers to C (68.2%), O (20.6%) and P (4.8%). After adsorption, the EDX spectra confirm the presence of Cu, Fe, and Pb metal ions on the surface of both commercial resins.

3.4 Cyclic Desorption Characteristics

For solution 1 (Cu^{+2} dominant solution) and for Amberlite IR 120H, the desorption efficiencies were the highest for 2 M HCl. For a variation in HCl concentration from
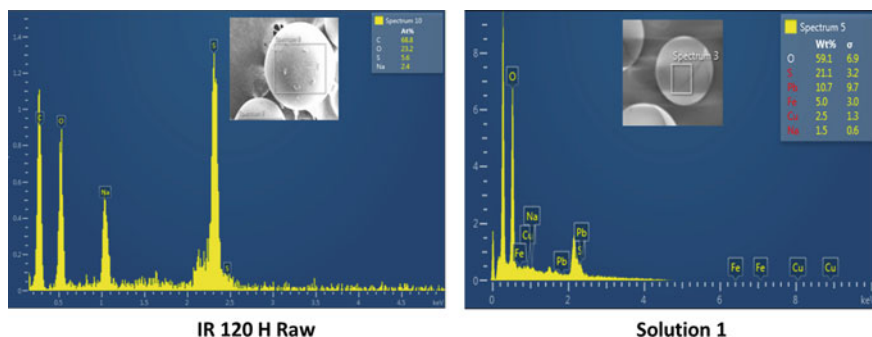
Fig. 11 FESEM EDX spectra of raw and metal loaded Amberlite IR 120H resin
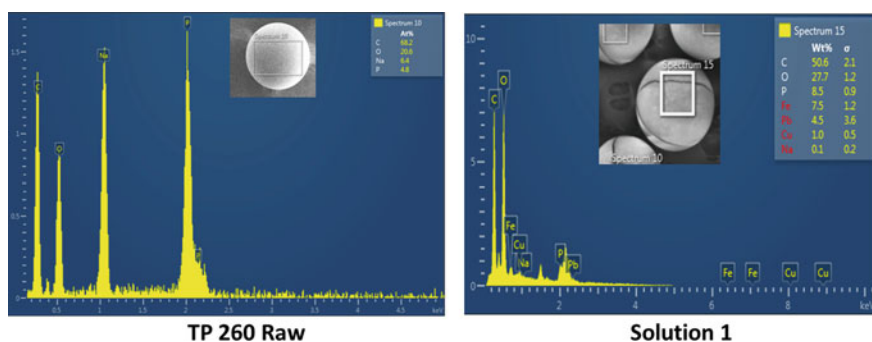
Fig. 12 FESEM EDX spectra of raw and metal loaded Lewatit TP 260 resin

0.1 to 2 M, the Cu^{+2} recovery efficiencies varied as 25.11–53.88, 10.9–28.1, and 3.64–12.3% for three consecutive cycles, respectively. The desorption efficiencies of all tested acidic eluents followed the hierarchy as $HCl > HNO_3 > H_2SO_4$. Corresponding cycle efficiencies for HNO_3 and H_2SO_4 comparatively lower and varied as 18.51–52.41, 5.27–25.8, and 1.72–11.3% and 16.74–49.59, 4.53–24.7, and 1.51–10.6% for three consecutive cycles, respectively. Thus, significant reduction in cycle 2 and 3 Cu^{+2} desorption efficiencies was apparent in conjunction with the desorption efficiencies (Fig. 13a). The desorption efficiencies of Fe^{+2} followed similar trends and correspondingly varied as 24.32–55.01, 10.34–25.98, and 6.35–16.47% for three consecutive cycles, respectively. The desorption efficiencies of all tested acidic eluents followed the hierarchy as $HCl > H_2SO_4 > HNO_3$. Corresponding cycle efficiencies for H_2SO_4 and HNO_3 were comparatively lower and varied as 22.0–47.06, 8.36–21.99, and 4.04–15.38% and 24.24–44.28, 10.79–21.75, and 4.30–14.45% for three consecutive cycles, respectively. The desorption efficiencies of Pb^{+2} followed the similar trends and correspondingly varied as 13.36–56.46, 5.01–21.65, and 2.24–12.15% for three consecutive cycles, respectively. The Pb^{+2} desorption efficiency of all tested acidic eluents followed the hierarchy as $HCl > HNO_3 > H_2SO_4$.

Corresponding cycle efficiencies for HNO$_3$ and H$_2$SO$_4$ were comparatively lower and varied as 13.50–47.21, 5.73–24.5, and 1.70–11.92% and 21.72–42.97, 8.15–27.81, and 3.81–11.86% for three consecutive cycles, respectively.

For solution 1 (Cu^{+2} dominant solution) and for Amberlite IR 120H, the desorption efficiencies varied as a comparatively lower range for basic eluents in conjunction with the acidic eluents (0.1–2 M). Corresponding cycle efficiencies for NaOH and KOH varied as 9.94–49.3.1, 3.81–21.0, and 1.49–8.46% and 10.77–36.40, 4.29–16.3, and 1.81–7.33% for three consecutive cycles, respectively. Thus, significant reduction in cycle 2 and 3 Cu^{+2} desorption efficiencies was observed with respect to cycle 1 desorption efficiencies (Fig. 13b). The desorption efficiencies of Fe^{+2} followed similar trend and the Fe^{+2} desorption efficiency of tested basic eluents followed the hierarchy as KOH > NaOH. Corresponding cycle efficiencies for KOH and NaOH have been determined as 13.12–41.05, 5.69–18.51, and 3.81–13.07% and 11.62–40.05, 5.06–17.98, and 3.42–11.32% for three consecutive cycles, respectively. Thus, significant reduction in cycle 2 and 3 Fe^{+2} desorption efficiencies with respect to cycle 1 Fe^{+2} efficiencies was observed. The desorption efficiencies of Pb^{+2} followed similar trend and the desorption efficiency of all tested basic eluents followed the hierarchy as NaOH > KOH. Corresponding cycle efficiencies for NaOH and KOH were 14.66–43.31, 6.08–24.36, and 3.21–13.08% and 13.72–40.09, 5.64–21.16, and 2.18–10.05% for three consecutive cycles, respectively. Thus, significant reduction in cycle 2 and 3 Pb^{+2} desorption efficiencies was observed in comparison with the Pb^{+2} cycle 1 desorption efficiencies.

Fig. 13 Desorption efficiency of **a**, **b** for Cu and **c**, **d** for Zn with Amberlite IR 120H

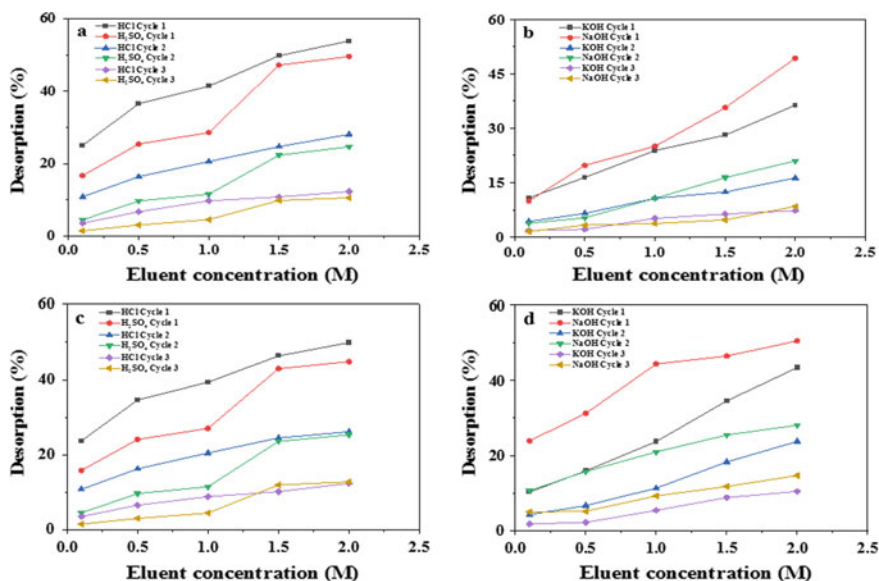For solution 1 (Cu^{+2} dominant solution) and for Lewatit TP 260, the desorption efficiencies were obtained promising for 2 M HCl. Corresponding variations in the Cu^{+2} recovery efficiencies varied as 20.64–44.30%, 8.62–21.2%, and 2.64–8.24% for 3 cycles, respectively, in the system constitution range of (0.1–2 M). The desorption efficiency of all tested acidic eluents followed the hierarchy as HCl > HNO_3 > H_2SO_4. Corresponding cycle efficiencies for HNO_3 and H_2SO_4 have been determined as 15.22–43.08%, 4.2–19.5%, 1.27–7.63% and 13.77–40.78%, 3.62–18.8%, 1.12–7.2% for 3 cycles, respectively. Thus, significant reduction in cycle 2 and 3 desorption efficiencies with respect to cycle 1 efficiencies was observed (Fig. 14a). The desorption efficiencies of Fe^{+2} followed the similar trends and varied as 15.12–47.18%, 10.88–23.73%, and 6.61–13.44% for 3 cycles, respectively, in the system constitution range of (0.1–2 M). The desorption efficiency of all tested acidic eluents followed the hierarchy as HCl > HNO_3 > H_2SO_4. Corresponding cycle efficiencies for HNO_3 and H_2SO_4 have been determined as 16.41–43.59%, 9.43–20.86%, 4.44–13.33% and 15.20–42.08%, 10.11–21.62%, 6.26–16.0% for 3 cycles, respectively. Thus, significant reduction in cycle 2 and 3 desorption efficiencies with respect to cycle 1 was observed. The desorption performance of Pb^{+2} followed the different trends with 2 N HNO_3 and varied as 14.27–44.89%, 6.25–24.81%, and 1.84–12.01% for 3 cycles, respectively, in the system constitution range of (0.1–2 M). The desorption efficiency of all tested acidic eluents followed the hierarchy as HNO_3 > H_2SO_4 > HCl. Corresponding cycle efficiencies for H_2SO_4 and HCl have been determined as 22.5–43.7%, 8.71–30.14%, 4.04–12.87% and 14.09–39.32%, 5.45–18.62%, and 2.42–9.89% for 3 cycles, respectively. Thus, significant reduction in cycle 2 and 3 desorption efficiencies with respect to cycle 1 efficiencies was observed.

For solution 1 (Cu^{+2} dominant solution) and for Lewatit TP 260, the desorption efficiencies were obtained highest for 2 M NaOH. Corresponding cycle efficiencies for NaOH and KOH have been determined as 16.24–51.06%, 4.22–24.7%, 2.43–12.0% and 8.87–33.29%, 3.46–17.2%, 1.35–8.55% for 3 cycles, respectively. Thus, significant reduction in cycle 2 and 3 desorption efficiencies with respect to cycle 1 efficiencies was observed. The desorption efficiencies of Fe^{+2} followed the similar trends and the desorption efficiency of tested basic eluents followed the hierarchy as NaOH > KOH. Corresponding cycle efficiencies for NaOH and KOH have been determined as 13.78–49.93%, 5.79–26.09%, 3.80–13.65% and 15.55–46.74%, 6.52–22.01%, 4.24–15.10% for 3 cycles, respectively (Fig. 14b). Thus, significant reduction in cycle 2 and 3 desorption efficiencies with respect to cycle 1 was observed. The desorption performance of Pb^{+2} followed the similar trends and the desorption efficiency of all tested basic eluents followed the hierarchy as NaOH > KOH. Corresponding cycle efficiencies for NaOH and KOH have been determined as 15.77–47.63%, 13.16–26.88%, 7.38–20.13% and 14.30–41.91%, 6.07–23.09%, 2.32–11.81% for 3 cycles, respectively. Thus, significant reduction in cycle 2 and 3 desorption efficiencies with respect to cycle 1 efficiencies was observed. For solution 2 (Zn^{+2} dominant solution) and for Amberlite IR 120H, Zn^{+2} recovery efficiencies were lesser for acidic eluents in the system constitution range of (0.1–2 M) and for all tested acidic eluents followed the hierarchy as HCl > HNO_3 > H_2SO_4. Corresponding cycle efficiencies for HCl, H_2SO_4 and HNO_3 have been determined as (23.71–48.9%,
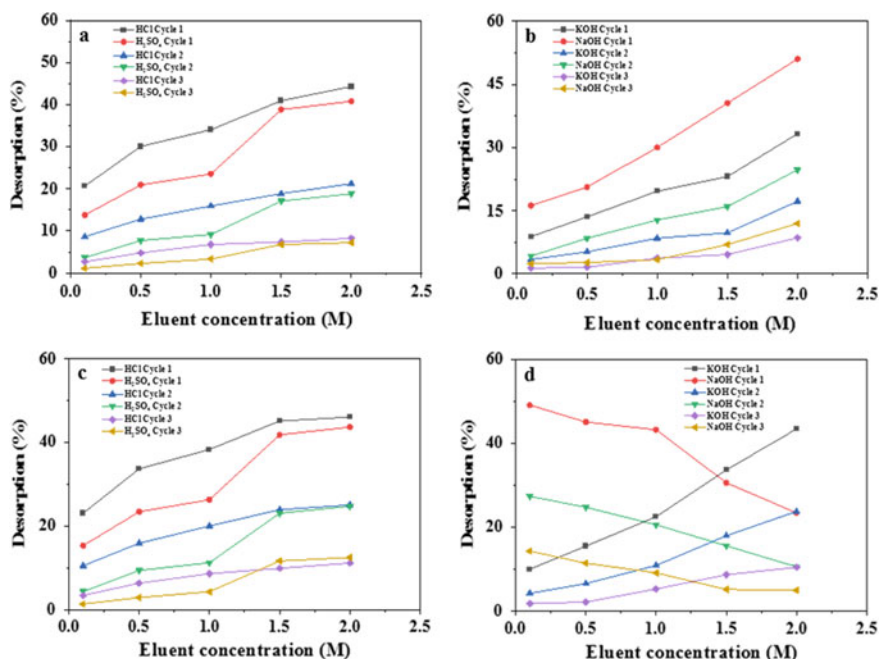
Fig. 14 Desorption efficiency of **a**, **b** for Cu and **c**, **d** for Zn with Lewatit TP 260

10.75–26.1%, 3.5–12.4%), (15.80–44.86%, 4.5–25.31%, 1.5–12.8%) and (17.10–47.6%, 5.3–27.8%, 1.7–12.1%) for 3 cycles, respectively (Fig. 13c). Thus, significant reduction in cycle 2 and 3 desorption efficiencies with respect to cycle 1 efficiencies was observed.

The desorption efficiencies of Fe^{+2} were highest for 2 M HCl and varied as 14.95–40.31%, 12.59–27.20%, and 9.45–22.54% for 3 cycles, respectively, in the system constitution range of (0.1–2 M). The desorption efficiency of all tested acidic eluents followed the hierarchy as $HCl > H_2SO_4 > HNO_3$. Corresponding cycle efficiencies for H_2SO_4 and HNO_3 have been determined as 13.56–29.01%, 10.37–22.8%, 6.21–19.72% and 14.93–27.18%, 13.18–24.82%, 6.4–21.4% for 3 cycles, respectively. Thus, significant reduction in cycle 2 and 3 desorption efficiencies with respect to cycle 1 was observed. The desorption performance of Pb^{+2} followed the similar trends and varied as 21.87–52.01%, 10.07–28.34%, and 4.75–14.81% for 3 cycles, respectively, in the system constitution range of (0.1–2 M). The desorption efficiency of all tested acidic eluents followed the hierarchy as $HCl > HNO_3 > H_2SO_4$. Corresponding cycle efficiencies for HNO_3 and H_2SO_4 have been determined as 17.29–46.3%, 7.07–26.8%, 2.95–15.2% and 17.5–44.4%, 7.53–24.03%, 3.46–13.17% for 3 cycles, respectively. Thus, significant reduction in cycle 2 and 3 desorption efficiencies with respect to cycle 1 efficiencies was observed. For solution 2 (Zn^{+2} dominant solution) and for Amberlite IR 120H, Zn^{+2} recovery efficiencies were highest for

2 M NaOH. Corresponding cycle efficiencies for NaOH and KOH have been determined as 23.9–50.63%, 10.7–28.1%, 5.1–14.7% and 10.24–43.5%, 4.27–23.8%, 1.8–10.4% for 3 cycles, respectively, in the system constitution range of (0.1–2 M) (Fig. 13d). Thus, significant reduction in cycle 2 and 3 desorption efficiencies with respect to cycle 1 efficiencies was observed. The desorption efficiencies of Fe^{+2} were obtained lesser for basic eluents and the desorption efficiencies for KOH and NaOH have been determined as 8.6–24.3%, 7.3–20.5%, 6.1–17.1% and 7.18–24.6%, 6.7–19.71%, 5.6–14.8% for 3 cycles, respectively. Thus, significant reduction in cycle 2 and 3 desorption efficiencies with respect to cycle 1 was observed. The desorption performance of Pb^{+2} followed the similar trends and the desorption efficiency of all tested basic eluents followed the hierarchy as KOH > NaOH. Corresponding cycle efficiencies for KOH and NaOH have been determined as 21.48–46.63%, 10.55–24.9%, 4.8–13.5% and 18.7–45.02%, 7.9–26.0%, 7.5–13.46% for 3 cycles, respectively. Thus, significant reduction in cycle 2 and 3 desorption efficiencies with respect to cycle 1 efficiencies was observed.

For solution 2 (Zn^{+2} dominant solution) and for Lewatit TP 260, Zn^{+2} recovery efficiencies were lesser for acidic eluents in the system constitution range of (0.1–2 M) and for all tested acidic eluents followed the hierarchy as HNO_3 > HCl > H_2SO_4. Corresponding cycle efficiencies for HNO_3, HCl, and H_2SO_4 have been determined as (17.24–46.3%, 5.2–25.2%, 1.7–11.8%), (23.1–46.1%, 10.6–25.2%, 3.5–11.2%), and (15.4–43.7%, 4.4–24.8%, 1.44–12.6%) for 3 cycles, respectively (Fig. 14c). Thus, significant reduction in cycle 2 and 3 desorption efficiencies with respect to cycle 1 efficiencies was observed. The desorption efficiencies of Fe^{+2} were highest for 2 M HCl and varied as 13.8–32.1%, 11.8–23.7%, and 8.3–20.2% for 3 cycles, respectively, in the system constitution range of (0.1–2 M). The desorption efficiency of all tested acidic eluents followed the hierarchy as HCl > H_2SO_4 > HNO_3. Corresponding cycle efficiencies for H_2SO_4 and HNO_3 have been determined as 12.6–26.9%, 9.7–21.3%, 5.8–18.4% and 13.8–25.2%, 12.3–23.2%, 6.1–20.1% for 3 cycles, respectively. Thus, significant reduction in cycle 2 and 3 desorption efficiencies with respect to cycle 1 was observed. The desorption performance of Pb^{+2} followed the similar trends and varied as 26.02–41.4%, 12.7–27.6%, and 5.9–15.7% for 3 cycles, respectively, in the system constitution range of (0.1–2 M). The desorption efficiency of all tested acidic eluents followed the hierarchy as HCl > HNO_3 > H_2SO_4. Corresponding cycle efficiencies for HNO_3 and H_2SO_4 have been determined as 19.6–41.3%, 8.5–24.4%, 3.5–13.3% and 20.2–39.2%, 9.2–25.6%, 4.1–15.03% for 3 cycles, respectively. Thus, significant reduction in cycle 2 and 3 desorption efficiencies with respect to cycle 1 efficiencies was observed.

For solution 2 (Zn^{+2} dominant solution) and for Lewatit TP 260, Zn^{+2} recovery efficiencies were highest for 0.1 M NaOH. Corresponding cycle efficiencies for NaOH and KOH have been determined as 49.2–23.4%, 27.4–10.5%, 14.3–4.9% and 10.01–43.5%, 4.2–23.8%, 1.7–10.4% for 3 cycles, respectively, in the system constitution range of (0.1–2 M) (Fig. 14d). Thus, significant reduction in cycle 2 and 3 desorption efficiencies with respect to cycle 1 efficiencies was observed. The desorption efficiencies of Fe^{+2} were obtained lesser for basic eluents and the desorption efficiencies for KOH and NaOH have been determined as 7.9–29.0%, 6.8–21.8%,

5.7–18.6% and 9.9–31.8%, 9.7–30.5%, 6.6–23.6% for 3 cycles, respectively. Thus, significant reduction in cycle 2 and 3 desorption efficiencies with respect to cycle 1 was observed. The desorption performance of Pb^{+2} followed the similar trends and the desorption efficiency of all tested basic eluents followed the hierarchy as NaOH > KOH. Corresponding cycle efficiencies for NaOH and KOH have been determined as 22.2–47.3%, 9.7–26.3%, 9.1–14.9% and 25.5–43.5%, 13.2–25.05%, 5.9–13.9% for 3 cycles, respectively. Thus, significant reduction in cycle 2 and 3 desorption efficiencies with respect to cycle 1 efficiencies was observed.

In summary, Amberlite IR 120H resin and 2 M HCl eluent are the best adsorbent and desorbent system for the copper, lead, and iron removal from both solutions. However, for the Zn^{+2} removal from solution 2, 2 M NaOH was the corresponding best desorbent system. Similarly, the Lewatit TP 260 resin performed the best for the reduction in copper, lead, and iron concentrations from both solutions. However, the Zn^{+2} removal indicated optimality of 0.1 M but not for 2 M NaOH. For the comparison with relevant literature, we have summarized our findings in Table 5. Compared to the literature, findings for Lewatit TP 260 resin were much superior. The literature refers to desorption efficiency of 0%, 45%, 70%, and 65% for Cd, Pb, Ni, and Cr, respectively [12]. In this present work, the adsorption properties of Lewatit TP 260 resin were unaffected by the existence of other metal ions such as Na$^+$, Al^{+3}, Mg^{+2}, and K$^+$, and desorption efficiencies were affected due to their presence. We can say that if we reduce the concentration of K, Na, Mg, and Al concentrations prior to adsorption–desorption processes, better efficiencies can achieve. For comparison studies, Amberlite IR 120H resin does not have any relevant published data.

4   Conclusions

From modeling and experimental studies conducted in this study to examine the performance of Amberlite IRA 120H and Lewatit TP 260 for recovery and reuse of copper, lead, zinc, and iron from synthetic industrial wastewater solutions, including (copper, lead, zinc, and iron), several prospective can be deduced. Firstly, Lewatit TP 260 resin confirms promising adsorptive capabilities of 204.1, 57.1, and 5.2 mg g^{-1} for Cu^{+2}, Fe^{+2}, and Pb^{+2} recovery from Cu^{+2}-based multi-metal wastewater solution and 196.1, 133.3, and 1.8 mg g^{-1} for Zn^{+2}, Fe^{+2}, and Pb^{+2} recovery from Zn^{+2}-based multi-metal wastewater solution. Secondly, Lewatit TP 260 resin offered promising performance with a lower resin dose (1.2 g L^{-1}) and lesser adsorption time (300 min). Thirdly, the pseudo-second-order model and non-homogeneous pattern confirmed the chemisorption process. Fourthly, heavy metal adsorption mechanism with resin and the species present at optimum pH was achieved with speciation analysis. Fifthly, Lewatit TP 260 resin shows higher desorption capabilities of 53.9, 55.0, and 56.5% for Cu^{+2}, Fe^{+2}, and Pb^{+2} utilizing 2 M NaOH solution in Cu^{+2}-based multi-metal wastewater solution and 50.6, 40.3, 52.0% after 3rd cycle for Zn^{+2} (using 0.1 M NaOH), Fe^{+2}, and Pb^{+2} using 2 M NaOH solution in Zn^{+2}-based multi-metal wastewater solution. Sixthly, if we neglect the cost of the commercial resin used

Table 5 A summary of the adsorptive and desorptive properties of the various resins studied in this study and published in the articles

S.No	Adsorbent	Functional group	Metal ion	Conc. (mg/l)	pH	Ads. Caps (mg/g)	Removal (%)	Desorption (%)	References
1	Amberlite IR 120H	Sulfonic acid	**Pb+2** **Pb+2** **Cu+2** **Zn+2** **Fe+2** **Fe+2** Zn+2 Cu+2 Mg+2 Mg+2 Al+3 Al+3 Na+ Na+ K+ K+	10.4 5.3 375.4 389.8 123.7 209.6 3.5 6.1 98.6 77.4 201.2 168.8 497.6 366.9 49.8 10.4	3.8 3.6	4.3 1.9 196.1 192.3 54.3 133.3	82.1 69.8 65.7 61.7 71.5 62.2	47.6–20.1 47.3–14.9 51.1–12.0 49.2–14.3 49.9–13.7 31.8–23.6 (2 M HCl; 1–3 cycles) (1–3 cycles; Pb & Fe; 2 M HCl & Zn; 2 M NaOH)	Present study
	Lewatit TP260	Aminomethyl phosphonic acid	**Pb+2** **Pb+2** **Cu+2** **Zn+2** **Fe+2** **Fe+2** Zn+2 Cu+2 Mg+2 Mg+2 Al+3 Al+3 Na+ Na+ K+ K+	10.4 5.3 375.4 389.8 123.7 209.6 3.5 6.1 98.6 77.4 201.2 168.8 497.6 366.9 49.8 10.4	3.8 3.6	5.2 1.8 204.1 196.1 57.1 133.3	69.8 61.4 61.7 67.0 62.2 72.1	56.5–12.2 51.96–14.8 53.9–12.3 50.6–14.7 55.0–12.2 40.31–22.5 (2 M NaOH; 1–3 cycles) (1–3 cycles; Pb & Fe; 2 M NaOH & Zn; 0.1 M NaOH)	Present study
2	Lewatit TP 260 Lewatit TP 208 Amberlite IRA743	(Aminomethyl) phosphoric acid Iminosiacetic acid N-methylglucamine	Al+3 Cu+2 Ni+2 Pb+2 Zn+2	–	3.9	64.8 66.7 35.3 1.8 1.9 1.3 3.3 2.7 1.2	–	> 90 (low molar sulfuric acid)	[15]

Table 5 (continued)

S.No	Adsorbent	Functional group	Metal ion	Conc. (mg/l)	pH	Ads. Caps (mg/g)	Removal (%)	Desorption (%)	References
3	Polyvinyl tetrazole grafted PS resins	Tetrazolyl groups	Pb^{+2} Cu^{+2} Cr^{+2}	4 (mmol/l)	5	1.5 2.6 3.4 (mmol/g)	35.5 60.3 84 (Binary)	94% 1 M HCl (10 cycle) 2 h desorption time	[6]
4	Styrene–DVB copolymer	Iminodiacetic acid	Cr^{+2} Ni^{+2} Pb^{+2} Cd^{+2}	–	3.5	–	99.7 65 59 28	65 70 45 (0.1 N NaOH) Cycles not given	[12]
5	Amberlite IRC748 NDC702	Iminodiacetic acid (IDA)	Cu^{+2} Pb^{+2} Cd^{+2}	0.1–4.0 (mmol/l)	5	2.8/2.1 1.2/1.3 0.9/0.9	–	~ 100% (15wt% HCl) Cycles not given	[11]
6	GMA/DVB magnetic resin	Iminodiacetate	Pb^{+2} Cd^{+2} Zn^{+2} Ca^{+2} Mg^{+2}	5 (mmol/l)	6 6.6 6.5 6.5 7.0	2.68 2.39 2.00 1.99 1.83	–	96 (0.2 M EDTA) 5 Cycles Efficiency of each cycle given	[4]

Bold values signify the results of the targeted metal ions

in the present study, then Lewatit TP 260 resin shows better results in comparison with Amberlite IR 120H. In summary, the efficiency of performance capabilities and process dimensions has been suggested and investigated as just a promising strategy for selecting the most productive resin for removing heavy metal ions from different systems.

References

1. Abo-Farha, S.A., Abdel-Aal, A.Y., Ashour, I.A., Garamon, S.E.: Removal of some heavy metal cations by synthetic resin purolite C100. J Hazard. Mater. **169**, 190–194 (2009)
2. Alyüz, B., Veli, S.: Kinetics and equilibrium studies for the removal of nickel and zinc from aqueous solutions by ion exchange resins. J. Hazard Mater. **167**, 482–488 (2009)
3. Anbazhagan, S., Thiruvengadam, V., Sukeri, A.: An Amberlite IRA-400 Cl-ion-exchange resin modified with: Prosopis juliflora seeds as an efficient Pb2+adsorbent: adsorption, kinetics, thermodynamics, and computational modeling studies by density functional theory. RSC Adv. **11**, 4478–4488 (2021)
4. Atia, A.A., Donia, A.M., Yousif, A.M.: Removal of some hazardous heavy metals from aqueous solution using magnetic chelating resin with iminodiacetate functionality. Sep. Purif. Technol. **61**, 348–357 (2008)
5. Das, P. P., Mondal, P., Sinha, A., Biswas, P., Sarkar, S., & Purkait, M. K.: Treatment of steel plant generated biological oxidation treated (BOT) wastewater by hybrid process. Sep. Purif. Technol. **258**, 118013 (2021)
6. Chen, Y., He, M., Wang, C., Wei, Y.: A novel polyvinyltetrazole-grafted resin with high capacity for adsorption of Pb(ii), Cu(ii) and Cr(iii) ions from aqueous solutions. J. Mater. Chem. A **2**, 10444–10453 (2014)
7. Demirbas, A., Pehlivan, E., Gode, F., Altun, T., Arslan, G.: Adsorption of Cu(II), Zn(II), Ni(II), Pb(II), and Cd(II) from aqueous solution on Amberlite IR-120 synthetic resin. J. Colloid Interface Sci. **282**, 20–25 (2005)
8. Hubicki, Z., Gęca, M., Kołodynska, D.: The effect of the presence of metatartaric acid on removal effectiveness of heavy metal ions on chelating ion exchangers. Environ. Technol. **32**, 805–816 (2011)
9. Kołodyńska, D., Hubicki, Z.: FT-IR/PAS studies of Cu(II)–EDTA complexes sorption on the chelating ion exchangers (2009)
10. Sontakke, A. D., Das, P. P., Mondal, P., & Purkait, M. K.: Thin-film composite nanofiltration hollow fiber membranes toward textile industry effluent treatment and environmental remediation applications. Emergent mater. **5**, 1–19 (2021)
11. Das, P. P., Mondal, P., Sinha, A., Biswas, P., Sarkar, S., & Purkait, M. K.: Integrated ozonation assisted electrocoagulation process for the removal of cyanide from steel industry wastewater. Chemosphere, **263**, 128370 (2021)
12. Purkait, M. K., Gusain, D. S., DasGupta, S., & De, S.: Adsorption behavior of chrysoidine dye on activated charcoal and its regeneration characteristics by using different surfactants. Sep. Sci. Technol. **39**, 2419–2440 (2005)
13. Morcali, M.H., Zeytuncu, B., Baysal, A., Akman, S., Yucel, O.: Adsorption of copper and zinc from sulfate media on a commercial sorbent. J. Environ. Chem. Eng. **2**, 1655–1662 (2014)

14. Das, P. P., & Purkait, M. K.: Treatment of cold rolling mill (CRM) effluent of steel industry. Sep. Purif. Technol. **274**, 119083 (2021)
15. Nekouei, R.K., Pahlevani, F., Assefi, M., Maroufi, S., Sahajwalla, V.: Selective isolation of heavy metals from spent electronic waste solution by macroporous ion-exchange resins. J. Hazard Mater. **371**, 389–396 (2019)
16. Niu, L., Deng, S., Yu, G., Huang, J.: Efficient removal of Cu(II), Pb(II), Cr(VI) and As(V) from aqueous solution using an aminated resin prepared by surface-initiated atom transfer radical polymerization. Chem. Eng. J. **165**, 751–757 (2010)
17. Das, P. P., Sharma, M., & Purkait, M. K.: Recent progress on electrocoagulation process for wastewater treatment: A review. Sep. Purif. Technol. **292**, 121058 (2022)
18. Pehlivan, E., Altun, T.: The study of various parameters affecting the ion exchange of Cu^{2+}, Zn^{2+}, Ni^{2+}, Cd^{2+}, and Pb^{2+} from aqueous solution on Dowex 50W synthetic resin. J. Hazard Mater. **134**, 149–156 (2006)
19. Prekob, Á., Hajdu, V., Muránszky, G., Kocserha, I.: Application of carbonized ion exchange resin beads as catalyst support for gas phase hydrogenation processes. React. Kinet. Mech. Catal. (2019)
20. Rengaraj, S., Kim, Y., Joo, C.K., Choi, K., Yi, J.: Batch adsorptive removal of copper ions in aqueous solutions by ion exchange resins: 1200H and IRN97H. Korean J. Chem. Eng. **21**, 187–194 (2004)
21. Samanta, N.S., Das, P.P., Mondal, P., Bora, U., Purkait, M.K.: Physico-chemical and adsorption study of hydrothermally treated zeolite A and FAU-type zeolite X prepared from LD (Linz–Donawitz) slag of the steel industry. Int. J. Environ. Anal. Chem. **00**, 1–23 (2022)
22. Taha, M.H.: Sorption of U(VI), Mn (II), Cu(II), Zn(II), and Cd(II) from multi-component phosphoric acid solutions using MARATHON C resin. Environ. Sci. Pollut. Res. **28**, 12475–12489 (2021)
23. Vergili, I., Gönder, Z.B., Kaya, Y., Gürdağ, G., Çavuş, S.: Sorption of Pb (II) from battery industry wastewater using a weak acid cation exchange resin. Process Saf. Environ. Prot. **107**, 498–507 (2017)
24. Samanta, N. S., Das, P. P., Mondal, P., Changmai, M., & Purkait, M. K.: Critical review on the synthesis and advancement of industrial and biomass waste-based zeolites and their applications in gas adsorption and biomedical studies. J. Indian Chem. Soc. **99**, 100761 (2022)
25. Yurtsever, M., Şengil, I.A.: Biosorption of Pb(II) ions by modified quebracho tannin resin. J. Hazard Mater. **163**, 58–64 (2009)
26. Zawierucha, I., Kozlowska, J., Kozlowski, C., Trochimczuk, A.: Sorption of Pb(II), Cd(II) and Zn(II) performed with the use of carboxyphenylresorcinarene-impregnated Amberlite XAD-4 resin. Desalin Water Treat. **52**, 314–323 (2014)

Investigation of Microalgae Growth in a Mixture of Kraft Paper Industry Effluent and Biogas Slurry: Wastewater Treatment and Biodiesel Production

Isfakur Rasul, Bikram Chakraborty, and Dhanapati Deka

1 Introduction

Around 97.4% of the water on the planet is present in the oceans which are excessively saline and not useful without treatment. The remaining 2% of water locks up in glacial masses or polar ice, where it is inaccessible. Only the excess 0.6% should keep humans and other remaining earthbound life alive [1]. Approximately 1.1 billion people, or one in six people, lack adequate access to clean drinking water. Moreover, approx. 2.6 billion people (two out of six) do not have proper sanitation [2]. The demand for essential goods expanded along with the population growth. To meet the requirement, new industries must be established, which will raise freshwater consumption. Water pollution is primarily caused by rapid industrialization; in developing countries, one-fourth of children under the age of five die from diseases caused by contaminated water. In general, roughly 30,000 individuals every day die from diseases associated with water [3]. Paper and pulp are one of the major industries that use a significant amount of freshwater and also generate a huge amount of polluted water. From the total freshwater supplied to a paper mill, around 75% of it comes as wastewater [4]. The average quantity of wastewater produced by the paper pulp industry is 80 m^3 t^{-1} of paper. The effluents produced by the various phases of the papermaking process contain more than 250 chemical compounds [5]. Based on the generation of hazardous waste, the paper and pulp sector is ranked sixth globally and among India's top 17 most polluting industries [6]. The discharge of effluents from paper mills without treatment may result in several environmental issues, such as water clarity, the solubility of gases in water, rise in harmful chemical components that impact aquatic life, and a reduction in dissolved oxygen due

I. Rasul (✉) · B. Chakraborty · D. Deka
Department of Energy, Tezpur University, Tezpur, Assam, India
e-mail: isfakur.rasul@gmail.com

D. Deka
e-mail: dhanapati@tezu.ernet.in

to eutrophication [7]. Several treatment systems (aerobic, anaerobic, photocatalysis, electrochemical, coagulation–flocculation, and adsorption) have been used to reduce the environmental effects of the effluents, but there is very little information available regarding toxic removal efficiencies. Due to the different manufacturing processes involved in different paper mills (Kraft paper mill, packaging, recycling), it is very difficult to evaluate the pollutant removal efficiency of the effluent treatment system [8].

Algae was once considered a plant, but due to its absence of stems, leaves, roots, and embryos, it is now classified into different groups. Algae are an extremely diverse and fast-growing group of organisms that can be found in almost every ecosystem on the planet, contain chlorophyll, and carry on photosynthesis. Photosynthesis is a biological process that converts carbon dioxide and solar energy into chemical energy and helps lower the atmospheric concentration of greenhouse gases. In addition, these microorganisms necessitate inorganic nitrogen and phosphorus sources as macronutrients. Microalgae in wastewater treatment give a new dimension to the wastewater system; it effectively reduces the effluent's nitrogen and phosphorus levels. Some of the most important advantages of a microalgal-based wastewater treatment system are absorption of nutrients, removal of toxic heavy metals, and increase in dissolved oxygen in water [9]. Due to the high concentration of polysaccharides, lipids, proteins, and other beneficial compounds that are present in microalgal biomass, microalgae are an important resource for a large number of uses, including the production of bioenergy, biofertilizers, and natural colorants and dyes [10, 11]. The main bottlenecks in algae production are large amounts of water and essential nutrients. On the other hand, microalgae can grow in unclean water, including sewage, industrial wastewater, and municipal wastewater. Using wastewater for algae cultivation accomplishes two goals: availability of vital nutrients and avoidance of the use of freshwater [12].

A variety of factors influence algal growth and lipid deposition in algal cells, including the availability of vital nutrients and a few critical physical factors. P^H, light intensity, temperature, CO_2, and biotic factors are that have the greatest effect on growth and lipid productivity [13, 14]. Among the biotic factors, algal density has an impact on algal growth; the higher the density, the greater the density, and the better the growth and nutrient removal capacity [15]. Although, it can have a negative effect by causing self-shading, which reduces the photosynthesis efficiency of microalgae culture [16]. In the production of microalgae, P^H plays a crucial role because it specifies the amount of dissolved CO_2 and the availability of nutrients in the media, as well as has a major effect on microalgal metabolism [17]. Each strain of microalgae species has a different P^H limit in terms of biomass and lipid productivity [18]. Temperature is another crucial physical component that affects the growth of algae, the number of lipids in their cells, and the content of their fatty acid. Different microalgae have different optimum temperatures which vary from species to species [19]. Most microalgae strains can perform photosynthesis and cell division in a temperature range of 15–30 °C, with 20–25 °C being the optimum temperature for mesophilic species [18]. Microalgae species that are thermophilic can grow at temperatures above 40 °C, whereas psychrophilic species can grow at

temperatures as low as 10 °C [20]. Temperature regulation is only possible in a closed photobioreactor, while it is difficult to maintain the temperature in an open system, maintaining optimum temperature is critical for commercially cultured microalgae. Closed system cultivation is the preferred approach for maintaining the optimum temperature for better lipid and biomass productivity [19]. Microalgae growth and biomass productivity are significantly influenced by light's wavelength and intensity. Light is needed for photoautotrophic microalgae to grow because it serves as an energy source for their bioprocessing operation, and microalgae cells typically have a photosynthetic spectrum between 400 and 700 nm [21]. The use of a combination of red (600–700nm) and blue (400–500nm) light will boost biomass productivity in *Chlorella* sp. [22].

The work aimed to investigate the growth of microalgae in wastewater of the Kraft paper industry and biogas slurry and analyzes the physiochemical characteristic of cultured media before and after being treated with microalgae. After treatment of wastewater, lipid and biomass contents were studied further for biodiesel production. The confirmation of produced biodiesel was done by NMR spectroscopy.

2 Materials and Methods

2.1 Collection of Samples

The effluent was collected from Kraft paper industry Brahmaputra Paper Mill located in, Dolabari, Assam (latitude 26.67293, longitude 92.8364), and biogas slurry was obtained from the biogas plant (50 m^3 capacity) located near the Patkai Men's Hostel, Tezpur University (Figs. 1 and 2).

Fig. 1 Kraft paper mill effluent

Fig. 2 Biogas slurry

2.2 Pre-treatment of the Effluent

Before the sample can be cultivated with algae, all heavy particles and debris must be removed. The wastewater was pre-treated in three stages: sedimentation, traditional sand filtration, and Whatman filter paper filtering. Sedimentation is a water treatment procedure that eliminates suspended impurities from the water that sink owing to gravity. The wastewater sample is then filtered via a traditional filter comprised of stones, charcoal, sand, and cloth (Fig. 3). Finally, the sample is filtered using Whatman filter paper (Figs. 4 and 5).

2.3 Media Preparation

Kraft paper mill and biogas slurry were mixed after pre-treatment. Prepare the sample in Erlenmeyer flasks with two replicate each containing 300 ml. Both the samples were mixed as shown in Table 1.

Preparation of BG11 Medium

The BG11 medium contains: $NaNO_3$ (1.5 g/L), $FeCl_3 \cdot 6H_2O$ (3.15 mg/L) and Na_2CO_3 (20 mg/L), $K_2HPO_4 \cdot 3H_2O$ (40 mg/L), $CaCl_2 \cdot 2H_2O$ (36 mg/L), $MgSO_4 \cdot 7H_2O$ (75 mg/L), citric acid (6 mg/L), and 1 mL of microelements solution contains: H_3BO_3 (2.86 mg/L), $CuSO_4.5H_2O$ (0.08 mg/ L), $Na_2MoO_4 \cdot 2H_2O$ (0.39 mg/L), $Co(NO_3)2.6H_2O$ (0.05 mg/L), $ZnSO_4 \cdot 7H_2O$ (0.22 mg/L), $MnCl_2 \cdot 4H_2O$ (1.81 mg/L), $Co(NO_3)_2 \cdot 6H_2O$ (0.05 mg/L), and concentrated H_2SO4 (1 mL).

Characterization of the sample

Physiochemical analysis of the prepared samples was done according to the ASTM method, before and after being treated with algae to analyze the pollutant loads
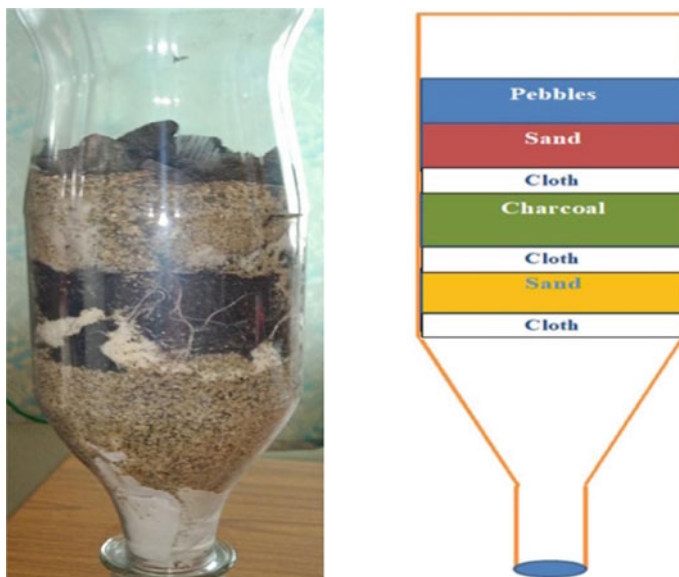
Fig. 3 Conventional filtration process
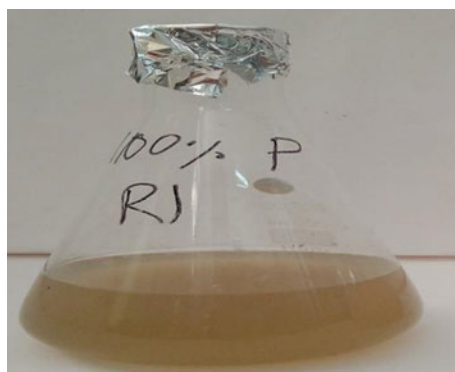
Fig. 4 Kraft paper effluent (after pre-treatment)

in the effluents. Physical parameters were analyzed in NERIWALM, Assam, and metal elements were analyzed in SAIC, Tezpur University. Percentage reduction of chemical parameters in the sample was determined by:

$$\text{Percentage reduction} = (\text{Initial value} - \text{final value})/\text{Initial value} * 100 \quad (1)$$

Fig. 5 Biogas slurry (after
pre-treatment)
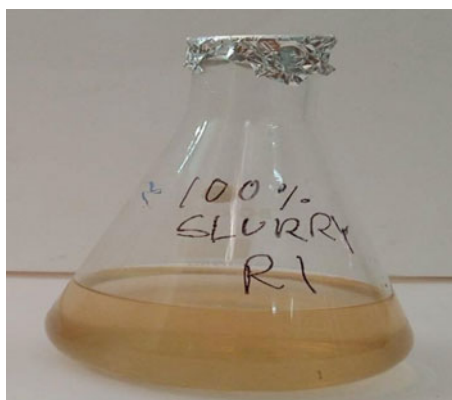
Table 1 Media preparation from Kraft paper mill and biogas slurry

Particular	Sample 1 (20%P)	Sample 2 (40%P)	Sample 3 (60%P)	Sample 4 (80%P)	Sample 5 (1 00%P)	Sample 6 (100%slurry)
Kraft paper effluent quantity (percentage), v/v	20%	40%	60%	80%	100%	0%
Biogas slurry quantity (percentage), v/v	80%	60%	40%	20%	0%	100%

2.4 Microorganism Selection and Growth Condition

Chlorella vulgaris microalgae strain was collected from the Department of Energy, Tezpur University, India. *Chlorella vulgaris* was grown on the prepared media in Biomass Conversion Laboratory, Department of Energy, Tezpur University, India. The culture media was provided with 24 h illumination using fluorescent tube light (14 W; BAJAJ CO, India), and continuous aeration was provided with an air pump. The growth of algae was determined from the initial day of inoculum till it reached the stationary growth phase, by taking optical density in the interval of 24 h at 750 nm using a UV-Vis spectrophotometer (Model: UV 1700, Shimadzu, Japan) (Figs. 6 and 7).

Fig. 6 Microalgae culture
(first day of culture)

Fig. 7 *Chlorella vulgaris*
microscopic image, first day
of culture (40X, RADICAL)
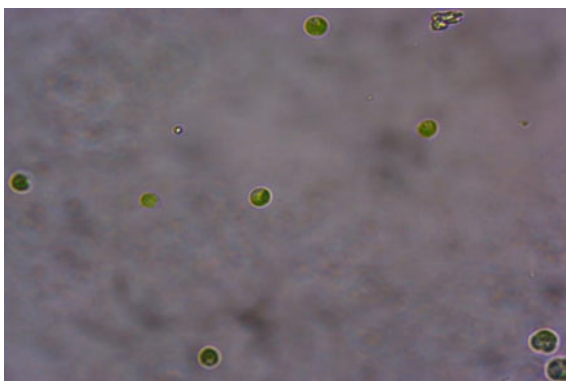
2.5 The Dry Weight of Algal Biomass

Algal biomass was obtained after the stationary growth phase of algae (18 days). To determine the dry weight of algae, 50 ml samples from each replicate were taken, and centrifugation at 5000 rpm for five minutes was used to extract the algal biomass (REMI, C-30BL). The algal biomass remained in the bottom of the centrifuge tube after centrifugation, and the biomass samples were placed in the pre-weighted tube after discarding the liquid component. After drying at 105 °C in an oven, the total dry weight of the algal biomass was calculated (Sartorius CPA225D, Germany). Biomass productivity (mg/l/day) was estimated as follows,

$$\text{Biomass Productivity (mg/L/day)} = (DW_2 - DW_1)/\text{Total no. of days} \qquad (2)$$

where DW_2 and DW_1 represent final dry weight and initial dry weight of algal biomass, respectively.
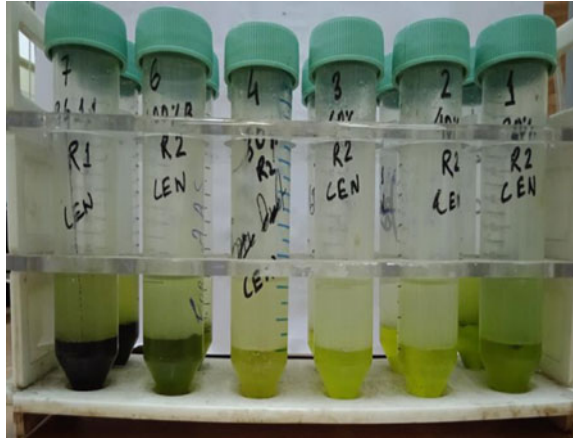
2.6   Lipid Extraction (Lipid Percentage)

The lipid extraction was carried out using a modified Bligh & Dyer method, in which methanol, chloroform, and a weak salt solution were used at a ratio of 2:2:1.8 (v/v). At first, harvested dried algal biomass obtained from the replicates was mixed with methanol and chloroform in the ratio of 2:1, then the samples were put into the shaker for 24 h with continuous shaking. Then, in a 1:1.8 (v/v) ratio, chloroform and a weak salt solution (NaCl 73%) were added. The lipid was deposited in the bottom layer with chloroform, while the topmost layer was made up of methanol and water. Carefully withdraw the bottom with a pipette and place it in pre-weighed glass vials, allowing the solvent to evaporate. Lipid content percentage was calculated as shown below (Figs. 8 and 9):

$$\text{Lipid content}(\%) = \text{Total lipids/Dry biomass} \qquad (3)$$

2.7   Biodiesel Production

Selected media 20%P, 1:4 (v/v), were used for further growth of algae to produce biodiesel, based on the lipid content percentage and growth analysis. The algae were cultured using the selected media in a photobioreactor made of glass. Algae were cultivated in 2 l of that media with 24 h of continuous light and aeration (Fig. 10).

Harvesting of algae

Harvesting was done after 18 days, by flocculation method, and $FeCl_3$ was used as a flocculating agent. After adding the flocculating agent to the completely developed cultured media, stir at a high rpm at first, and then gradually lower the speed. The

Fig. 9 Extracted lipid
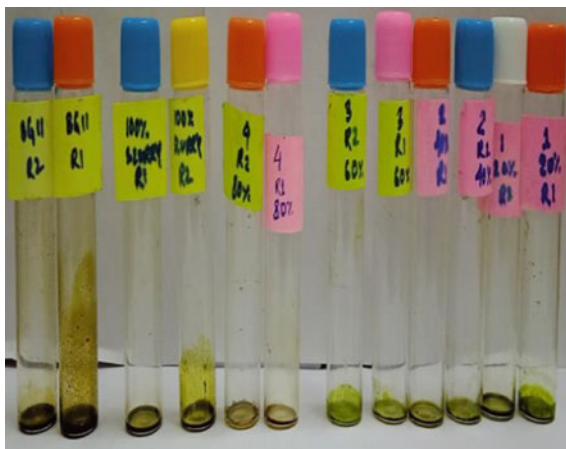
algal biomass settled down to the bottom of the sample after being left undisturbed for 24 h, and dewatering was done to remove the water. The algal biomass was collected and dried in a 105 °C oven (Fig. 11).

Lipid extraction

Lipids were extracted using a modified Bligh & Dyer method. Methanol, chloroform, and a weak salt solution were employed at a ratio of 2:2:1.8 (v/v). Using the Soxhlet apparatus, lipid was extracted from dried algal biomass that was placed in the cellular thimble. Initially, the material was heated at 60 °C for 12 h in a 2:1 (v/v) mixture of methanol and chloroform. The solvent-extracted lipid was removed and mixed at a ratio of 1:1.8 with chloroform and a weak salt solution (NaCl 73% v/v). The mixture was then placed in the separating funnel for 24 h. Three distinct layers were produced, with the lipid accumulating in the lower layer and a small quantity of chloroform being removed, and the solvent is eliminated by evaporation (Figs. 12 and 13).

Fig. 10 Algae culture in 2 l media

Fig. 11 Dry algal biomass

Fig. 12 Lipid extraction process
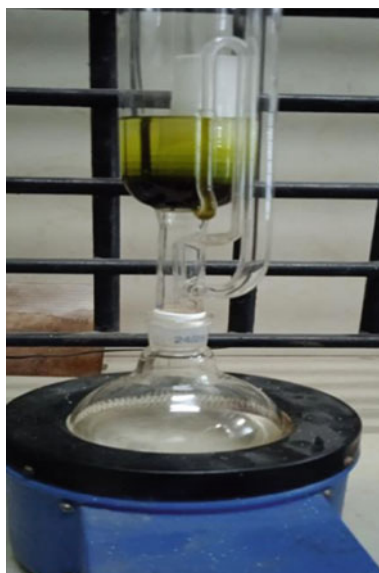
Transesterification

Transesterification was used to convert the extracted lipid to fatty acid methyl ester (FAME), also known as biodiesel (Fig. 14). Methanol and concentrated sulfuric acid (acid catalyst) were utilized in a 6:1 ratio in this process. Methanol and concentrated sulfuric acid were added to the lipid obtained from the algal biomass in a round bottom flask with a magnetic stirrer. The reaction temperature was maintained at 60 °C for 3 h. The sample was allowed to cool to room temperature once the reaction was complete. The mixture was left undisturbed for 24 h, and two layers began to

Fig. 13 Layer formation

form. To confirm biodiesel synthesis and conversion efficiency, FAME was analyzed using $^+$H NMR and ^{13}C NMR spectrometer (Oxford, AS400, China). The following equation was used to estimate the yield of biodiesel [23, 24]:

$$\text{Conversion}(\%) = \frac{2\text{AMe}}{3\text{ACH2}} \times 10 \qquad (4)$$

where

AMe   integration value of the methoxy protons in biodiesel
ACH_2 integration value of α-methylene protons in biodiesel

Fig. 14 Conversion of lipid to biodiesel

3 Results and Discussions

3.1 *Microalgal Growth*

All of the findings in the research are the average of two replicates. The optical density at 750 nm was measured in different culture media and plotted against time to determine the growth of *Chlorella vulgaris*. The greater the value of OD, the more cells were present in the sample, indicating that the algae were growing faster. The result analyzed from the growth curve showed the highest growth in the BG11 (control) media compared with other media. The growth in the industrial effluent and biogas slurry was observed highest in 100% slurry followed by 20%P (1:4), 40%P (2:3), and 60%P (3:2), 80%P (4:1); Kraft paper mill effluent: biogas slurry, v/v. The growth of algae decreases with increase in the quantity of Kraft paper effluent as shown in the figure. The media with 100% Kraft paper effluent are uninhabitable for algal growth as it has very less amount of available nitrogen present that is essential for algal growth; also, the formation of flakes in media hampers the growth (Fig. 15).
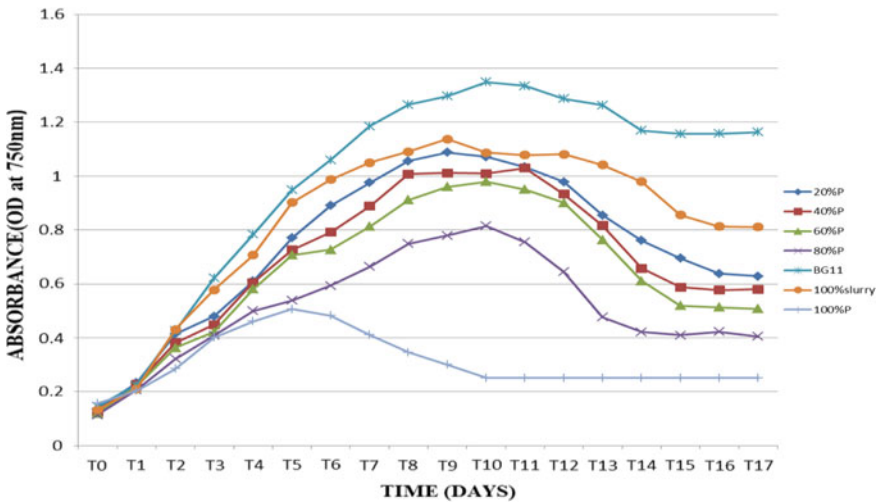
Fig. 15 Growth curve of *Chlorella vulgaris* in different culture media

Table 2 Physical parameter analysis of Kraft paper mill effluent and biogas slurry

Sample	pH	EC (mS)	DO (ppm)	TDS (ppt)	Turbidity (NTU)	Salinity (ppt)
Kraft paper mill effluent	8.94	16.2	1.5	8.86	510	8.93
Biogas slurry	6.53	6.16	3.3	340	23	3.31

3.2 Physical Parameters of the Prepared Samples (After and Before Being Treated with Algae)

According to the measurement of physical parameters, samples treated with algae had an excellent result in terms of removing pollutant loads. An increase in dissolved oxygen is a favorable indication of an algae-based wastewater treatment system. The bar graph shows that microalgae are capable of successfully removing pollutant load from the prepared media of Kraft paper effluent and biogas slurry (Fig. 16; Tables 3 and 4).
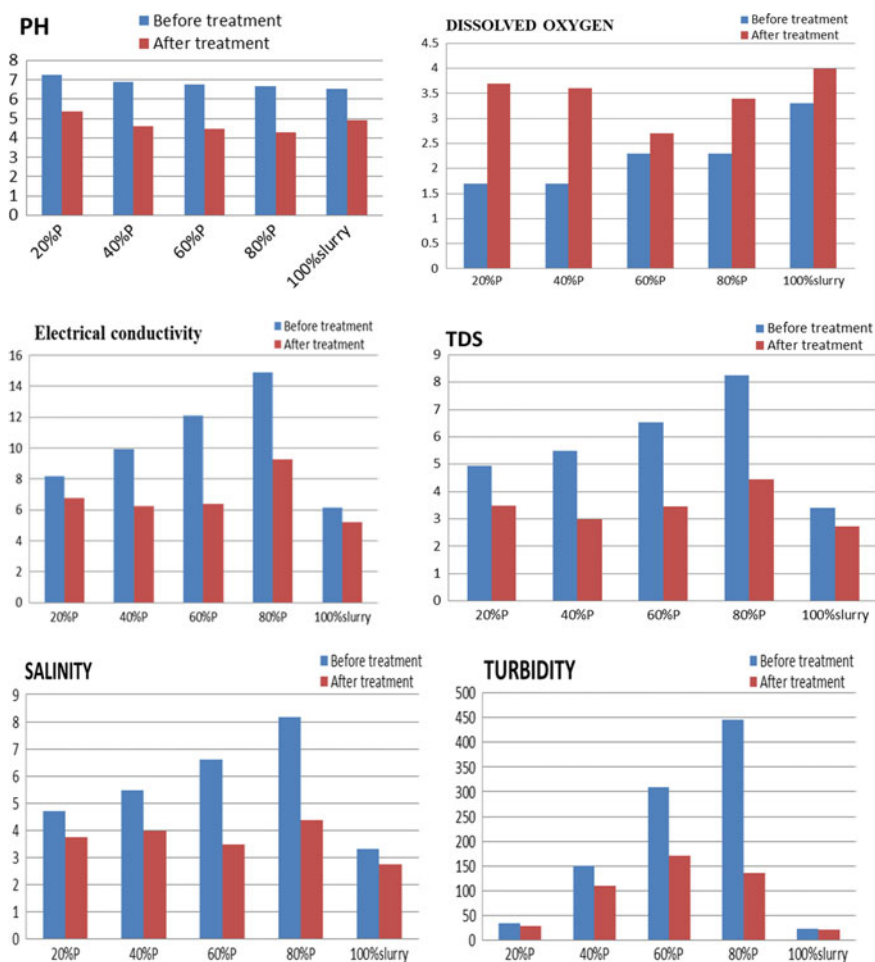
Fig. 16 Comparison of physical parameters (before and after treatment with algae)

Table 3 Before treatment physical parameters

Sample	pH	EC (mS)	DO (ppm)	TDS (ppt)	Turbidity (NTU)	Salinity (ppt)
20%P	7.24	8.17	1.7	4.94	33	4.72
40%P	6.89	9.90	1.7	5.50	150	5.49
60%P	6.76	12.1	2.3	6.53	310	6.62
80%P	6.65	14.9	2.3	8.26	445	8.17
100% slurry	6.53	6.16	3.3	3.40	23	3.31

Table 4 After treatment physical parameters

Sample	pH	EC (mS)	DO (ppm)	TDS (ppt)	Turbidity (NTU)	Salinity (ppt)
20%P	5.35	6.75	3.7	3.48	28.5	3.74
40%P	4.54	6.22	3.6	2.99	110	3.97
60%P	4.37	6.36	2.7	3.45	170	3.49
80%P	4.1	8.26	3.4	4.46	135	4.38
100% slurry	5.37	5.19	4.0	2.72	20.5	2.74

3.3 Chemical Parameter of Kraft Paper Mill Effluent and Biogas Slurry

A significant reduction of the chemical parameter is observed from the analysis of the sample treated with algae. Recovery of the chemical from the water sample was observed in all the prepared media. Nitrogen reduction is analyzed and found to be higher in 20%P (1:4, v/v) and biogas slurry as it is an essential element for the growth of algae. From the analysis of chemical parameters, it was observed that with an increase in growth, the reduction efficiency of pollution load has also increased. All of the parameters in the wastewater sample have been decreased to the effluent discharge threshold limit after being treated with algae (Fig. 17; Tables 5, 6 and 7).

3.4 Biomass and Lipid Production

After the stationary phase of algal growth, biomass was extracted from various cultured media. When comparing different growth media, the dry weight of algal biomass was found to be highest in BG11 (control) media. Between Kraft paper mill effluent and biogas slurry, 100% slurry yields the highest dry biomass production, followed by 20% P, 1:4 (v/v).

Lipid production from the dried algal biomass was carried out and found to be the highest in BG11 media. Lipid content percentage is found higher in 20%P, 1:4 (v/v) as compared with other culture media. Although 100% slurry has a higher biomass yield, the lipid percentage is found less than 20%P, 1:4 (v/v), and higher
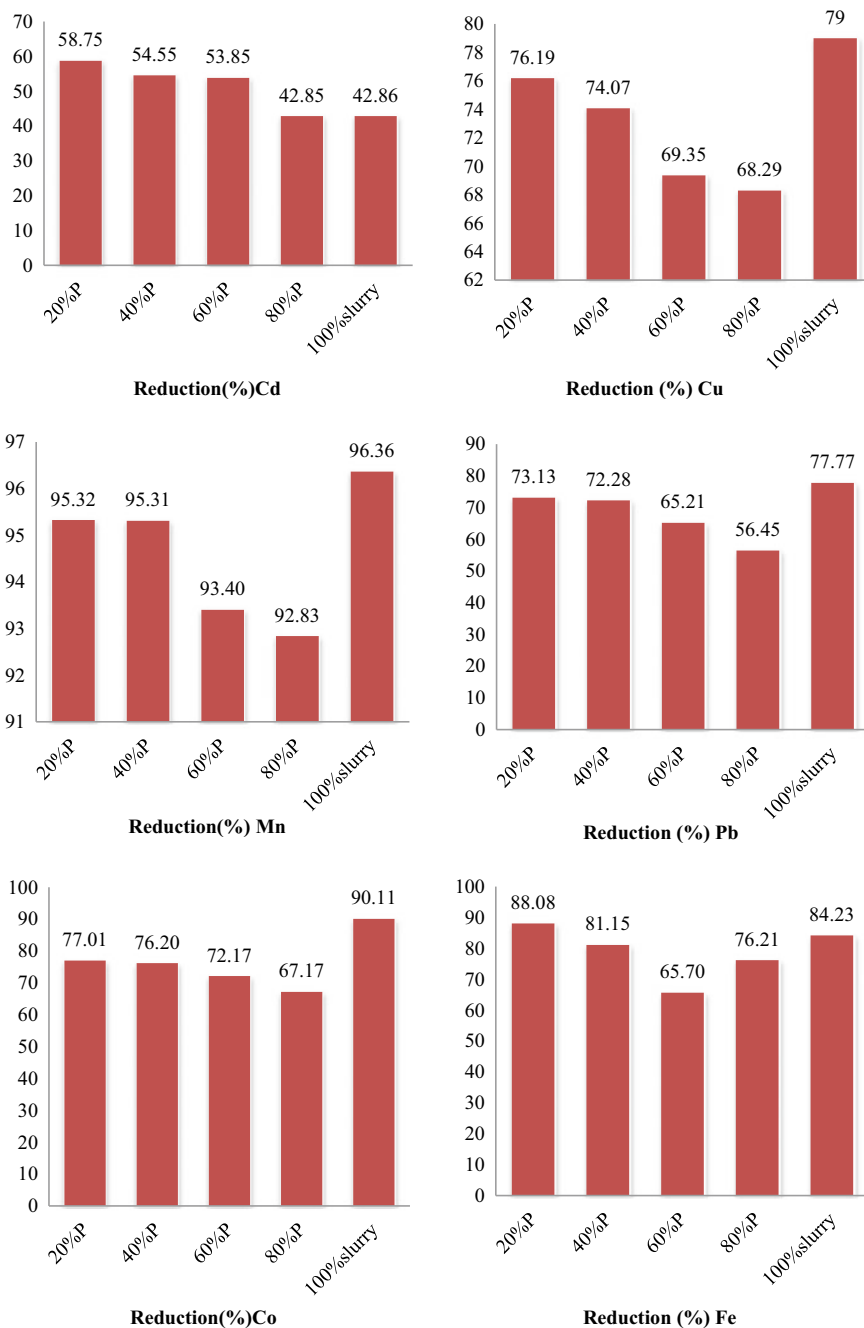
Fig. 17 Reduction (%) of chemical parameters after being treated with algae

Reduction (%) Total Nitrogen
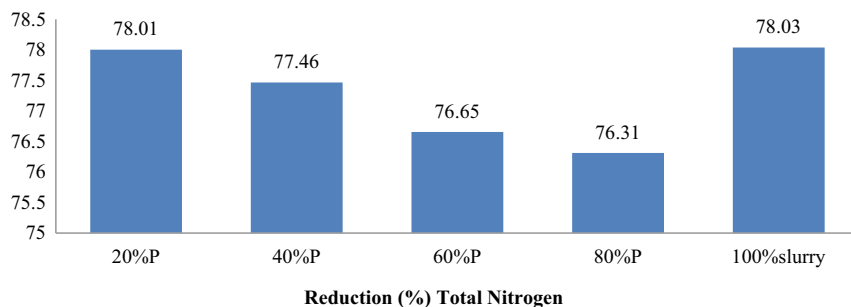
Fig. 17 (continued)

Table 5 Physicochemical characterization of Kraft paper mill effluent and biogas slurry

Sample	Cu (mg/L)	Fe (mg/L)	Cd (mg/L)	Mn (mg/L)	Pb (mg/L)	Co (mg/L)	Total nitrogen (mg/L)
Kraft paper mill effluent	0.042	0.586	0.016	0.554	0.146	0.185	7.96
Biogas slurry	0.01	0.222	0.014	0.011	0.009	0.09	144.8

Table 6 Parameters before treated with algae

Sample	Cu (mg/L)	Fe (mg/L)	Cd (mg/L)	Mn (mg/L)	Pb (mg/L)	Co (mg/L)	Total nitrogen (mg/L)
20%P	0.021	0.361	0.008	0.107	0.067	0.097	117.432
40%P	0.027	0.382	0.011	0.209	0.083	0.108	91.056
60%P	0.031	0.414	0.013	0.288	0.092	0.138	63.696
80%P	0.041	0.492	0.014	0.405	0.124	0.156	34.328
100%slurry	0.01	0.222	0.014	0.011	0.009	0.09	144.8

Table 7 Parameters after treatment with algae

Sample	Cu (mg/L)	Fe (mg/L)	Cd (mg/L)	Mn (mg/L)	Pb (mg/L)	Co (mg/L)	Total nitrogen (mg/L)
20%P	0.005	0.043	0.004	0.005	0.018	0.0223	25.832
40%P	0.007	0.072	0.005	0.0098	0.023	0.0247	20.518
60%P	0.0095	0.142	0.006	0.019	0.032	0.0274	14.87
80%P	0.013	0.117	0.008	0.029	0.054	0.0302	8.132
100%slurry	0.0021	0.035	0.008	0.0004	0002	0.0089	31.8
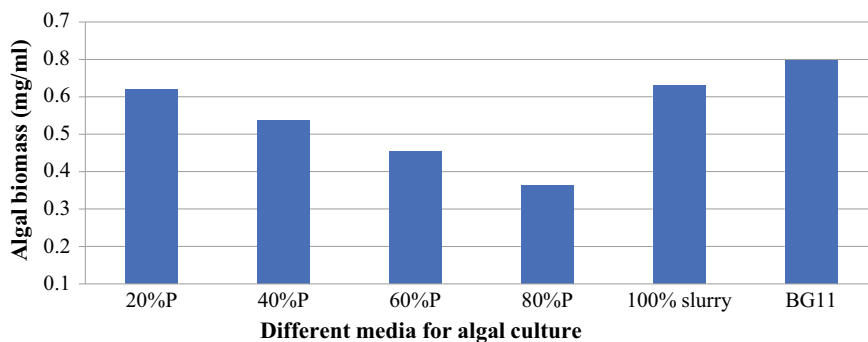
Fig. 18 Dried algal biomass

lipid accumulated might be due to a lack of nitrogen present in the media. The lipid content of algal cells is crucial for producing biodiesel economically (Figs. 18 and 19; Tables 8 and 9).
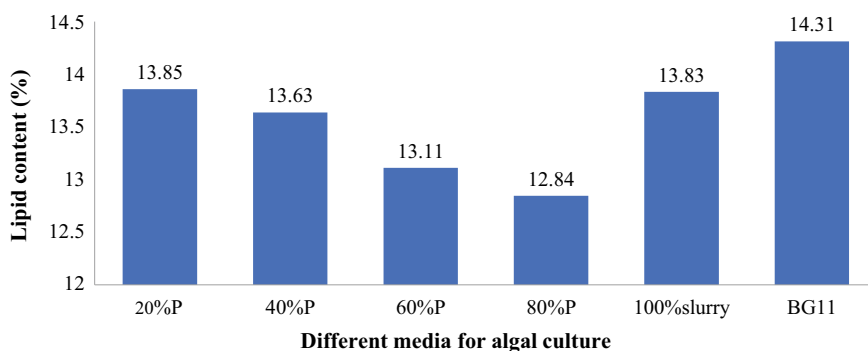
Fig. 19 Comparison of lipid content (%)

Table 8 Dried algal biomass

Sample	Dry weight (mg/mL)	Biomass productivity (mg/L/day)
20%P	0.52	36.82
40%P	0.44	30.87
60%P	0.35	24.92
80%P	0.26	18.41
100% slurry	0.53	37.53
BG11	0.59	42.38

Table 9 Lipid productivity

Sample	Lipid (mg/mL)	Lipid content (%) w/w
20%P	0.072	13.85
40%P	0.059	13.63
60%P	0.046	13.11
80%P	0.040	12.84
100% slurry	0.074	13.83
BG11	0.086	14.31

3.5 Biodiesel Analysis—NMR Spectroscopy

Biodiesel produced from the algal lipid by transesterification reaction. In this process triglyceride was converted to fatty acid methyl ester (FAME). Researchers utilize ^{1}HNMR spectroscopy to investigate biodiesel synthesis by transesterification reactions and to estimate the conversion efficiency of lipid to methyl esters. Hence, extracted methyl ester (biodiesel) from algal lipid was examined using ^{1}HNMR to confirm that the algal lipid is converted to methyl esters. From Fig. 20, a singlet peak at 3.62 ppm verifies the presence of the methoxy group, and an intense significant peak at 2.26 ppm, which pertains to the α-carbonyl methylene group, proves the presence of the methyl ester in the biodiesel sample. These relevant signals (3.62 and 2.26 ppm) in the methoxy group and α-carbonyl methylene group were chosen for integration to quantify the conversion efficiency. The lipid to methyl ester conversion percentage was calculated and determined to be 83.24%. The ^{13}CNMR spectrum of the produced biodiesel from algal lipid is shown in Fig. 21. The signal at 48.21 ppm in the spectrum indicates the formation of methyl ester. The signals ranging from 13.05 to 33.36 ppm indicate the presence of methylene and methyl carbons, respectively.

4 Conclusion

Global energy demand and environmental concerns are at an all-time high. Algae are one of the most promising options for simultaneously addressing both challenges. The main bottleneck of the cultivation of algae is the requirement for a huge amount of water and essential nutrients for growth. Wastewater treatment combined with algae growing achieves a dual goal of nutrient removal and biofuel production. But all type of wastewater is not suitable for the cultivation of algae. This study shows how the mixing of different wastewater from Kraft paper mill effluent and biogas slurry makes it habitable for algal growth. Effluent from Kraft paper is loaded with toxic chemicals and very limited amount of nitrogen which inhibits algal growth. Mixing biogas slurry achieves two goals. The slurry is an excellent supply of nitrogen, and it eliminates the need for freshwater to dilute extremely polluted water, making it ideal for algal growth. From the study, growth of *Chlorella vulgaris* was found to be the
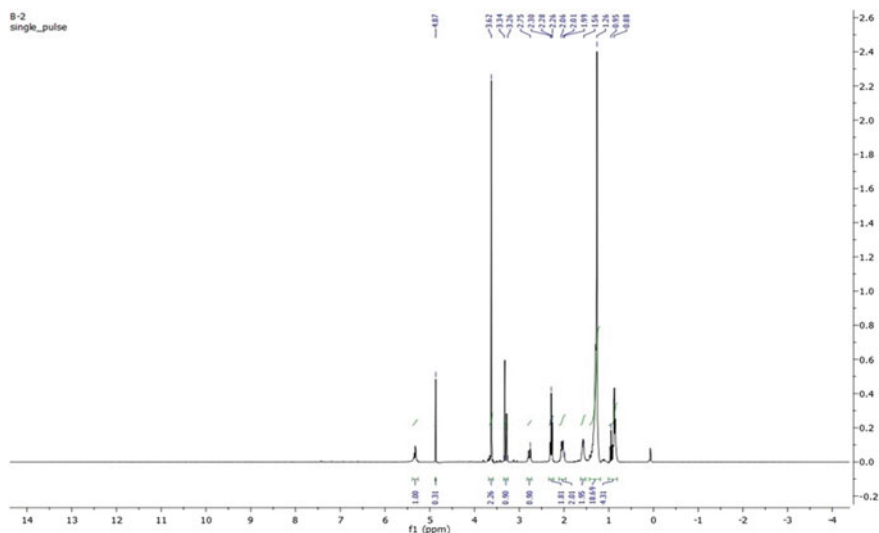
Fig. 20 ^{1}HNMR spectrum of produced biodiesel from *Chlorella vulgaris* algae lipid
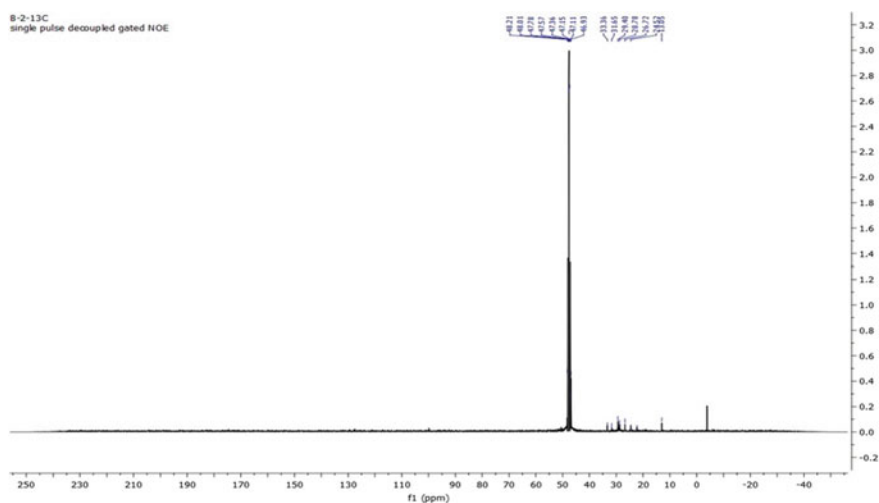
Fig. 21 ^{13}C NMR spectrum of produced biodiesel from *Chlorella vulgaris* algae lipid

highest with 100% slurry, and in the mixer of paper mill effluent and biogas slurry, maximum growth was obtained with 20%P (Kraft paper effluent: biogas slurry, 1:4). The decreasing trend in growth was observed with an increase in Kraft paper mill effluent quantity. Biomass productivity was found higher in the slurry media with 37.53 mg/L/day followed by 36.82 mg/L/day in 20%P. Lipid content was determined higher in 20%P media with 13.85% (w/w) than in slurry media with 13.83 % (w/w).

When comparing the growth curve to the pollution load, it was discovered that as growth increased, the polluting load dropped. The percentage reductions of heavy metals Cd, Cu, Mn, Pb, Co, and Fe from the 20% P (1:4, v/v) media were determined to be 58.75%, 76.19%, 95.32 %, 73.13%, 77.01%, and 88.08%, respectively. Above 75% reduction of total nitrogen was observed from all cultured media.

Finally, biodiesel was made by transesterification of lipid extracted from algal biomass grown on a medium with the maximum lipid content. The biodiesel sample was analyzed using NMR spectroscopy, and the conversion yield was determined and found to be 83.24%.

According to the findings, biogas slurry is a good substrate for *Chlorella vulgaris* cultivation and can be used with biogas production. The ideal mixing ratio for optimal growth, biomass production, and lipid content was determined to be 20%P.

References

1. Raskin, P., Gleick, P.H., Kirshen, P., Pontius, R.G., Jr., Strzepek, K.: Comprehensive Assessment of the Freshwater Resources of the World, 1st edn. Stockholm Environmental Institute, Sweden (1997)
2. Das, P. P., Sharma, M., & Purkait, M. K.: Recent progress on electrocoagulation process for wastewater treatment: A review. Sep. Purif. Technol., **292**, 121058 (2022)
3. Peavy, H.S., Rowe, D.R., Tchobanoglous, G.: Environmental Engineering, 1st edn. McGraw-Hill Book Company, New York (1985)
4. Virendra, K., Purnima, D., Sanjay, N., Anil, K., Rita, K.: Biological approach for the treatment of pulp and paper industry effluent in sequence batch reactor. J. Bioremediat Biodegradation **5**(3) (2014)
5. Bautista, P., Mohedano, A.F., Casas, J.A., Zazo, J.A., Rodriguez, J.J.: An overview of the application of Fenton oxidation to industrial wastewaters treatment. J. Chem. Technol. Biotechnol.: Int. Res. Process Environ. Clean Technol. **83**(10), 1323–1338 (2008)
6. Sonkar, M., Kumar, M., Dutt, D., Kumar, V.: Treatment of pulp and paper mill effluent by a novel bacterium Bacillus sp. IITRDVM-5 through a sequential batch process. Biocatal. Agric. Biotechnol. **20**, 101232 (2019)
7. Reid, N.M., Bowers, T.H., Lloyd-Jones, G.: Bacterial community composition of a wastewater treatment system reliant on N_2 fixation. Appl. Microbiol. Biotechnol. **79**(2), 285–292 (2008)
8. Das, P. P., Mondal, P., Sinha, A., Biswas, P., Sarkar, S., & Purkait, M. K.: Integrated ozonation assisted electrocoagulation process for the removal of cyanide from steel industry wastewater. Chemosphere, **263**, 128370 (2021).
9. Rawat, I., Kumar, R.R., Mutanda, T., Bux, F.: Dual role of microalgae: phycoremediation of domestic wastewater and biomass production for sustainable biofuels production. Appl. Energy **88**(10), 3411–3424 (2011)
10. Samanta, N. S., Das, P. P., Mondal, P., Changmai, M., & Purkait, M. K.: Critical review on the synthesis and advancement of industrial and biomass waste-based zeolites and their applications in gas adsorption and biomedical studies. J. Indian Chem. Soc. **99**, 100761 (2022)

11. Das, P. P., Mondal, P., Sinha, A., Biswas, P., Sarkar, S., & Purkait, M. K.: Treatment of steel plant generated biological oxidation treated (BOT) wastewater by hybrid process. Sep. Purif. Technol. **258**, 118013 (2021)
12. Sharma, M., Das, P. P., Sood, T., Chakraborty, A., & Purkait, M. K.: Ameliorated polyvinylidene fluoride based proton exchange membrane impregnated with graphene oxide, and cellulose acetate obtained from sugarcane bagasse for application in microbial fuel cell. J. Environ. Chem. Eng. **9**, 106681 (2021)
13. Samanta, N. S., Das, P. P., Mondal, P., Bora, U., & Purkait, M. K.: Physico-chemical and adsorption study of hydrothermally treated zeolite A and FAU-type zeolite X prepared from LD (Linz–Donawitz) slag of the steel industry. J. Environ. Anal. Chem. **13**, 1–23 (2022)
14. Das, P. P., & Purkait, M. K.: Treatment of cold rolling mill (CRM) effluent of steel industry. Sep. Purif. Technol. **274**, 119083 (2021)
15. Lau, P.S., Tam, N.F.Y., Wong, Y.S.: Effect of algal density on nutrient removal from primary settled wastewater. Environ. Pollut. **89**(1), 59–66 (1995)
16. Darley, W.M.: Algal biology: a physiological approach. Basic Microbiol. **9**, 30–52 (1982)
17. Chen, C.Y., Durbin, E.G.: Effects of pH on the growth and carbon uptake of marine phytoplankton. Mar. Ecol.-Prog. Ser. **109**, 83–83 (1994)
18. Haldar, D., & Purkait, M. K.: A review on the environment-friendly emerging techniques for pretreatment of lignocellulosic biomass: Mechanistic insight and advancements. Chemosphere, **264**, 128523 (2021)
19. Haldar, D., & Purkait, M. K.: Micro and nanocrystalline cellulose derivatives of lignocellulosic biomass: A review on synthesis, applications and advancements. Carbohydr. Polym. **250**, 116937 (2020)
20. Li, W.K.: Temperature adaptation in phytoplankton: cellular and photosynthetic characteristics. Primary Prod. Sea, 259–279 (1980)
21. Varshney, P., Mikulic, P., Vonshak, A., Beardall, J., Wangikar, P.P.: Extremophilic micro-algae and their potential contribution in biotechnology. Biores. Technol. **184**, 363–372 (2015)
22. Haldar, D., & Purkait, M. K.: Thermochemical pretreatment enhanced bioconversion of elephant grass (Pennisetum purpureum): insight on the production of sugars and lignin. Biomass Convers. Biorefin. **12**, 1–14 (2020)
23. Knothe, G.: Monitoring a progressing transesterification reaction by fiber-optic near infrared spectroscopy with correlation to 1H nuclear magnetic resonance spectroscopy. J. Am. Oil. Chem. Soc. **77**(5), 489–493 (2000)
24. Basumatary, S., Barua, P., Deka, D.C.: Identification of chemical composition of biodiesel from Tabernaemontana divaricata seed oil. J. Chem. Pharm. Res **5**(1), 172–179 (2013)

Pharmaceutically Active Compounds' (PhACs) Threat: An Environmental Prospective

Ravi Ravi and Animes Kumar Golder

1 Introduction

In the last few decades, the production and consumption of pharmaceuticals extensively increased due to huge population growth. Pharmaceuticals, one of humans' greatest development, have a great impact on humans and other organisms, i.e., increased life span, treatment of severe diseases, improved health quality, and healthy livestock animals. Recent knocking of Covid-19, swine flu and bird flu outbreaks increased the use of pharmaceutically active compounds (PhACs) in humans and livestock animals. According to the *Center for Disease Dynamics, Economics & policy's* report, over 1.3 lakh tons of antibiotics are used annually in animal feed. China is reported as the highest consumer of antibiotics, whereas India stands in the fourth position in the highest use of antibiotics after the USA and Brazil [1].

Consequently, the generation of PhACs containing wastewater has increased. Now, PhACs are exposed in all tested waterbodies. Emerging contaminants, especially PhACs, receive high attention from researchers and the government due to their hazardous behavior in the environment. Unfortunately, the lack of appropriate data on contaminants in industrial effluents, hospital waste, household waste, animal excretion, and agriculture runoff is a major concern for scientists, which hamper the modeling and management of the treatment plants. Additionally, the lack of eco-toxicity studies and the long-lasting effects of persistent PhACs on

R. Ravi · A. K. Golder (✉)
Centre for the Environment, Indian Institute of Technology Guwahati, Guwahati, Assam 781039, India
e-mail: animes@iitg.ac.in

R. Ravi
e-mail: r.vashist@iitg.ac.in

A. K. Golder
Department of Chemical Engineering, Indian Institute of Technology Guwahati, Guwahati, Assam 781039, India

microbes and animals augment the need for the PhACs treatment system. PhACs waste has long-lasting and life-threatening consequences due to PhACs (lower than their minimum inhibitory concentration) being most likely to develop antimicrobial resistance microbes and several diseases [2].

PhACs industry effluent, healthcare centers, household waste, and animal excretions are familiar sources of PhACs in aquatic bodies. Expansion of the antibiotic resistance microbes, i.e., bacteria, and fungi, is a major concern that can give rise to some lethal microbes, and we will be a victim/witnesses of even more severe pandemics in upcoming years [3]. Contamination of PhACs and their diverse effects on organisms and water treatment plants have been reported in various studies. Although, the presence of the PhACs in domestic discharge has not been explored well. Various conventional treatment methods have been used for the treatment of the PhACs containing wastewater with their own pros and cons. Inhibition of microbial growth by PhACs obstructs the efficiency of the biological treatment process [4]. The indulged PhACs contamination must be highlighted globally, and its drastic effects on the environment must be investigated for appropriate rectification. Based on addressed discretions, this review focused on the framework of the reign of PhACs on waterbodies at the local and global scale to state the direction of future research overcoming the PhACs threat. Hence, the following themes are discussed:

- Overview of the PhACs and potential sources
- Sweeping of PhACs in the environment: Indian and Global scale distribution of PhACs contaminated water bodies and treatment plants.
- Drastic effects of PhACs on the environment, i.e., Humans, aquatic organisms, microbes, and water treatment plants.
- Review of various PhACs waste treatment methods.

2 Pharmaceutically Active Compounds (PhACs)

Earlier, plant extract-based pharmaceutical compounds have been used for medical practice since ancient time. Until the mid-nineteenth century, only natural pharmaceuticals were used for treatment, but the discovery of chloral hydrate, a first synthetic drug, in 1869, introduced a gateway for new synthetic drugs [5]. Nevertheless, the discovery of the penicillin by Alexander Fleming in 1928 revolute the pharmaceutical industries [6]. After that, synthetic pharmaceuticals are continuously produced with paced industrialization to compensate for the fast-growing population. An increase in the demand for disease-free livestock animals for food further enhanced the production of antibiotics, which ultimately trigger the production of the PhACs containing effluents. Flow through of PhACs in environment via various sources is illustrated in the Fig. 1. PhACs are the group of biologically active compounds which possess pharmaceuticals, namely, antibiotics, analgesics, tranquillizers, diuretics, hormones, etc. [7]. Some mainly used pharmaceutically active compounds and their chemical structure are tabulated in Table 1. PhACs have toxicological impacts on all types of organisms. Among all PhACs, the persistent amount of antibiotics in waterbodies is a major
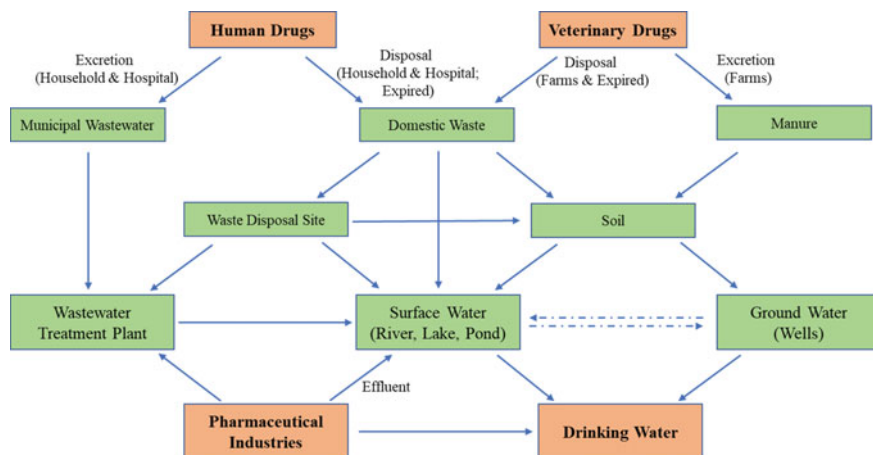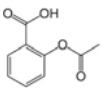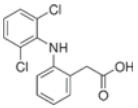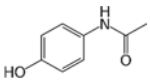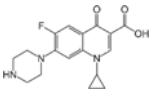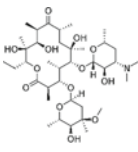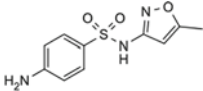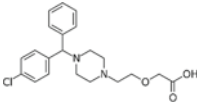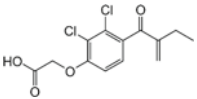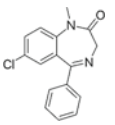
Fig. 1 Flow through of PhACs in the environment via various sources

concern due to development of the antimicrobial resistant microbes, i.e., bacteria and fungi [8]. Moreover, the impact of PhACs on human and aquatic animals is also alarming, affecting their health. Appropriate monitoring of the PhACs in the water bodies, i.e., lakes, rivers, estuarine, drainage, domestic water storage sites, drinking water reservoirs, and groundwater, must be accomplished to model the treatment process and enlighten the direction of the research. Herein, PhACs contamination in waterbodies at local and global scale is highlighted in further section.

2.1 PhACs: Indian Prospective

The pharmaceutical sector of India is expanding quickly to fulfill the demand of the second largest population in the world. According to IBEF, in terms of the pharmaceutical industry market, India is the third-largest in volume and the 14th largest by value. The Indian pharmacy network is expanded with more than 3K pharmaceutical companies established with more than 10K manufacturing units (https://www.ibef.org/industry/pharmaceutical-india). Massive production of pharmaceuticals and inappropriate treatment, monitoring and management system resulted in the disposal of the PhACs waste in the environment. Several case studies have been executed to detect the contamination of the water bodies, especially rivers and water bodies near the pharmaceutical industries. Hyderabad is the primary hub of pharmaceutical industries in India, and several case studies have been reported to highlight the PhACs contamination in drinking water (wells water), lakes and industrial effluents. Fick et al. (2010) collected the samples from 6 villages (wells), two lakes and industrial effluent to investigate the presence of PhACs by LC–MS analysis [9]. Several PhACs were detected in all the samples where the concentration of ciprofloxacin

Table 1 List of commonly used PhACs with their molecular weight and chemical structure

Category	Compound	Molecular weight (g/mol)	Chemical structure
Analgesic	Aspirin	180.158	
	Diclofenac	296.148	
	Paracetamol	151.163	
Antibiotics	Ciprofloxacin	331.346	
	Erythromycin	733.930	
	Sulfamethoxazole	235.279	
Antihistamine	Cetirizine	388.890	
Diuretics	Ethacrynic acid	303.138	
Tranquilizer	Diazepam	284.700	

(CIP) antibiotic was found to be highest in industrial effluents and lake samples at 14,000 and 6500 μg L^{-1}, respectively.

Vimalkumar et al. (2018) detected the antimicrobial ingredients, triclocarban and benzotriazole, in south India's Kaveri, Vellar, and Thamiraparani rivers. Among all rivers, Kaveri was highly contaminated with triclocarban, while Thamiraparani is reported as highly contaminated with benzotriazole [10]. Renganathan et al. (2021) investigated the presence of heavy metals and PhACs in the Cauvery river and its tributaries. The obtained result confirmed the highest concentration of carbamazepine (3330.7 ng L^{-1}), followed by caffeine (435.3 ng L^{-1}), and diclofenac (293.2 ng L^{-1}) [11]. In another study, Subedi et al. (2017) detected the presence of various PhACs in the influents and effluents of the sewage treatment plants (STPs) in Udupi and Mangalore [12]. The reported studies concluded that escaping the treatment process by most of the PhACs in both the STPs due to improper treatment, indicating the requirement for an improved treatment process. All the observed PhACs contaminants in several water bodies are reported in Table 2.

Nevertheless, the reviewed studies are not summarizing the whole scenario of the PhACs in India. Detection and monitoring of the PhACs contamination at a small scale, i.e., ponds in villages and small towns, are still lacking. Government and other relevant agencies should come forward to quantify the PhACs contamination at each scale to overcome its hazardous impacts.

2.2 PhACs: Global Prospective

The global pharmaceutical market has shown tremendous growth in the last few decades, where the USA, China, and India are the highest contributors. The global situation of the PhACs contamination is somewhat similar to Indian scenarios, especially in developed and developing nations. Several investigations have been performed worldwide to quantify the PhACs contamination in the rivers, marshlands, wastewater treatment plants, estuary, hospitals, and domestic effluents. Verlicchi et al. (2012) reported 9 and 5 out of 73 PhACs above the critical concentration in the hospital and WWTPs effluent, respectively [13]. In another study, Vazquez-Roig et al. (2012) reported the presence of the 17 PhACs in different sample types from Pego–Oliva Marshlands. The persistent concentrations of the PhACs in the sediment and soil samples were lower than PhACs in the water [14]. As per the council of Canadians report, approx. 3/4th of water resources crossed the critical contamination concertation and are at high risk. Most of the Canadian population relies on treated wastewater for domestic use, but the inappropriate functioning of WWTPs is a major concern. Guerra et al. (2014) reported the presence of the 62 PhACs in the influent and effluent of 5 different WWTPs in Canada. On average, the concentration of PhACs in the effluents of WWTPs is higher than the critical concentration, granting the removal efficiency is ~90% [15]. Hossain et al. (2018) concluded the detection of the 9 PhACs in the old Brahmaputra river, although the pharmaceutical industries of Bangladesh are not much developed [16]. Hanamoto et al. (2018) monitored 55

Table 2 Level of various PhACs in different types of samples collected from several contaminated waterbodies in India

Source	Type of sample	PhACs	Concentration (ng L^{-1})	Reference
Patancheru Enviro Tech Ltd., Hyderabad (pharmaceutical industries effluent treatment plant)	Pharmaceutical industries effluent	Cetirizine	2,100,000	[9]
		Ciprofloxacin	14,000,000	
		Citalopram	430,000	
		Enrofloxacin	210,000	
		Ofloxacin	55,000	
		Norfloxacin	25,000	
Lakes (near pharmaceutical industries in Hyderabad)	Water	Cetirizine	5000–1,200,000	
		Ciprofloxacin	ND–6,500,000	
		Citalopram	2000–8000	
		Enrofloxacin	ND–25,000	
		Ofloxacin	ND–11,000	
		Norfloxacin	60,000–200,000	
Wells (near pharmaceutical industries in Hyderabad)	Water	Cetirizine	900–28,000	
		Ciprofloxacin	40–14,000	
		Citalopram	ND–1400	
		Enrofloxacin	ND–70	
		Ofloxacin	ND–480	
		Norfloxacin	ND–31	
Kaveri (Cauvery)	Water	Triclocarban	8–1119	[10]
	Sediment		ND–26.3	
	Water	Benzotriazole	ND–29.3	
	Sediment		ND–6.59	
Vellar	Water	Triclocarban	2.2–103	
	Sediment		ND–4.3	
	Water	Benzotriazole	ND–15.9	
	Sediment		ND–7.3	
Thamiraparani	Water	Triclocarban	3.3–168	
	Sediment		ND–9.2	
	Water	Benzotriazole	ND–31.3	
	Sediment		ND–4.6	
Cauvery and its tributaries	Water	Perindopril	ND–46.1	[11]
		Atenolol	ND–84.8	
		Caffeine	20.8–435.3	
		Carbamazepine	27.4–3330.7	
		Diclofenac	4.6–293.2	

(continued)

Table 2 (continued)

Source	Type of sample	PhACs	Concentration (ng L^{-1})	Reference
		Ibuprofen	ND–76.2	
		Triclosan	ND–46.6	
		Ciprofloxacin	ND–87.4	
Sewage treatment plants, Udupi	Influent	Sulfamethoxazole	55–690	[12]
	Effluent		120–420	
	Influent	Mefenamic acid	ND-2800	
	Effluent		320–750	
	Influent	Acetaminophen	5400–11,000	
	Effluent		330–1200	
Sewage treatment plants, Udupi	Influent	Sulfamethoxazole	ND–170	
	Effluent		ND–25	
	Influent	Mefenamic acid	490–3800	
	Effluent		250–750	
	Influent	Acetaminophen	2900–7500	
	Effluent		ND–490	

*ND = Not detected

PhACs in 4 different rivers and 3 STPs in the Yodo river watershed [17]. Ma et al. (2017) studied the spatiotemporal distribution of the 33 PhACs in the Beiyun river and its tributaries. After 2013, 37 and 30% decrease in the level of some PhACs and caffeine, respectively, indicating the improvement in the water quality of the Beiyun river. Although, concentration of various PhACs were higher than the critical concentration [18]. As per the review, as mentioned earlier, the majorly present PhACs contaminants in aquatic bodies are tabulated in Table 3. Conclusively, PhACs contamination in water bodies is worldwide spread. Conventional WWTPs and STPs are not efficient enough to degrade the PhACs, which results in the presence of PhACs in the effluents of the WWTPs.

3 Upshots of PhACs on Environment

The exposure of PhACs to non-target organisms is a major concern due to their ecotoxic impacts. Compared to terrestrial organisms, aquatic organisms, and microbes are at high risk due to contaminated water bodies. That is why contemporary investigations focus more on risk assessment and the impact of PhACs on aquatic organisms and microbes. Globally, hundreds of PhACs have been detected in water bodies, soil, and WWTPs. The exposure of surface water, especially rivers, is polluted with a high concentration of PhACs, which raised severe concerns among

Table 3 Level of various PhACs in different types of samples collected from several contaminated waterbodies worldwide

Source and country	Type of sample	PhACs	Concentration (ng L^{-1})	Reference
Hospital, North Italy	Hospital effluent	Naproxen	340–11,000	[13]
		Ciprofloxacin	1400–26,000	
		Ofloxacin	3300–37,000	
		Sulfamethoxazole	900–6500	
		Furosemide	5300–18,000	
WWTP, North Italy	WWTP (Effluent–influent)	Naproxen	100–910	
		Ciprofloxacin	290–3700	
		Ofloxacin	220–2200	
		Sulfamethoxazole	170–740	
		Furosemide	80–470	
Pego–Oliva Marshlands (Spain)	Water	Acetaminophen	104.8–119.6	[14]
		Codeine	46.0–79.4	
		Ibuprofen	42.7–75.3	
	Sediment (ng g^{-1})	Acetaminophen	12.7–17.5	
		Codeine	3.2–4.0	
		Ibuprofen	ND	
WWTP (Canada)	Influent	Acetaminophen	5700–130,000	[15]
		Ibuprofen	2500–45,000	
		Clarithromycin	48–8000	
		Ciprofloxacin	17–2500	
		Sulfamethoxazole	59–3100	
	Effluent	Acetaminophen	16–62,000	
		Ibuprofen	16–47,000	
		Clarithromycin	130–7000	
		Ciprofloxacin	22–620	
		Sulfamethoxazole	33–1800	
Old Brahmaputra river (Bangladesh)	Water	Sulfadiazine	ND–11.4	[16]
		Trimethoprim	ND–17.2	
		Metronidazole	0.1–13.5	
		Tylosin	ND–16.7	
Beiyun River Basin (China)	Water	Acetaminophen	ND–3577	[18]
		Caffeine	31.3–2714.1	
		DEFT	2.5–1356.1	
		Erythromycin	ND–1320	

scientists and the government. The PhACs contamination in drinking water does not possess severe impacts on humans due to its very less concentration. Different types of PhACs possess a unique impact on the organisms. PhACs, especially antibiotics, have persistent and threatening outcomes due to PhACs (< minimum inhibitory concentration, MIC) that are most likely to develop antimicrobial resistance microbes and several diseases. Development of the antibiotic resistance microbes, i.e., bacteria, and fungi, is a major concern that can give rise to some lethal microbes.

According to the 'scoping report on antimicrobial resistance in India' by "The *Center for Disease Dynamics, Economics & Policy*", gram-negative microbes have more tendency to resist the action of antibiotics. More than 70% of isolates of *E. coli*, *K. pneumonia*, and *P. aeruginosa* were reported to be resistant to fluoroquinolones in a PhACs contaminated water body [1]. Flach et al. (2015) isolated the bacterial colonies from PhACs contaminated Kazipally lake and Asanikunta tank (in Hyderabad) and found 52% (approx.) of bacterial strains were ciprofloxacin-resistant, while 60% of strains were sulfamethoxazole resistant [19]. Akiba et al. (2015) concluded the risk of expansion of the antimicrobial resistance microbes in the STPs (South India) due to hospital waste than domestic waste; for instance, the isolated *E. coli* was reported to be resistant to 17 antibiotics [20]. Machado et al. (2014) reported antibiotic resistant bacteria in the wells and observed their seasonal distribution. A variant of *chryseobacterium* spp. was found to be resistant to all the tested antibiotics, while most isolates were concluded to be resistant to ampicillin. Tao et al. (2010) detected tetracycline and six antibiotic resistant Enterobacteriaceae in the Pearl river [21]. In another study, approx. 2.4% isolates of *S. aureus* (isolated from bovine and caprine milk) were vancomycin-resistant [22]. Dos Santos et al. (2016) also detected multi-antibiotic resistant staphylococcus spp. in bovine milk [23]. All the reported antimicrobial resistant microbes present in different water bodies have been listed in Table 4. The observed concentration of PhACs in drinking water is very less, but the impact of the persistent PhACs on humans and domestic animals cannot be undervalued.

Fluoroquinolones are a class of highly used antibiotics for treatment of the bacterial infections. However, obstinate consumption of these antibiotics creates severe health impacts on humans, i.e., memory loss, stroke, vomiting, Nausea, joint and abdominal pain, liver failure, and lung infection [24]. Use of antihistamine drugs to treat the allergies due to consumption of contaminated air, food, and water. Cetirizine and diphenhydramine are highly used antihistamine drugs, but several studies confirmed their health impacts on humans, i.e., disturbed motor function, improper kidney function, constipation, and dizziness (https://www.nhs.uk/medicines/cetirizine/). PhACs are reported to affect the metabolic process in plants by disturbing the various pathways. The indirect impacts of the PhACs on plants are more concerning. PhACs kill the plant growth-promoting rhizobacteria, consequently decreasing the availability of fixed nitrogen and enzymes required for the growth of plants [25]. PhACs are majorly water contamination that drastically affects aquatic animals' health. The presence of PhACs decreases the egg-laying capacity and decreases life span, disturbing biochemical pathways and fertility of the aquatic animals [26]. Vimalkumar et al. (2018) reported the presence of the PhACs (triclocarban and

Table 4 Review of antimicrobial resistance microbe's distribution due to PhACs contamination

Source and sample type	Microorganism	Resistance to PhACs	Reference
Kazipally lake and Asanikunta tank (Sediment)	*Escherichia coli*	Ciprofloxacin	[19]
		Sulfamethoxazole	
Sewage treatment plants effluent (household and hospital waste)	*Escherichia coli*	Ampicillin	[20]
		Cefazolin	
		Cefotaxime	
		Nalidixic Acid	
		Ciprofloxacin	
Four major wells, Guinea-Bissau, West Africa (drinking water)	*Acinetobacter* spp.	Ampicillin	[8]
		Chloramphenicol	
	Chromobacterium spp.	Ampicillin	
		Amoxicillin + Clavulanic acid	
		Gentamicin	
	Ralstonia spp.	Chloramphenicol	
		Ampicillin	
		Amoxicillin + Clavulanic acid	
		Gentamicin	
	Acidovorax spp.	Ampicillin	
	Xenophilus spp.	Chloramphenicol	
		Ampicillin	
		Amoxicillin + Clavulanic acid	
		Doxycycline	
	Pseudomonas spp.	Chloramphenicol	
		Ampicillin	
		Amoxicillin + Clavulanic acid	
		Doxycycline	
	Chryseobacterium spp.	Chloramphenicol	
		Ampicillin	
		Amoxicillin + Clavulanic acid	
		Doxycycline	
		Gentamicin	
Pearl River, China (water)	*Enterobacteriaceae*	Ampicillin	[21]
		Chloramphenicol	

(continued)

Table 4 (continued)

Source and sample type	Microorganism	Resistance to PhACs	Reference
		Ciprofloxacin	
		Levofloxacin	
		Sulfamethoxazole	
		Tetracycline	
		Trimethoprim	
Bovine (milk sample)	*Staphylococcus aureus*	Vancomycin	[22]
Caprine (milk sample)			
Bovine (milk sample)	*Staphylococcus epidermidis*	Methicillin	[23]
		Oxacillin	
	Coagulase-negative *staphylococci* (CNS)	Cephalothin	
		Erythromycin	
		Tetracycline	

benzotriazole) in the fishes of the Kaveri and Vellar rivers of India [10]. The presence of the PhACs in the fishes increases the risk of bio-magnification, which might increase the spontaneous consumption of high concentrations of PhACs by higher organisms via food. The impact of PhACs contamination is not limited to aquatic organisms, but it also hinders the activity of the WWTPs by killing the microbes used in the biological treatment process. Conclusively, the development of the pharmaceutical sector improved the lifestyle and health of humans and other animals but generation of huge PhACs waste is major concern due to its severe impact on the environment. Hence, an appropriate treatment system must be used elucidate the PhACs contaminant through the environment.

4   Methods for PhACs Degradation

Escaping of organic pollutants, specially PhACs, from WWTPs and STPs augmented the presence of the PhACs in most water bodies in the world. Guerra et al. (2014) reported the presence of acetaminophen and ibuprofen with the maximum concentration of 62,000 and 47,000 ng L^{-1}, respectively, in the effluent of WWTPs in Canada, which are still higher than their critical concentrations [15]. Verlicchi et al. (2012) concluded that escaping the more than 10% concentration of PhACs from WWTPs with a concentration near their critical value [13]. Hence, proper treatment of the PhACs cannot be possible with conventional WWTPs and STPs, which triggers the need for some highly efficient treatment processes. Various separation (adsorption, coagulation, ion exchange, and filtration) and degradation methods (chemical oxidation, electrochemical, biodegradation, and advanced oxidation process) have been

used at laboratory and industrial scales for the degradation of the organic pollutants, as given in Fig. 2 [27–29]. All the mentioned processes come with their advantages and disadvantages. Adsorption of pollutants is the cheapest and most used process for wastewater treatment. However, hindering adsorption efficiency by other contaminants and incomplete removal due to concentration equilibrium and the requirement of safe disposal lowered the interest of researchers and industrialists for adsorption [30]. The chemical treatment strategy is the strongest contender for the rapid degradation of PhACs, but the use and production of toxic chemicals are major concerns [31]. Fouling, high reject to permeate ratio, and high maintain and operating costs are problems with membrane filtration systems [31]. Interfering of charged compounds and its expensive nature neglect the use of electrochemical processes for degradation of the PhACs [32]. Biological or microbial degradation of organic pollutants is done by biological agents, especially bacteria and fungi. This process is the ecofriendly process, but safe management of produced antimicrobial resistant microbial biomass is complex. Additionally, antimicrobials present in the PhACs encumbered the degradation efficiency by killing the biological agents [4].

Unlikely, photocatalysis is the most suitable method for degradation of the PhACs at any scale due to the ecofriendly, highly efficient and complete mineralization process, but the requirement of UV light by native catalysts, i.e., TiO_2 and ZnO, is a major problem with this process. Various modification methods, i.e., doping, heterojunction formation, and surface functionalization, can lower their bandgap for use under visible light. Chelli and Golder (2018) lower the bandgap energy of TiO_2 from 3.13 to 2.8 eV by doping Ag metal [33]. Degradation of various PhACs, i.e., CIP, tetracycline, diclofenac, and sulfamethoxazole, were performed by photocatalysis process using different photocatalysts [34–37]. Plant extract-based green synthesis-based photocatalysts provide double benefit with high catalytic efficiency and ecofriendly
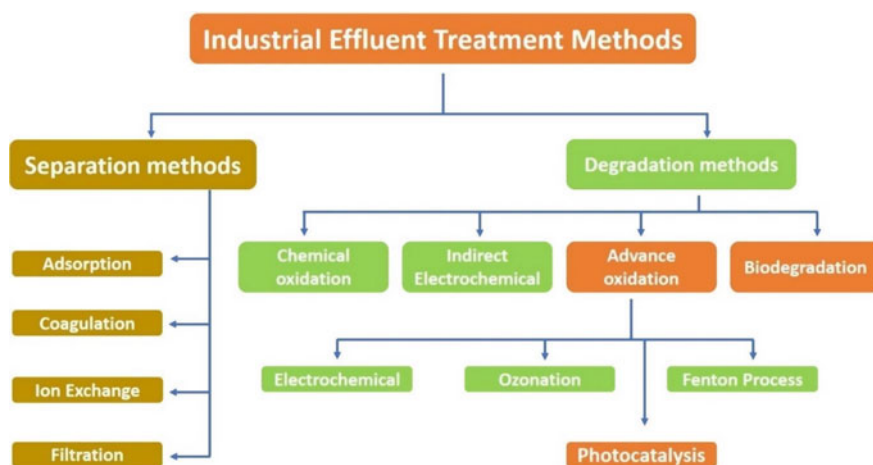
Fig. 2 Various treatment methods used for degradation of the industrial effluent

development nature. Dubiously, the plant parts can be used for adsorption of pollutants [38]. All the reported studies concluded efficient degradation of PhACs with a wide range of light energy. Although, pilot-scale and industrial-scale degradation of PhACs by photocatalysis process is lacking.

5 Conclusions and Future Perspective Toward Elimination of PhACs Contaminants

PhACs contamination has increased over the last two decades due to improper treatment of a high volume of generated PhACs containing wastewater. Detection and monitoring of the PhACs contamination are limited to urban and a few sites of the rivers. Additionally, the risk assessment of PhACs and their effect on humans, aquatic animals, plants, and microorganisms are not entirely understood. The concentration of PhACs in surface water, especially rivers and lakes, is higher than in drinking water (wells water) which augment the health risk in aquatic organisms than humans and domestic animals. Although, toxic effects on a human being cannot be neglected. Persistent contamination of PhACs has increased the expansion of the antimicrobial resistant microbes, which is the major concern with PhACs. Developed antimicrobial resistant microbes might escape the antibiotics during the treatment and can cause some severe diseases, which would result in a few more epidemics.

Additionally, the impact of PhACs on humans and plants through contaminated agriculture fields is not being observed even on a small scale. Although, the chances of bio-magnification of the PhACs are quite low. The topic of detection, monitoring and risk assessment of PhACs in our ecosystem, which includes all the biotic and abiotic things, is high of interesting due to flaws in the monitoring system. Some new pharmaceuticals come into the market every year, which can cause unique and severe health issues in flora and fauna. Hence, detection and timely monitoring of PhACs contamination in rural and small towns is highly recommended. Various studies concluded that inefficient WWTPs and STPs for PhACs waste treatment, globally as more than 10% PhACs escape the treatment process. This review addresses various conventional degradation methods, but photocatalysis (advance oxidation process) was reported as the most efficient degradation process. Photocatalysis is more limited to laboratory scale with some flaws of high bandgap energy and rapid recombination. For upcoming research, the modification of photocatalysts and upscaling of the photocatalysis process are suggested. Furthermore, governments and other agencies should increase their efforts by providing improved detection techniques and more advanced treatment plants at small and large scales to make our ecosystem pollution-free.

References

1. Gandra, S., Joshi, J., Trett, A., Lamkang, A.S., Laxminarayan, R.: Scoping report on antimicrobial resistance in India. Center for Disease Dynamics, Economics & Policy (2017)
2. Bernier, S.P., Surette, M.G.: Concentration-dependent activity of antibiotics in natural environments. Front. Microbiol. **4**, 20 (2013)
3. Das, P. P., Sharma, M., & Purkait, M. K.: Recent progress on electrocoagulation process for wastewater treatment: A review. Sep. Purif. Technol. **292**, 121058 (2022)
4. Wu, G., Yin, Q.: Microbial niche nexus sustaining biological wastewater treatment. Npj Clean Water **3**(1), 1–6 (2020)
5. Jones, A.W.: Early drug discovery and the rise of pharmaceutical chemistry. Drug Test. Anal. **3**, 337–344 (2011)
6. Bentley, R.: Different roads to discovery; Prontosil (hence sulfa drugs) and penicillin (hence β-lactams). J. Ind. Microbiol. Biotechnol. **36**, 775–786 (2009)
7. Silva, S., Rodrigues, J.A., Coelho, M.R., Martins, A., Cardoso, E., Cardoso, V.V., Benoliel, M.J., Almeida, C.M.: Occurrence of pharmaceutical active compounds in sewage sludge from two urban wastewater treatment plants and their potential behaviour in agricultural soils. Environ. Sci.: Water Res. Technol. **7**, 969–982 (2021)
8. Machado, A., Bordalo, A.A.: Prevalence of antibiotic resistance in bacteria isolated from drinking well water available in Guinea-Bissau (West Africa). Ecotoxicol. Environ. Saf. **106**, 188–194 (2014)
9. Fick, J., Söderström, H., Lindberg, R.H., Phan, C., Tysklind, M., Larsson, D.J.: Contamination of surface, ground, and drinking water from pharmaceutical production. Environ. Toxicol. Chem. **28**, 2522–2527 (2009)
10. Vimalkumar, K., Arun, E., Krishna-Kumar, S., Poopal, R.K., Nikhil, N.P., Subramanian, A., Babu-Rajendran, R.: Occurrence of triclocarban and benzotriazole ultraviolet stabilizers in water, sediment, and fish from Indian rivers. Sci. Total Environ. **625**, 1351–1360 (2018)
11. Renganathan, J., Ramakrishnan, K., Ravichandran, M.K., Philip, L.: Spatio-temporal distribution of pharmaceutically active compounds in the River Cauvery and its tributaries, South India. Sci. Total Environ. **800**, 149340 (2021)
12. Subedi, B., Balakrishna, K., Joshua, D.I., Kannan, K.: 2017: Mass loading and removal of pharmaceuticals and personal care products including psychoactives, antihypertensives, and antibiotics in two sewage treatment plants in southern India. Chemosphere **167**, 429–437 (2017)
13. Verlicchi, P., Al Aukidy, M., Galletti, A., Petrovic, M., Barceló, D.: Hospital effluent: investigation of the concentrations and distribution of pharmaceuticals and environmental risk assessment. Sci. Total Environ. **430**, 109–118 (2012)
14. Vazquez-Roig, P., Andreu, V., Blasco, C., Picó, Y.: Risk assessment on the presence of pharmaceuticals in sediments, soils and waters of the Pego-Oliva Marshlands (Valencia, eastern Spain). Sci. Total Environ. **440**, 24–32 (2012)
15. Guerra, P., Kim, M., Shah, A., Alaee, M., Smyth, S.A.: Occurrence and fate of antibiotic, analgesic/antiinflammatory, and antifungal compounds in five wastewater treatment processes. Sci. Total Environ. **473**, 235–243 (2014)
16. Hossain, A., Nakamichi, S., Habibullah-Al-Mamun, M., Tani, K., Masunaga, S., Matsuda, H.: Occurrence and ecological risk of pharmaceuticals in river surface water of Bangladesh. Environ. Res. **165**, 258–266 (2018)
17. Hanamoto, S., Nakada, N., Yamashita, N., Tanaka, H.: Source estimation of pharmaceuticals based on catchment population and in-stream attenuation in Yodo River watershed, Japan. Sci. Total Environ. **615**, 964–971 (2018)
18. Ma, R., Wang, B., Lu, S., Zhang, Y., Yin, L., Huang, J., Deng, S., Wang, Y., Yu, G.: Characterization of pharmaceutically active compounds in Beijing, China: occurrence pattern, spatiotemporal distribution and its environmental implication. J. Hazard. Mater. **323**, 147–155 (2017)

19. Flach, C.F., Johnning, A., Nilsson, I., Smalla, K., Kristiansson, E., Larsson, D.J.: Isolation of novel IncA/C and IncN fluoroquinolone resistance plasmids from an antibiotic-polluted lake. J. Antimicrob. Chemother. **70**, 2709–2717 (2015)
20. Akiba, M., Senba, H., Otagiri, H., Prabhasankar, V.P., Taniyasu, S., Yamashita, N., Lee, K.I., Yamamoto, T., Tsutsui, T., Joshua, D.I., Balakrishna, K.: Impact of wastewater from different sources on the prevalence of antimicrobialresistant *Escherichia coli* in sewage treatment plants in South India. Ecotoxicol. Environ. Saf. **115**, 203–208 (2015)
21. Tao, R., Ying, G.G., Su, H.C., Zhou, H.W., Sidhu, J.P.: Detection of antibiotic resistance and tetracycline resistance genes in *Enterobacteriaceae* isolated from the Pearl rivers in South China. Environ. Pollut. **158**, 2101–2109 (2010)
22. Bhattacharyya, D., Banerjee, J., Bandyopadhyay, S., Mondal, B., Nanda, P.K., Samanta, I., Mahanti, A., Das, A.K., Das, G., Dandapat, P., Bandyopadhyay, S.: First report on vancomycin-resistant *Staphylococcus aureus* in bovine and caprine milk. Microb. Drug Resist. **22**, 675–681 (2016)
23. Dos Santos, F.F., Mendonça, L.C., de Lima Reis, D.R., de Sá Guimarães, A., Lange, C.C., Ribeiro, J.B., Machado, M.A., Brito, M.A.V.P.: Presence of mecA-positive multidrug-resistant *Staphylococcus epidermidis* in bovine milk samples in Brazil. J. Dairy Sci. **99**, 1374–1382 (2016)
24. Mathews, B., Thalody, A.A., Miraj, S.S., Kunhikatta, V., Rao, M., Saravu, K.: Adverse effects of fluoroquinolones: a retrospective cohort study in a South Indian tertiary healthcare facility. Antibiotics **8**, 104 (2019)
25. Gallego, S., Martin-Laurent, F.: Impact of PhACs on Soil Microorganisms, Interaction and Fate of Pharmaceuticals in Soil-Crop Systems, pp. 267–310. Springer, Germany, (2020).
26. Patel, M., Kumar, R., Kishor, K., Mlsna, T., Pittman, C.U., Jr., Mohan, D.: Pharmaceuticals of emerging concern in aquatic systems: chemistry, occurrence, effects, and removal methods. Chem. Rev. **119**, 3510–3673 (2019)
27. Das, P. P., Mondal, P., Sinha, A., Biswas, P., Sarkar, S., & Purkait, M. K.: Treatment of steel plant generated biological oxidation treated (BOT) wastewater by hybrid process. Sep. Purif. Technol. **258**, 118013 (2021)
28. Samanta, N. S., Das, P. P., Mondal, P., Bora, U., & Purkait, M. K.: Physico-chemical and adsorption study of hydrothermally treated zeolite A and FAU-type zeolite X prepared from LD (Linz–Donawitz) slag of the steel industry. J. Environ. Anal. Chem. **13**, 1–23 (2022)
29. Das, P. P., & Purkait, M. K.: Treatment of cold rolling mill (CRM) effluent of steel industry. Sep. Purif. Technol. **274**, 119083 (2021)
30. Samanta, N. S., Das, P. P., Mondal, P., Changmai, M., & Purkait, M. K.: Critical review on the synthesis and advancement of industrial and biomass waste-based zeolites and their applications in gas adsorption and biomedical studies. J. Indian Chem. Soc. **99**, 100761 (2022)
31. Changmai, M., Das, P. P., Mondal, P., Pasawan, M., Sinha, A., Biswas, P., ... & Purkait, M. K.: Hybrid electrocoagulation–microfiltration technique for treatment of nanofiltration rejected steel industry effluent. J. Environ. Anal. Chem. **102**, 62–83 (2022)
32. Radjenovic, J., Sedlak, D.L.: Challenges and opportunities for electrochemical processes as next-generation technologies for the treatment of contaminated water. Environ. Sci. Technol. **49**, 11292–11302 (2015)
33. Chelli, V.R., Golder, A.K.: Ag-doping on ZnO support mediated by bio-analytes rich in ascorbic acid for photocatalytic degradation of dipyrone drug. Chemosphere **208**, 149–158 (2018)
34. Elangovan, M., Bharathaiyengar, S.M., PonnanEttiyappan, J.: Photocatalytic degradation of diclofenac using TiO_2CdS heterojunction catalysts under visible light irradiation. Environ. Sci. Pollut. Res. **28**, 18186–18200 (2021)
35. Purkait, M. K., & Chang, C. T.: Experimental evaluation of Pt/TiO2/rGO as an efficient HER catalyst via artificial photosynthesis under UVB & visible irradiation. Int. J. Hydrog. Energy. **45**, 17174–17190 (2020)
36. Singh, R., Yadav, V. S. K., & Purkait, M. K.: Cu2O photocatalyst modified antifouling polysulfone mixed matrix membrane for ultrafiltration of protein and visible light driven photocatalytic pharmaceutical removal. Sep. Purif. Technol. **212**, 191–204 (2019)

37. Yadav, V. S. K., & Purkait, M. K.: Solar cell driven electrochemical process for the reduction of CO2 to HCOOH on Zn and Sn electrocatalysts. Sol. Energy. **124**, 177–183 (2016)
38. Golder, A.K., Chauhan, S., Ravi, R.: Synthesis of low-cost bentonite/Duranta erecta's fruit powder imbedded alginate beads and its application in surfactant removal. Environ. Sci. Pollut. Res. **28**, 58945–58957 (2021)

Removal of Methylene Blue Dye from Textile Industry Wastewater Using Plantain Pith

P. B. Lakshmipriya, Rosemary Francis, and B. Gayathri

1 Introduction

One of the major contributors to industry waste water is the textile industry. At different stages of the textile industry, coloring the textiles demands multiple types of dyes. This process in turn produces huge amount of waste water, which is often released directly into the nearby water bodies. This disposal degrades the water and poses a direct threat to the aquatic eco system and the environmental [1].

Annually, 7.1×10^5 metric tons of textile dye is produced across the world to meet the commercial need of the industry. Of which the dye lost during the dyeing process is estimated to be 10–25%. About one-fifth of this lost dye is released into the water bodies without proper treatment. It is estimated that globally water bodies receive 0.28 million tons of textile dye which impacts the surface as well as the ground water. According to the World Bank, major textile water contamination arises from the dyeing as well as the treatment process. The disposal of untreated effluents to water streams in many developing nations such as India, China, Bangladesh, etc. has caused severe harm to human health and the environment. Among all these dyes, methylene blue (C16H18ClN3S) is frequently for dyeing [2].

The textile industry uses different types of dyes, chemicals, auxiliary chemicals, and sizing materials during the processing of textiles resulting in various environmental problems unless proper treatment is carried out before its disposal. The pollutants such as color, dissolved solids, trace metals, etc. are not effectively removed by conventional treatment methods. On the other hand, advanced treatment methods offer scope for reduction of these pollutants along with recovery and recycling of water and chemicals but are resource intensive [3].

Plantain (Musa paradisiaca) is one among the widely consumed fruits, and constitutes second largest fruit industry in India. It is grown in about 120 countries. With

P. B. Lakshmipriya (✉) · R. Francis · B. Gayathri
Department of Civil Engineering, SCMS School of Engineering and Technology, Karukutty, India
e-mail: lakshmipriyapb95@gmail.com

an annual production of 14.2 million tons of plantain, India is one among the top producers of plantain in the world. The stem of the fruit goes to waste once the fruit is cut off [4]. In order to make the dyeing wastewater treatment economical, it is imperative to go for low-cost adsorbents. Initially, the effect of adsorbent on water mixed with known quantities of methylene blue dye will be studied [5]. The effectiveness of plantain pith as an economical natural adsorbent in the removal of dye with varying parameters like color, pH, adsorption capacity, and time is studied in this paper. For detailed study, adsorption graphs are plotted.

2 Materials and Method

2.1 Materials Used

Materials used are glass tank, methylene blue dye, adsorbent used includes fresh plantain pith, dried plantain pith, fresh plantain pith bark, dried plantain pith bark, beakers, pipettes, std flask, spectrophotometer, water quality analyses, sulfuric acid, and sodium hydroxide.

2.2 Adsorption

The adsorption technique gave the best results in the removal of dye among other treatment options explored. Adsorption is measured using a spectrophotometer, which measures light absorbed by a chemical substance. The measurement is carried out by calculating the light intensity as a beam when passed through a solution. The principle involved is that over a particular range of wavelength each compound either absorbs or transmits light. The following measurement also helps to quantify a known chemical substance [6].

2.3 Plantain Pith and Bark as Adsorbents

The efficiency of plantain fiber as an adsorbent in the elimination of methylene blue dye was studied. The adsorbent is eco-friendly, renewable, and easily disposable [7]. The benefit of using plantain fibre as such is two fold as it not only helps in better management of the plant but also in effective utilization of its fiber [8].

Fig. 1 Calibration chart
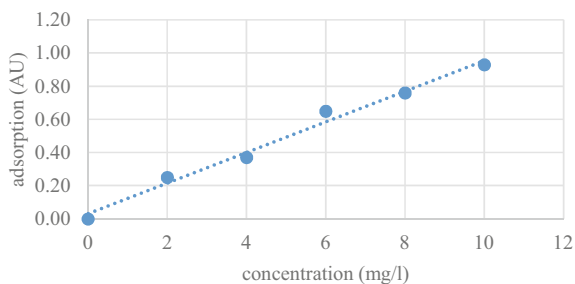
3 Scope and Objective

Developing countries face many major problem during effluent treatment of which the huge expense and the cost of importing technologies and chemicals outcasts the rest. The development of treatment technologies and chemicals locally or the use of locally available materials is a solution for this problem [9]. With regard to this, in many developing nations, the usage of certain low-budget technology for the waste water treatment has been initiated. The pre-treatment procedure with appropriate biomaterials after proper understanding of the biosorbent mechanism is widely adapted. The initial concentration, effect of pH, contact time, and adsorbent dose on adsorption of methylene blue dye are thoroughly studied.

4 Methodology

4.1 Preparation of Calibration Chart

The calibration chart required for finding out the concentration of dye removed was prepared by plotting a graph of adsorption versus concentration. The maximum absorbance wavelength was found to be 640 nm. A concentration of 10 mg/L of methylene blue was prepared, and its absorbance was found under various wavelengths to get the maximum absorbance wavelength. Preparation of different concentrations of dye solution like 2, 4, 6, 8, and 10 mg/L was done to prepare the calibration chart (Fig. 1).

4.2 Tests Conducted

Different tests were conducted using plantain pith and bark under varying conditions to get the maximum removal efficiency. Parameters like initial dye concentration, pH, adsorbent surface area and amount of adsorbent were checked. Each experiment

was conducted separately in a glass aquarium, and absorbance was found using spectrophotometer. Effect of shape of the adsorbent, initial concentration, effect of pH, effect of the amount of adsorbent used were tested using both fresh and dried samples of plantain pith and plantain pith bark and absorbance rate was checked.

The adsorbents were immersed in the prepared dye solution in the given amount for 24 h in a glass aquarium. Absorbance of the solution collected from the aquarium was tested after every 1, 2, and 24 h. Time versus concentration graph were plotted for the given amount of adsorbent and the amount of adsorbent giving maximum removal efficiency was obtained (Fig. 2).

Plantain pith (fresh). The plantain pith which is the innermost portion of the banana stem. 100 mg/L of adsorbents was used for each experiment (Figs. 3 and 4).

Fig. 2 Experimental setup (glass aquariums with dye solution and adsorbents)

Fig. 3 Plantain pith pieces before adsorption of dye

Fig. 4 Plantain pith pieces after adsorption of dye

Effect of adsorbent shape. The collected sample of plantain pith which is the innermost portion of the banana stem was cut into different shapes to check the variation of removal efficiency with respect to the surface area of pith. The pith was cut into squares, circular plates and long stripes. At pH 7, the initial concentration was 6 mg/L.

Effect of initial dye concentration. Samples of concentration 2, 4, 6, 8, and 10 mg/L were prepared for testing.

Effect of Ph. Removal efficiency for a sample of initial concentration 6 mg/L was checked (6 mg/L was selected because it gave maximum removal efficiency in the previous experiment). pH range for which test was conducted includes 4, 7, and 12.

Effect of the amount of adsorbent used. Removal efficiency for samples of initial concentration 6 mg/L and pH 4 was checked. Tests were conducted for different amount of adsorbents like 200, 150, 100, and 50 g/L (6 mg/L and pH 4 were selected because it gave maximum removal efficiency in the previous experiments).

Plantain pith (dried). Plantain pith collected was cut into small cubes of size roughly $2 \times 2 \times 2$ cm and sun-dried to remove all the water content from it (Fig. 5 and 6).

Effect of initial concentration. Samples of concentration 2, 4, 6, 8, and 10 mg/L were prepared for testing. At pH 7, 4 g/L of adsorbent was used.

Effect of the Ph. Samples of concentration 6 mg/L were prepared to check removal efficiency due to the effect of pH (6 mg/L was selected because it gave maximum removal efficiency in the previous experiment). 4 g/L of adsorbents were used at a pH 4, 7, and 12.

Effect of the amount of adsorbent used. Samples of concentration 6 mg/L and pH 7 were prepared to check removal efficiency due to the effect of amount of adsorbent used. (6 mg/L and pH 4 were selected because it gave maximum removal efficiency in the previous experiments). The amount of adsorbents used were 4, 8, and 12 g/L.

Fig. 5 Dried plantain pith

Fig. 6 Dried pith immersed
in dye solution

Bark of plantain stem (fresh). The bark of plantain stem was collected and cut into stripes to conduct the experiment. 200, 150, 100, and 50 g/L of adsorbents were used in the experiments (Figs. 7 and 8).

Effect of the initial concentration. Different concentrations like 2, 4, 6, 8, and 10 mg/L were prepared for testing.

Effect of the pH. Samples of initial concentration 8 mg/L were prepared for testing (8 mg/L was selected because it gave maximum removal efficiency in the previous experiment).

Fig. 7 Fresh plantain pith stripes

Fig. 8 Plantain pith stripes after adsorption of dye

Effect of the amount of adsorbent used. Samples of initial concentration 8 mg/L and pH 7 were prepared for testing (8 mg/L and pH 7 were selected because it gave maximum removal efficiency in the previous experiments).

Bark of plantain stem (dried). The bark of plantain stem was collected and chopped into pieces and dried under sun for 24 h to remove all the water to conduct the experiment (Figs. 9 and 10).

Effect of the initial concentration. Concentrations like 2, 4, 6, 8, and 10 mg/L were prepared for testing. 20 g/L of adsorbents was used at a pH 7.

Fig. 9 Dried bark of plantain pith before adsorption of dye

Fig. 10 Dried bark of plantain pith after adsorption of dye

Effect of the pH. Samples of initial concentration 8 mg/L were prepared for testing (8 mg/L was selected because it gave maximum removal efficiency in the previous experiment).

Effect of the adsorbent amount. Samples of initial concentration 8 mg/L and pH 7 were prepared to check the effect of amount of adsorbent used on removal efficiency (8 mg/L and pH 7 were selected because it gave maximum removal efficiency in the previous experiments).

5 Results and Discussions

All the data collected from the experiments conducted were tabulated and plotted to find out the conditions and parameters giving removal efficiency at its maximum.

The following formula was used to calculate removal efficiency,

$$\text{Removal efficiency}(\%) = \frac{C_o - C_t}{C_o} \tag{1}$$

where

C_o Initial concentration of the dye solution (mg/L)
C_t Concentration of the dye at any time (mg/L)

5.1 Fresh Plantain Pith

Effect of shape of adsorbent. Plantain pith was cut into small cubes, circular plates and elongated stripes to check the influence of surface area on adsorption. The experiment was conducted under pH 7 with the dye concentration as 6 mg/L, and adsorbent amount used is 100 g/L. Removal efficiency of each shape was calculated by collecting the sample after 24 h (Table 1).

Effect of initial concentration. Experiment was conducted under different initial concentration with pH 7 and taking 100 g/L of the adsorbent (Fig. 11; Table 2).

Effect of pH. From the above conducted experiments on varying initial concentration, it was found out that 6 mg/L gave the maximum removal efficiency. By keeping the

Table 1 Variation of removal efficiency with the shape of adsorbent	Shape of adsorbent	Removal efficiency (%)
	Cubes	79.00
	Circular plates	73.20
	Elongated stripes	71.50

Fig. 11 Concentration versus contact time graph for varying dye concentration

Table 2 Variation of removal efficiency with initial concentration

Initial concentration (mg/L)	Removal efficiency (%)
10	70.00
8	73.80
6	75.00
4	62.50
2	64.00

initial concentration as 6 mg/L, the test was conducted on varying pH. Amount of adsorbent used is 100 g/L (Fig. 12; Table 3).

Effect of the amount of adsorbent used. Experiment was conducted by altering the amount of adsorbent used under a pH 4 and initial concentration 6 mg/L (which gave maximum removal efficiency from the above conducted experiments) (Table 4).

Fig. 12 Concentration versus contact time graph for varying pH
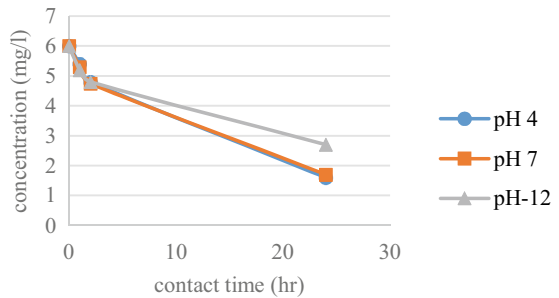
Table 3 Variation of removal efficiency with pH

pH	Removal efficiency (%)
4	76.36
7	75.00
12	60.00

Table 4 Variation of removal efficiency with the dosage of adsorbent used

Amount of adsorbent used (g/L)	Removal efficiency (%)
50	70.12
100	76.36
150	77.05
200	76.92

5.2 Plantain Pith (Dried)

Plantain pith was cut into cubes and dried under sun for 24 h to remove all the water content.

Effect of initial concentration. Experiment was conducted under different initial concentration with pH 7 and taking 4 g/L of the adsorbent. Absorbance of the sample was checked after every 1, 2, and 24 h using spectrophotometer (Fig. 13; Table 5).

Effect of pH. From the above conducted experiments on varying initial concentration, it was found out that 6 mg/L gave the maximum removal efficiency (Fig. 14; Table 6).

Effect of the amount of adsorbent used. Experiment was conducted by altering the amount of adsorbent used under a pH 7 and initial concentration 6 mg/L (which gave maximum removal efficiency from the above conducted experiments) (Fig. 15; Table 7).

Fig. 13 Concentration versus contact time graph for varying dye concentration
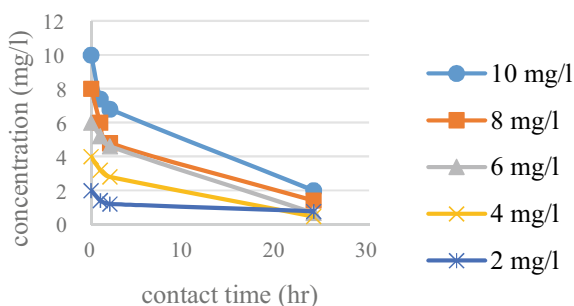
Table 5 Variation of removal efficiency with initial concentration

Initial concentration (mg/L)	Removal efficiency (%)
10	81.11
8	81.42
6	89.69
4	87.90
2	87.30

Fig. 14 Concentration versus contact time graph (varying pH)
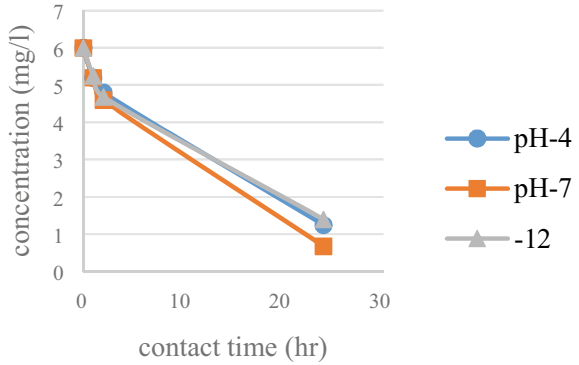
Table 6 Variation of removal efficiency with pH

pH	Removal efficiency (%)
4	80.23
7	89.69
12	70.65

Fig. 15 Concentration versus contact time graph (varying dosage of adsorbent)

Table 7 Variation of removal efficiency with the dosage of adsorbent used

Amount of adsorbent used (g/L)	Removal efficiency (%)
4	89.69%
8	90.66%
12	92.45%

5.3 Bark of Plantain Stem (Fresh)

Bark of banana stem was cut into small pieces to conduct the experiment.

Effect of initial concentration. Experiment was conducted under different initial concentration with pH 7 and taking 100 g/L of the adsorbent (Fig. 16; Table 8).

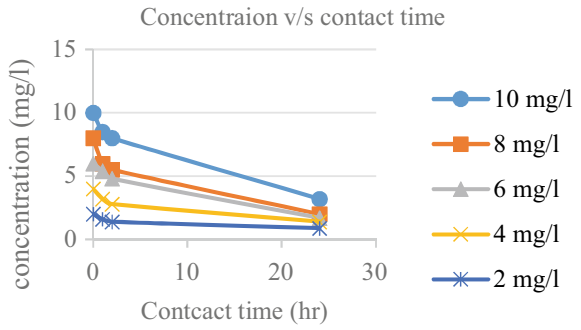**Fig. 16** Concentration versus contact time graph (varying dye concentration)
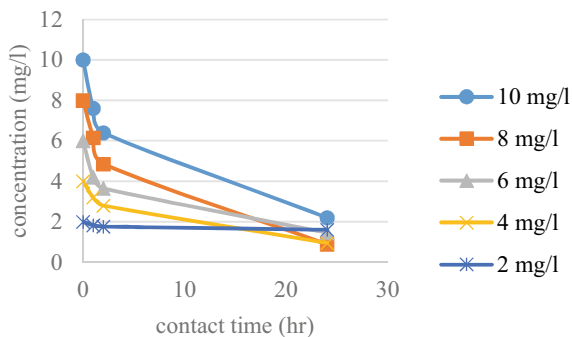
Table 8 Variation of removal efficiency with initial concentration

Initial concentration (mg/L)	Removal efficiency (%)
10	80.30
8	87.40
6	78.40
4	73.03
2	56.01

Effect of pH. From the above conducted experiments on varying initial concentration, it was found out that 8 mg/L gave the maximum removal efficiency. By keeping the initial concentration as 8 mg/L, the test was conducted on varying pH. Amount of adsorbent used is 100 g/L (Fig. 17; Table 9).

Fig. 17 Concentration versus contact time graph (varying pH)
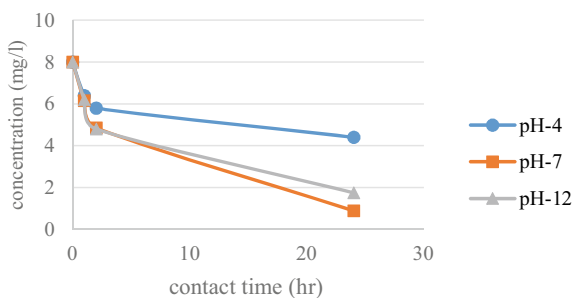
Table 9 Variation of removal efficiency with pH

pH	Removal efficiency (%)
4	43.40
7	87.40
12	78.09

Fig. 18 Concentration versus contact time graph (varying adsorbent dosage)
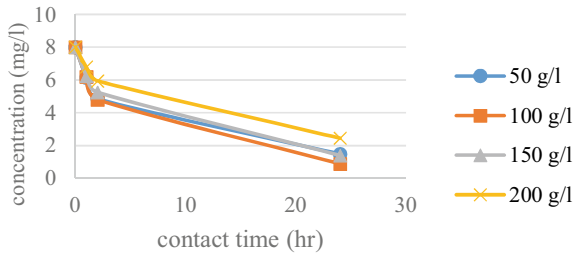
Table 10 Variation of removal efficiency with the amount of adsorbent used

Amount of adsorbent used (g/L)	Removal efficiency (%)
50	80.20
100	87.40
150	83.10
200	70.20

Effect of the amount of adsorbent used. Experiment was conducted by altering the amount of adsorbent used under a pH 7 and initial concentration 8 mg/L (which gave maximum removal efficiency from the above conducted experiments) (Fig. 18; Table 10).

5.4 Dried Bark of Plantain Stem

Bark of banana stem was cut into pieces and sun-dried for 24 h to conduct the experiment.

Effect of the initial concentration. Experiment was conducted under different initial concentration with pH 7 and taking 20 g/L of the adsorbent (Fig. 19; Table 11).

Effect of pH. From the above conducted experiments on varying initial concentration, it was found out that 8 mg/L gave the maximum removal efficiency. By keeping the

Fig. 19 Concentration versus contact time graph (varying dye concentration)
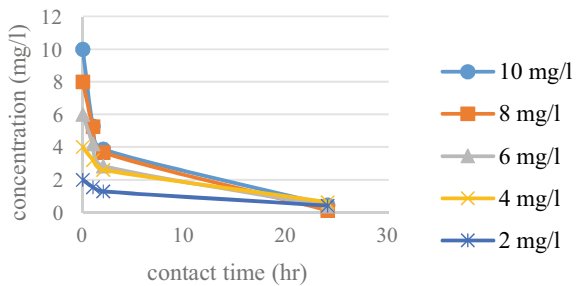
Table 11 Variation of removal efficiency with initial concentration

Initial concentration (mg/L)	Removal efficiency (%)
10	95.29
8	98.11
6	93.20
4	86.27
2	85.31

initial concentration as 8 mg/L, the test was conducted on varying pH. Amount of adsorbent used is 20 g/L (Fig. 20; Table 12).

Effect of the amount of adsorbent used. Experiment was conducted by altering the amount of adsorbent used under a pH 7 and initial concentration 8 mg/L (which gave maximum removal efficiency from the above conducted experiments) (Fig. 21; Table 13).

Fig. 20 Concentration versus contact time graph (varying pH)
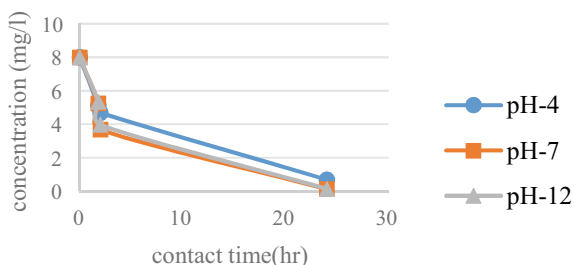
Table 12 Variation of removal efficiency with pH

pH	Removal efficiency (%)
4	90.63
7	98.11
12	80.16

Fig. 21 Concentration versus contact time graph (varying adsorbent dosage)
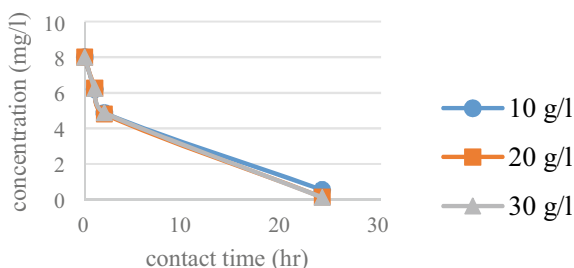
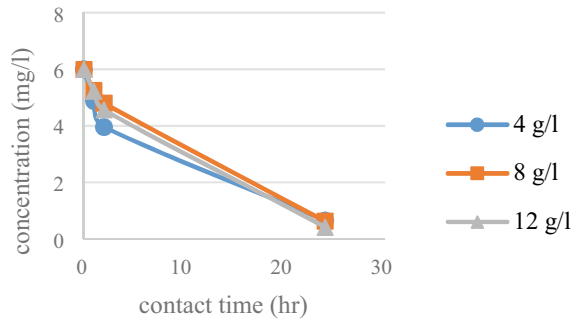**Table 13** Variation of removal efficiency with the amount of adsorbent used

Amount of adsorbent used (g/L)	Removal efficiency (%)
10	91.23
20	98.11
30	98.24

## 5.5 *Reusability of Dried Plantain Bark*

Reusability of adsorbents were tested. Out of the four adsorbents, only the dried plantain bark showed reusability properties, since others deteriorated due to 24 h contact time. The used dried plantain bark was sun-dried to use as adsorbent again. An initial dye concentration of 8 mg/l was used. Absorbance was checked after 1, 2, and 24 h. The observations gave very poor result.

6 Conclusion

It was found that methylene blue dye was effectively removed by the plantain pith and bark in the present work. The pH of the dye, dye concentration, adsorbent amount, and contact time were found to affect the removal efficiency of the adsorbent. Of all the pH values, pH 7 was found the most effective in removing dye, whereas removal efficiency drops with a rise in pH. Out of the adsorption measured for 24 h, quick adsorption was observed in the initial hours. A concentration of 6 mg/L under a pH of 4 gave the best result for fresh pieces of plantain pith when cut into cubes and for the bark of plantain stem, maximum removal efficiency was observed when the initial concentration was 8 mg/L and under a pH 7. The dried samples of plantain pith gave maximum removal efficiency at a concentration of 6 mg/L and under a pH of 7. The dried samples of banana stem bark gave maximum removal efficiency when the initial concentration was 8 mg/L and under a pH of 7. Amount of adsorption increases with the amount of adsorbent used.

From all the experimental observations, it can be concluded that dried adsorbent samples (dries plantain pith and dried plantain stem bark) gives maximum removal efficiency under normal pH and among dried plantain pith and plantain stem bark the latter gives the best removal efficiency. Hence in this study, the use of plantain pith and bark as a sustainable adsorbent could effectively remove methylene blue dye from textile waste water.

References

1. Haris, M., Kathiresan, S.: The removal of methyl red from aqueous solutions using banana pseudostem fibers. Am. J. App. Sci. **6**, 1690–1700 (2009)
2. Das, P. P., Sharma, M., & Purkait, M. K.: Recent progress on electrocoagulation process for wastewater treatment: A review. Sep. Purif. Technol. **292**, 121058 (2022)
3. Sontakke, A. D., Das, P. P., Mondal, P., & Purkait, M. K.: Thin-film composite nanofiltration hollow fiber membranes toward textile industry effluent treatment and environmental remediation applications. Emergent mater. **5**, 1–19 (2021)
4. Das, P. P., & Purkait, M. K.: Treatment of cold rolling mill (CRM) effluent of steel industry. Sep. Purif. Technol. **274**, 119083 (2021)
5. Das, P. P., Mondal, P., Sinha, A., Biswas, P., Sarkar, S., & Purkait, M. K.: Treatment of steel plant generated biological oxidation treated (BOT) wastewater by hybrid process. Sep. Purif. Technol. **258**, 118013 (2021)
6. Samanta, N. S., Das, P. P., Mondal, P., Changmai, M., & Purkait, M. K.: Critical review on the synthesis and advancement of industrial and biomass waste-based zeolites and their applications in gas adsorption and biomedical studies. J. Indian Chem. Soc. **99**, 100761 (2022)
7. Khaleque, A., Roy, D.: Removing reactive dyes from textile effluent using banana fibre. Int. J. Basic Appl. Sci. IJBAS-IJENS **16**, 14–20 (2016)
8. Namasivayam, C., Prabha, D., Kumutha, M.: Removal of direct red and acid brilliant blue by adsorption on to plantain pith. Bioresourc. Technol. **64**, 77–79 (1998)
9. Crini, G.: Non-conventional low-cost adsorbents for dye removal: a review. Bioresour. Technol. **97**, 1061–1085 (2006)
10. Bin, F., Rahman, A., Akter, M., Abedin, M.: Dyes removal from textile wastewater using orange peels. Int. J. Sci. Technol. Res. **2**(9), 47–51 (2013)

Enhancement of Biomass and Lipid Production via Algal-Bacteria Consortia by Treating Rubber Wastewater

Angana Chaudhuri, Nongmaithem Debeni Devi, Dipesh Kumar, Surajit Das, and Vaibhav V. Goud

1   Introduction

With the rise in urbanization and various anthropogenic activities, such as pollution, and exploitation of resources have led to critical consequences on the ecosphere [1]. Another impact of such activities is the depletion of the huge reservoirs of fossils, resulting in energy crisis. The utilization of these fossil fuel reserves has also contributed to about 51% rise in greenhouse gas emissions [2]. Hence, there is a dire need to develop a sustainable solution. Recently, strenuous research has been focused on the generation of biofuels derived from oil-rich biomass, waste cooking oil, as an alternative renewable source of energy [3]. Some studies are gaining interest in microalgae for the generation of biofuels owing to the following properties such as (a) sequestration of atmospheric carbon dioxide [4] (b) higher lipid content (20–80%) as compared to food crops [5] (c) capability to assimilate nutrients from wastewater

A. Chaudhuri · N. D. Devi · D. Kumar · V. V. Goud (✉)
School of Energy Science and Engineering, Indian Institute of Technology Guwahati, Guwahati, Assam 781039, India
e-mail: vvgoud@iitg.ac.in

A. Chaudhuri
e-mail: achaudhuri@iitg.ac.in

N. D. Devi
e-mail: debeni@iitg.ac.in

D. Kumar
e-mail: k.dipesh@iitg.ac.in

S. Das
Department of Life Science, National Institute of Technology, Rourkela, Odisha 769008, India

V. V. Goud
Department of Chemical Engineering, Indian Institute of Technology Guwahati, Guwahati, Assam 781039, India

[6] (d) growth in non-arable land [7] (e) no land competition between food crops and oil production.

However, approximately 6000 L of water was required to produce 1 L microalgal oil which added up the cost of cultivation [8]. Recent studies started using various types of wastewater (industries, municipality, domestic, etc.) to cultivate microalgae to reduce the water footprint [9]. The major contributor of wastewater is rubber plantation which discharges about 80 bil L/d globally [10]. The rubber industry of India ranked 5th across the world, processing 8.645 lakh MT of dry natural rubbers to generate 12.96–17.29 billion liters of rubber wastewater (RWW). This has led to a huge release of untreated effluent into the environment [10]. The effluent released from the rubber processing plants contains high amount of ammonium (300–400 mg/L) and phosphorous (5–20 mg/L) that may cause a serious threat to the environment. According to EPA, the level of phosphate, ammonia, COD, BOD present in the wastewater exceed the permissible limit (17 mg for ammonia and 0.05 mg/L for phosphate concentration) established by USEPA, thus fetching the attention to treat the effluent [11]. In treating this RWW, microalgae culture is integrated with wastewater remediation for simultaneous removal of nutrient and metabolic growth. Considering the property of algae to assimilate nutrients, researchers have stated that algae have the potential to remove nutrients like ammonia and phosphorus by 99% [12, 13].

Nevertheless, the existing cultivation of microalgae is associated with several drawbacks. For example, biomass separation from suspended conditions requires high-cost and energy-intensive harvesting techniques [12]. Therefore, in recent years algae-bacteria consortium cultivation method has gained the attention of researchers [14]. Bacteria degrades organic matters into smaller compounds, which is further assimilated by the algae. This metabolic process led the bacteria to produce carbon dioxide which is taken up by the microalgae. The algae in turn release oxygen, which is used by bacteria for its growth and metabolic activities. During the degradation of compounds and exchange of gases, the nutrient removal from the wastewater is enhanced [15]. In addition, the bacteria has the potential to release EPS in the medium which helps in aggregation of cells and the formation of biofilm. The biofilm helps in enhanced growth and increased harvesting efficiency [16]. A handful of studies have been reported on treating different types of wastewater by microalgal biofilm [17, 18]. However, none have investigated the treatment of RWW by microalgae-bacteria consortium. Hence, the current study targets to analyze bioremediation of rubber wastewater through symbiotic association between indigenous bacteria that are readily available in RWW and a novel microalga, *Scenedesmus* sp. DDVG I.

In this present study, we have demonstrated an easy harvesting method by algae-bacteria consortia which helps in enhanced biomass production. Initially, the microalgae were acclimatized in different concentrations of RWW to investigate the highest growth of algae in a particular concentration. Further, the readily available indigenous bacteria were also acclimatized in various concentrations. The optimized conditions of RWW suitable for the growth of both algae and bacteria were used for designing the consortia in RWW, and the consortium was confirmed through TEM analysis. This study also evaluated the biomass productivity and accumulation of

Table 1 Initial RWW characterization

Parameters	Initial conc. (sterilized RWW)	Initial conc. (non-sterilized RWW)
pH	4.17	4.25
COD (mg/L)	1428	1489
BOD (mg/L)	104.5	110.1
Alkalinity (mg/L)	1492	1504
Hardness (mg/L)	310	320
TSS (mg/L)	0.0058	0.0063
TDS (mg/L)	0.0046	0.0051
Phosphate (mg/L)	5.12	5.79
Nitrate (mg/L)	7.8	8.32
Ammonium nitrogen (mg/L)	203.71	210

lipid in the consortium–based biomass which will be established as a prospective feedstock for biodiesel production. In addition, these nutrient removal efficiencies of monoculture and the consortium were analyzed and compared. Overall, this study represents an ideal approach toward a cleaner and sustainable environment.

2 Material and Methodology

2.1 Rubber Wastewater (RWW) Procurement and Its Characterization

The RWW was procured from a local Rubber Processing Plant of Bongaigaon, Assam. The wastewater was filtered with the aid of Whatman Filter Paper (Grade I). Further, the filtered wastewater was sterilized by autoclaving at 121 °C, 15 lb pressure for 30 min. The physicochemical properties of the sterilized and non-sterilized RWW including total phosphorus (TP), nitrate nitrogen (NO_3–N), ammonia nitrogen (NH_3–N), COD, BOD, total suspended solids (TSS), and total dissolved solids (TDS) were analyzed by following the APHA protocols [19] and summarized in Table 1.

2.2 Strains and Inoculum Preparation

The microalga, *Scenedesmus* sp. DDVG I having accession no. MN630585, was formerly isolated by the bioenergy group obtained from a source of freshwater and maintained in BG11 media [16]. Initial inoculum was prepared by culturing

Scenedesmus sp. DDVG I in 250 ml Erlenmeyer flask holding 100 ml BG11 medium (pH = 7) with inoculum size of 10% (v/v). Inoculum was maintained at 27 °C with an intensity of light having 40.5 μmol m^{-2} s^{-1}, 12:12 light–dark cycle. The 7th-day-old cells which were in logarithmic phase were accumulated through the conventional method centrifugation of 6000 rpm for 10 min and used for the experimentation. Indigenous bacterial strains *Bacillus* sp. 0S26, *Bacillus cereus* 0S36, *Lysinibacillus macrolides* ST13, *Burkholderia cepacia* DF12 used in this study were isolated from the RWW. Bacterial inoculum was prepared by culturing all the strains in 250 mL Erlenmeyer flask comprising 100 ml LB Broth with inoculum size of 10% (v/v). The inoculum was maintained at 27 °C in an orbital shaker of 150 rpm. After 24 h, the bacterial cells were accumulated by centrifugation at 6000 rpm for 10 min and used for further experimentation.

2.3   *Experimental Setup for Acclimatization*

Initially, the algal strain was acclimatized both in sterilized and non-sterilized RWW by diluting in different concentrations using distilled water (DI) ranging from 5 to 100%v/v (RWW: DI) in 250 mL flasks (Erlenmeyer) comprising 100 mL of the medium. The experiment was regulated at 27 $\pm$ 1 °C with an intensity of light of 40.5 μmol m^{-2} s^{-1} with 12 h: 12 h (light to dark periods). The growth was evaluated in the form of biomass concentration. The content of chlorophyll was also determined to confirm the algal growth. For acclimatization of bacteria, the similar range of wastewater concentrations was supplemented with 50 mM of urea to support the growth of bacteria, as urea was a minimum requirement for the growth of the strains isolated [20]. The acclimatization of bacteria cultures in RWW was conducted in the similar conditions of microalgal cultivation. The culture conditions which showed superior growth for both microalgae and bacteria were used for further consortium experiment.

2.4   *Experimental Setup for Consortium*

To investigate the consortium study, the 7th-day-old *Scenedesmus* sp. culture and 12th h old bacteria culture were co-cultivated in different ratios of 1:1, 1:2, 2:1 (based on *Scenedesmus*: bacteria cell density) in 80% RWW supplemented with 50 mM of urea. The experiment was conducted in 250 mL Erlenmeyer culture flasks comprising 100 mL media and kept in orbital shakers at 50 rpm. The cultures were maintained at 27 $\pm$ 1 °C with intensity of light 40.5 μmol /m^2/s^1 having periods of 12 h:12 h (light: dark). The consortium systems were regulated for a minimum of 20–22 days and further harvested post reaching a stable state. The consortium condition which showed the maximum biomass was further analyzed for the lipid content and compared with the monoculture of *Scenedesmus* sp.

2.5 Analytical Methods

Cell Growth

The microalgal biomass concentration (dry weight g/L) was estimated by using total suspended solids (TSS) [19]. To examine the growth rate of bacteria, 1 mL of bacterial culture was taken out every 4 h and optical density (OD) was obtained at 600 nm. The growth rate (d^{-1}) was evaluated with the help of Eq. 1.

$$\text{Growth Rate} = (\ln OD_t - \ln OD_0)/t \tag{1}$$

where OD_t and OD_0 denote optical density at time 't' at time '0', respectively.

For chlorophyll estimation, algal culture of quantity 1 mL was centrifuged at 6000 rpm for about 10 min and the pellet was suspended in 1.5 mL containing methanol and incubated in a water bath for 30 min at 45 °C. Finally, the sample was centrifuged at 6000 rpm for 10 min and absorbance at 480, 652, 665, and 680 nm was measured. Chlorophyll content was analyzed as per Eq. (2).

$$\text{Chlorophyll in (mg/L)} = 16.5169\ A_{665} - 8.0962\ A_{652} \tag{2}$$

where A_{665} and A_{652} denote absorbance at 665 nm and 652 nm, respectively.

Biomass Productivity and Lipid Content

The suspended *Scenedesmus* sp. cells in RWW medium were harvested by centrifugation at 6000 rpm for 10 min to retrieve the biomass. The biomass was washed two to three times with 0.9% NaCl to remove the unwanted particulate matters and was oven dried for 16 h. The biomass was used to determine biomass productivity by Eq. (3):

$$\text{Biomass Productivity (g/L.d)} = (DCW \times 1000)/(\text{No. of days} \\ \times \text{Volume of sample culture}) \tag{3}$$

where DCW represents dry cell weight.

For the consortium study, after removal of the culture from the shaker, the culture was settled down for 2 h. After settling down, the supernatant was discarded and the settled bottom layer was used for determining the biomass productivity using Eq. (4). The dry biomass of algal monoculture and consortium was used for extraction of lipid by following the modified Bligh and Drier method [21]. Briefly, the biomass was dissolved in 10 ml of a mixture of chloroform and methanol (2:1 v/v) and kept for 16 h in orbital shaker. Subsequently, 3 mL of water was used to dissolve the sample and mixed for around 1 min. The separation was done by using a separating funnel by respective solvents (chloroform and methanol). The bottom layer was collected, where the lipid was extracted into the chloroform (the organic layer). The lipid content was estimated using formula (4):

$$\text{Lipid content } (\%) = (\text{Weight of lipid extracts} \times 100)/\text{Weight of DCW} \quad (4)$$

The supernatant obtained from the monoculture and consortium was used for estimating the harvesting efficiency. The harvesting efficiency was estimated by formula (5):

$$\text{Harvesting efficiency}(\%) = (F_{OD} - I_{OD}) \times 100/I_{OD} \quad (5)$$

where F_{OD} and I_{OD} are the final OD and initial OD before settling, respectively.

TEM Analysis of Consortium

The monoculture of *Scenedesmus* sp. and its symbiotic association with bacterium to form biofilm were visualized through a transmission electron microscope (TEM). The cells suspension was drop casted on a copper mesh and dried overnight in a hot air oven. The sample was visualized under a JEOL Model: 2100F TEM (Japan).

Nutrient Removal

The concentrations of COD, BOD, alkalinity, hardness, TSS, TDS were determined through APHA protocols [19]. The nitrate estimation in the centrifuged supernatant was done by salicylic acid method by calibrating $NaNO_3$ (standard solution). The ascorbic method was used to estimate the concentration of phosphate using dibasic potassium hydrogen phosphate as standard [22]. The removal efficiency of the nutrients was evaluated by using Eq. (5).

$$\text{Removal efficiency}(\%) = (S_0 - S_T/S_0) \times 100$$

where S_0 and S_T portrayed the initial and final concentration of the nutrients, respectively.

3 Results and Discussion

3.1 Rubber Wastewater Characterization

The initial influent RWW was characterized to determine COD, BOD, phosphate, ammonia, nitrate, TSS and TDS concentration. Results in Table 1 demonstrate the parameters characterized. High concentrations of ammonia, phosphate, COD, BOD were observed which fetched attention for further treatment.

3.2 Acclimatization of the Algae (Scenedesmus DDVG I) in RWW

The monocultural growth of *Scenedesmus* sp. in different RWW was determined through biomass concentration and illustrated in Fig. 1. Results in Fig. 1a represent an increasing trend in the growth of the algae with the increase in the concentration in RWW. This increment is caused due to the presence of more nutrients in media for growth of the algae [10]. The highest biomass concentration of 1.230 and 1.20 g/L was observed at 100 and 80% dilution in non-sterilized RWW. The sterilized RWW represented a lower concentration of biomass having 1.19, 1.15 g/L and growth at 100% and 80% dilution, respectively. In one of the recent reports by Shen et al. (2017) [23], it was reported that sterilizing the wastewater remarkably reduces the algal biomass growth. In accordance with the report, the present study also indicated lower biomass concentration in sterilized RWW. This difference in the biomass growth can be explained by the presence of other indigenous microbes in the non-sterilized RWW. The increase in biomass concentration with concentration of wastewater has also been explained by Zhu et al. [24] where the optimal concentration of *Chlorella zofingiensis* in piggery wastewater (COD_{1900}) had the highest algal growth of 2.9 g/L which was higher than the lower concentrations. Further, to support the growth of the algae with increasing concentration of RWW, the chlorophyll content was also determined (Fig. 1b). The chlorophyll content followed the similar trend as biomass concentration, i.e., enhanced chlorophyll content in algae with increased RWW concentration. The highest chlorophyll content (21 mg/g of biomass) was observed at 100% concentration of non-sterilized wastewater, followed by 80% concentration of RWW (20.6 mg/g of biomass). Finally, the algal growth in terms of rate was determined. As per, the growth profile represented in Fig. 1c, d, the logarithmic phase varies from 0th day to the 6th day. On the 8th day, the growth rate (1.75 day^{-1}) was highest for the 100% concentration of sterilized (1.72 day^{-1}) and non-sterilized ((1.75 day^{-1}) RWW, following which the stationary phase continues until the 16th day. The growth rate of 100% concentration of wastewater was followed by the 80% concentration with growth rate of 1.69 day^{-1} for non-sterilized and 1.65 day^{-1} for sterilized RWW. The probable reason for the stationary phase and a slightly decline biomass productivity might be due to the limitation of utilized carbon sources [25]. The comparison between the lipid content of *Scenedesmus* in BG11 media and non-sterilized, sterilized media is illustrated in Fig. 2e. The lipid content of *Scenedesmus* sp. in sterilized and non-sterilized RWW (~25%) is higher than the lipid content of *Scenedesmus* in BG11(~17%). The higher biomass concentration of *Scenedesmus* sp. in RWW contributed to higher lipid production. Hence, demonstrating that RWW can be utilized as a cheap source of nutrient for enhanced biomass growth.
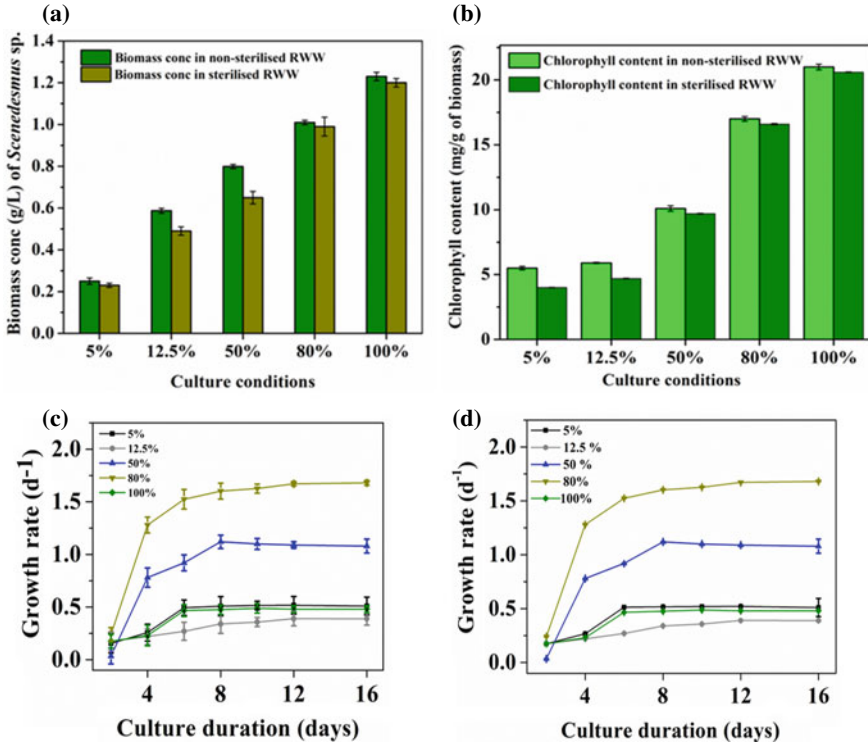
Fig. 1 **a** Biomass conc. of *Scenedesmus*, **b** Chlorophyll content of algal biomass, **c, d** Growth rate of *Scenedesmus* in sterilized and non-sterilized RWW

Fig. 2 Biomass productivity and lipid content of *Scenedesmus* sp.
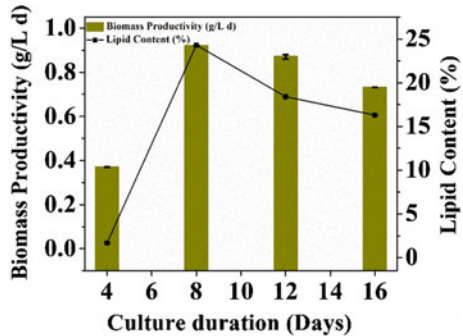
3.3 Biomass Productivity and Lipid Content of Algae in RWW

Results in Fig. 3 illustrated the lipid content, the biomass productivity of *Scenedesmus* sp. in RWW. The monoculture of *Scenedesmus* achieved its highest biomass productivity on 8th day of its cultivation. The biomass productivity was observed to increase

from 0.28 to 0.9 g/L. d grown in sterilized RWW. Significant enhancement of biomass productivity was not observed after 8th day and was found to be in stationary phase until the 16th day. Further, it can be explained that due to high quantities of BOD, COD, phosphate and ammonium aided as a cheap source of nutrient for the robust growth of the *Scenedesmus.* The lipid content represented in Fig. 2 indicates that the lipid content of Scenedesmus increased with the increasing days. The lipid (%) obtained was highest on the 8th day (25%) and lowest on 4th day. After the 8th day, the lipid content further decreased due to the decrease in biomass productivity. Current study by Nayak et al. [25] reported the same trend of biomass productivity where the biomass productivity (0.6517 g/L d) of *Scenedesmus* in domestic wastewater increased with the increase in cultivation days. Wang et al. [26] elaborated that the lipid content of pure culture in synthetic wastewater was found to be 21.5% which can be compared to the obtained lipid content in the present study.

3.4 Acclimatization of Bacteria in RWW

The biomass concentration of the bacteria grown in RWW was determined. Graphs in Fig. 3e represent the biomass concentration of the bacteria in different concentrations of RWW. As the concentration of the wastewater increased, a gradual increase of biomass conc. was observed in bacteria. The highest biomass concentration of all four bacteria was observed at a dilution of 80% RWW. *Burkholderia cepacia* DF12 had a maximal concentration of metabolic biomass of 1.39 g/L at 80% concentration of wastewater and minimum biomass concentration of 0.102 g/L at 100% concentration of wastewater. *Bacillus* sp. 0S26 had the similar pattern of biomass concentration, where the highest biomass concentration (1.44 g/L) was obtained at 80% of RWW. Similar trends were observed for *Bacillus cereus* 0S36, *Lysinibacillus macrolides* ST13, having biomass concentration of 1.413 g/L and 0.912 g/L, respectively. The least biomass concentration of all the bacteria was observed at 100% wastewater. This can be explained by the fact that, 100% RWW might have higher toxicity and organic compounds present which limited the growth of the bacteria. However, in 80% concentration of wastewater, the RWW was diluted with 20% tap water, thus providing a dilution of toxic compounds and optimum nutrient for the robust growth of the bacteria. Additionally, the growth rate was also determined and represented graphically in Fig. 3a–d. The growth profile indicates that the logarithmic phase of *Burkholderia cepacia* DF12 began from 2nd h to around 12th h for 80% concentration of wastewater having growth rate of 0.41 h^{-1}, whereas for 60% concentration of wastewater, the logarithmic phase began from 2nd h to around 15th h. Finally, the death phase began from around 15th–20th h and continues upto 28th h. At 100% concentration of wastewater, no growth of bacteria was observed. Similar growth profile was observed for *Bacillus* sp. 0S26, *Bacillus cereus* 0S36, *Lysinibacillus macrolides* ST13 with the highest growth rate (0.55, 0.49, 0.51 h^{-1}) at 80% concentration of wastewater in Fig. 3a–d, followed by 60% concentration of wastewater.
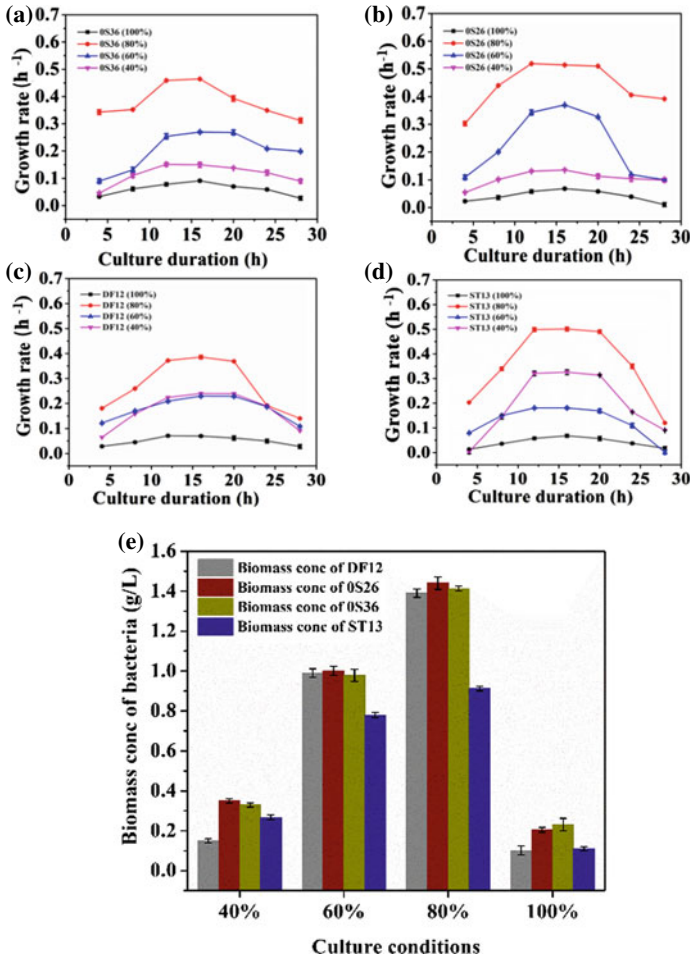
Fig. 3 **a** Growth rate of *Burkholderia cepacia* DF12 in RWW, **b** Growth rate of *Bacillus* sp. 0S26, **c** Growth rate of *Bacillus cereus* 0S36 0S26, **d** Growth rate *Lysinibacillus macrolides* ST13, **e** Biomass concentration of bacteria in different conc of RWW

The stationary and the death phase is generally due to the nutrient depletion and inhibition of secreted metabolites by the bacteria.

3.5 Consortium Formation and Its Characterization

The different combinations of consortia were analyzed to find the biomass productivity and harvesting efficiency. Results in Table 2 represent the different combinations of consortia. Scenedesmus DDVG I with *Bacillus* sp. 0S26, *Bacillus*

cereus 0S36 had the highest biomass productivity of 1.78 g/m^2.day, followed by Scenedesmus DDVG I with *Bacillus* sp. 0S26, *Bacillus cereus* 0S36, *Burkholderia cepacia* DF12, and *Lysinibacillus macrolides* ST13 having biomass productivity of 0.9 g/m^2.day. It is evident from the table that the other combinations of algae and bacteria were not suitable for the formation of biofilm and enhanced biomass production. Results in table also demonstrate the harvesting efficiency. The algae-bacteria consortia of the highest biomass productivity (Scenedesmus DDVG I with *Bacillus* sp. 0S26, *Bacillus cereus* 0S36) had the highest harvesting efficiency of 100%. The harvesting efficiency of Scenedesmus DDVG I with *Bacillus* sp. 0S26, *Bacillus cereus* 0S36, *Burkholderia cepacia* DF12, and *Lysinibacillus macrolides* ST13 had 74% harvesting efficiency. Further, on optimizing the ratios of the consortium, 1:1, 1:2, 2:1, the ratio of 1:1 v/v of algae-bacteria consortia had the highest biomass (1.78 g/m^2 day) and biofilm formation. The biofilm formation might be due to the secretion of EPS from the bacterial cultures. Past research, reported that EPS are unique metabolic products released by certain organisms when they are in stress-mediated condition, limited by irradiance, temperature, nitrogen or ammonium concentration and help in enhanced biomass production by forming biofilm [15]. Study by Makut et al. (2019) reports biomass productivity of 1.271 g/L.d in the consortium culture of algae and bacteria [14]. Results in Fig. 4 illustrate the lipid produced by the consortia in the RWW. The lipid content increased upto 41% until the 8th day, after which. Wang et al. [26] also elaborated that the co-culture of *Scenedesmus* and the bacteria (artificial consortium) contained a lipid content of 24.16%. The lipid (% content) in consortium reported was higher than the pure culture grown in synthetic wastewater. Similar trend is followed by the current study where lipid content by the algae-bacteria consortia is higher than the monoculture algae. However, the lipid content is higher than prior studies. Thus, indicating that *Scenedesmus* DDVG I is a highly potential microalgae which can yield higher biomass productivity in RWW.

Table 2 Biomass productivity of algae with its harvesting efficiency

Sl No	Consortium	Biomass (g/m^2/d)	Harvesting efficiency
1	*Scenedesmus* DDVG1 + 0S26	0.21	5
2	*Scenedesmus* DDVG1 + 0S36	0.17	3.2
3	*Scenedesmus* DDVG1 + ST13	0.001	0.3
4	*Scenedesmus* DDVG1 + DF12	0.02	0.9
5	*Scenedesmus* DDVG1 + 0S26 + DF12	0.072	4.6
6	*Scenedesmus* DDVG1 + 0S26 + ST13	0.95	32
7	*Scenedesmus* DDVG1 + 0S26 + 0S36	1.78	99.8
8	*Scenedesmus* DDVG1 + 0S36 + DF12	0.76	28
9	*Scenedesmus* DDVG1 + 0S36 + ST13	0.89	62
10	*Scenedesmus* DDVG1 + DF12 + ST13	0.02	3

Fig. 4 Biomass
productivity, lipid content of
consortia
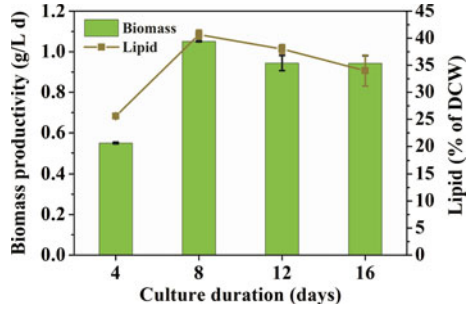
3.6 TEM Analysis of Algae-Bacteria Consortia

The TEM analysis of the consortia demonstrated the interaction exhibited by the algae and the bacteria. It is observed from the images that the bacteria has aided in the symbiotic interaction with the algae *Scenedesmus* sp. The images also displayed the secretion of EPS which further binds the algae to form a biofilm. This biofilm enhances the biomass and the interaction between them. Figure 5a represents an algal cell having a biofilm surrounding it, and Fig. 5b represents the bacteria present. Image in Fig. 5c, d shows interaction of algae and bacteria where few algal cells are surrounded by bacterial cells. Further, Fig. 5c illustrates EPS being secreted by bacteria which binds with algae. It can be interpreted from the images that the algae and bacteria consortia has been successfully formed. Studies by Chandrashekharaiah et al. [27] illustrated similar algae bacteria interaction in the consortia by SEM analysis. Another study by Wang et al. [28] demonstrated TEM analysis of the algae-bacteria consortia and were comparable to the images obtained in our study. The TEM analysis reported by Choudhary et al. [29] in Supplementary 1 (d) represents the biofilm formation around the algae like a sheath. Hence, the TEM images confirm the consortia and biofilm formation between the algae and the bacteria.
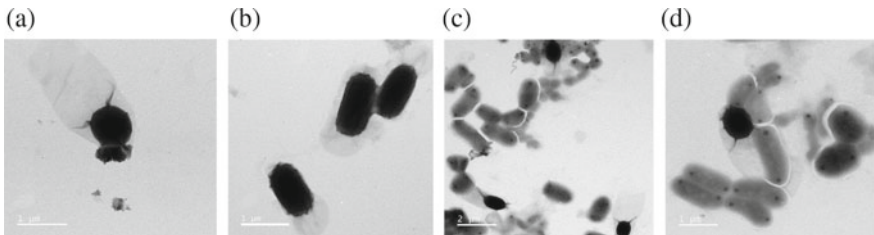

Fig. 5 TEM analysis of algae-bacteria consortia

3.7 *Wastewater Remediation by* Scenedesmus *DDVG I*

The chemical composition of the initial influent and final effluent wastewater are demonstrated in Table 3. The COD, BOD, TSS, TDS, nitrate, ammonium, and phosphate concentration in the initial RWW was quite high which could be hazardous for the marine life. The growth of the monoculture of *Scenedesmus* sp. reduced the chemical compositions of the wastewater, thus making the levels in compliance with the standards set by the environmental associations. The preliminary phosphate content observed in RWW was 5.8 mg/L, whereas due to the succeeding growth of the algal monoculture the phosphate concentration had reduced to about 1.01 mg/L. Thus, providing a nutrient removal of 91 and 95% for sterilized and non-sterilized wastewater, respectively. The robust growth and nutrient removal by the algae in high concentrations of phosphate indicated that the algal strain Scenedesmus DDVG I had a high tolerance toward increased phosphate concentration. The high removal efficiency maybe due to both algal metabolic uptake and phosphate precipitation. RWW has been found to have high amounts of ammonium concentration. Prior studies conducted by Posadas et al. [30] demonstrated that algae had the potential to remove 85% of phosphate concentration from the synthetic wastewater used which is comparable to the reported values in the current study. *Scenedesmus* sp. has been successful in removing the ammonium from the wastewater considerably. Table 3 shows a removal efficiency of about 88 and 89.5% ammonium-nitrogen, respectively, for sterilized and non-sterilized wastewater. Reports by Gou et al. 2018 [31] mention ammonia–nitrogen removal by algae of around 90%, which is similar to the removal efficiency obtained in this study. Thus, indicating that *Scenedesmus* had better potential in removing ammonia–nitrogen from RWW than the algae used in the report by Guo et al. (1990) reported that the removal of ammonium occurs due to the utilization of NH_3–N and NH_4 stripping. This ammonium stripping occurs due to absorption by algae and the presence of urea in media. Thus, owing to the presence of urea and algal absorption, there has been a drastic removal of ammonium. The nitrate concentration of the wastewater reduced slowly and the efficiency (61, 64.5% for sterilized and non-sterilized rubber wastewater) was comparatively lower when compared to the other nutrients. Reports from study by Kothari et al. [5] indicate similar nitrate reduction pattern where the removal efficiency has been reported to be 60%. This reduction efficiency is comparable to the current study. Lower removal of nitrate might indicate that the algal strain lacked the potential to remove nitrate effectively from RWW. Critically, the COD, BOD, TSS, and TDS were removed efficiently. The organic compounds resulting in high COD, BOD, TSS, and TDS acted as a macro- and micro-nutrient for the algal growth. This utilization by the algae led to a reduction in their concentrations. COD had a removal of around 92% while BOD had a removal of 88%. BOD is mainly caused because of the presence of high amounts of carbon, oxygen, and nitrogen which acts as a substrate for the algae to growth. Utilization of these compounds by algae as nutrient reduces the BOD content in RWW and hence the higher removal efficiency. Similar observations have been reported by

Wang et al. [28], where the COD removal has been observed to have reduction efficiency of 90%. Studies by Hena et al. [32] reported that *Chlorella* had a potential to remove BOD by a 93.4% which is concordant with the results observed in our study. TSS and TDS concentrations were also notable decreased. TSS had decreased from a higher conc. of 0.0058 mg/L to a lower conc. of 0.0051 mg/L for sterilized wastewater, with efficiency of 90.1%, whereas TDS decreased from a concentration of 0.0046–0.0027 mg/L for sterilized wastewater, having removal efficiency of 90.3%. Similar reduction patterns were observed when the algae was grown in non-sterilized wastewater with a slight increase in the removal efficiencies. In another study reported by Hena et al. [32], the TDS was reduced by 54% by the monoculture. The microalgae efficiently reduced the alkalinity and hardness of the wastewater. In non-sterilized wastewater, the algae reduced the alkalinity and hardness by 73% and 77%, respectively. Parallely, the algae in sterilized wastewater reduced the alkalinity and hardness by 72.5 and 75.9%, respectively. Similar reports by Arora et al. [33] state that the algae *Chlorella sorokiniana* (UUIND6) was successful in removing the alkalinity and hardness by 70 and 75% in the effluent. Results from Table 1 concluded that the various nutrient parameters have been successfully removed by the algal monoculture.

Table 3 Nutrient removal by algae

Parameters	Initial influent RWW		Final effluent RWW		Nutrient removal (%)	
	Sterilized rubber wastewater	Non-sterilized rubber wastewater	Sterilized rubber wastewater	Non-sterilized rubber wastewater	Sterilized rubber wastewater	Non-sterilized rubber wastewater
pH	4.17	4.25	7.51	7.59	–	
COD	1428	1489	128.52	96.79	91	93.5
BOD	104.5	110.1	16.72	14.31	84	87
Alkalinity (mg/L)	1492	1504	346.1	285.76	76.8	81
Hardness (mg/L)	310	320	23.25	292.4	92.5	92
TSS (mg/L)	0.0058	0.0063	0.0004	0.00063	93.1	90.1
TDS (mg/L)	0.0046	0.0051	0.00045	0.0005	95.65	90.3
Phosphate (mg/L)	5.12	5.79	0.46	0.29	91	95
Nitrate (mg/L)	7.8	8.32	1.25	1.22	64%	65

3.8 Wastewater Remediation by Consortium

A significant decrement was observed in the chemical composition of the wastewater when treated with consortia. The algae and bacteria consortia has proved to be a good association which reduced the COD, BOD, phosphate, nitrate, and ammonium. Past studies on these bacteria have demonstrated them as ureolytic and nitrifying bacteria. The presence of bacteria along with algae in the wastewater has enhanced the removal efficiency. The initial COD in non-sterilized wastewater was calculated to be 1428 mg/L, whereas the final COD value was found to be 71.4 mg/L, thus observing a steady decrease of about 96.7%. The COD removal efficiency by the algae in the sterilized wastewater was 95% which was lower than the COD efficiency in the non-sterilized wastewater. Similar trends were followed for BOD values, wherein initially it was 104.5 mg/L. After the growth of the algae bacteria consortium, BOD decreased by around 84%. Safanova et al. [34] reported in his study a reduction of BOD by 97% by algal-bacteria consortia. COD and BOD are caused due to the existence of increased amounts of organic compounds which act as a substrate for the growth of the algae, which in turn reduces the COD and BOD content in the RWW. COD and BOD removal of the consortium is slightly higher than the algal monoculture removal. This may be caused by the co-cultured bacteria in the consortium which enhances the COD removal [35]. The high amounts of phosphate in the wastewater were reduced drastically by the association, exchange, and reaction between the algae and the bacteria. The phosphate concentration dropped from 5.12 to 0.2 mg/L and 5.79 to 0.14 mg/L for non-sterilized and sterilized water, respectively. In both cases, the nutrient removal efficiency was observed to be approx. 97%. High phosphate removal efficiency maybe attributed to the fact that the algae and bacterial strain is highly tolerant toward increasing phosphate concentration, and hence removal is due to the algal metabolic uptake. The initial wastewater characterizations had denoted high concentrations of ammonium nitrogen. *Scenedesmus* sp. has potential to remove ammonium efficiently from the medium of growth. Ammonium reduction occurs due to a phenomenon called ammonia stripping, which is caused due to the presence of high urea concentration. The algal-bacteria consortium required supplementation of urea to support its growth. Thus along with the urea concentration and algal uptake, the ammonium removed efficiency [36]. Moreover, the bacteria being a nitrifying and ureolytic bacteria, the ammonium utilization was higher in the algae-bacteria consortia than the algae. Table 4 shows a nutrient reduction efficiency of 91 and 93.5% for sterilized and non-sterilized wastewater, respectively. Critically, the nitrate concentration was also decreased effectively by 61 and 64.5%, respectively, for sterilized and non-sterilized wastewater. Removal of TSS and TDS is an essential parameter for the wastewater characterization. The consortium effectively reduced the TSS and the TDS of the non-sterilized wastewater by 95 and 97% and 93.1 and 95.65 for sterilized wastewater. In a report by Hena et al. [32], the TDS had been reduced by the consortium by 59% approx. The present study reports TDS value higher than literature, and thus, *Scenedesmus* sp. is a highly potential algae

with the capability to reduce TDS from the wastewater, thus enhancing environ-
mental sustainability. The ability of consortium to reduce the hardness and alkalinity
enhanced the water quality. The consortium reduced the alkalinity and hardness by
77% and 93.4%, respectively, in non-sterilized wastewater. Similarly, in sterilized
wastewater, the consortium was able to reduce the alkalinity and hardness by 76.8 and
92.5%, respectively. The alkalinity is attributed by the presence of carbon dioxide,
carbonate, and bicarbonate ions. Microalgae in the consortium require CO_2 during
the photosynthesis thus reducing the level, and hence, the alkalinity also reduces.
Studies of equivalent observation were demonstrated by Nadersha et al. [37] where
indigenous microalgae cultivation (*Chlorella* sp. and indigenous bacteria) removed
86.4% of alkalinity. Wang et al. [38] reported a decrease in hardness of RWW by
84% when *Scenedesmus* sp. LX1, *Chlorella* sp. (ZTY4) were grown in domestic
wastewater. From the results observed in Table 2, it is demonstrated that there has
been a significant nutrient removal by the consortia which was considerably higher
than the removal by the monoculture algae.

Table 4 Nutrient removal by consortia

Parameters	Initial influent RWW		Final effluent RWW		Nutrient removal (%)	
	Sterilized rubber wastewater	Non-sterilized rubber wastewater	Sterilized rubber wastewater	Non-sterilized rubber wastewater	Sterilized rubber wastewater	Non-sterilized rubber wastewater
pH	4.17	4.25	7.45	7.59	–	
COD	1428	1489	71.4	49.137	95	96.7
BOD	104.5	110.1	20.1	16.5	84	85.01
Alkalinity (mg/L)	1492	1504	345	344.1	76.8	77
Hardness (mg/L)	310	320	23	21.1	92.5	93.4
TSS (mg/L)	0.0058	0.0063	0.0004	0.00031	93.1	95
TDS (mg/L)	0.0046	0.0051	0.00021	0.00015	95.65	97
Phosphate (mg/L)	5.12	5.79	0.2	0.14	96.5	97.6
Nitrate (mg/L)	7.8	8.32	0.5	0.55	68	69.6
Ammonium nitrogen (mg/L)	203.71	210	18.34	13.65	91	93.5
Urea (mg/L)	1.05	1.05	0.08	0.074	92.3	92.9

4 Conclusions

In this study, the RWW is used as a cheap source of nutrient for the growth of the algae, *Scenedesmus* DDVG I. The study focuses on designing an algae-bacteria consortia for enhanced biomass production. The Scenedesmus DDVG I with *Bacillus* sp. 0S26, *Bacillus cereus* 0S36 consortia with biomass productivity 1.15 g/L. d and 41% lipid content had the best biofilm formation and maximum harvesting efficiency. Additionally, the consortia was able to treat the wastewater by removing certain nutrients. The consortia successfully removed approximately 95% COD, 84% BOD. It also removed phosphate concentration by 97.6% and ammonium concentration by 93.5%. The overall results showed that the algae-bacteria consortia system has been successful in enhanced biomass production, efficient harvesting. The consortia also provided an alternative technology of remediating wastewater. In future, large-scale cultivation of the algae-bacteria consortia can be targeted while focusing on the techno-economic aspects.

Declaration of Competing Interest The authors declare no competing interests.

Author Contributions Angana Chaudhuri: Conceptualization, Investigation, Methodology, Formal analysis, Writing—Original Draft, Curation of Data, Writing—Editing & Reviewing, Visualization. **Nongmaithem Debeni Devi**: Formal analysis, Review & Editing, Writing-original Draft. **Dipesh Kumar**: Formal analysis, Resources, Review & Editing. **Surajit Das**: Supervision, Curation of Data and Conceptualisation, Reviewing & Edit, Validation, Visualization. Authors approved the final version of manuscript. **Vaibhav V. Goud**: Supervision, Conceptualization, Curation of Data, Edit & Review, Validation and Visualization. The final version of manuscript has been approved by all authors.

References

1. Das, P. P., Sharma, M., & Purkait, M. K.: Recent progress on electrocoagulation process for wastewater treatment: A review. Sep. Purif. Technol. **292**, 121058 (2022)
2. Nitsos, C., Filali, R., Taidi, B., Lemaire, J.: Current and novel approaches to downstream processing of microalgae: a review. Biotechnol. Adv. **45**, 107650 (2020)
3. Samanta, N. S., Das, P. P., Mondal, P., Changmai, M., & Purkait, M. K.: Critical review on the synthesis and advancement of industrial and biomass waste-based zeolites and their applications in gas adsorption and biomedical studies. J. Indian Chem. Soc. **99**, 100761 (2022)
4. Xu, X., Gu, X., Wang, Z., Shatner, W., Wang, Z.: Progress, challenges and solutions of research on photosynthetic carbon sequestration efficiency of microalgae. Renew. Sustain. Energy Rev. **110**, 65–82 (2019)
5. Haldar, D., & Purkait, M. K.: Thermochemical pretreatment enhanced bioconversion of elephant grass (Pennisetum purpureum): insight on the production of sugars and lignin. Biomass Convers. Biorefin. **12**, 1–14 (2020)
6. Ekendahl, S., Bark, M., Engelbrektsson, J., Karlsson, C.A., Niyitegeka, D., Strömberg, N.: Energy-efficient outdoor cultivation of oleaginous microalgae at northern latitudes using waste heat and flue gas from a pulp and paper mill. Algal Res. **31**, 138–146 (2018)
7. Chen, J., Wang, Y., Benemann, J.R., Zhang, X., Hu, H., Qin, S.: Microalgal industry in China: challenges and prospects. J. Appl. Phycol. **28**, 715–725 (2016). https://doi.org/10.1007/s10811-015-0720-4
8. Gayen, K., Bhowmick, T.K., Maity, S.K.: Sustainable Downstream Processing of Microalgae for Industrial Application. CRC Press (2019)
9. Xu, K., Zou, X., Xue, Y., Qu, Y., Li, Y.: The impact of seasonal variations about temperature and photoperiod on the treatment of municipal wastewater by algae-bacteria system in lab-scale. Algal Res. **54**, 102175 (2021)
10. Sinha, S.K., Gupta, A.: Acclimatization strategy of *Chlamydomonas* sp. BTA 4152 for growing in natural rubber latex processing wastewater. Int. J. Sci. Res. **4**, 1080–1085 (2015)
11. Epa, U.S.: United States environmental protection agency. Quality Assurance Guidance Document-Model Quality Assurance Project Plan for the PM Ambient Air, 2 (2001)
12. Haldar, D., & Purkait, M. K.: Micro and nanocrystalline cellulose derivatives of lignocellulosic biomass: A review on synthesis, applications and advancements. Carbohydr. Polym. **250**, 116937 (2020)
13. Das, P. P., Mondal, P., Sinha, A., Biswas, P., Sarkar, S., & Purkait, M. K.: Treatment of steel plant generated biological oxidation treated (BOT) wastewater by hybrid process. Sep. Purif. Technol. **258**, 118013 (2021)
14. Haldar, D., & Purkait, M. K.: A review on the environment-friendly emerging techniques for pretreatment of lignocellulosic biomass: Mechanistic insight and advancements. Chemosphere, **264**, 128523 (2021)
15. Su, M., Dell'Orto, M., Scaglia, B., D'Imporzano, G., Bani, A. and Adani, F.: Growth performance, biochemical composition and nutrient recovery ability of twelve microalgae consortia isolated from various local organic wastes grown on nano-filtered pig slurry. Molecules **27**(2), 422 (2022)
16. APHA,: Standard Methods for the Examination of Water and Wastewater, 21st edn, American Public Health Association/American Water Works Association/Water Environment Federation, Washington DC (2005)
17. Sharma, M., Das, P. P., Sood, T., Chakraborty, A., & Purkait, M. K.: Ameliorated polyvinylidene fluoride based proton exchange membrane impregnated with graphene oxide, and cellulose acetate obtained from sugarcane bagasse for application in microbial fuel cell. J. Environ. Chem. Eng. **9**, 106681 (2021)
18. Devi, N.D., Tiwari, R., Goud, V.V.: Cultivating *Scenedesmus* sp. on substrata coated with cyanobacterial-derived extracellular polymeric substances for enhanced biomass productivity: a novel harvesting approach. Biomass Convers. Biorefinery, 1–13 (2021)

19. Wang, L., Addy, M., Lu, Q., Cobb, K., Chen, P., Chen, X., Liu, Y., Wang, H., Ruan, R.: Cultivation of *Chlorella vulgaris* in sludge extracts: nutrient removal and algal utilization. Biores. Technol. **280**, 505–510 (2019)
20. Proom, H., Knight, B.C.J.G.: The minimal nutritional requirements of some species in the genus *Bacillus*. Microbiology **13**(3), 474–480 (1955)
21. Bligh, E.G., Dyer, W.J.: A rapid method of total lipid extraction and purification. Can. J. Biochem. Physiol. **37**(8), 911–917 (1959)
22. Mahesh, R., Naira, V.R., Maiti, S.K.: Concomitant production of fatty acid methyl ester (biodiesel) and exopolysaccharides using efficient harvesting technology in flat panel photo-bioreactor with special sparging system via Scenedesmus abundans. Bioresour. Technol. **278**, 231–241 (2019)
23. Khoo, K.S., Chia, W.Y., Chew, K.W., Show, P.L.: Microalgal-bacterial consortia as future prospect in wastewater bioremediation, environmental management and bioenergy production. Indian J. Microbiol. **61**(3), 262–269 (2021)
24. Zhu, L.D., Takala, J., Hiltunen, E., Wang, Z.M.: Recycling harvest water to cultivate *Chlorella zofingiensis* under nutrient limitation for biodiesel production. Biores. Technol. **144**, 14–20 (2013)
25. Nayak, M., Karemore, A., Sen, R.: Performance evaluation of microalgae for concomitant wastewater bioremediation, CO_2 biofixation and lipid biosynthesis for biodiesel application. Algal Res. **16**, 216–223 (2016)
26. Wang, R., Xue, S., Zhang, D., Zhang, Q., Wen, S., Kong, D., Yan, C., Cong, W.: Construction and characteristics of artificial consortia of *Scenedesmus obliquus*—bacteria for *S. obliquus* growth and lipid production. Algal Res. **12**, 436–445 (2015)
27. Chandrashekharaiah, P.S., Gupte, Y., Sarkar, P., Prasad, S., Sanyal, D., Dasgupta, S., Banik, A.: Algae-bacterial aquaculture can enhance heavy metals (Pb^{2+} and Cd^{2+}) remediation and water re-use efficiency of synthetic streams. Resour. Conserv. Recycl. **180**, 106211 (2022)
28. Wang, Y., Gong, X., Huang, D., Zhang, J.: Increasing oxytetracycline and enrofloxacin concentrations on the algal growth and sewage purification performance of an algal-bacterial consortia system. Chemosphere **286**, 131917 (2022)
29. Choudhary, P., Prajapati, S.K., Kumar, P., Malik, A., Pant, K.K.: Development and performance evaluation of an algal biofilm reactor for treatment of multiple wastewaters and characterization of biomass for diverse applications. Biores. Technol. **224**, 276–284 (2017)
30. Posadas, E., García-Encina, P.A., Soltau, A., Domínguez, A., Díaz, I., Muñoz, R.: Carbon and nutrient removal from centrates and domestic wastewater using algal–bacterial biofilm bioreactors. Biores. Technol. **139**, 50–58 (2013)
31. Gou, Y., Yang, J., Fang, F., Guo, J., Ma, H.: Feasibility of using a novel algal-bacterial biofilm reactor for efficient domestic wastewater treatment. Environ. Technol. **41**(4), 400–410 (2020)
32. Hena, S., Fatimah, S., Tabassum, S.: Cultivation of algae consortium in a dairy farm wastewater for biodiesel production. Water Resour. Ind. **10**, 1–14 (2015)
33. Arora, N., Jaiswal, K.K., Kumar, V., Vlaskin, M.S., Nanda, M., Pruthi, V., Chauhan, P.K.: Small-scale phyco-mitigation of raw urban wastewater integrated with biodiesel production and its utilization for aquaculture. Biores. Technol. **297**, 122489 (2020)
34. Safonova, E., Kvitko, K.V., Iankevitch, M.I., Surgko, L.F., Afti, I.A., Reisser, W.: Biotreatment of industrial wastewater by selected algal-bacterial consortia. Eng. Life Sci. **4**(4), 347–353 (2004)
35. Mishra, S., Mohanty, K.: Comprehensive characterization of microalgal isolates and lipid-extracted biomass as zero-waste bioenergy feedstock: an integrated bioremediation and biorefinery approach. Biores. Technol. **273**, 177–184 (2019)
36. Tam, N.F.Y., Wong, Y.: Effect of ammonia concentrations on growth of *Chlorella vulgaris* and nitrogen removal from media. Biores. Technol. **57**(1), 45–50 (1996)
37. Nadersha, S., Hassan, A.A.: Biodesalination and treatment of raw hypersaline produced water samples using indigenous wastewater algal consortia. Desalination **528**, 115638 (2022)
38. Wang, X.X., Wu, Y.H., Zhang, T.Y., Xu, X.Q., Dao, G.H., Hu, H.Y.: Simultaneous nitrogen, phosphorous, and hardness removal from reverse osmosis concentrate by microalgae cultivation. Water Res. **94**, 215–224 (2016)

Assessment of Water Quality Parameters of Three Tributaries of the Brahmaputra River System Flowing Along Urban Settlements and Industrial Clusters with Special Reference to Their Respective Catchment Characteristics

Simanta Goswami, Mridul Dev Adhikary, Ankuran Pathak, and Arup Kumar Misra

1 Introduction

The Northeast Region is endowed with abundant water resources comprising a dense network of rivers, streams, and wetlands. Brahmaputra and Barak are the two major rivers of the region which have been joined by tributaries in abundance.

In Assam, the Brahmaputra basin covers an area of around 70,634 km^2 and has numerous tributaries. Although large parts of the Brahmaputra catchment is covered by pristine forests and vegetation, several tributaries flowing through urban and industrial stretches have turned into causes of concern due to increasing pollution and degradation of water quality.

The Pollution Control Board Assam has been mandated under section 17 (c) of The Water (Prevention and Control of Pollution) Act, 1974, to collect and disseminate information relating to water pollution and the prevention, control or abatement thereof. Accordingly, The Board monitors water quality in 206 locations across the state of Assam. Out of which 139 locations comprises surface water sources which includes rivers, creeks, ponds, lakes, wetlands, etc., and 67 locations from ground water sources [1].

S. Goswami · M. D. Adhikary (✉) · A. Pathak · A. K. Misra
Pollution Control Board, Guwahati, Assam, India
e-mail: madhikary.pcba@gmail.com

In this study, emphasis has been laid on the status of water quality of the tributaries namely Mora Bharali, Digboi, and Bega Rivers. These three rivers have been identified considering the fact that these rivers flow through urban agglomerations and industrial clusters. The assessment has been made in terms of Water Quality Index (WQI) parameters namely pH, Biochemical Oxygen Demand (BOD), Dissolved Oxygen (DO) and Fecal Coliform following standard methods [2].

2 Water Quality Assessment

For the purpose of this study, the water quality data as analyzed by the Board has been taken into consideration for a period of one year, i.e., from January 2021 to December 2021 with respect to the aforementioned parameters. Subsequently, assessment of the data has been undertaken in order to understand the seasonal variations in water quality and correlate it with the impact of increasing urbanization and industrialization in their respective catchment areas.

2.1 Bega River

Bega River originates from the foothills of Bhutan Himalayas and flows from north to south before confluence with Brahmaputra River.

The river Bega flows through the heart of Mangaldoi Town, the district headquarter of Darrang district. During its course in the plain, it is joined by another tributary called Mangaldoi River and then flows to the west after passing through Mangaldoi Town and then to the southwest till it joins the Noanadi and later, stream of the Brahmaputra river after a complex course of about 9 km.

It has been observed from Table 1 that there is significant variation in the BOD values and fecal coliform count. Moreover in multiple occasions, the BOD values have exceeded the permissible limit which is ≤ 3 mg/l and similarly in case of fecal coliform count in multiple instances have been observed to exceed the desirable limit of 500 MPN/100 ml. It may also be mentioned that the maximum permissible limit for fecal coliform is 2500 MPN/100 ml (Fig. 1).

2.1.1 Brief Analysis of the Contributing Factors in Terms of Major Pollutants in the Bega Catchment Area

The river Bega flows through the urban settlements of Mangaldoi Town which has a population of around 26,000(as per 2011 census). More than 3 MLD of sewage is being generated in the catchment which eventually drains into the Bega River without adequate treatment. Further with rapid increase in population, the quantity of sewage has increased considerably. Untreated sewage is known to have high organic

Table 1 Water quality status of Bega River with respect to WQI

River Bega MG Road, Mangaldoi (Lat: 26.407684, Long: 92.076405) Year: 2021

Sampling month	DO (mg/L)	pH	BOD (mg/L)	Fecal coliform (MPN/100 ml)	Total coliform (MPN/100 ml)
Jan	5.6	7.7	2.2	730	2000
Feb	4.7	7.4	2.6	910	2000
Mar	5.4	7.2	2.8	360	1500
Apr	5	7.3	2.4	730	1500
Jul	5.6	7.2	2.5	720	2100
Aug	5.5	7.3	3.2	910	2000
Sep	5.8	7.4	3.8	1100	2100
Oct	5.8	7.5	3.7	910	2000
Nov	5	7.5	3.8	910	2000
Dec	5.2	7.8	3.9	1100	2700
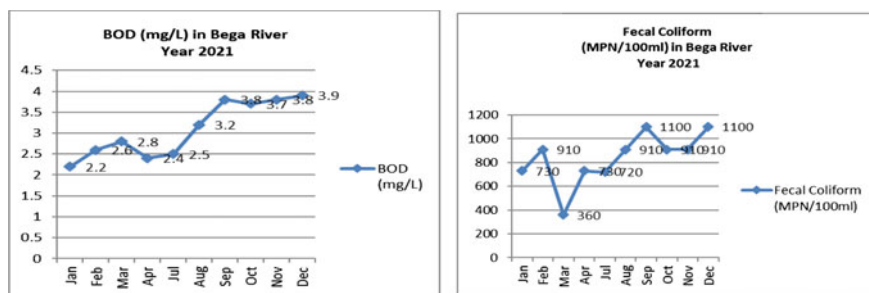
Fig. 1 Trends in BOD and fecal coliform in Bega water samples

load which consequently exerts a significant Biochemical Oxygen Demand in the receiving water body. Moreover, it increases the bacteriological load as evident from the above table.

Apart from sewage, it has been quantified that around 33.5 KLD of industrial effluent finds its way to the river. Although most of them have installed effluent treatment plants, the likelihood of discharge of inadequately treated waste water from these industries cannot be ruled out (Fig. 2).

2.2 Mora Bharali

Mora Bharali River is an abandoned channel by the river Jia Bharali. Sometimes prior to 1824 the Jia Bharali River abandoned this channel and followed the more or less straight course up to its confluence with the Brahmaputra. Subsequently, the
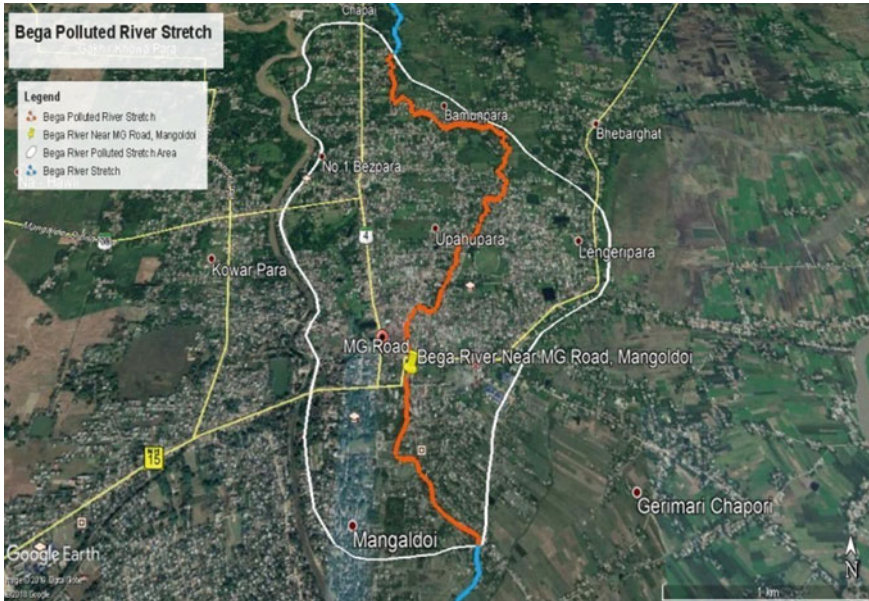
Fig. 2 Landuse pattern of Bega catchment area
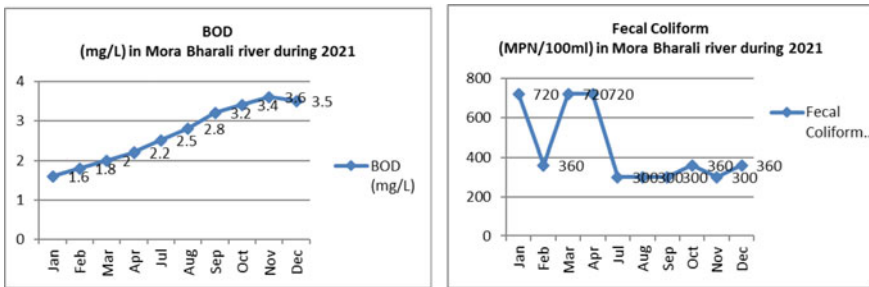
Fig. 3 Trends in BOD and fecal coliform in Mora Bharali water samples

Mora Bharali channel got silted up and it is now carrying hardly any flow except in the stretch between Bamgaon and Kakokuli (Fig. 3; Table 2).

2.2.1 Brief Analysis of the Contributing Factors in Terms of Major Pollutants in the Mora Bharali Catchment Area

The river flows through Tezpur which is a major urban center with a population of around 282,000 (as per 2011 census). Around 30 MLD of sewage is generated

Table 2 Water quality status of Mora Bharali River with respect to WQI

River Mora Bharali at Tezpur, Assam
(Lat: 26.848745, Long: 92.840375) Year: 2021

Sampling month	DO (mg/L)	pH	BOD (mg/L)	Fecal coliform (MPN/100 ml)	Total coliform (MPN/100 ml)
Jan	4.8	7.5	1.6	720	1400
Feb	4.8	7.2	1.8	360	910
Mar	6.8	7.4	2	720	2000
Apr	4.6	7.2	2.2	720	1400
Jul	5.4	7	2.5	300	1100
Aug	5	7.3	2.8	300	730
Sep	4.5	7.1	3.2	300	1100
Oct	5	7.4	3.4	360	720
Nov	5	7.3	3.6	300	1100
Dec	4.5	7.6	3.5	360	1500

from Tezpur Town, a portion of which finds its way into the river Mora Bharali. Contribution of industries pertaining to the pollutant load is to be quantified.

Considering the proximity of municipal solid waste dumpsite of Tezpur Town, there is a likelihood of contaminated runoff from the dumpsite contributing to the Pollutant concentration in the river Mora Bharali (Fig. 4).

Fig. 4 Landuse pattern of Mora Bharali catchment area
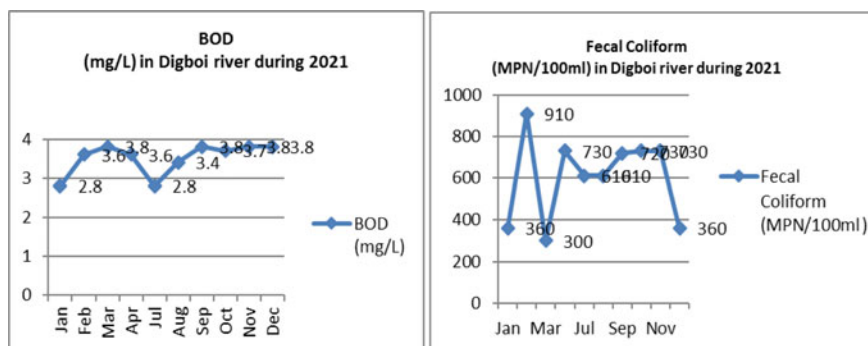
Fig. 5 Trends in BOD and fecal coliform in Digboi water samples

2.3 Digboi River

The Digboi River is a small river which is a sub-tributary of the Burhi Dihing River and crisscrosses the Dihing Reserve Forest. The river has its origin at upper Dihing Reserve Forest and flows toward the Tipling River. The river after flowing through the Tipling River, finally turns toward Buridihing and then confluence with the river. It has its entrance point to the Digboi Town at Ram Nagar Bridge, Digboi. The catchment of the river extends to a number of villages, Lakhipathar Reserve Forest, Oil collecting stations and paddy fields.

The river flows for about 32 km from here to its confluence point flowing along Bamunigaon, Ushapur and falls in the river Burhi Dihing, which is the largest tributary of the Brahmaputra. It is a perennial river and carries water throughout the year (Fig. 5; Table 3).

2.3.1 Brief Analysis of the Contributing Factors in Terms of Major Pollutants in the Digboi Catchment Area

Digboi Town and Digboi Oil Township are the major localities situated on the bank of the Digboi River. The approximate total population of the Digboi Town and Digboi Oil Town is 34,462 as per Census 2011 with 7508 numbers of households. The river receives storm water along with municipal sewage by two drains coming from Digboi Township at Borbil no.3 at a distance of 1 km from Ram Nagar Bridge, Digboi. Around 5 MLD of sewage generated from these settlements discharges into the river Digboi. Apart from sewage around 9 MLD of industrial effluent is generated by industries located in the catchment of the river, the major industry being Digboi refinery. Although the industries have been reported to be equipped with adequate Effluent Treatment plant, there is a likelihood of contaminated runoff from industrial premises discharging into the river (Fig. 6).

Table 3 Water quality status of Digboi River with respect to WQI

River Digboi at Lakhipathe, reserve forest, Digboi, Assam
(Lat: 27.381964, Long: 95.622819) Year: 2021

Sampling month	DO (mg/L)	pH	BOD (mg/L)	Fecal coliform (MPN/100 ml)	Total coliform (MPN/100 ml)
Jan	3.6	7.2	2.8	360	1400
Feb	4.5	7.4	3.6	910	2000
Mar	2.6	7.2	3.8	300	1100
Apr	7	7.4	3.6	730	2000
Jul	3.8	7.8	2.8	610	2000
Aug	4.2	7.6	3.4	610	2000
Sep	5.8	7.7	3.8	720	1400
Oct	3.3	7.6	3.7	730	1500
Nov	7.8	7.7	3.8	730	2000
Dec	2.6	7.4	3.8	360	1100
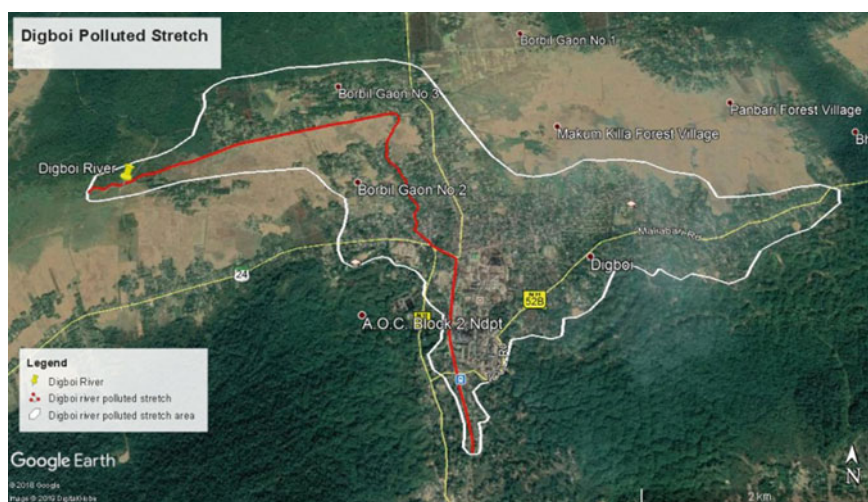
Fig. 6 Landuse pattern of catchment area of Digboi River

3 Proposed Pollution Abatement Strategies for Rejuvenation of the Rivers

From the assessment of water quality of the rivers and correlation observed with the landuse pattern of the catchment areas of the respective rivers, it implies that the primary contributor of pollutant load in all the rivers is untreated sewage.

Untreated trade effluent from industrial and commercial establishment and contaminated runoff from unscientific garbage disposal sites can be considered as secondary contributors of contaminants in these river systems. However, detailed source apportionment studies including analysis of water quality of streams and drains discharging into the rivers have to be conducted in order to quantify the pollutant load contributed by each of the sources.

Based on the above observations, the following abatement measures are suggested in order to bring the Water Quality Index (WQI) parameters within desirable limits and subsequently preserve the wholesomeness of water flowing in the water bodies.

(a) **Sewage treatment plants (STPs)**: None of the urban settlements in the catchment areas of these rivers have any common sewage treatment plant. Adequately designed STPs equipped with primary, secondary, and tertiary treatment systems have to be installed in suitable locations. A sewerage network starting from every single source of sewage generation draining into the STP inlet has to be established.

(b) **Decentralized Grey water recycling systems**: In order to reduce the burden on common sewage treatment plants, a policy framework has to be chalked out, in order to promote grey water recycling (GWR) systems, for installation in individual households and residential colonies. GWR can be an effective tool to arrest contaminants at the source of generation and subsequently preserve fresh water resources. Including GWR as mandatory requirement in building byelaws can be an effective step in towns and cities with less space available for common STPs.

(c) **Performance evaluation of Effluent Treatment Plants**: Effluent treatment plants installed and operated by industries located in the catchment have to be continuously monitored in order to ascertain if these ETPs are adequate in terms of concentration of pollutants in the treated effluent. Accordingly, necessary directives have to be issued in case of any violations observed.

(d) **Scientific Municipal Solid Waste treatment and disposal systems**: Contaminated runoff and leachate from MSW dumping grounds usually find its way into water bodies in their vicinity. Provisions for Engineered Secured Landfills equipped with leachate treatment systems and liners of impermeable membranes have to be incorporated in order to prevent pollution of the waterbodies along urban settlements.

(e) **Innovative Environmental Management Practices (EMPs)**: Research and development in the field of environmental engineering and emerging innovative environmental management practices have created a conducive ecosystem for preservation of our environment in general and our rivers in particular. Floating Treatment Wetlands (FTWs), in situ bioremediation of contaminated rivers beds and wetlands and other emerging natural systems for waste water treatment can play an important role in abatement of pollution in water bodies and subsequently act as tools for remediation to achieve their natural state.

4 Conclusion

Rivers are the lifeline of human civilization. Wholesomeness of the water quality in a river has a profound impact on the quality of life of the inhabitants residing along it. Therefore, it is the primary duty of the people in general and the statutory authorities in particular to undertake all necessary steps to check contamination of the rivers and water bodies. As an integrated part of the ecosystem, human beings should pledge not to engage in activities that adversely impact the rivers. And with the growing awareness among the common masses and sincere intent to preserve the environment, it is utterly possible that the pristine nature of our rivers shall be restored for our future generation.

References

1. National Water Quality Monitoring Programme (NWMP) sponsored by Central Pollution Control Board, New Delhi
2. APHA, Standard methods for examination of water and waste water by American Public Health Association, American Water Works Association

Environment Pollution and Remediation

Bioremediation of Oil Spill Cleanup: Case Studies of Two Major Oil Spills

Bikashita Shyam, Ranjan Phukan, and Chinmoy Das

1 Introduction

The spill of oil on land or water surface mostly at sea and freshwater bodies whether accidentally or intentionally sometimes is called oil spillage. It happens when a significant amount of hydrocarbons seep into the environment when moving oil through pipelines, tanks, etc., or when there are unforeseen, unexpected incidents such as drilling failures, kicks followed by blowouts, and improper waste disposal techniques [1, 2]. Moreover, sometimes spills may also occur due to natural processes such as earthquakes and submarine seeps, and also each year some amount of crude oil is discharged from natural seeps. In addition, spillage may also occur during the consumption, storage, and usage of oil products such as in fueling an aircraft, gas stations, and truck stops. The consequences of oil spills on the environment are huge and unavoidable.

The ecology and health of mankind are at risk from oil spills in land and marine areas [3]. When oil is spilled on land, it hampers the environment including its flora and fauna as shown in Fig. 1. This can cause water pollution, can have explosions thereby causing air pollution, and even soil pollution, destroying the habitat of animals on both land and marine and having a huge impact on the ecosystem thereby the economy of that particular country. The consequences of oil spills on the environment are already known by the various devastating accidents that occurred in history, which should not repeat again due to carelessness or human error. As a

B. Shyam (✉) · R. Phukan · C. Das
Department of Petroleum Technology, Dibrugarh University, Dibrugarh, Assam, India
e-mail: bikashitashyam2106@gmail.com

R. Phukan
e-mail: r.phukan@dibru.ac.in

C. Das
e-mail: chinmoydas2107@gmail.com

result, a supported logistical and skilled staff is required to respond appropriately in a timely manner following the occurrence of oil spills [4].

When oil is spilled into water bodies, it harms the aquatic organisms, deep ocean plants, coral reefs, etc., thereby damaging the underwater ecosystem and the overall food chain (Fig. 2). Marine animals are also vulnerable to spillages as their body and skin get affected by the contact of oil and also the ingestion of oils causes various toxicity and health problems to these organisms. Since the fish and other sea organisms we consume get contaminated, the intake of these will eventually cause various health problems to human beings.

Exxon Valdez in 1987, when over 11 million gallons of oil were spilled [7], and Deepwater Horizon in the year 2010, where roughly 4.9 million barrels of oil were leaked, are two noteworthy oil spill events that are remembered in history as being particularly harmful to the marine environment. Additionally, there was the 2002

Fig. 1 Damaged mangrove forest caused by oil spillage [5]

Fig. 2 Impact of oil spill on creatures [6]

prestige disaster and the 1978 Amoco Cadiz oil leak [8]. Among the condensate oil spill accidents, notable ones happened in Uniacke G-72 oil drilling, Nova Scotia, 1984, Montara offshore oil field, Timor Sea, 2009, Elgin production platform, North Sea, 2012 MT Sanchi, East China Sea, 2018 and the most recent one in Baghjan, well no. 5, Duliajan, Assam, 2020.

There are various methods to treat oil spillages such as physical or mechanical, chemical, and biological methods. Physical methods include skimmers and booms, which are some floating devices that prevent oil spills. Skimmers are devices that, like a vacuum cleaner, suck up oil from the ocean surface that is restricted by booms. Chemical approaches employ emulsifiers, dispersants, and other chemicals. Oil spills are treated using dispersants to reduce the size of the droplets. Incorporating microorganisms, nutrients, or oxygen to boost bacterial growth and, as a result, biodegradation of the oil spill are examples of biological techniques [8]. Following its successful use in the Exxon Valdez oil disaster, bioremediation has gained attention as a viable solution for the cleaning of oil spills. Compared to physicochemical methods, bioremediation is a more environmentally friendly technique that is also more inexpensive. Both bioaugmentation and biostimulation involve refilling the polluted environment with nutrients and/or introducing natural or genetically modified microorganisms to a polluted site. These approaches of removing oil spills have primarily been explored in the laboratory and to a minor extent in actual circumstances.

Several regulations, laws, and directives involve oil spill prevention, response, handling, and recovery. Accidental oil spills are, nevertheless, unavoidable, and governments should be prepared to respond appropriately in the event of a leak. The US Environmental Protection Agency has made oil spill prevention and preparation one of its key goals (US EPA 2013). Oil spills can be remedied using a variety of methods, and bioremediation is the greener approach among them, and it is the subject of this report.

1.1   History of Oil Spill Accidents

The first oil spill accident occurred on November 30, 1903, when 1300 tonnes of oil leaked at Port Philip Bay, Victoria, Australia, marking the beginning of the oil spill era. Another incident occurred in 1907 when 7400 tonnes of paraffin oil poured into the sea and along the British shoreline [9].

The Amoco Cadiz oil spill, which contaminated more than 320 km of shoreline by releasing over 227,000 tonnes of crude oil into the sea, was another oil leak incident that happened in 1978. On March 24, 1989, the Exxon Valdez oil tanker collapsed on Bligh Reef in William Sound. Oiling was most intense on the shorelines of Prince William Sound islands which is shown in Fig. 3.

The Deepwater Horizon (DWH) catastrophe that occurred in the Gulf of Mexico in 2010 as a result of a drilling rig explosion is among the most well-known oil spills. More than 700,000 tons of crude were released into the Atlantic Ocean as a result of the catastrophe [9]. As a result of this occurrence, the biodiversity of the living

Fig. 3 Exxon Valdez oil spillage [10]

Fig. 4 BP Deepwater horizon oil spill [11]

organisms was diminished. Cleaning up after the catastrophe was expected to cost tens of billions of dollars. This incident may rank as the major oil leak mishap in recorded history which is shown in Fig. 4 (Table 1).

1.2 Remediation Method of Oil Spillage

The greater the probability of preventing and stopping contamination, the faster the response to the spill [12]. So, the main reason for the oil spill response should be that it must focus on how to remedy the negative things that have already occurred. So, anyhow the spread of this must be stopped, and also the source must not keep on continuing the spill. Also, when there occurs such horror then we must make use of

Table 1 Observation between the Exxon Valdez oil spill and the BP deepwater horizon oil spill

	Exxon Valdez oil spill	BP deepwater horizon blowout
Reason for the occurrence of oil spill	It happened in the year 1989 on March 24, which flooded the shorelines of Prince William Sound islands after the oil tanker of Exxon Valdez turned over in the ocean	It happened on April 20, 2010, when high-pressure oil and gas leaked out from the exploration well and the rig got caught on fire, which then got destroyed in the next two days
Gallons of oil spilled	11 million gallons	4.9 million gallons
Type of oil spilled	North slope Heavy oil	Light Louisiana Oil
API of oil	29	35.2
Impact on living beings, water, and land surface	Life in Alaska was impacted, by various marine creatures, flora, fauna, and livelihood of the people near it, etc	Killed thousands of marine creatures, flora fauna, and their habitat, destroyed deep-sea coral communities, and a reduction in planktonic grazers led to phytoplankton blooms etc
Remediation method used	Bioremediation is extensively used, mostly biostimulation where fertilizers containing nitrogen nutrients were used, and bioaugmentation, various microorganisms such as species of bacteria, fungi, etc., are used	Although chemical subsurface dispersants such as COREXIT 9500 were used. Bioremediation or the hidden microorganisms have played a crucial role in the cleanup
The success of bioremediation	1. A field test revealed that fertilizer increased the rate of degradation when it was added to the microorganisms that feed on hydrocarbons, resulting in the decrease of the spilled hydrocarbons of up to 1.2 percent in a single day 2. Even though these locations had been intensive to moderately oiled in 1989. In 2001 and 2003, the NOAA conducted a test and found out that 97.8% of the dug pits have no traces of oil or minor remains if it was found	In the deep marine cloud of scattered oil, bacterial activity was found which was observed through RNA microarray, and this clearly signifies that microbial degradation or the microorganisms that feed on hydrocarbons are responsible for the decrease in a large portion of the hydrocarbon (PAHs) though it was not seen through naked eyes

the mechanical spill clearance equipment which will be handy and clear the oil spill [13].

The main goal of these treatments is that we must lower the oil spill and transform it into less reactive materials that will not affect our environment much. There are a variety of remedies and reactions to oil spills, including mechanical, synthetic, and eco-friendly techniques [14].

1.2.1 Mechanical or Physical Methods

Mechanical or physical methods include the use of booms, skimmers, wiping with absorbent materials, sediment relocation and tilling, in situ burning, etc.

(a) Oil booms: It is a very easy way to manage the oil spill through the use of oil booms. Here, there are containment booms that are connected through cables, and these structures float around on the water surface. This helps the oil spill to be kept concentrated at a certain place and this way the oil spillage won't spread to a large area. But this process is disadvantageous during storms, tides, or high speeds of wind.

(b) Skimmers: These are used after the oil booms are placed. These skimmers are like vacuum cleaners that would suck the oil from the floor of the water body and helps us to recover the health of the environment back. It generally can collect most of the oil which is spilled, and this is also economically helpful to us.

(c) Sorbents: These are the elements which are used to absorb the oil spill from the water body through absorption or adsorption. This is generally done in a small area or to absorb or adsorb the traces of a large oil spill area.

(d) Burning in situ: In this process, oil on the beach is commonly burned when it comes into contact with something that burns, but this approach has the potential to pollute the air and kill plants and animals [14, 15].

(e) Sediment relocation and tiling: This is done to recover the land area of an oil spill and here the soil from the beach could be relocated to another place or also, or tilling and mixing might be done. Oil may penetrate deep into the seashore sediments as a result of tilling.

(f) Using manual labor: This method is used when manually a person needs to clean the oil spill using different tools for his help. Mechanical equipment is required to clean the oil spills, and also if we want to clean any inaccessible location. This procedure can only be used to clean up sloppy shorelines. The procedure is more cost effective since it may be carried out by untrained personnel with little training.

1.2.2 Chemical Methods

The chemical methods include the use of dispersants, demulsifiers, solidifiers, etc. Here, notably, dispersants have long been employed as a response option in many

nations. Dispersants are the first choice in some countries where harsh coastline conditions don't let us use mechanical reactions easily [14]. Chemical approaches, on the other hand, have not been widely employed in the USA because of concerns about their toxicity and long-term environmental impacts, as well as disagreements over their efficacy (US EPA 1999) [15]. Some of the chemicals used are as follows:

(a) Dispersants: These are substances that are used to break up the oil molecules that are present on the ocean floor due to the oil spill. This breakdown of the oil molecule increases the area of the oil molecule leading it to mix with water. Also, this helps the bacteria which will be used to break down the oil. But the main disadvantage is that these are chemicals that would become tarballs that would affect the marine as well as the life on the sea bed [15].
(b) Demulsifiers: These are the substances that would break the emulsion which is created from the oil and water of the ocean [14].
(c) Solidifiers: These are the substances that would polymerize the oil molecules thus not letting them spill any further or allowing them to react to different elements [14].
(d) Film-forming compounds: These are the substances that are used upon the oil spill so that they do not get attached to the shoreline substrates [14].
(e) Chemical stabilization by elastomers: Sometimes elastomers such as gelatin are used upon the oil spill so that it stops the spread of the oil spill, and then it can be chemically held for the further cleaning of the oil spill. But these elastomers are very much toxic to marine species and can suffocate them.

1.2.3 Natural Recovery

Another one is to give natural recovery to the spillages. This is employed only when the oil spillage location is very far away from the shore, then it is allowed to dry from the natural heat of the sun, and the microbial bacteria which is already present in the ocean waters will degrade the oil spill that has occurred. It's one of the most budget-friendly options. It's a time-consuming and unpredictable procedure that needs continual and vigilant supervision. It is not to be confused with "sitting around doing nothing." The location of an oil spill is a critical consideration in its cleanup.

1.2.4 Biological Method

Among the biological methods, bioremediation is proved to be effective, and it is a greener approach. Although traditional measures, such as physical removal, are the first line of defense, they seldom result in comprehensive oil spill cleaning [14]. Bioremediation is the process described as when materials are introduced to accelerate natural biodegradation. This strategy is predicated on the idea that a significant portion of oil components break down rapidly in nature. The effectiveness of remediation of spillages biologically is dependent on how we create and sustain conditions in

the polluted environment that encourage increased oil biodegradation rates. Bioaugmentation is the process in which a bacteria family is introduced to the oil spillage area and would reduce the fatalities of the oil spill; another method is biostimulation, where new bacteria families are allowed to grow along with the addition of nutrients in it [14]. In this report, mainly this bioremediation method will be discussed broadly with context to condensate oil spillage.

2 Bioremediation of Oil Spillage

Bioremediation, specifically biostimulation, has been demonstrated to improve oil biodegradation on polluted shorelines in both laboratory and field investigations. Also, biostimulation is a successful strategy, as adding hydrocarbon-degrading bacteria does not improve oil breakdown any more than just adding nutrients. Bioremediation provides several benefits over traditional approaches. For starters, bioremediation is a comparatively low-cost process. For example, the cost of bioremediating 120 km of shoreline during the Exxon Valdez spill cleanup was less than one day's physical washing expenditures.

To detoxify ecologically dangerous pollutants, bioremediation uses microorganisms such as bacteria, fungus, and plants, as well as plants. Phytoremediation is the term for when plants are utilized in the process, while mycoremediation is the term for when fungi are used. To break down pollutants, mycoremediation uses fungi's digestive enzymes. All of these bioremediation sources are aided by the addition of inorganic nutrients, which aid their development and speed up the biodegradation process.

Bioremediation is a time-consuming procedure that might take weeks or months to complete. It is a cost-effective technology, even though a comprehensive economic study of the process has yet to be completed. Other advantages of this procedure include the absence of substantial negative consequences such as the development of secondary pollutants, limited physical damage to the site, efficacy in eliminating harmful substances, simpler mechanical technology, and lower costs. A downside of this procedure is that it necessitates a unique strategy for each contaminated location and spill type [3]. In the sea, bioremediation is a less successful treatment technique, and the existing information is still rudimentary, focusing mostly on the employment of prokaryotic organisms.

The absence of standards for when and how to utilize oil bioremediation is now one of the most significant obstacles to its implementation. Although substantial research on oil bioremediation has been undertaken over the last decade, the majority of already available studies focused on assessing the use of bioremediation in the oil spills around the globe. Only a few experiments have been done and tested, and the results are quite extraordinary. There is an immediate need for a comprehensive and practical set of instructions for oil spill responders to answer issues like when to utilize bioremediation, which bioremediation agents to use, how to apply them, and how to monitor and assess the effects.

As it is evident that natural biodegradation is a very slow process, and it would take a very much time to clean up all the oil spills in time. So, bioremediation strategies are used to control the oil spill. Also, to maximize the impact of bioremediation the physical, chemical, and biological processes must be followed [16].

2.1 Bioaugmentation

Bioaugmentation is used when the main microbes which are required to degrade the petroleum products are used in the oil spills. It is generally required when the microbes which degrade petroleum products are at a low number [16].

To augment the microorganisms which have the highest capacity to feed on hydrocarbons are added to these contaminated areas. This strategy can be approached using a variety of approaches. Nonindigenous microorganisms from other contaminated settings are frequently employed to populate the target location [16]. Microbes from the target location can also be isolated, and mass has grown in bioreactors under laboratory conditions before being employed as inoculum for the target site, and it refers to circumstances where the bioaugmentation is carried out by the polluted site's natural bacteria following enrichment and then reintroduced to the site. Seeding microorganisms in a polluted location can shorten the time it takes for biodegradation to begin [16].

Bioaugmentation was successfully carried out on a minor-scale under controlled circumstances. However, it must be remembered that real-world situations may be unpredictable. Many merchants provide microbial agents that claim to speed up the biodegradation of oil. Bioaugmentation research in the lab, on the other hand, has shown mixed results. 12 commercial microorganisms were tested in the laboratory for the remediation of crude biologically from Alaska's North Slope. When compared to a nutritional control, four products demonstrated an increase in oil biodegradation after 28 days, with considerably greater alkane and aromatic breakdown rates. In several laboratory investigations, microbial seeding was shown to improve oil breakdown in saltwater but in freshwater used weathered Alaskan crude oil in shaker flask microcosms to evaluate ten different commercial microbial products to see if they could compete with indigenous populations. Thus, bioaugmentation may be beneficial in minor-scale research with well-controlled environmental conditions, but this does not imply that it will be effective in the field.

2.2 Biostimulation

Biostimulation is the use of desired microorganisms that can degrade the hydrocarbons specifically [17]. Among the nutrients, some elements such as carbon, phosphorous, and nitrogen are also used to limit the growth of the oil spill. Also, changing the temperature and aeration rate will affect the biostimulation. This is generally

done to expand the spread of the bio degraders so that the oil spills can be reduced and stopped. This is also called as nutrient enrichment. Although the biodegradation of oil improves with the use of nitrogen and phosphorus, it is seen that it also depends upon the quality of oil as well as different conditions and quantities of the microorganisms used [18].

Also, to improve the conditions further, aeration can be done where oxygen is introduced to the porous soil which then makes it more ambient for the microorganisms to grow. And this method has shown a good success percentage of 85 from the data. Since the use of nitrogen and phosphorus is detrimental to the environment so uric acid is used which can make a nice association with the hydrocarbons present. But it should be noted that the use of nitrogen has no bad effect because it is already present in the atmosphere in different strata [16].

Biodegradation normally occurs when we have an oil and water interface. As a result, the efficiency of biostimulation is determined by the nutrient content in oily sediment interstitial pore water. The nutrient content should be kept at a level that allows bacteria to grow easily. Excessive quantities of nutrients, like ammonia, can cause toxic reactions when it comes in contact with marine animals; therefore, vigilance is advised [19]. Maintaining an adequate concentration of the nutrient added to that of the oil is one of the most difficult aspects of biostimulation in oil-contaminated coastal environments. The efficiency of these nutritional items in stimulating hydrocarbon biodegradation rates has been compared in several articles.

In conclusion, data from laboratory reports have demonstrated that biostimulation in certain situations and bioaugmentation can speed up the biodegradation of oil and more generally in oceanic habitats. Under specific conditions, oxygen might be in limited quantity just like in freshwater marshlands, etc. Field assessments are still required to validate these findings, though.

2.3 Microorganisms Used for Bioremediation of Oil Spills

Certain species of bacteria, fungi, and yeasts in around 200 numbers are found to be capable to degrade the hydrocarbons containing petroleum. These microbes can be found in the atmosphere in almost all the strata, may it be land or water, and there are many hydrocarbon-degrading microorganisms [16].

Various kinds of indigenous soil bacteria have the capacity of diminishing different petroleum hydrocarbon molecules. Some bacteria can aid in the production of biosurfactants, which improve bioremediation by lowering surface tension and increasing hydrocarbon absorption. However, elements including the availability of food and the kind of oil pollutants have an effect on how quickly hydrocarbons degrade. [20].

Also, there are certain fungi that are capable of this degradation of the hydrocarbons, but they require quite an amount of time to degrade all the hydrocarbons in the pool [21]. Again, there are some yeasts as well who can do this degradation of the petroleum hydrocarbons.

3 Bioremediation Methods Used in Exxon Valdez Oil Spill

In the year 1989, the crushing of the tanker Exxon Valdez on Bligh Reef in Alaska, the US EPA, in collaboration with Exxon Corporation and the state of Alaska, launched the world's biggest oil spill bioremediation effort. Extensive field testing was undertaken at numerous locations [22]. The degradation of hydrocarbons by native microflora on the beaches of Prince William Sound was hastened by supplying fertilizers directly to the contaminated areas, according to field research done by scientists. Laboratory tests confirmed the oleophilic fertilizer's value as a nutrition source [23].

Most decision-makers involved in oil spill cleanup have a strong desire to generate "site-specific" information concerning bioremediation capability. The increase of oil degraders in oil spillage zones may not be the deciding factor for first bioremediation in other incidents due to circumstances. Even though these markers were not first employed in Alaska, they are nevertheless important to consider.

Mineralization investigations that include the total CO_2 generated, for example, can provide valuable preliminary data. The method gives quick, somewhat unambiguous time-course data that can be used to compare different biological therapy alternatives (e.g., the results of supplying nutrients). If crude oil deterioration occurs in contaminated beach, oil mineralization should release significant levels of CO_2 in comparison with an unpolluted beach. Similarly, nutrient additions such as nitrogen could accelerate the biodegradation of oil-contaminated areas (Fig. 5).

Oil mineralization rates from contaminated beach debris can be measured using biometer flask systems intended to capture CO_2 sideways which contains an alkaline solution. After that these beach oil-contaminated materials are taken in the flask, and the saltwater which is fresh is circulated to form a tidal exchange. This experiment was done after the bioremediation field demonstration. This biometer flask experiment is a technique that can become handy for short-term use at a particular site to gather the data of the oil catastrophe for its remedy. Also, this might happen that there might be certain other organic matter which may release carbon dioxide, so we must first measure the oil mineralization. Also, a radio-labeled hydrocarbon can be used along with the uncontaminated beach material to ensure that mineralization in the presence of the oil is much higher than the background.

The following are some of the most important findings and lessons acquired from these investigations:

(a) Oil biodegradation on the Prince Williams Sound shoreline was found to be limited by nutrient concentrations, mainly nitrogen, rather than a lack of hydrocarbon-degrading microorganisms. Snug Harbor's test beaches, for field demonstration of its efficiency of the bioremediation, where Inipol was used, generated some unexpected results. The beaches of the region were chosen because the oil concentration and distribution were supposed to resemble physically washed beaches.

(b) Some oleophilic, as well as some inorganic fertilizers, were used to put into a test on the field. Each was demonstrated to have varying degrees of effectiveness. So,
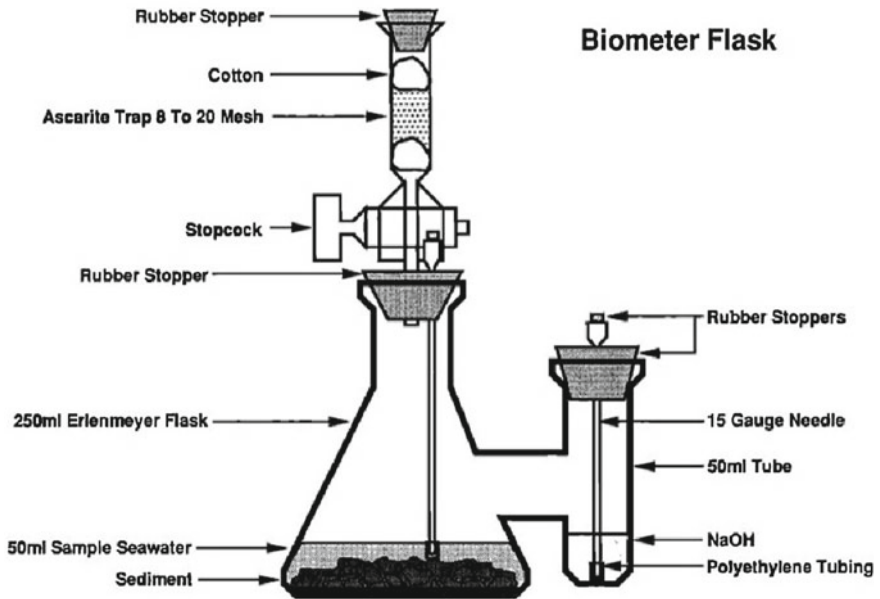
Fig. 5 Modified biometer flasks that are used to count the mineralization of hydrocarbons from contaminated areas samples [24]

nitrogen and phosphorus were used along with Inipol EAP22 and Customblen as bioremediation agents. The section of the solution looked clean and clear two weeks after fertilizer application than the untreated region which is shown in Fig. 6. However, it was later discovered that the oil on the cobble's surfaces had been removed and re-deposited within the beach's surface interstices.

Fig. 6 Snug Harbor on Knight Island, Prince William Sound Effect on test plots by using the Inipol fertilizer to remove oil spillages. We can clearly see the difference between the right to that of the left [24]

(a) It was challenging to assess the rates of oil biodegradation using existing techniques due to the heterogeneous oil dispersion on the polluted beaches. They also discovered that classic biomarkers like pristane and phytane rapidly deteriorated on Alaskan beaches. As a result of this finding, using such biomarkers to draw clear judgments about bioremediation success is no longer possible. Instead, 17(H),21(H)-hopane was utilized. Studies demonstrated that fertilizer treatment increased the rate of oil elimination by a factor of five when compared to natural attenuation, using hopane as the biomarker. This conclusion was reached based on samples obtained repeatedly from a single location.

(b) Bioremediation may improve oil biodegradation on some maritime shorelines, according to the findings of the fertilizer application following the Exxon Valdez spill. However, the Exxon Valdez study's results on bioremediation efficacy are somewhat dubious, in part because the experimental design was not wholly based on basic statistical principles. The lack of replication and the effort to determine too many parameters in a small number of studies, resulting in the confounding of diverse effects, were also major faults. As a result of the lessons learnt from the Exxon Valdez project, "post-Exxon Valdez enthusiasm" has been replaced with more scientifically sound techniques [25].

4 Oil Biodegradation and Bioremediation in British Petroleum Deepwater Horizon Oil Spill

The high-pressure oil and gas erupted from the exploratory well in the Deepwater horizon on April 20, 2010, which was located 77 km offshore in Mississippi Canyon Block 252. 11 guys sadly died as a result of the subsequent fire and explosions. The rig caught on fire and finally sank after two days. This led to the damage of the emergency shutoff equipment, including the blowout preventer (BOP). This also led to the damage of the riser pipe and the riser pipe as well as the BOP equipment leaking the oil from the bottom at multiple broken points. Finally, the well stopped production after 84 days.

This event changed the history of the world and the public and the media compared it to the Exxon Valdez oil spill, which had been the greatest disaster of oil spills till then. The Exxon Valdez disaster came into the picture because of its impact on the wildlife of Alaska as well as the long lawsuits which have been going on for a long time now. Although both the disasters were related to the oil and gas industry, they were completely different in terms of the type of oil spilled, the quantity of oil, and the natural ecosystems affected. Also, the BP Deepwater Horizon was greater in magnitude and it spilled methane (natural gas) into the ocean floor [25] (Fig. 7).

The Exxon Valdez oil spill occurred near the shore, but the Deepwater Horizon oil spill happened 80 km inside the ocean, that too, 1500 m below the surface of ocean water.

Deepwater Horizon oil that was spilled was lighter oil, so it was more biodegradable at first than that of the Exxon Valdez oil spill which had heavy crude. Also,
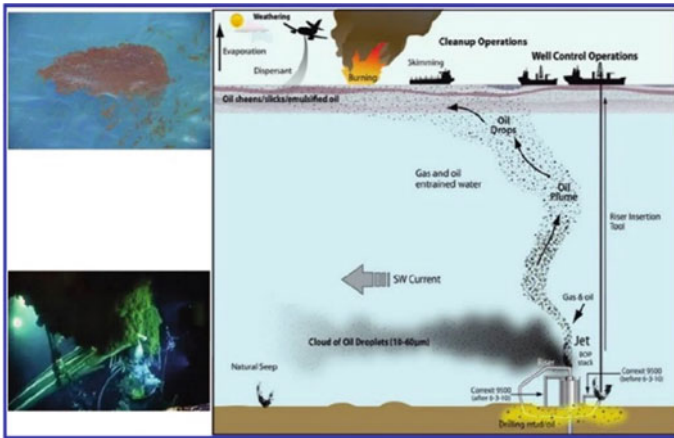
Fig. 7 Deepwater horizon oil spill effect and cleanup [25]

the habitat harmed was also different, the Exxon Valdez oil spill took place at a sub-Arctic zone and the Deepwater Horizon spill occurred in a subtropical region.

The main reason that the bioremediation technique was considered because of the oil that had seeped into the ocean beneath the surface of the water, and it was not possible by any other means to stop this spillage, and after weeks of the spill, the bioremediation was identifies as a new possible way.

At Deepwater Horizon, at a sea depth of 1500 m, COREXIT 9500, a dispersant, was put at the wellhead to decrease the environmental degradation by the oil spill. The main aim was to spread the oil underwater, and not on the surface of the ocean because this may happen that the oil might reach the shores from the surface and also many ships had been there to stop the leaks from the riser pipe and the BOP. And this injecting of the dispersant gave results within 4 h, and the leakage stopped, and the oil spills decreased [25].

Since the oil was allowed to spread underwater, at high pressure and temperature, some droplets floated to the surface and some carried away by currents up to 900–1300 m. This dispersion in the deep sea could lead to reductions in the oxygen concentrations of the ocean but did not result in anoxic conditions of the sea. This type of dispersions in the deep sea having total petroleum hydrocarbon concentrations less than 10 ppm is called das "cloud" [25].

In those "cloud" bacterial activity was seen which showed lower potassium oxide and dissolve oxygen concentrations. Also, the ammonia concentration was higher, and the lower nitrous oxide concentrations were seen. The bacterial activity was higher than that outside of the "cloud." A 16S rRNA microarray identified 951 bacterium subfamilies from 62 phyla; however, only 16 proteobacteria subfamilies were considerably enriched in the cloud, with three Oceanospirillales families dominating.

During the discharge, polynuclear aromatic hydrocarbon concentrations dropped rapidly as distance from wellhead increased reaching 1.0 ppb within 24–32 km in every direction except to the southwest, where a few samples surpassed 1 ppb out to 64 km. Microbial breakdown is responsible for much of the decrease in PAHs [25].

5   Conclusion

The oil spill incidents of the Prince William Sound and the British Petroleum Deepwater Horizon teach us hundreds of importance of degradation through indigenous microorganisms in case of the oil spillages. Most inflamed hydrocarbons can be removed through manner of biodegradation and distinct natural weathering processes, but this may take some time in varying from regions to regions based on the concentration of crude oil. The Exxon Valdez oil spill had a similar effect on oil on shorelines. While there was research on lowering oil concentrations, no particular biodegradation studies were undertaken for the Exxon Valdez spill with its unique deepwater cloud of dispersed oil, as they were for the BP spill with its unique deepwater cloud of dispersed oil.

Biodegradation of oil was mostly due to microorganisms in the Gulf of Mexico, because of the natural seepages and offshore drilling that happen every year which makes the microbiota adapted to it. In some cases, like in the case of Prince William Sound, bioremediation with addition of fertilizer was found to be effective in a way to accelerate oil biodegradation rates and this had enhanced tv.

The main effects of the oil spill must be kept in mind, and then the risk control of the overall process must be looked upon. It must also follow the guidelines to make the environment healthy so that the living organisms as a whole won't be affected. Also, it must be noted that the natural degradation of the oil spills is a great cause but there are certain bacteria, fungi, as well as yeasts who can degrade the spillage of oils and can bring the disaster to under control. The main factor that should be kept in mind is that the ecosystem should be maintained [25].

References

1. Si-Zhong, Y., Hui-Jun J.I.N., Zhi W.E.I., Rui-Xia H.E., Yan-Jun J.I., Xiu-Mei L.I., Shao-Peng Y.U.: Bioremediation of oil spills in cold environments: a review. Pedosphere **19**(3), 371–381 (2009)

2. Das, P. P., & Purkait, M. K.: Treatment of cold rolling mill (CRM) effluent of steel industry. Sep. Purif. Technol. **274**, 119083 (2021)
3. Bikkina, P. K., Uppaluri, R., & Purkait, M. K.: Evaluation of surfactants for the cost effective enhanced oil recovery of Assam crude oil fields. Pet. Sci. Technol. **31**, 755–762 (2013)
4. Marzan, L.W., Sultana, T., Hasan, M.M., Mina, S.A., Islam, M.R., Rakibuzzaman, A.G.M. and Khan, M.I.H.: Characterization of furnace oil bioremediation potential of hydrocarbonoclastic bacteria isolated from petroleum contaminated sites of the Sundarbans, Bangladesh. J. Gene. Eng. Biotechnol. **15**(1), 103–113 (2017)
5. Numbere, A.O.: The impact of oil and gas exploration: invasive nypa palm species and urbanization on mangroves in the Niger River Delta, Nigeria. In: Threats to Mangrove Forests, pp. 247–266. Springer, Cham, 2018
6. Nsenergybusiness Home Page. https://www.nsenergybusiness.com/features/exxon-valdez-oil-spill-1989/. Last accessed: 5 June 2020
7. Carson, R.T., Mitchell, R.C., Hanemann, M., Kopp, R.J., Presser, S., Ruud, P.A.: Contingent valuation and lost passive use: damages from the Exxon Valdez oil spill. Environ. Resource Econ. **25**(3), 257–286 (2003)
8. Azubuike, C.C., Chikere, C.B., Okpokwasili, G.C.: Bioremediation techniques–classification based on site of application: principles, advantages, limitations and prospects. World J. Microbiol. Biotechnol. **32**(11), 1–18 (2016)
9. Mapelli, F., Scoma, A., Michoud, G., Aulenta, F., Boon, N., Borin, S., Kalogerakis, N., Daffonchio, D.: Biotechnologies for marine oil spill cleanup: indissoluble ties with microorganisms. Trends Biotechnol. **35**(9), 860–870 (2017)
10. National Geographic Home Page. https://www.nationalgeographic.com/environment/article/oil-spills-30-years-after-exxon-valdez
11. Florida Politics Home Page. https://floridapolitics.com/archives/252472-cori-henderson-picked-evaluate-deepwater-horizon-settlement-applications/. Last accessed: 15 May 2022
12. Nandi, B. K., Uppaluri, R., & Purkait, M. K.: Microfiltration of stable oil-in-water emulsions using kaolinbased ceramic membrane and evaluation of fouling mechanism. Desalin. Water Treat. **22**, 133–145 (2010)
13. Walker, A.H.: Oil spills and risk perceptions. In: Oil Spill Science and Technology, pp. 1–70. Elsevier (2017)
14. Jain, P.K., Gupta, V.K., Gaur, R.K., Lowry, M., Jaroli, D.P., Chauhan, U.K.: Bioremediation of petroleum oil contaminated soil and water. Res. J. Environ. Toxicol. **5**(1), 1 (2011)
15. Zhu, X., Venosa, A.D., Suidan, M.T., Lee, K.: Guidelines for the bioremediation of marine shorelines and freshwater wetlands. US Environmental Protection Agency (2001)
16. Jafarinejad, S.: Solid-Waste management in the petroleum industry. In: Jafarineja, S. (ed.) Petroleum Waste Treatment and Pollution Control, pp. 269–345. Butterwoth-Heinemann, Oxford, United Kingdom (2017)
17. Soleimani, M., Farhoudi, M., Christensen, J.H.: Chemometric assessment of enhanced bioremediation of oil contaminated soils. J. Hazard. Mater. **254**, 372–381 (2013)
18. Wrenn, B.A., Haines, J.R., Venosa, A.D., Kadkhodayan, M., Suidan, M.T.: Effects of nitrogen source on crude oil biodegradation. J. Ind. Microbiol. **13**(5), 279–286 (1994)
19. Pritchard, P.H., Costa, C.F.: EPA's Alaska oil spill bioremediation project. Part 5. Environ Sci Technol **25**(3), 372–379 (1991)
20. Bovio, E., Gnavi, G., Prigione, V., Spina, F., Denaro, R., Yakimov, M., Calogero, R., Crisafi, F. and Varese, G.C.: The culturable mycobiota of a Mediterranean marine site after an oil spill: isolation, identification and potential application in bioremediation. Sci. Total Environ. **576**, 310–318 (2017)
21. Volli, V., & Purkait, M. K.: Physico-chemical properties and thermal degradation studies of commercial oils in nitrogen atmosphere. Fuel. **117**, 1010–1019 (2014)
22. Venosa, A.D.: Oil spill bioremediation on coastal shorelines: a critique. Bioremediat Principles Pract. **3**, 259–301 (1998)
23. Bragg, J.R., Prince, R.C., James Harner, E., Atlas, R.M.: Effectiveness of bioremediation for the Exxon Valdez oil spill. Nature **368**(6470), 413–418 (1994)

24. Pritchard, P.H., Mueller, J.G., Rogers, J.C., Kremer, F.V., Glaser, J.A.: Oil spill bioremediation: experiences, lessons and results from the Exxon Valdez oil spill in Alaska. Biodegradation **3**(2), 315–335 (1992)
25. Atlas, R.M., Hazen, T.C.: Oil biodegradation and bioremediation: a tale of the two worst spills in US history, pp. 6709–6715 (2011)

Fabrication of Borate Cross-Linked Graphene Oxide Framework (GOF)-Laminated UF Membrane for Heavy Metal Removal

Ankush D. Sontakke, Ankit Tiwari, and Mihir K. Purkait

1 Introduction

The scarcity of freshwater resources in today's globe has created significant challenges for humans, animals, and plants. Rapid infrastructure and industrial growth result in a variety of environmental and water toxins, which have a negative impact on both human and animal health. The heavy metal pollutants, in particular, Pb^{2+}, Cr^{3+}, and Cd^{2+}, can have major consequences for all living beings; thus, wastewater treatment, environmental remediation application, and water purification technologies have received much attention. Meanwhile, the emergence of nanomaterials such as graphene and other treatment techniques has led to substantial advances in environmental remediation [1, 2]. In addition, pressure-driven ultrafiltration (UF) techniques provided significant advantages for the separation of water contaminants via Donnan repulsion and molecular sieving or size exclusion mechanisms [3]. In recent, many research findings have advocated the usage of graphene-imparted membranes to separate both the monovalent and divalent ions [4–6].

Graphene, a perfect single-layer material, because of its π-orbital configuration, forms a dense, the delocalized cloud, which makes it gap free within its aromatic ring. This barrier in material and the defect-free structure, chemical inertness, and high mechanical strength of the graphene have inspired researchers to artificially

---

Ankush D. Sontakke and Ankit Tiwari are equally contributed.

A. D. Sontakke (✉) · A. Tiwari · M. K. Purkait
Department of Chemical Engineering, Indian Institute of Technology Guwahati, Guwahati, Assam 781039, India
e-mail: ankus176107025@iitg.ac.in

A. Tiwari
e-mail: vijaysha@alumni.iitg.ac.in

M. K. Purkait
e-mail: mihir@iitg.ac.in

create a hole in graphene nanosheets for developing nanoporous graphene-based membranes. Graphene oxide being the most important graphene derivative has been widely used as a building block entity for membranes. Like graphene, GO contains a single-atom-thick sheet with additional oxygenated functional groups to ensure GO is a versatile material for surface modification with an aim to construct a well-defined nanostructure and provide opportunities to fabricate GO-based membrane [7–9]. In-plane nanopores of GO provide the main transport channel in the nanosheet membrane; on the other hand, along with basal nanopores, the d-spacing between GO nanosheets allows the flow of molecules. The oxygenated functional group of GO makes it water dispersible and enhances the specific interaction with different transport molecules via hydrogen bonding and electrostatic bonding. With water-dispersible features and a high aspect ratio, GO nanosheets can be readily assembled in the form of the laminar membrane by vacuum filtration [7, 10], spin coating [11, 12], drop-casting [13], and LBL deposition [14]. One of the most convenient and straightforward ways to form the GO membrane is vacuum filtration. By varying GO concentration in the suspension, membrane thickness can be easily controlled [7].

However, the hydrophilic nature of GO causes instability in water due to increased intersheet spacing [15], which may reduce the overall strength of GO-imparted membranes due to the weak interaction of GO nanosheets. This issue can be resolved by creating stronger chemical bonding within GO sheets, such as by its covalent cross-linking using polyallylamine [16], dopamine [17], diamine monomers [18], dicarboxylic acids, borate [19], and different divalent metal ions [20]. This process produces a chemically stable and high-strength membrane. Such type of surface modification of GO is termed as graphene oxide framework (GOF). By optimizing the functional group, substituent and chain length of the crosslinker, the elastic modulus, d-spacing, and flux of the membrane can be adjusted [15]. The stable bonding can be created between GO nanosheets by choosing suitable crosslinkers. The cross-linking is done for the tuning of d-spacing of GO nanosheet and examining their effect on the separation process. However, the synthesis of GOF via organic groups may impart serious issues of fouling. Also, the organic linkers are easily oxidized by oxidants, thus weakening the cross-linking bond and oxidation resistance which is an essential parameter for membrane as oxidants are frequently used for the cleaning of fouled membrane surfaces. These hurdles can be subsided via cross-linking of GO with inorganic crosslinkers such as sodium tetraborate. As an oxidation resistive, sodium tetraborate can be reacted with the hydroxyl functional groups of GO to establish a stable and robust –B–O–C cross-linking.

In this study, an endeavor has been made to prepare a graphene oxide thin-film composite membrane by cross-linking the inorganic borate group in between the GO nanosheets (GOF). The borate group was perfectly cross-linked with the hydroxyl group of GO, which may improve its aqueous stability. To prepare the thin film membrane, polysulfone (PSF) was used as a support with polyethylene glycol (PEG) as a pore-forming agent. PEG yielded uniform pores in the PSF membrane, and due to its non-ionic and protein resistive characteristics, improved hydrophilicity and antifouling properties were imparted on PSF support. The PSF–PEG support was further treated with dopamine to give the anchoring sites to borate-GO (GOF)

solution by virtue of the property of electrostatic interaction through the oxygenated functional group of GO. The GOF film got linked by the amine group of dopamine and easily deposited on the PSF–PEG substrate. Furthermore, the obtained GOF solution was used to fabricate thin-film composite (TFC) membranes. The fabricated TFC membranes were further tested for the separation of heavy metal ions using a batch filtration setup. The fabricated membranes have demonstrated their potential to act on the adsorptive mechanism and reject the heavy metal ions based on the Donnan repulsion and size exclusion principles.

2 Experimental

2.1 Materials

Graphite powder (synthetic) was procured from SRL Pvt. Ltd. and used to synthesize graphene oxide. Phosphorous pentoxide ($P_2O_5 \geq 98.0\%$), sulfuric acid (98%), and hydrochloric acid (37%) were acquired from Sigma Aldrich. Potassium permanganate (98.5%), sodium nitrate (99%), potassium peroxide disulfate (98%), *N*-methyl-2-pyrrolidone (NMP), and hydrogen peroxide aqueous solution (30%) was obtained from Merck. Sodium tetraborate decahydrate (99.5%) and ethylene diamine were obtained from Sigma Aldrich and Qualigens and used for the crosslinker of GO. Polysulfone (PSF) was obtained from Sigma Aldrich and used as a polymer in membrane fabrication. Polyethylene Glycol (PEG-6000) was purchased from Otto chemical and used as a pore-forming agent. All the chemical was used as customary without any further purification.

2.2 Synthesis of Borate Cross-Linked Graphene Oxide (GOF)

The graphene oxide (GO) was synthesized using low-cost synthetic grade graphite via the modified Hummers method. Details on GO synthesis can be obtained from our previous work [21, 22]. GOF was synthesized via cross-linking of GO with borate and amine functional groups. For the borate group functionalization, 50 mL GO suspension of concentration 8.6 mg/L was initially prepared and sonicated for 15 min. Further, sodium tetraborate solution (2.5 mmol/L) was inserted into the GO suspension and sonicated for 30 min to confirm the suitable mixing and cross-linking of borate functional groups. The GOF suspension was filtered and dried in the oven for further characterization.

In addition, amine cross-linked GO was also synthesized, and the cross-linking was compared with the borate functionalized GOF. The best suitable cross-linked material was further used to fabricate the GOF-based membrane. For the amine cross-linked GO, a 400 ppm GO aqueous solution was initially prepared and sonicated

to form uniform dispersion. Later, a diamine monomer, EDA, was mixed with an aqueous GO suspension to obtain a 0.1 M solution in relation to the monomer. The suspension was run through the filter, and a thin film formed on filter paper was collected and dried in the oven to indorse cross-linking amongst GO and diamine. The film was further soaked in methanol to remove the physically bonded amine group. The cross-linking of both borate and amine groups functionalized GO was further verified using FTIR and XRD analysis.

2.3   Fabrication of GOF-Laminated UF Membranes

The GOF-laminated membranes were fabricated using a PSF–PEG substrate and a layer-by-layer assembly method. To fabricate the PSF–PEG substrate, an essential quantity of PSF and PEG was inserted into the beaker comprising NMP as a solvent. The mixture was stirred at 200 rpm and at 60 °C for 18 h. The optimized composition of the membranes was finalized to be 12 wt% PSF, 5 wt% PEG, and 83 wt% NMP. The phase inversion method was adopted for the fabrication of membranes. After the predefined reaction time, the mixture was kept for degassing for 2 h at the reaction temperature. The polymer suspension was casted on a spotless glass plate using a glass rod, upholding a 120 μm thickness. Followed by the casting process, the glass plate was quickly submerged in a DI coagulation water bath. A uniform thin film appeared on a glass plate and separated from the plate after a certain time. Membranes were then dried at ambient temperature for 24 h and characterized to process for the specific application.

After confirmation of cross-linking of GO with the borate group, the different quantities of GO borate (GOF) solutions were run through the PSF–PEG substrate. To improve the homogeneity of GOF nanosheets on the substrate, the PSF–PEG membrane was first treated with a dopamine solution of 2 g/L concentration by contacting the active surface of a substrate to the solution for 3 h. During this step, dopamine self-polymerizes itself and forms an adhesive layer on the substrate, thereby providing anchoring sites for GOF; the support was then dried and put in the batch filtration setup. 50, 100, and 150 mL of GOF with optimized concentration were filtered, and perfect deposition with a 9.6 μm thickness of GO film was obtained with 150 mL of solution. The composition of fabricated membranes is provided in Table 1.

Table 1 GOF-based membrane composition

Membrane	PSF (w/w %)	NMP (w/w %)	PEG (w/w %)	Volume of GOF suspension (mL)
M01	12	83	5	0
M02	12	83	5	50
M03	12	83	5	100
M04	12	83	5	150

2.4 Characterization of Membrane

The surface properties of the membrane, like its morphology, size and shape of pores, along with pore size distribution, play a significant role in evaluating its separation enactment. The prepared membranes were characterized for morphological studies and permeability experiments. Also, their performance was analyzed by equilibrium water content (EWC) and PWF with the help of a batch filtration setup. The EWC, porosity, hydraulic permeability and, PWF were determined using the following equations.

$$EWC(\%) = \frac{W - W_d}{W_d} \times 100 \tag{1}$$

$$Porosity = \frac{W_w - W_d}{\rho_w \times V} \tag{2}$$

$$Pure\ water\ flux\ (J_w) = \frac{Q}{A \times t} \tag{3}$$

$$Permeability(Pm) = \frac{J_w}{\Delta P} \tag{4}$$

where W_w and W_d are the mass of wet and dry membrane (g), ρ_w is the water density at ambient temperature (Kg/m^3), V is wet membrane volume (m^3), J_w is pure water flux (Lm^{-2} h^{-1}), Q is a volume of water collected (L), A is the effective area of a membrane (m^2), and t is sample collection time (h). Pm is hydraulic permeability (Lm^{-2} h^{-1} bar^{-1}), and ΔP is transmembrane pressure (TMP) (bar).

2.5 Performance Evaluation of Membranes for Heavy Metal Removal

Herein, a membrane cell with a 350 mL capacity was applied for the membrane permeation experiments. The permeation cell is competent in acquiring a membrane with a diameter of 3.3×10^{-2} m with a 7.065×10^{-4} m^2 operative area. Membrane compaction is done to find the compaction factor at 5 bars transmembrane pressure (TMP) for 2 h. The permeate was accumulated in a separate flask/tank at the bottom of the permeation cell. The pressure gauge was installed at the top of the membrane cell, and pressure was maintained using an air compressor. Figure 1 represents the graphic of the permeation cell. The permeate flux profile was computed using time data and the cumulative volume of permeate. Permeate aliquots were obtained on an intermittent basis for analysis. To maintain feed concentration, permeate gathered underneath the cell was circulated back to the feed side. The feed concentration of each metal ion (Pb^{2+}, Cr^{3+}, and Cd^{2+}) was set at 50 mg/L for filtering of individual
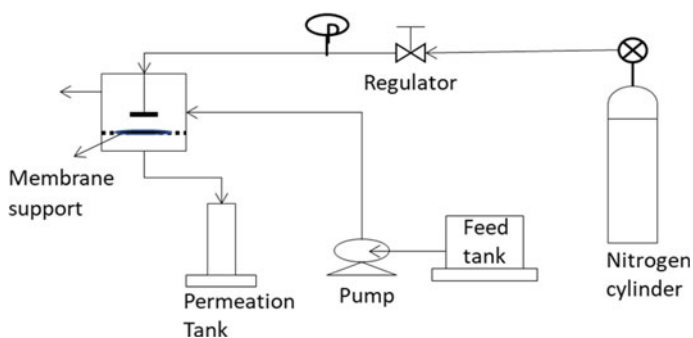
Fig. 1 Schematic representation of batch filtration setup

heavy metals, as this is often the upper limit of heavy metals [1]. The concentrations of several heavy metals in aqueous suspension were determined using an atomic absorption spectrophotometer. The rejection rate of heavy metal ions was calculated using the following equation.

$$\text{Rejection}(\%) = \frac{\text{Conc. in Feed} - \text{Conc. in permeate}}{\text{Conc. in Feed}} \times 100 \qquad (5)$$

3 Result and Discussion

3.1 Characterization of GO and GOF

3.1.1 Field Emission Scanning Electron Microscopy (FESEM)

The surface morphology of GO and GOF nanosheets is provided in Fig. 2. A rumpled layer structure of GO with the accumulation of multiple single atomic thin nanosheets can be observed in Fig. 2a. Similarly, a wrinkled surface was exhibited by the GOF synthesized via both borate and amine-functionalized GO, as displayed in Fig. 2b, c respectively. The GO was produced via oxidation of synthetic graphite, which leads to the incorporation of hydroxyl, carboxyl, and epoxy functional groups on the basal planes and edges of GO nanosheets. The incorporation of various oxygen-containing functional entities was validated by EDX analysis. In the case of GO, the C/O weight % ratio was found to be 1.65 (Fig. 2d). However, during the formation of GOF, the borate and amine functional groups were attached to the carboxyl and hydroxyl functional groups of GO, which further reduces the oxygen content within the GO and increases the C/O ratio. The elemental composition of borate cross-linked GO, and amine cross-linked GO is shown in Fig. 2e, f. The borate group from sodium tetraborate and amine group from ethylene diamine were attached with GO, and
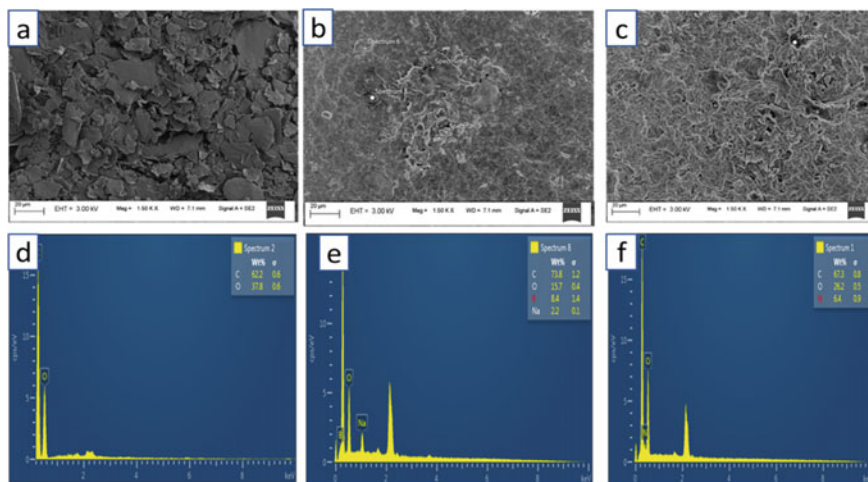
Fig. 2 FESEM images and EDX spectra of GO, borate, and amine cross-linked GO

thereby, the existence of boron and nitrogen elemental confirms the cross-linking of the group in GO. The cross-linking of GO during GOF synthesis has partially reduced GO and increased the C/O ratio to 4.70 and 2.56 for borate and amine group functionalization, respectively. The functionalization of GO was also confirmed via IR spectroscopy.

3.1.2   Chemical Interaction Study

The qualitative analysis of pristine graphite synthesized GO and GOF via cross-linking of GO with borate and amine functional groups was done using FTIR analysis to confirm the existence of major functional groups within these materials. As shown in Fig. 3, a broad peak at 3430 cm^{-1} resembles hydroxyl functional entities of stretching vibrations that can be observed for GO, representing phenolic OH from carboxylic groups [17, 21]. In addition, the existence of carboxyl and epoxy functional entities was advocated by the peak positions at 1730, 1630, and 1052 cm^{-1} with inferior transmittance that signifies a dense presence of bonds in GO to that of graphite [21, 23]. Further, successful cross-linking of GO was confirmed via the presence of the respective functional group. The B-C vibration at 1076 cm^{-1} along with NH bond vibration positioned at 1554 cm^{-1} indicated the joining of the borate and amine group in GO [19, 24]. The absorption peak of GO at 3430 cm^{-1} disappeared for borate and amine cross-linked GO indicating the participation of the hydroxyl group in the cross-linking process.
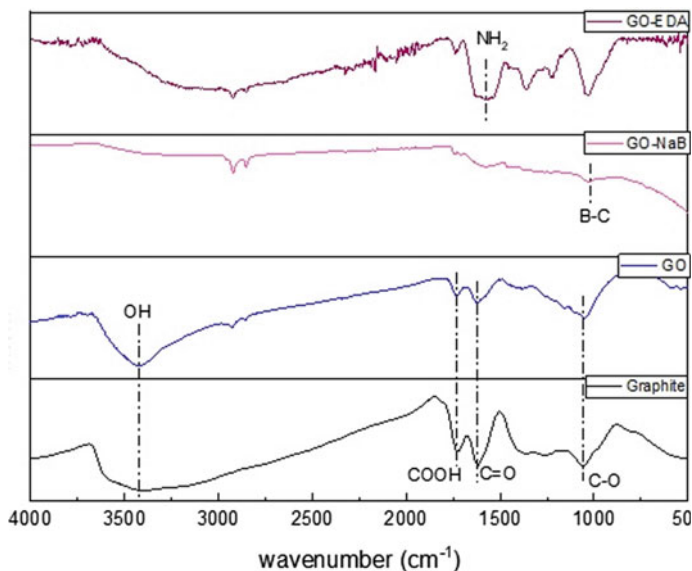
Fig. 3 FTIR spectra of graphite, GO, borate cross-linked GO (GO-NaB), and amine cross-linked GO (GO-EDA)

3.1.3 X-Ray Diffraction Study

Figure 4 represents the XRD patterns of synthetic graphite, GO, and borate and amine cross-linked GO (GOF). Herein the graphite exhibited a sharp and distinct peak at $2\theta = 26.56°$, corresponding to the strongly ordered structure of graphite with higher van der Waals interactions. Modified Hummer's approach to graphite oxidation decreases these interactions, resulting in totally exfoliated GO nanosheets. After graphite had been oxidized, the graphitic peak around 26.54° disappeared altogether and resulted in a diffraction peak of GO at 10.14° of (0 0 1) plane of 0.88 nm interlayer spacing. The increment in the interlayer spacing of GO nanosheets from graphite (0.35 nm) further confirms the successful incorporation of oxygenating functional groups with GO [21, 25].

In the case of borate and amine cross-linked GO, the shift in the (0 0 1) plane from 10.14° for GO to 10.76° for GO-EDA and 9.96° for GO-NAB suggested parallel functionalization of these groups to GO nanosheets [19]. In addition, the reappearance of graphitic peak positions in GO-EDA and GO-NAB suggests the partial reduction within GO as advocated by elemental composition in EDX analysis. However, the amine cross-linked GO exhibited a higher amorphous structure due to the existence of ethylenediamine, which may result in instability during membrane fabrication. Also, while noting the antifouling characteristics of inorganic borate groups, the borate cross-linked GO was further considered for the fabrication of GOF-laminated membranes.
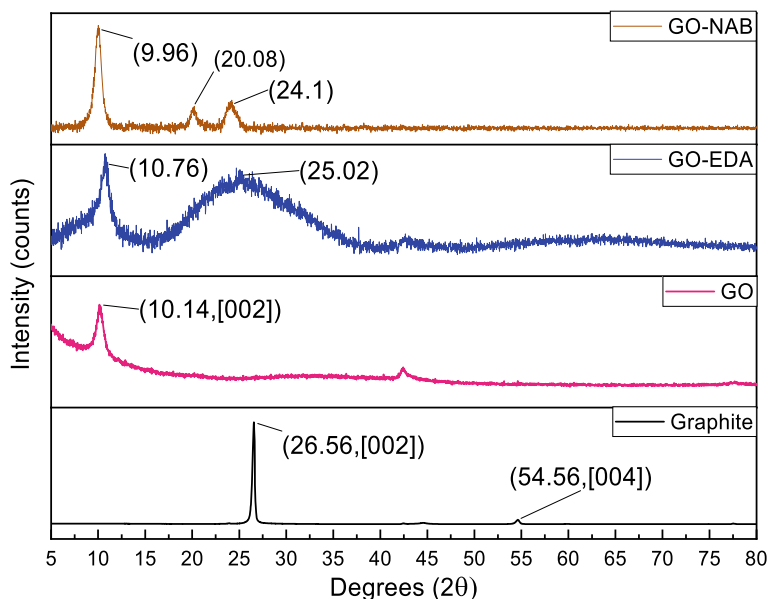
Fig. 4 X-ray diffraction pattern of graphite, GO, borate cross-linked GO (GO-NaB), and amine cross-linked GO (GO-EDA)

3.2 Membrane Characterization

3.2.1 Surface Morphology

The cross-sectional and surface morphology of the PSF–PEG substrate is shown in Fig. 5. It can be easily depicted below Fig. 5a that the asymmetric structure of the substrate was formed with a top dense skin layer having uniform nanocapillaries in addition to a porous sub-layer. In the PSF–PEG substrate (M 01), a finger-like structure was observed due to the PSF material and the strong mutual affinity of the NMP solvent in water, resulting in immediate de-mixing. The substrate of the thickness of 110 μm was made by lab casting, as also visible in Fig. 5a.
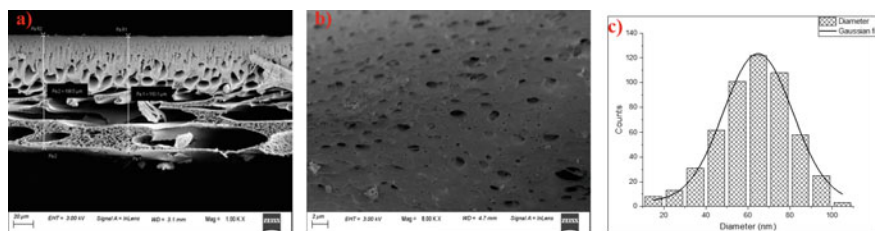
Fig. 5 FESEM images and pore size distribution of PSF–PEG substrate (M 01)

Table 2 Fitting data of pore size distribution

Model	Gauss
Equation	$y = y0 + (A/(w*\mathrm{sqrt}(pi/2)))*\exp(-2*((x - xc)/w)^2)$
Plot	Counts
Xc	64.79011 ± 0.52283
W	32.92492 ± 1.69819
A	4926.52855 ± 338.97617
Adj. R-Square	0.98928

The top surface morphology of M 01 with a nearly uniform cylindrical pore is presented in Fig. 5b. The pore formation mechanism is attributed to the diffusion of solvent and additive PEG on the feed solvent side. PEG diffuses through the PSF substrate, thereby giving uniform cylindrical pore throughout. The pore size distribution of the PSF–PEG substrate was done by ImageJ software via the method of thresholding (Fig. 5c). The distribution was performed over the whole surface. The presence of a larger void and edge cavity was neglected during the calibration so as to give the actual pore analysis in the substrate. The pore distribution was obtained with different pore diameters, which were plotted as a histogram. The distribution resulted in the average pore diameter (Xc) as 64.79 nm, with an R^2 value of 0.9985, as presented in Table 2.

The prepared substrate was treated with dopamine solution before depositing borate-GO solution onto it. Dopamine formed an adhesive layer by self-polymerization and provided anchoring sites to GO. The borate-GO solution after batch filtration at an optimized solution concentration of 8.6 and 50 mL of the solution resulted in around 6 μm thickness of GOF film over the M 02 membrane, as shown in Fig. 6. The treatment with dopamine had enhanced the bonding of substrate with GO solution due to the incorporation of the amine group on the external surface of the substrate, thereby increasing electrostatic interaction between borate-GO and dopamine. It was observed that the GOF suspension was uniformly distributed over the substrate. Also, the inbound integralities of GO were modified by borate group interaction with the hydroxyl (OH) group of GO. This bounding had removed the hurdle of instability of weak H-bond between GO nanosheets in the wet state. With an increase in deposition of GOF solution, the layer thickness of GOF over the substrate was increased.

3.2.2 Permeation Study of GOF Membranes

The PWF of the membranes was evaluated at different TMP (0–5 bar) to investigate the flux of the substrate as well as GOF-laminated membranes, as presented in Fig. 7. It is seen that the PWF upsurges with transmembrane pressure; it serves as a driving force for membrane studies. The slope of the plot, which is the hydraulic permeability of the membrane, was determined, and it is observed that the permeability value is
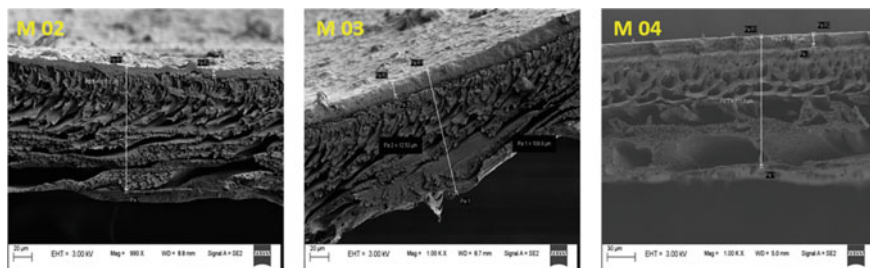
Fig. 6 FESEM images of borate cross-linked GO (GOF) based membranes

influenced by the addition of copolymer in the membrane. The EWC and porosity of the PSF–PEG substrate were observed as 59.60% and 0.3, respectively. The hydraulic permeability of PSF–PEG substrate and GOF-laminated membranes is reported in Table 3. The permeability of obtained membranes was decreased with the increase in the GOF layer over the substrate because of the additional resistance offered by the GOF layer. However, it may boost the rejection rate for heavy metal ions. M 04 membrane with the permeability of 21.29 ($Lm^{-2}\,h^{-1}\,bar^{-1}$) was chosen to evaluate its separation performance for rejecting heavy metal ions considering a higher amount of borate cross-linked GO (GOF).

Fig. 7 Pure water flux of M 01, M 02, M 03, and M 04 membranes
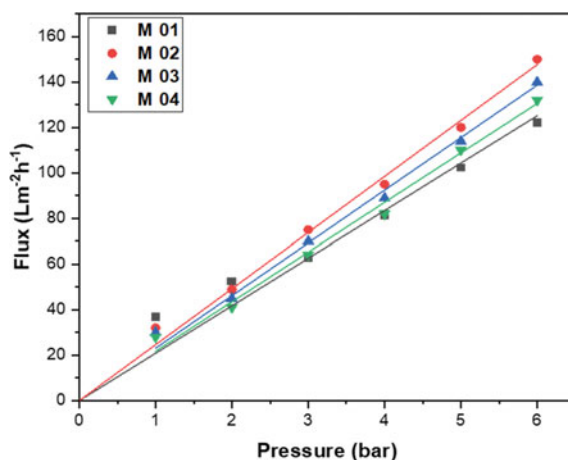
Table 3 Permeability of fabricated membranes

Membranes	Permeability ($Lm^{-2}\,h^{-1}\,bar^{-1}$)	Adj-R^2
M01	19.38	0.9651
M02	24.54	0.9924
M03	22.18	0.9930
M04	21.29	0.9888

3.2.3 Separation Performance of GOF Membranes

A rejection study to remove the heavy metal ions of 50 mg/L feed concentration by M04 membrane is presented in Fig. 8. The rejection of Pb^{2+}, Cr^{3+}, and Cd^{2+} was > 96%, > 90%, and > 94% throughout the experiment, respectively. The aqueous feed solution of metal salts has a pH of 6.5 (nearly neural) except for Cr, as it forms chromic acid in an aqueous solution; therefore, the chromium aqueous solution of lower pH of 3.5 was used to examine the separation performance of the membrane. The borate cross-linked GO solution persists a negative charge over the surface of a membrane (ζ potential –26.4 mV); therefore, the rejection of heavy metal ions was established via the electrostatic adsorption process, which was mainly driven by Donnan repulsion; also, the interchannels between the layers of GOF provide the access for the size exclusion principle. The adsorption capacity of metal ion salts varies depending on their stability constant and electronegativity, and also the sequence of elimination of Pb^{2+}, Cd^{2+}, and Cr^{3+} comprehends the track of the highest adsorption capacity [26]. The chromium solution at pH 3.5 has a much lower surface charge than the other metal ions at pH 6.5. As the metal ion rejection results from the electrostatic interaction within the positively charged metal ions and the negatively charged membrane surface, a lower rejection rate of 90–92% was observed for the Cr ions. Furthermore, the existence of H^+ ions interacts with Cr^+ ions for adsorption sites on the membrane surface, diminishing the ion elimination rate even further [1].

4 Conclusion

In the present work, GO nanosheets were successfully prepared using the modified Hummers method by considering their properties and flow mechanism through nanosheets. Further, the interchannel of GO was modified by cross-linking of borate and amine functional groups to obtain GOF. However, more amorphous structure and reduced nature of amine cross-linked GO may cause instability for the membranes; therefore, it was omitted during the fabrication of GOF-laminated membranes. The borate cross-linked GO was selected for the membrane fabrication by noting the antifouling characteristics and suitable aqueous stability of the inorganic borate group. The existence of oxygenated function groups in GO and successful cross-linking of borate functional groups on GO for the formation of GOF has been confirmed by FTIR, EDX, and XRD analysis. Further, the PSF-supported membranes with PEG as a pore-forming agent were obtained by the phase inversion method. The PSF–PEG substrate exhibited an average pore size of 64.79 nm with a permeability of 19.32 ($Lm^{-2}\ h^{-1}\ bar^{-1}$). The deposition of the borate-GO layer over the substrate was established using the layer-by-layer method. It was observed that the GOF lamination had increased the PWF owing to the hydrophilicity of GOF and frictionless flow through its nanochannels; however, further deposition has decreased the flux. The amine group from the dopamine layer on the PSF–PEG substrate contributed to the effective deposition of the GOF solution. The GOF layer was chemically coupled
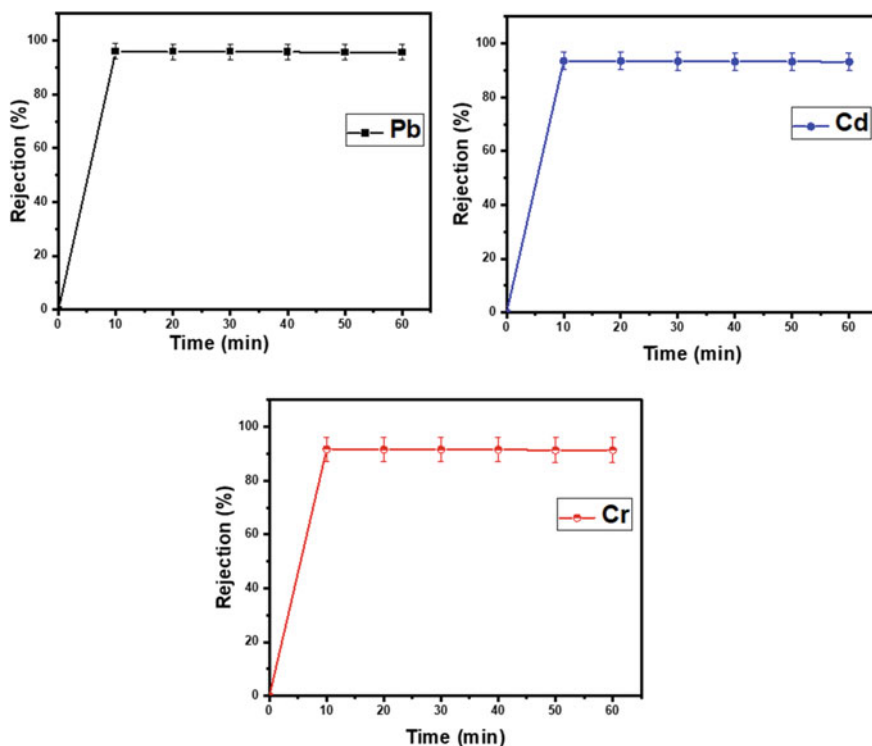
Fig. 8 Rejection of Pb^{2+}, Cd^{2+}, and Cr^{3+} heavy metal ions using M 04 membrane

with the amine group due to electrostatic interaction, and the remaining sheet was cross-linked by the borate group. The working mechanism of the membranes is contributed to Donnan repulsion due to functional group and size exclusion principle due to sub nanochannel of borate-GO sheets. The GOF-laminated membrane M04 was tested for the rejection of Pb^{2+}, Cr^{3+}, and Cd^{2+} ions. The rejection rate was $> 96\%$, $> 94\%$, and $> 90\%$ of feed (50 ppm) for the Pb^{2+}, Cd^{2+}, and Cr^{3+} ions, respectively. It can be concluded that the prepared membranes have the capability to stand effectively for ion-selective separation.

References

1. Das, P. P., Sharma, M., & Purkait, M. K.: Recent progress on electrocoagulation process for wastewater treatment: A review. Sep. Purif. Technol. **292**, 121058 (2022). https://doi.org/10.1016/j.seppur.2022.121058

2. Singh, R., Yadav, V.S.K., Purkait, M.K.: Cu$_2$O photocatalyst modified antifouling polysulfone mixed matrix membrane for ultrafiltration of protein and visible light driven photocatalytic pharmaceutical removal. Sep. Purif. Technol. **212**, 191–204 (2019). https://doi.org/10.1016/j.seppur.2018.11.029

3. Purkait, M.K., Bhattacharya, P.K., De, S.: Membrane filtration of leather plant effluent: Flux decline mechanism. J. Memb. Sci. **258**, 85–96 (2005). https://doi.org/10.1016/j.memsci.2005.02.029

4. Purkait, M.K., DasGupta, S., De, S.: Micellar enhanced ultrafiltration of phenolic derivatives from their mixtures. J. Colloid Interface Sci. **285**, 395–402 (2005). https://doi.org/10.1016/j.jcis.2004.11.036

5. Purkait, M.K., Sinha, M.K., Mondal, P., Singh, R.: Chapter 1—Introduction to membranes. In: Interface Science and Technology, Stimuli-Responsive Polymeric Membranes, pp. 1–37. Elsevier, Netherlands (2018)

6. Zhang, P., Gong, J.L., Zeng, G.M., Deng, C.H., Yang, H.C., Liu, H.Y., Huan, S.Y.: Cross-linking to prepare composite graphene oxide-framework membranes with high-flux for dyes and heavy metal ions removal. Chem. Eng. J. **322**, 657–666 (2017). https://doi.org/10.1016/j.cej.2017.04.068

7. Han, Y., Xu, Z., Gao, C.: Ultrathin graphene nanofiltration membrane for water purification. Adv. Funct. Mater. **23**, 3693–3700 (2013). https://doi.org/10.1002/adfm.201202601

8. Sontakke, A.D., Das, P.P., Mondal, P., Purkait, M.K.: Thin-film composite nanofiltration hollow fiber membranes toward textile industry effluent treatment and environmental remediation applications: review. Emergent Mater. (2021). https://doi.org/10.1007/s42247-021-00261-y

9. Changmai, M., Das, P. P., Mondal, P., Pasawan, M., Sinha, A., Biswas, P., ... & Purkait, M. K.: Hybrid electrocoagulation–microfiltration technique for treatment of nanofiltration rejected steel industry effluent. J. Environ. Anal. Chem. **102**, 62–83 (2022). https://doi.org/10.1080/03067319.2020.1715381

10. Sharma, M., Das, P. P., Sood, T., Chakraborty, A., & Purkait, M. K.: Reduced graphene oxide incorporated polyvinylidene fluoride/cellulose acetate proton exchange membrane for energy extraction using microbial fuel cells. J. Electroanal. Chem. **907**, 115890 (2022). https://doi.org/10.1016/j.jelechem.2021.115890

11. Bulasara, V.K., Thakuria, H., Uppaluri, R., Purkait, M.K.: Effect of process parameters on electroless plating and nickel-ceramic composite membrane characteristics. Desalination **268**, 195–203 (2011). https://doi.org/10.1016/j.desal.2010.10.025

12. Sharma, M., Das, P. P., Sood, T., Chakraborty, A., & Purkait, M. K.: Ameliorated polyvinylidene fluoride based proton exchange membrane impregnated with graphene oxide, and cellulose acetate obtained from sugarcane bagasse for application in microbial fuel cell. J. Environ. Chem. Eng. **9**, 106681 (2021). https://doi.org/10.1016/j.jece.2021.106681

13. Patel, P. K., Pandey, L. M., & Uppaluri, R. V.: Adsorptive removal of Zn, Fe, and Pb from Zn dominant simulated industrial wastewater solution using polyvinyl alcohol grafted chitosan variant resins. Chem. Eng. J. 141563 (2023). https://doi.org/10.1016/j.cej.2023.141563

14. Hu, M., Mi, B.: Enabling graphene oxide nanosheets as water separation membranes. Environ. Sci. Technol. **47**, 3715–3723 (2013). https://doi.org/10.1021/es400571g

15. Jia, Z., Wang, Y.: Covalently cross-linked graphene oxide membranes by esterification reactions for ions separation. J. Mater. Chem. A **3**, 4405–4412 (2015). https://doi.org/10.1039/c4ta06193d

16. Park, S., Dikin, D.A., Nguyen, S.T., Ruoff, R.S.: Graphene oxide sheets chemically cross-linked by polyallylamine. J. Phys. Chem. C **113**, 15801–15804 (2009). https://doi.org/10.1021/jp907613s

17. Das, P. P., & Purkait, M. K.: Treatment of cold rolling mill (CRM) effluent of steel industry. Sep. Purif. Technol. **274**, 119083 (2021). https://doi.org/10.1016/j.seppur.2021.119083

18. Hung, W.S., Tsou, C.H., De Guzman, M., An, Q.F., Liu, Y.L., Zhang, Y.M., Hu, C.C., Lee, K.R., Lai, J.Y.: Cross-linking with diamine monomers to prepare composite graphene oxide-framework membranes with varying d-spacing. Chem. Mater. **26**, 2983–2990 (2014). https://doi.org/10.1021/cm5007873

19. Han, J.L., Haider, M.R., Liu, M.J., Wang, H.C., Jiang, W.L., Ding, Y.C., Hou, Y.N., Cheng, H.Y., Xia, X., Wang, A.J.: Borate inorganic cross-linked durable graphene oxide membrane preparation and membrane fouling control. Environ. Sci. Technol. **53**, 1501–1508 (2019). https://doi.org/10.1021/acs.est.8b04194

20. Park, S., Lee, K.S., Bozoklu, G., Cai, W., Nguyen, S.B.T., Ruoff, R.S: Graphene oxide papers modified by divalent ions—enhancing mechanical properties via chemical cross-linking. ACS Nano. **2**, 572–578 (2008). https://doi.org/10.1021/nn700349a

21. Sontakke, A.D., Purkait, M.K.: Fabrication of ultrasound-mediated tunable graphene oxide nanoscrolls. Ultrason. Sonochem. (2020)

22. Sontakke, A.D., Purkait, M.K.: A brief review on graphene oxide nanoscrolls: Structure, synthesis, characterization and scope of applications. Chem. Eng. J. **420**, 129914 (2021). https://doi.org/10.1016/j.cej.2021.129914

23. Amadei, C.A., Stein, I.Y., Silverberg, G.J., Wardle, B.L., Vecitis, C.D.: Fabrication and morphology tuning of graphene oxide nanoscrolls. Nanoscale **8**, 6783–6791 (2016). https://doi.org/10.1039/c5nr07983g

24. Srinivas, G., Burress, J.W., Ford, J., Yildirim, T.: Porous graphene oxide frameworks: Synthesis and gas sorption properties. J. Mater. Chem. **21**, 11323–11329 (2011). https://doi.org/10.1039/C1JM11699A

25. Tang, B., Xiong, Z., Yun, X., Wang, X.: Rolling up graphene oxide sheets through solvent-induced self-assembly in dispersions. Nanoscale **10**, 4113–4122 (2018). https://doi.org/10.1039/c7nr08415c

26. Samanta, N. S., Das, P. P., Mondal, P., Changmai, M., & Purkait, M. K.: Critical review on the synthesis and advancement of industrial and biomass waste-based zeolites and their applications in gas adsorption and biomedical studies. J. Indian Chem. Soc. **99**, 100761 (2022). https://doi.org/10.1016/j.jics.2022.100761

Fluorescent Carbons Dots from Bio-Wastes Immobilized on Mesoporous Silica as an Affordable Next-Generation Catalyst for Adsorptive Removal of Lead

Tuhin Bhattacharjee, Smriti Rekha Das, Hiranya Kumar Choudhury, Deepmoni Deka, and Gitanjali Majumdar

1 Introduction

Carbon nanodots are zero-dimensional material sub 10 nm in size and were first obtained during the refining of carbon nanotube [1] from a mixture in 2004. Carbon dots synthesized from biogenic sources have become the center of research activity in the present times, because of their relatively easy preparation with highly fluorescent properties resulting in their wide range of applications [2]. Carbon dots could be synthesized via low-cost methods from a wide variety of raw materials in nature [3, 4]. These captivating properties bestow the C-dots with great prospective in emerging research activities like optronics, cell-tracking and imaging, drug delivery, and water pollution remediation [5].

Carbon is generally a black powder with low water solubility. Such tiny C-dots has strong fluorescence, hence commonly refereed as fluorescent carbon [6, 7]. The tunable photoluminescence (PL) C-dots are exploited to design a wide range of

T. Bhattacharjee · G. Majumdar (✉)
Department of Chemistry, Assam Engineering College, Jalukbari, Guwahati, Assam 781013, India
e-mail: gitanjalic@gmail.com

S. R. Das · H. K. Choudhury
Department of Chemistry, Handique Girl's College, Dighalipukhuri, Guwahati, Assam 781001, India

D. Deka (✉)
Centre for the Environment, Indian Institute of Technology Guwahati, Guwahati, Assam 781039, India
e-mail: deepmoni@iitg.ac.in

sensors, in vivo imaging platforms, multicolor light emitting systems [8], and efficient light absorbent in the whole spectrum [9].

With added advantage over traditional quantum dots and commercial dyes such carbon quantum dots are preferable with regard to water solubility, chemical inertness, photostable, not known cytotoxicity, and being biocompatibile. Therefore, emphasis has been given to studies on its application in bio-imaging, biological labeling, and drug delivery [10].

The photoluminescence C-dots can be decreased significantly either by using an electron donor–acceptor system in solution, thereby exhibiting that C-dots can have donor and acceptor properties [4]. The photoinduced transfer of electron of C-dots may open access to exciting opportunities involving photovoltaics, light energy conversion, and related applications [10]. It can also be used as sensor probe for ion detection [11].

There has been much development in various methods like laser ablation, electrothermal, combustion/thermal, microwave heating, etc., to produce multicolor, fluorescent, biocompatible carbon dots. Currently, hydrothermal, solvothermal, and microwave synthesis methods are emerging due to easy operation [12].

Heavy metals currently are possibly the most ubiquitous pollutants that has raised serious environmental and health concerns. They are toxic for organisms with their habitats in aqueous environment but at the same time pile up in the food chain that in return may also adversely affect human beings [13]. Contamination from lead metal is a consequence from textile drying, glass and ceramic industries, battery electrode and mining operations, and also from motor vehicle exhaust gases. Lead poisoning causes severe health problems including physical as well as neuro-damage [14].

Therefore, these pollutants need to be reduced to a concentration below the hazardous level before there are discharged into the water ecosystem. Although many procedures are reported for the elimination of toxic metals from wastewater [15]. With ever increasing concentration of environmental pollutants, there is an urgent need for developing novel materials with higher efficacy for the removal of toxic pollutants in an inexpensive way.

Mesoporous material has received immense interest because of it having well-defined pore size, high surface area, and shape. The inner pores of MCM-41 were obtained from the condensation of silicate sources in template micelles, whereas the ordinary structure is the outcome as a micellar array in a hexagonal arrangement. It has a 1D channel system with a p6 mm space group which is identical to a honeycomb network [16–18]. Surface functionalizations of mesoporous silica have gathered significant interest as a solid support due to its large surface-to-volume ratio, faster kinetics for adsorption, manageable porosity, and hierarchically arranged three-dimensional pore arrangement. Using such mesoporous materials researchers have already reported improved removal of heavy metals from wastewater [19–21]. MCM-41 has been modified with different functional groups and has been used to adsorb traces of heavy metals from wastewater [22, 23]. Yoshitake et al. [24] looked into amino-modified mesoporous silica for the treatment of electroplating wastewater. Lam et al. [25] synthesized target-specific MCM-41 functionalized with organic amines. Algarra et al. [26] used aminopropyl groups to estimate the ability to remove hazardous metals from electroplating wastewaters embedded with MCM-41. Adsorptive removal of heavy metals with conventional as well as nanostructured materials has been reported by Burakov et al. [27].

Since the porosity of mesoporous silica-based materials ranges from 2 to 50 nm, it is consistent with QDs of various sizes. Therefore, mesoporous silica can be implanted with QDs forming a composite having mesoporous silica with fluorescent properties of QDs [28]. Reports on QDs embedded mesoporous silica/CQDs composite for Fe^{3+} detection in solution are available [29]. These studies enabled us to venture into the making of novel adsorbent with varied combinations of QDs and mesoporous materials.

Therefore, our main aim is to study the efficacy of the carbon dot MCM-41 nanocomposites prepared from waste biomass material in the adsorption of heavy metal. This composite may be used as a possible adsorbent for the removal of lead from wastewater.

2   Materials and Methods

Camellia sinensis (tea), tea leaves, *Terminalia chebula* (silikha), silikha leaves, *Carica papaya* (papaya) leaves, *Piper betle* (paan), and peel of *Citrus paradise* (grape fruit) were collected from nearby areas. Tetraethylorthosilicate (TEOS) (Sigma-Aldrich) and all other chemicals such as Ammonia, Cetyltrimethylammoniumbromide (CTAB), lead acetate were used of reagent grade purchased from Merck. All the experiments were performed in double distilled water.

2.1   Characterization and Analysis

Fluorescence measurements in aqueous solution at room temperature were performed using a Horiba Fluoromax-4c fluorescence spectrometer. The adsorption of heavy metal was characterized using UV–VIS spectrophotometer (LABINDIA 3200 UV–VIS). Surface charge analysis with zeta potential measurements was performed on a Malvern ZS 90 zeta potential analyzer. Atomic absorption spectrophotometry (AA 7000 Shimadzu) was conducted to measure concentration of lead and iron.

2.2   Synthesis of Water Soluble Carbon Nanodots (ws C-dots)

To synthesize water soluble carbon nanodots, we choose some of the locally available bio masses such as tea leaves, papaya leaves, betel leaves, etc., prior to drying in hot air oven the biomasses were washed properly to remove any dirt or dust particle, then heated at 180° to 200 °C for 30 h. Dried materials were finely grounded and again heated for 36 h at 180 °C and cooled to room temperature. The black finely grinded powder were collected. To generate the water soluble C-dots, a small amount of the black powder were treated with distilled water with 10 min stirring and filtered to get

the carbon dots in soluble form. The solution was then subjected to microwave intensification, which resulted in an intense brown-colored solution. The resulting brown solution showed green fluorescence which was used in the subsequent experiments as an aqueous carbon nanodot solution.

2.3 Synthesis of MCM-41

In a typical synthesis procedure, 153.4 mL distilled water was taken in a 500 mL beaker and added to it 1 g of CTAB slowly with continuous stirring using an electrical stirrer. Then 122.4 mL NH_4OH was added slowly with constant stirring. 4.9 mL TEOS was added drop-wise with stirring. Then the entire mixture was stirred for 2 h. After that, the mixture was allowed to settle for 10 min, which was then filtered and washed to remove the excess ammonia and dried in an oven at 100 °C and calcined at 550 °C obtaining a powdered form of MCM-41.

2.4 Synthesis of C-dots Embedded MCM-41

Aqueous C-dots solution with MCM-41 was stirred using a magnetic stirrer for nearly 5 h. Then the mixture is filtered using fine filter paper and after washing with distilled water, dried in an oven at 95 °C. The dried product is collected. The overall scheme of the synthetic process is shown in Fig. 1.

2.5 Adsorption of Heavy Metals

Aqueous lead acetate solution was used as a model system for the study of the adsorption of heavy metals.

Procedure for adsorption of heavy metal

In a typical synthesis method, 10 mL aqueous solution of heavy metal and 0.08 mg C-dot embedded MCM-41 was stirred in a test tube for 10 min and allowed to settle for 5 min and filtered by using a fine filter paper. The filtrate is used for measuring the concentration of heavy metal using AAS. The same procedure was applied for MCM-41, which was not embedded with c-dot.
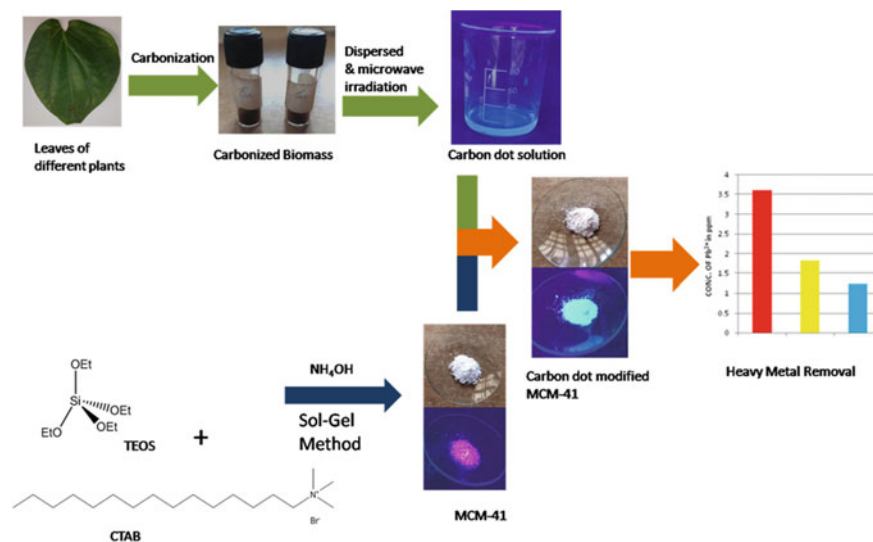
Fig. 1 Overall process in synthesis of carbon dot modified MCM-41

3　Results and Discussion

Carbon nanodots have been synthesized using six different biomass waste through pyrolysis and microwave process. Among them C-dots from Carica papaya (papaya) leaves have shown better adsorption of lead from aqueous solutions as compared to the others. The DLS data shows the size of all the C-dots within the range 8.9–1.8 nm, all having negative zeta potentials within the range −13.4 to −18.9 (Figs. 2, 3 and Table 1). The negative zeta potential is due to the presence of COO– group as evidenced by the IR spectroscopy (Fig. 4). The synthesized C-dots have been embedded in synthesized MCM-41. The decrease in the lead concentration shows the adsorption capacity of MCM-41. The lead adsorption is more effective when papaya C-dot embedded MCM-41 is used as an adsorbent.

The negative zeta potential of the C-dot is due to the presence of –COOH group, which was proved by the IR spectrum of the aqueous solution of all carbon dots. The IR spectrum shows broad bands around 3400 cm^{-1} suggesting the presence of H-bonded –OH group. Further, the sharp bands around 1700 cm^{-1} indicate the presence of >C=O group of carboxylic acid (Fig. 4).

The X-ray diffraction (Fig. 5) of the C-dots shows an intense broad peak at 2θ = 23.8 as a result of graphite lattice spacing. This is due to the existence of highly disordered (sp^3) carbon atoms.

3.1 Fluorescence Emission Spectra of Synthesized Carbon Dots

To check the luminescence properties of the synthesized carbon dots, a small amount of the black powder as dispersed in water and microwaved for 5 min, the resulting yellow solution was used for the photoluminescence (PL) study. The solution is found to have wavelength-dependent fluorescence in the wavelength range of (350–390) nm as shown in Fig. 6.
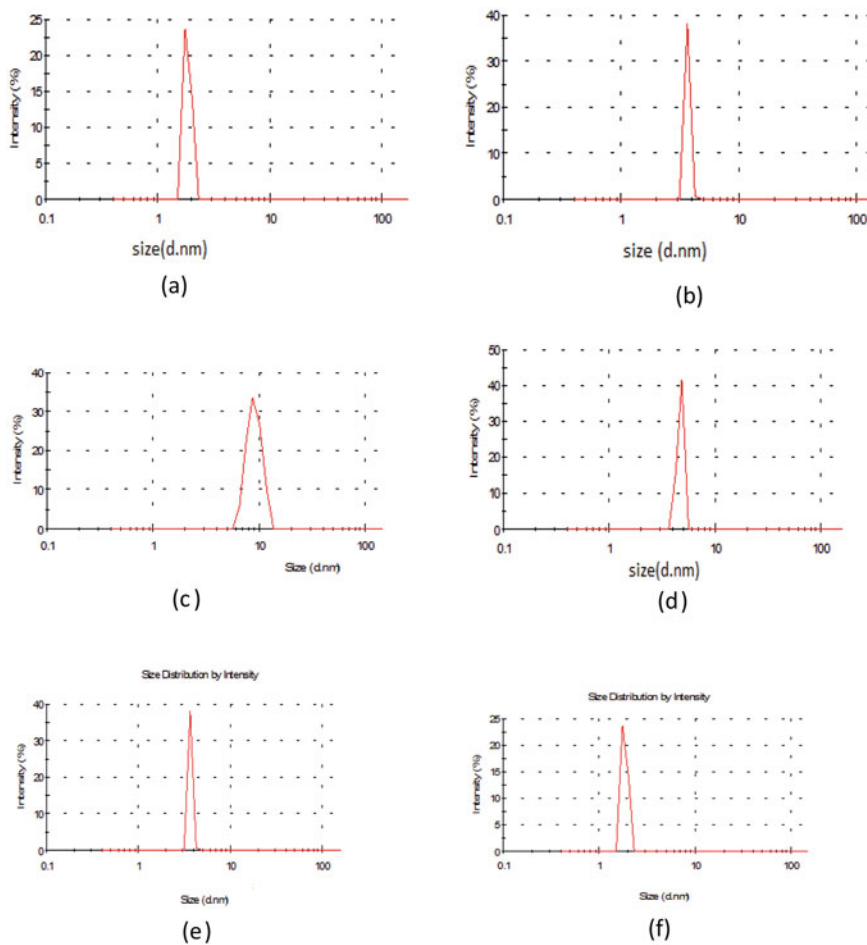
Fig. 2 Dynamic light scattering patterns for particle size determination. Particle size of synthesized C-dot **a** tea, **b** tea leaf, **c** silikha, **d** paan, **e** robab, and **f** papaya
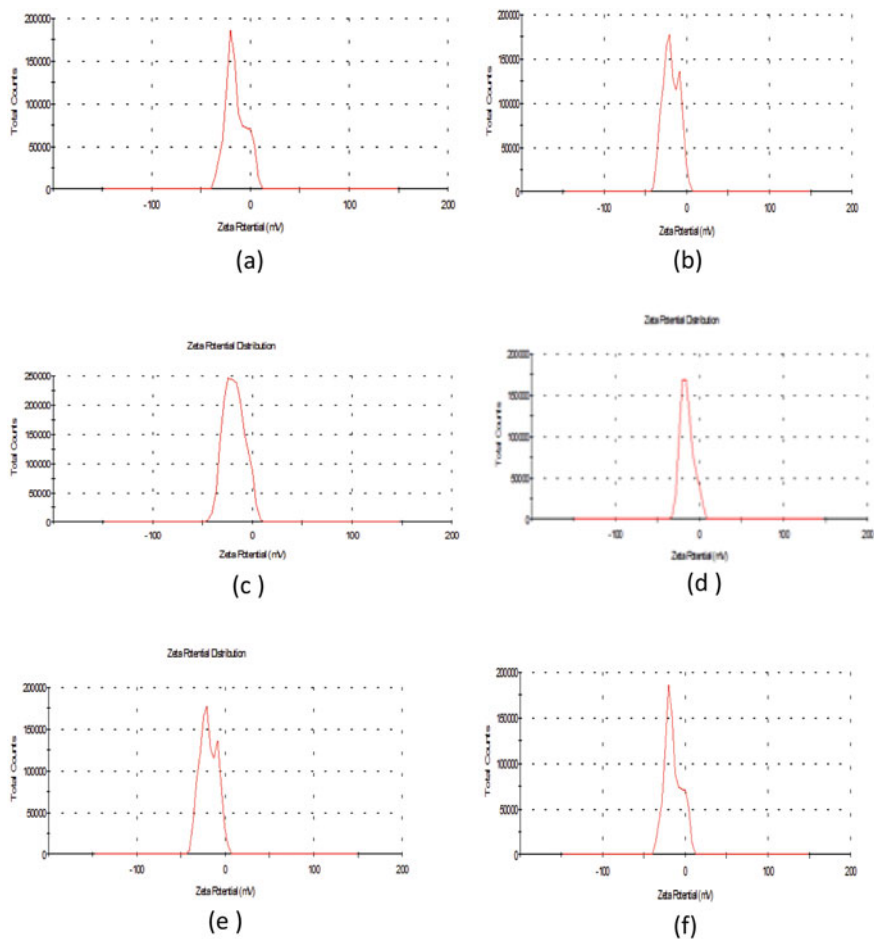
Fig. 3 Zeta potential of C-dots **a** tea, **b** tea leaf, **c** silikha, **d** robab, **e** papaya, and **f** paan

Table 1 DLS data of particle size and zeta potential of the synthesized C-dots

C-dot	Particle size (nm)	Zeta potential (mV)
Tea	3.6	−18.8
Tea leaf	1.83	−18.9
Silikha	8.9	−15.0
Paan	4.6	−13.4
Robab	3.62	−18.6
Papaya	1.8	−18.0
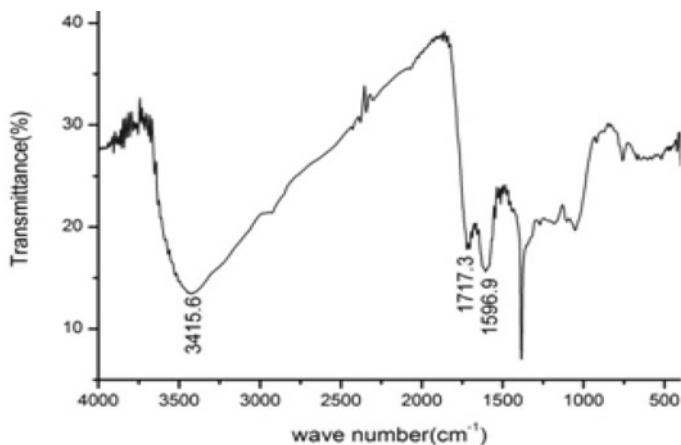
Fig. 4 IR spectrum of C-dots
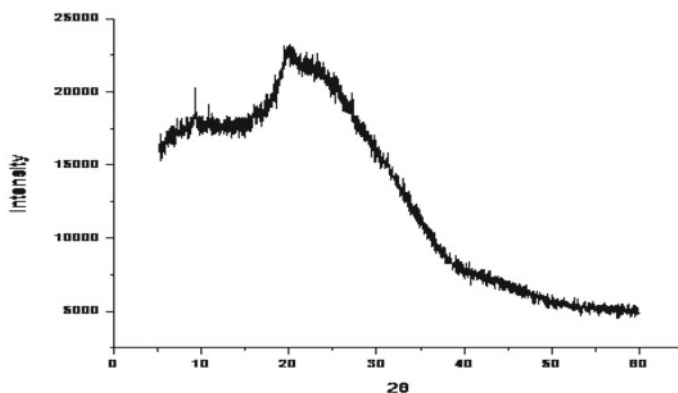
Fig. 5 X-ray diffraction pattern of the carbon dot

All the synthesized C-dots showed fluorescence, and the maximum fluorescence was observed at the exciting wavelength of 390 nm. This also supports the formation of C-dot in the aqueous solution.

In the XRD pattern of C-dot broad peak at $2\theta = 23$ confirms that C-dot is successfully incorporated into MCM-41 (Fig. 7).

3.2 Adsorption of Lead

The concentrations of Pb^{2+} have been measured by using atomic absorption spectroscopy technique. The Pb^{2+} solutions, after stirring with MCM-41, with and without
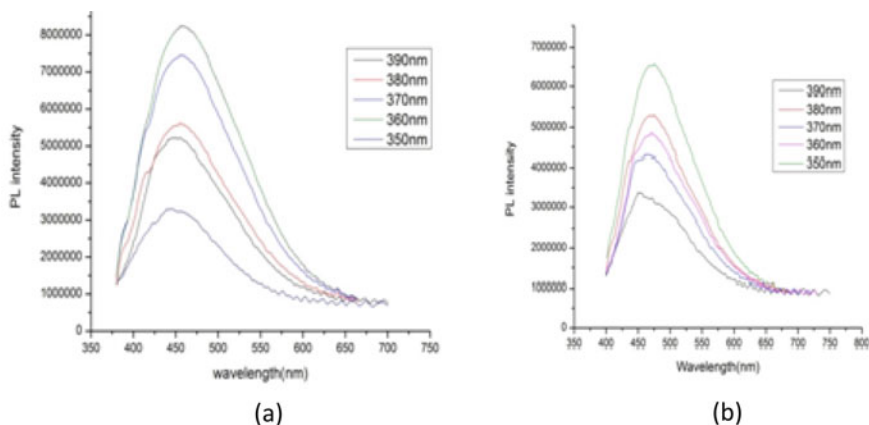
Fig. 6 Tunable fluorescence spectra of C-dot **a** silikha and **b** tea

Fig. 7 XRD pattern of
C-dot embedded MCM-41
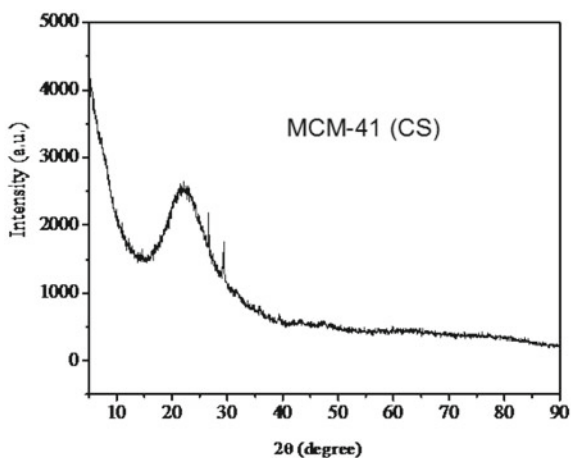
C– dots were filtered out and were subjected to measurement of concentrations of the
metal ion. The result has been presented in Fig. 8. From this data it is clear that the
concentration of lead is much decreased when adsorption is carried out in presence
of C-dots embedded MCM-41 than with MCM-41 alone. Thus, the incorporation
of C-dots in MCM-41 effectively increases the adsorption of Pb^{2+} ions from the
solution.
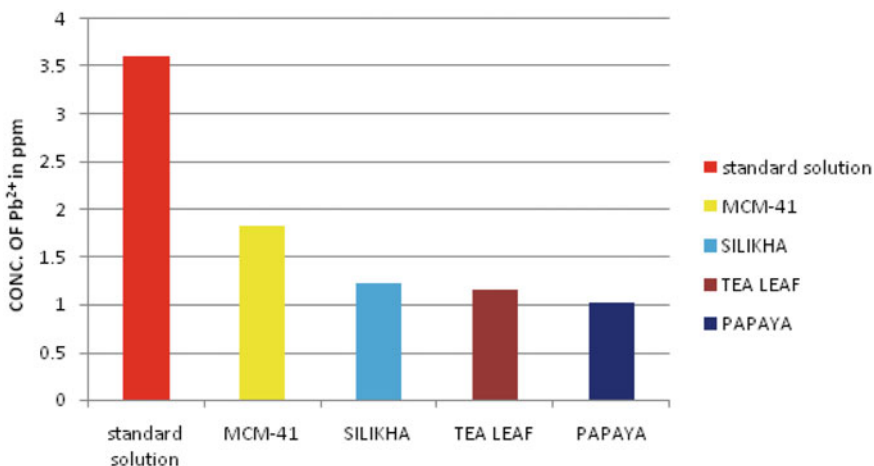
Fig. 8 Concentration of Pb^{2+} in presence of MCM-41 and C-dots embedded MCM-41

3.3 Probable Mechanism of Adsorption of Lead

IR spectrum analysis of C-dots reveals it to contain –COOH group, and by determining zeta potential value of carbon dot, it is found to be negatively charged. When carbon dot is embedded with MCM-41 the surface becomes negatively charged due to the presence of –COO⁻ group. This negatively charged functional group binds with the positively charged heavy metal. So, adsorption occurs due to the chemical interaction between surface functional group and heavy metal (Fig. 9).

4 Conclusion

In summary, pyrolysis and microwave-assisted treatment of waste material has been reported as a green approach for the synthesis of fluorescent C-dots. Furthermore, this synthesis process offers the advantage of simplicity and cost efficiency. The C-dots have a particle sizes within the range of 8.9–1.8 nm and zeta potential value within the range of −13.4 to −18.9. This synthesized C-dot is embedded in prepared MCM-41 and studied for adsorption of heavy metal lead. Among the biogenic materials, the papaya C-dot is found to be more effective in adsorption of heavy metal lead.
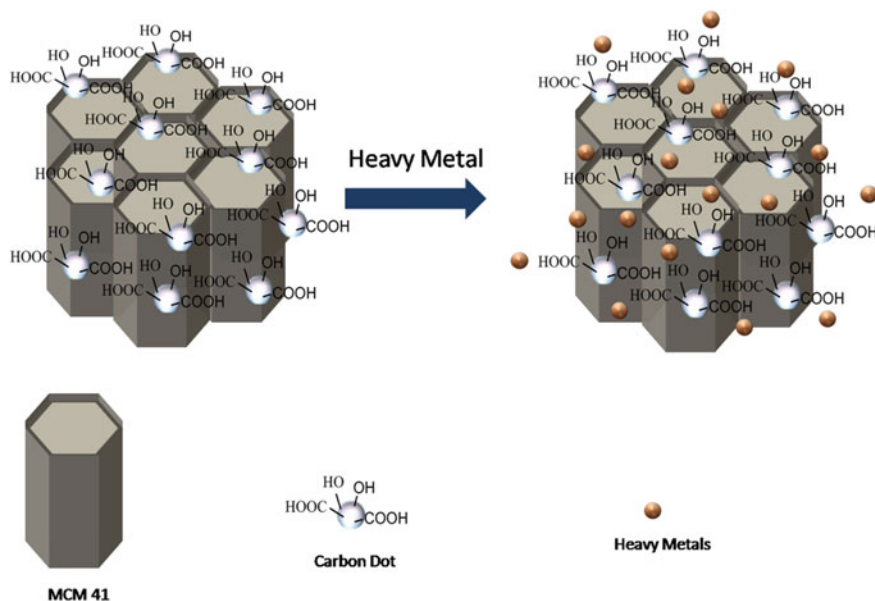
Fig. 9 Mechanism of adsorption of heavy metal

Appendix

See the Table 2.

Table 2 Atomic absorption spectroscopy (AAS) data of Pb^{2+} concentration in ppm

Adsorbent	Concentration of Pb^{2+} in ppm
Standard lead solution	3.599
MCM-41	1.8227
Silikha C-dot embedded MCM-41	1.2303
Robab C-dot embedded MCM-41	1.2987
Tea leaf C-dot embedded MCM-41	1.1620
Papaya C-dot embedded MCM-41	1.0253

References

1. Xu, X., Ray, R., Gu, Y., Ploehn, H.J., Gearheart, L., Raker, K., Scrivens, W.A.: Electrophoretic analysis and purification of fluorescent single-walled carbon nanotube fragments. J. Am. Chem. Soc. **126**, 12736–12737 (2004)
2. Humaera, N.A., Fahri, A.N., Armynah, B., Tahir, D.: Natural source of carbon dots from part of a plant and its applications: a review. Luminescence **36**(6), 1354–1364 (2021)
3. Long, C., Jiang, Z., Shangguan, J., Qing, T., Zhang, P., Feng, B.: Applications of carbon dots in environmental pollution control: a review. Chem. Eng. J. 126848 (2020)
4. Perumal, S., Atchudan, R., Edison, T.N.J.I., Lee, Y.R.: Sustainable synthesis of multifunctional carbon dots using biomass and their applications: a mini-review. J. Environ. Chem. Eng. **9**(4), 105802 (2021)
5. Ng, H.K.M., Lim, G.K., Leo, C.P.: Comparison between hydrothermal and microwave-assisted synthesis of carbon dots from biowaste and chemical for heavy metal detection: a review. Microchem. J. **165**, 106116 (2021)
6. Li, M.L., et al.: Carbon dots: synthesis, formation mechanism, fluorescence origin and sensing applications. Green Chem. **21**(3), 449–471 (2019)
7. Wang, B., Lu, S.: The light of carbon dots: from mechanism to applications. Matter **5**(1), 110–149 (2022)
8. He, C., Peng, X., Zhang, X., Long, W.: The synthetic strategies, photoluminescence mechanisms and promising applications of carbon dots: current state and future perspective. Carbon **186**, 91–127 (2022)
9. Saini, D., Garg, A.K., Dalal, C., Anand, S.R., Sonkar, S.K., Sonker, A.K., Westman, G.: Visible-light-promoted photocatalytic applications of carbon dots: a review. ACS Appl. Nano Mater. **5**(3), 3087–3109 (2022)
10. Wang, B., Cai, H., Waterhouse, G.I., Qu, X., Yang, B., Lu, S.: Carbon dots in bioimaging, biosensing and therapeutics: a comprehensive review. Small Sci. 2200012 (2022)
11. Chattopadhyay, S., Mehrotra, N., Jain, S., Singh, H.: Development of novel blue emissive carbon dots for sensitive detection of dual metal ions and their potential applications in bioimaging and chelation therapy. Microchem. J. **170**, 106706 (2021)
12. Ng, H.K., Melvin, G.K., Lim, C. P. Leo.: Comparison between hydrothermal and microwave-assisted synthesis of carbon dots from biowaste and chemical for heavy metal detection: a review. Microchemi. J. **165**, 106116 (2021)
13. Das, P. P., & Purkait, M. K.: Treatment of cold rolling mill (CRM) effluent of steel industry. Sep. Purif. Technol. **274**, 119083 (2021)
14. Debnath, B., Singh, W.S., Manna, K.: Sources and toxicological effects of lead on human health. Indian J. Med. Specialities **10**(2), 66 (2019)
15. Das, P. P., Mondal, P., Sinha, A., Biswas, P., Sarkar, S., & Purkait, M. K.: Treatment of steel plant generated biological oxidation treated (BOT) wastewater by hybrid process. Sep. Purif. Technol. **258**, 118013 (2021)
16. Liu, J., et al.: Preparation and adsorption properties of mesoporous material PS-MCM-41 with low-silicon content peanut shell ash as silicon source. Mater. Chem. Phys. **241**, 122355 (2020)
17. Bhandari, R., Volli, V., & Purkait, M. K.: Preparation and characterization of fly ash based mesoporous catalyst for transesterification of soybean oil. J. Environ. Chem. Eng. **3**, 906–914 (2015)
18. Li, X.-D., Zhai, Q.-Z.: Evaluation of eosin Y removal from aqueous solution using nano-mesoporous material MCFs: adsorption equilibrium, kinetics, and adsorption isotherms. Int. J. Ind. Chem. **11**(1), 55–67 (2020)
19. Bhattacharjee, A., Gumma, S., & Purkait, M. K.: Fe3O4 promoted metal organic framework MIL-100 (Fe) for the controlled release of doxorubicin hydrochloride. Microporous Mesoporous Mater. **259**, 203–210 (2018)
20. Samanta, N. S., Das, P. P., Mondal, P., Changmai, M., & Purkait, M. K.: Critical review on the synthesis and advancement of industrial and biomass waste-based zeolites and their applications in gas adsorption and biomedical studies. J. Indian Chem. Soc. **99**, 100761 (2022)

21. Das, P. P., Sharma, M., & Purkait, M. K.: Recent progress on electrocoagulation process for wastewater treatment: A review. Sep. Purif. Technol. **292**, 121058 (2022)
22. Cashin, V.B., et al.: Surface functionalization and manipulation of mesoporous silica adsorbents for improved removal of pollutants: a review. Environ. Sci. Water Res. Technol. **4**(2), 110–128 (2018)
23. Fu, Y., et al.: Rapid and selective removal of Hg (II) ions and high catalytic performance of the spent adsorbent based on functionalized mesoporous silica/poly (m-aminothiophenol) nanocomposite. J. Mol. Liq. **286**,110746 (2019)
24. Yoshitake, H., Yokoi, T., Tatsumi, T.: Adsorption behavior of arsenate at transition metal cations captured by amino-functionalized mesoporous silicas. Chem. Mater. **15**, 1713 (2003)
25. Alg, M., Jiménez, M.V., Rodríguez-Castellón, E., Jiménez-López, A., Jiménez-Jiménez, J.: Heavy metals removal from electroplating wastewater by aminopropyl-Si MCM-41. Chemosphere **59**, 779 (2005)
26. Ho, Y.S., McKay, G.: Sorption of dyes and copper ions onto biosorbents. Process Biochem. **38**, 1047 (2003)
27. Gupta, N., Singh, H.P., Sharma, R.K.J.: Metal nanoparticles with high catalytic activity in degradation of methyl orange: an electron relay effect. J. Mol. Catal. A: Chem. **335**(1–2), 248–252 (2011)
28. Wang, M., et al.: Preparation of mesoporous silica/carbon quantum dots composite and its application in selective and sensitive Hg^{2+} detection. Microporous Mesoporous Mater. **284**, 378–384 (2019)
29. Dong, Y., et al.: Ordered mesoporous silica encapsulated carbon quantum dots and its application in Fe^{3+} detection. Ceram. Int. **46**(8), 11115–1112 (2020)

Numerical Analysis of Particulate Matter 2.5 to Get the Diffusion Model of North-East India Using Anomalous Diffusion Equation

Somnath Das and Dilip Pal

1 Introduction

Diffusion is a process where particles or molecules spreads from higher concentration region to lower concentration region via a slow mixing process, to a state where they are uniformly scattered. Diffusion is a fundamental transport mechanism that helps many non-equilibrium systems reach equilibrium. Diffusion is an idea that is commonly utilised in a variety of disciplines in physics, chemistry and cell biology. Robert Brown's discovery of a very irregular condition of motion for microscopic pollen grains suspended in water created one amongst science's most interesting topics. The significance of such a finding is really immeasurable. This irregular motion called as Brownian motion can be based on a random walk where the mean square displacement can be written as using Einstein's relation [1],

$$\langle (\Delta x)^2 \rangle = 2t \mathrm{d}D \tag{1}$$

where Δx is the displacement of Brownian particles, d is the dimension of the space we are working on, D is diffusion constant. In this paper, we basically work on Einstein's relation using environments particles data.

In contrast to this, a significant class of systems and processes exhibit anomalous diffusion behaviour, which is characterised by a nonlinear temporal dependency of the same variable. From last few decades, various fields were gaining the attention of scientific community. Unlike ordinary diffusion, anomalous diffusion explains by a power law

S. Das (✉) · D. Pal
Department of Physics, Indian Institute of Technology Guwahati, Guwahati, Assam, India
e-mail: somnath.das@iitg.ac.in

D. Pal
e-mail: dpal@iitg.ac.in

$$\langle (\Delta x)^2 \rangle = D_\alpha t^\alpha \tag{2}$$

where t is the elapsed time and D_α is generalised diffusion coefficient; if we put $\alpha = 1$, we can get the normal diffusion equation, subdiffusion occurs when $\alpha < 1$ and superdiffusion happens when $\alpha > 1$ this is known as anomalous diffusion type. Superdiffusion can occur as a result of active cellular transport mechanisms [2].

2 Mathematical Preliminaries

2.1 A Brief About Fractional Calculus

The strength of fractional calculus-based mathematical tools has drawn the attention of the pure and applied mathematics community. In practice, the combination of these methodologies with the diffusional problem represents a new field of research. It has been demonstrated in numerous ways that fractional calculus, while not unique, is an acceptable or even natural mathematical framework for dealing with the tremendous complexity of anomalous diffusion processes. One effective technique of applying these mathematical tools to the study of diffusion processes necessitates the search for fractional linear and nonlinear diffusion equation solutions.

Normally, we are familiar with derivatives where orders are integers like $\frac{dy}{dx}$ which we can solve or analyse easily, but problem starts when are facing the derivatives with fractional orders like $\frac{d^{1/2}y}{dx^{1/2}}$, to solve this type of equation we need fractional calculus. Not individually but with the help of many mathematician fractional calculus was improved step by step.

2.1.1 Mathematical Operations for Fractional Calculus

Riemann–Liouville Fractional Integral

$$\,_a^{RL}I_x^\alpha f(x) = \frac{1}{\Gamma(\alpha)} \int_a^x (x-t)^{\alpha-1} f(t) \mathrm{d}t \; \alpha \in R, \; 0 < \alpha < 1 \tag{3}$$

where a and x are terminal points.

Properties of RF Fractional Integral

$$\,_a^{RL}I_x^0 f(x) = f(x) \tag{4}$$

$$\,_0^{RL}I_x^\alpha C = \frac{C}{\Gamma(\alpha+1)} x^\alpha \; \alpha > 0 \tag{5}$$

$$\substack{RL\\0}I_x^\alpha(x^n) = \frac{\Gamma(n+1)}{\Gamma(n+\alpha+1)}x^{n+\alpha}\, n > -1, \ \alpha > 0 \tag{6}$$

Properties of Riemann–Liouville Fractional Derivative

$$\substack{RL\\a}D_x^\alpha f(x) = \frac{1}{\Gamma(n-\alpha)}\left(\frac{d}{dx}\right)^n \int_0^x (x-t)^{n-\alpha-1}f(t)dt, \ \alpha > 0, \ n-1 < \alpha \le n$$

$$\tag{7}$$

$$\substack{RL\\0}D_x^\alpha C = \frac{1}{\Gamma(1-\alpha)}x^{-\alpha}\ \alpha > 0 \tag{8}$$

$$\substack{RL\\0}D_x^\alpha(x^n) = \frac{\Gamma(n+1)}{\Gamma(n-\alpha+1)}x^{n-\alpha}\, n > -1, \ \alpha > 0 \tag{9}$$

Properties of Caputo Fractional Derivative

$$\substack{C\\a}D_x^\alpha f(x) = \frac{1}{\Gamma(n-\alpha)}\int_a^x (x-t)^{n-\alpha-1}f^n(t)dt\ \alpha > 0, \ n-1 < \alpha \le n \tag{10}$$

$$\substack{C\\0}D_x^\alpha(c) = 0 \ \ \alpha > 0 \tag{11}$$

$$\substack{C\\0}D_x^\alpha(x^n) = \frac{\Gamma(n+1)}{\Gamma(n-\alpha+1)}x^{n-\alpha}\, n > -1, \ \alpha > 0 \tag{12}$$

Mittag–Leffler Function

This function is taken from the paper [3]

$$E_{\alpha,\beta}(z) = \sum_{k=0}^{\infty} \frac{Z^k}{\Gamma(\alpha k + \beta)} \tag{13}$$

$$E_{0,1}(z) = \frac{1}{(1-z)}\ |z| < 1 \tag{14}$$

$$E_{1,1}(z) = e^z \tag{15}$$

$$E_{1,2}(z) = \frac{e^z - 1}{z} \tag{16}$$

Laplace Transform of Fractional Operation

$$L\{f(t)\} = \int_0^\infty e^{-st} f(t)dt = F(s) \tag{17}$$

Laplace transform of Riemann–Liouville derivative

$$L\{^{RL}_0 D^\alpha_x f(x)\} = s^\alpha F(s) - \sum_{k=0}^{n-1} s^k {}^{RL}_0 D^{\alpha-k-1}_x f(0) \tag{18}$$

Laplace transform of Caputo derivative

$$L\{^C_0 D^\alpha_x f(x)\} = s^\alpha F(s) - \sum_{k=0}^{n-1} s^{\alpha-k-1} f^k(0) \tag{19}$$

Laplace transform of Mittag–Leffler function

$$L\{x^{\beta-1} E_{\alpha,\beta}(\lambda x^\alpha)\} = \frac{s^{\alpha-\beta}}{s^\alpha - 1} \tag{20}$$

Pochhammer Symbol

Let $z \in C$ and $n \in N$ then the pochhammer symbol $(z)_n$ with integer order n written as

$$(z)_0 = 1, (z)_n = z(z+1)\ldots(z+n-1)[n = 1, 2, \ldots]$$
$$(1)_n = n!$$

Binomial Coefficients

Let $\alpha \in C$ and $n \in N$ then the binomial coefficients are defined by

$$\binom{\alpha}{n} = \frac{(-1)^n(-\alpha)_n}{n!}$$

Or

$$\binom{n}{m} = \frac{n!}{m!(n-m)!} \cdots [m \geq n \geq 0, \; n = 0, 1, 2, \ldots m]$$

This binomial coefficients can also define as for minteger as

$$\binom{\alpha}{m} = \frac{\Gamma(\alpha + 1)}{\Gamma(m + 1)\Gamma(\alpha - m + 1)} \tag{21}$$

Gamma Function

$$\Gamma(z) = \int_0^\infty x^{z-1} \exp(-x)\mathrm{d}x \quad [z \in C]$$

is defined as Gamma function, the recurrence relation that is going to help us

$$\Gamma(n + 1) = n\Gamma(n)$$

$$\Gamma(-x) = \frac{\Gamma(-x + m)}{\prod_{k=0}^{m-1}(-x + k)} \quad \text{(m is an integer)} \tag{22}$$

2.2 Grunwald–Letnikov Operator

It helps us to calculate the fractional derivative of a density function, to calculate the diffusion coefficient of a particular space.

From the definition of derivative of $y(x)$, using the elementary calculus we can write [4]

$$y'(x) = \frac{\mathrm{d}y}{\mathrm{d}x} = \lim_{h \to 0} \frac{y(x) - y(x - h)}{h} \tag{23}$$

where h is a step function, we have 1 h interval data, that's why we will take $h = 1$

Similarly for second-order derivative, we have

$$y''(x) = \frac{\mathrm{d}^2 y}{\mathrm{d}x^2} = \lim_{h \to 0} \frac{y'(x) - y'(x - h)}{h}$$

$$= \lim_{h \to 0} \frac{y(x) - 2y(x - h) + y(x - 2h)}{h^2}$$

Same way it will permit us to do nth order derivative, which gives

$$y^n(x) = \frac{\mathrm{d}^n y}{\mathrm{d}x^n} = \lim_{h \to 0} \frac{1}{h^n} \sum_{m=0}^{\infty} (-1)^m \binom{n}{m} y(x - mh) \tag{24}$$

$$\binom{n}{m} = \frac{n!}{m!(n - m)!} = \frac{n(n - 1)(n - 2)\ldots\ldots\ldots(n - m + 1)}{m!}$$

For the convenience of our calculation, we will convert factorials into gamma function.

Using the gamma function property from (3), we can write [5]

$$D^\alpha y(x) = \lim_{h \to 0} \frac{1}{h^n} \sum_{m=0}^{\infty} (-1)^m \frac{\Gamma(\alpha+1)}{\Gamma(m+1)\Gamma(\alpha-m+1)} y(x-mh) \qquad (25)$$

(α denotes the fractional parameters).

2.3   Log-Normal Distribution Function

The probability distribution function that will be widely used in this paper is log-normal distribution.

If the natural logarithm of a random variable has a normal distribution, it is said to have a log-normal distribution. In other words, a normal random variable's exponential has a log-normal distribution.

The PDF of log-normal distribution for x positive random variables is given by

$$f(x) = \frac{1}{x\sigma\sqrt{2\pi}} \exp\left(-\frac{(\ln x - \mu)^2}{2\sigma^2}\right) \qquad (26)$$

where σ^2 is variance and μ is the mean of sample
$f(x) = 0$ for $x < 0$, where $-\infty < \mu < \infty, \sigma > 0$

$$\text{for}\quad x > 0 \quad P(X \le x) = P(\ln X \le \ln x)$$
$$= P(Y \le \ln x) = P\left(\frac{Y-\mu}{\sigma} \le \frac{\ln x - \mu}{\sigma}\right)$$
$$= \emptyset\left(\frac{\ln x - \mu}{\sigma}\right)$$

$\emptyset$ is a cumulative distribution function of $N(0,1)$.

Relation between Normal and Log-Normal Distribution

Let us take a random variable Y for which σ^2 is variance and μ is the mean of sample.
Then we can say

$$X = \exp(Y)$$

will give the log-normal distribution with parameters σ and μ.

If Y has a normal distribution, then its probability density function is

$$f_Y(y) = \frac{1}{\sqrt{2\pi\sigma^2}} \exp\left(-\frac{1}{2}\frac{(y-\mu)^2}{\sigma^2}\right) \qquad (27)$$

the function $X = g(Y) = \exp(Y)$

which is a strictly increasing function

we can write

$$f_X(x) = f_Y\big(g^{-1}(x)\big)\frac{\mathrm{d}g^{-1}}{\mathrm{d}x}$$

At certain point, we have

$$g^{-1}(x) = \ln(x)$$

$$\frac{\mathrm{d}g^{-1}}{\mathrm{d}x} = 1/x$$

So that $f_X(x) = f_Y\big(g^{-1}(x)\big)\frac{\mathrm{d}g^{-1}}{\mathrm{d}x}\ f_X(x) = f_Y\big(g^{-1}(x)\big)\frac{\mathrm{d}g^{-1}}{\mathrm{d}x}$

$$= \frac{1}{x\sigma\sqrt{2\pi}}\exp\left(-\frac{(\ln x - \mu)^2}{2\sigma^2}\right)$$

Parameters in Log-Normal Distribution

Mean	$\exp(\mu + \sigma^2/2)$
Median	$\exp(\mu)$
Mode	$\exp(\mu - \sigma^2)$
Variance	$[\exp(\sigma^2) - 1]\exp(2\mu + \sigma^2)$
Skewness	$[\exp(\sigma^2) + 2]\sqrt{\exp(\sigma^2) - 1}$

3   Historical Background—Normal to Anomalous Diffusion

No discussion of diffusion would be complete without including the work of Albert Einstein, Robert Brown, Marian Smoluchowski and Paul Langevin. Base point of any type of diffusion is random motion of particles which is also known as Brownian motion. Robert Brown (1773–1858), an English botanist, was one of the first scientists to notice and report on the random motion of particles. He discovered microscopic particles moving in a continuous, irregular zigzag pattern in an aqueous sample of pollen from the plant Clarkia pulchella.

First paper of Einstein on Brownian motion gives the diffusion coefficient D, which can be expressed as,

$$D = \frac{RT}{N} \times \frac{1}{6\pi kr} \tag{28}$$

where k is the coefficient of viscosity of outers liquid, r is the radius of the spherical particle, R is ideal gas constant, T is the temperature at which the experiment takes place.

In this consequence, the diffusion equation governed by the Brownian motion can be described by the equation

$$\frac{df}{dt} = D\frac{d^2 f}{dx^2} \tag{29}$$

$f(x, t)$ is the number of particles per unit volume at a distance x at a time t.

To deduce this equation let us take a liquid chamber containing 'n' number of molecules, suppose in an interval δ time particles increased by 'y', now the probability of the particle displaced between y and y +dy is $\varphi(y)$dy at a time interval δ,

Now $\int\limits_{-\infty}^{\infty} \varphi(y)dy = 1$ with the symmetry

$$\varphi(y) = \varphi(-y) \tag{30}$$

Number of particles $f(x, t)$ per unit volume located at time $(t + \delta)$, at x and $x +$ dx will be

$$f(x, t + \delta)dx = dx \int\limits_{-\infty}^{\infty} f(x + y, \delta)\varphi(y)dy$$

$$\approx f(x, t) + \delta\frac{df}{dx} \tag{31}$$

When δ is very small $f(x + y)$ of RHS of Eq. (31) can be written as

$$f(x + y, t) = f(x, t) + y + \frac{df}{dx} + \frac{y^2}{2}\frac{d^2 f}{dx^2} + \text{higher−order terms}$$

from Eq. (31)

$$f(x, t + \delta)dx = f(x, t)\int\limits_{-\infty}^{\infty} \varphi(y)dy + \frac{df}{dx}\int\limits_{-\infty}^{\infty} y\varphi(y)dy + \frac{d^2 f}{dx^2}\int\limits_{-\infty}^{\infty}\frac{y^2}{2}\varphi(y)dy$$

using Eq. (30) we can show

$$\int\limits_{-\infty}^{\infty} y\varphi(y)dy = 0,$$

Now we can write

$$\delta \frac{\mathrm{d}f}{\mathrm{d}t} = \frac{\mathrm{d}^2 f}{\mathrm{d}x^2} \int\limits_{-\infty}^{\infty} \frac{y^2}{2} \varphi(y)\mathrm{d}y \tag{32}$$

Let us define

$$D = \frac{1}{\delta} \int\limits_{-\infty}^{\infty} \frac{y^2}{2} \varphi(y)\mathrm{d}y$$

Hence, Eq. (29) $\frac{\mathrm{d}f}{\mathrm{d}t} = D\frac{\mathrm{d}^2 f}{\mathrm{d}x^2}$ is deduced.

From the central limit theorem, the solution of Eq. (27) around $t = 0$ can be written as

$$f(x, t) = \frac{n}{\sqrt{4\pi t D}} e^{-\frac{x^2}{4tD}}$$

$$n = \int\limits_{-\infty}^{\infty} f(x, t)\mathrm{d}x \tag{33}$$

so now the mean square displacement can be written as

$$\langle x^2 \rangle = \frac{1}{n} \int\limits_{-\infty}^{\infty} x^2 f(x, t)\mathrm{d}x = 2tD \tag{34}$$

Using (28) and (34) we can write, the mean square displacement

$$\langle x^2 \rangle = \frac{RT}{N} \times \frac{1}{3\pi kr} \times t \tag{35}$$

Avogadro's number can also be determined from the above equation. From Langevin's treatment, we can also determine this above equation.

3.1 Langevin's Treatment

The equipartition theorem is the beginning point for Langevin's quantitative method. It is necessary for a molecule immersed in any form of liquid to have an average kinetic energy such that when multiplied by a large number of identical particles of mass m, the average is equal to

$$m\langle v^2 \rangle = \frac{RT}{N} \tag{36}$$

where $v = \frac{\mathrm{d}x}{\mathrm{d}t}$ velocity of particle some particular point. Then the E.O.M can be written as

$$m\frac{\mathrm{d}^2x}{\mathrm{d}t} = -6\pi\mu av + Y \tag{37}$$

where $F_v = -6\pi\mu av$ (viscous dragging force related to stokes law) and for Y Langevin treat it as 'complementary force'. The complimentary force is such that it keeps the particle excited; otherwise, the viscous resistance would halt it. The mass m is given by solving the equation, and we can deduce

$$\left\langle \frac{\mathrm{d}x^2}{\mathrm{d}t} \right\rangle = \frac{RT}{N}\frac{1}{3\pi\mu a}$$

Or,

$$\langle x^2 \rangle = \frac{RT}{N} \times \frac{1}{3\pi\mu a} \times t \tag{38}$$

Same as obtained by Einstein.

Langevin provided a method for dealing with Gaussian white noise and a stochastic/contemporary differential equation that has inspired new mathematical approach and gives a new thing. Let us rewrite Eq. (40) in the form to examine this element of the technique in further depth,

$$\frac{\mathrm{d}v}{\mathrm{d}t} = -\gamma v + S(t) \tag{39}$$

where $\gamma = \frac{6\pi\mu a}{m}$ and $S(t)$ is contemporary force or stochastic force per unit mass. This is linked to the system's characteristics. Thus, the choice of $S(t)$ from normal to anomalous diffusion determines whether the system is described in a Markovian or non-Markovian manner [6] depending on the features of the system under examination (non-Markovian will be discussed later).

So the characteristics equation to illustrate the process

$$\langle S(t) \rangle = 0$$
$$\langle S(t)S(t') \rangle = \overline{m}\delta(t - t') \tag{40}$$

where $\overline{m} = \frac{2S^2D}{m^2}$ and $D = \frac{KT}{Sm}$ (Einstein–Smoluchowski relation).

This selection of $S(t)$ is characteristic of a Markovian process, i.e. Brownian motion, and is commonly referred to as white noise. In order to explain other types of diffusive processes, we must find additional relevant formulations for $S(t)$ for an anomalous process, i.e. a non-Markovian process.

Using the co-relation function in this case, we can also establish

$$\langle x^2 \rangle = 2tD \tag{41}$$

Anomalous diffusion, on the other hand, is defined by a distinct time dependency in Eq. (44), which may be a power law depending on the behaviour of the process.

$$\langle x^2 \rangle \propto t^{\alpha} \tag{42}$$

For $\alpha > 1$, it shows superdiffusion and $\alpha < 1$ shows subdiffusion, whereas $\alpha = 1$ shows normal diffusion [7].

4 Numerical Analysis of Anomalous Diffusion Equation Using the data of North-East India

Different types of pollutants (like SO_2, CO_2, PM2.5, PM10) are present in our environment which exhibit Brownian motion. To study the anomalous diffusion equation, we will use the data of PM2.5. 'Central Pollution Control Board' of India publish every 1 h interval data of these pollutants in the form of concentration. We will basically take four different stations of North-East region (Assam Railway Station, Pan Bazar, Lumpyngngad-Meghalaya and PWD Junction-Kohima).

4.1 What is PM2.5?

PM is a combination of several chemical species, not a single pollutant. Small liquid droplets, dry solid fragments and solid cores with liquid coatings make up this complicated blend of solids and aerosols. Particles come in a variety of sizes, shapes and chemical compositions and may contain inorganic ions, metallic compounds, elemental carbon, organic molecules and chemicals from the earth's crust. For the purposes of air quality regulation, particles are classified according to their diameter. PM2.5 is the particulate matter having aerodynamic diameter less than or equal to 2.5 microns.

4.1.1 Assam Railway Station

We have every 1 h interval data of PM2.5. We will take those data to get the time series plot, from that we will also find the fluctuation of those particles in every 1 h (Figs. 1, 2 and Table 1).
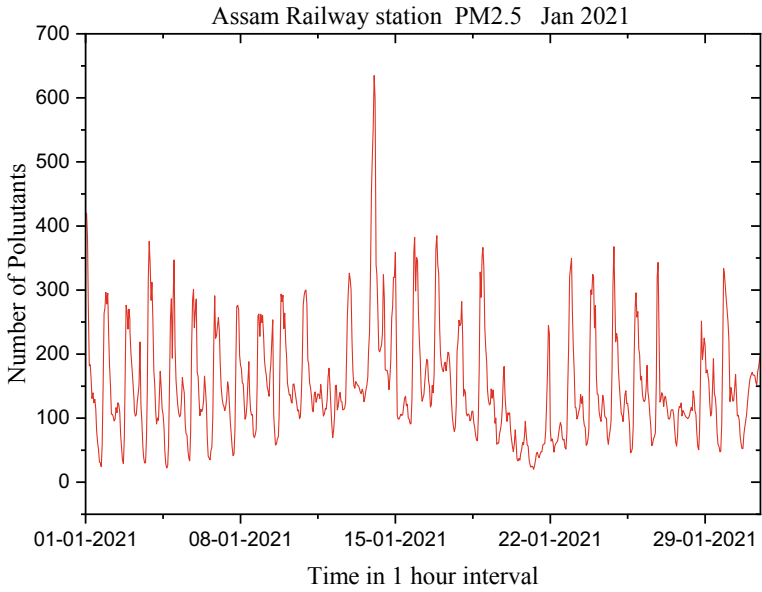
Fig. 1 Time series plot of pollutants(PM2.5)
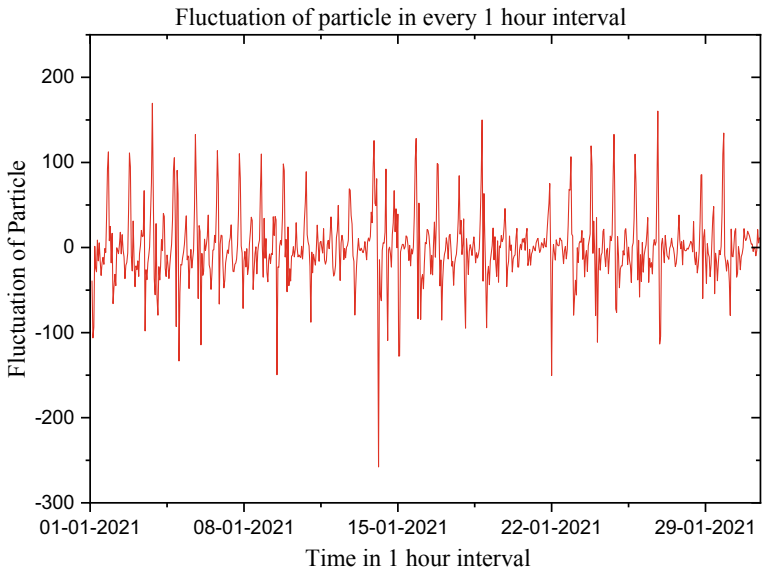
Fig. 2 Fluctuation of pollutants about mean position

Table 1 Concentration of PM2.5 in every 1 h interval

From date	To date	PM2.5
01–01–2021 00:00	01–01–2021 01:00	420.48
01–01–2021 01:00	01–01–2021 02:00	381.69
01–01–2021 02:00	01–01–2021 03:00	275.4
01–01–2021 03:00	01–01–2021 04:00	181.97
01–01–2021 04:00	01–01–2021 05:00	183.47
01–01–2021 05:00	01–01–2021 06:00	159.44
01–01–2021 06:00	01–01–2021 07:00	130.81
01–01–2021 07:00	01–01–2021 08:00	139.6
01–01–2021 08:00	01–01–2021 09:00	123.94
01–01–2021 09:00	01–01–2021 10:00	129.5
01–01–2021 10:00	01–01–2021 11:00	113.58
01–01–2021 11:00	01–01–2021 12:00	80.75
01–01–2021 12:00	01–01–2021 13:00	62.45
01–01–2021 13:00	01–01–2021 14:00	50.89
01–01–2021 14:00	01–01–2021 15:00	31.2
01–01–2021 15:00	01–01–2021 16:00	29.94
01–01–2021 16:00	01–01–2021 17:00	24.23
01–01–2021 17:00	01–01–2021 18:00	58.53
01–01–2021 18:00	01–01–2021 19:00	151.18
01–01–2021 19:00	01–01–2021 20:00	263.61
…….	……	……

Frequency Distribution of Assam Railway Station (PM2.5-2021)

Next we will do the binning of time series data for the whole year of 2021 to find the frequency distribution plot (Fig. 3).

The above log-normal distribution can be verified by taking log of the number of pollutants and again if we plot the frequency distribution of that data, then we will get a well-fitted Gaussian curve, which verify the above distribution plot (Fig. 4).

4.1.2 Pan Bazar Assam

We have every 1 h interval data of PM2.5. We will take those data to get the time series plot, from that we will also find the fluctuation of those particles in every 1 h (Figs. 5 and 6).

4.1.3 Frequency Distribution of Pan Bazar—Assam (PM2.5-2021)

See the Fig. 7.

Descriptive Statistics of the Frequency Distribution	
Mean	111.2838
Standard Error	20.06129
Median	41
Mode	6
Standard Deviation	172.5737
Sample Variance	29781.69
Kurtosis	7.416744
Skewness	2.629275
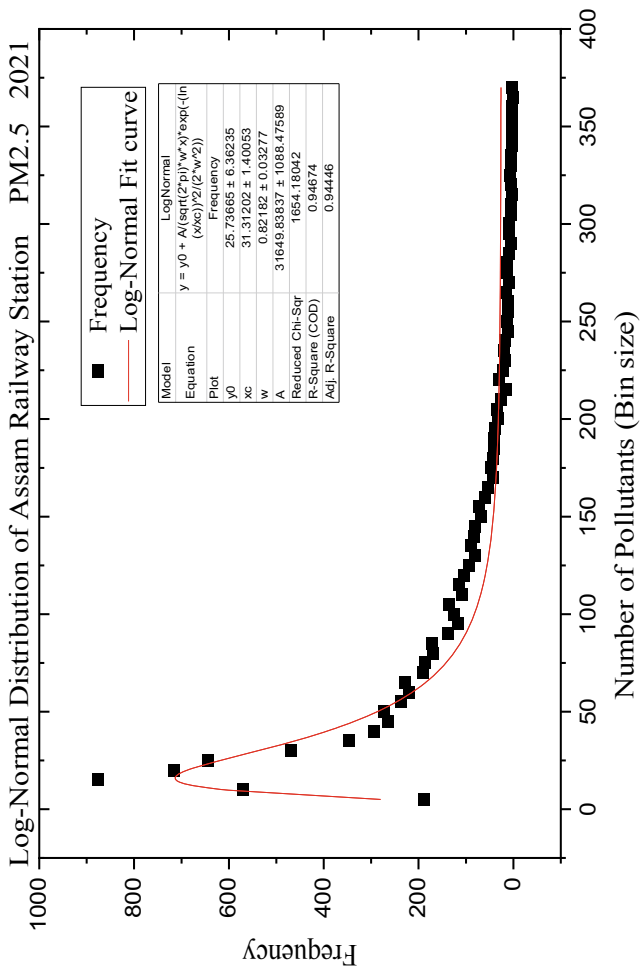
Fig. 3 Log-normal distribution of Assam Railway Station

Descriptive Statistics of the Frequency Distribution	
Mean	515.6875
Standard Error	128.7563
Median	326
Standard Deviation	515.0254
Sample Variance	265251.2
Kurtosis	-1.84116
Skewness	0.343286

Plot to verify above Log-Normal Distribution

Model	Gauss
Equation	y=y0 + (A/(w*sqrt(pi/2))) *exp(-2*((x-xc)/w)^2)
Plot	FREQ
y0	-101.8983 ± 95.26188
xc	1.70977 ± 0.03298
w	1.12488 ± 0.11969
A	1984.70035 ± 294.9851
Reduced Ch	16970.01324
R-Square (	0.94882
Adj. R-Squa	0.93602

Frequency
— Gausian Fit curve

Number of Pollutants (Bin size)

Fig. 4 Normal distribution of Assam Railway Station

Fig. 5 Time series plot of pollutants
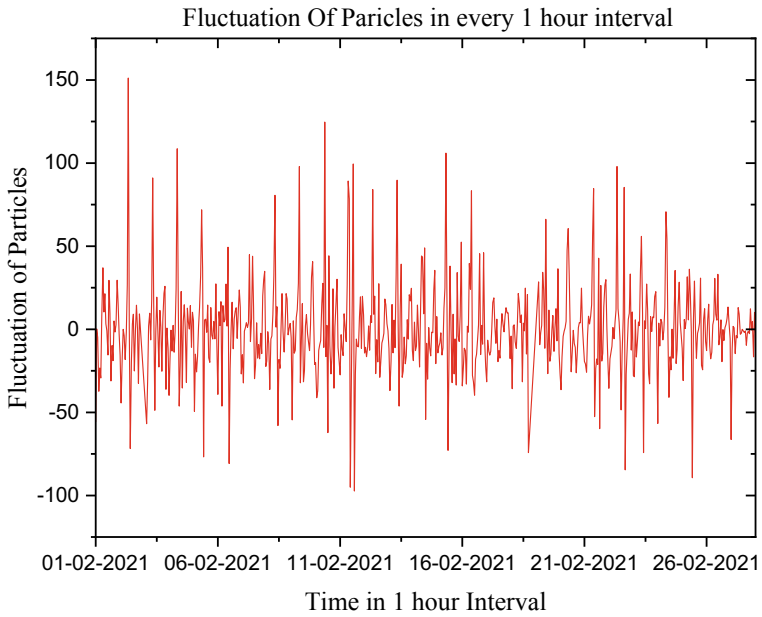
Fig. 6 Fluctuation of pollutants about mean position
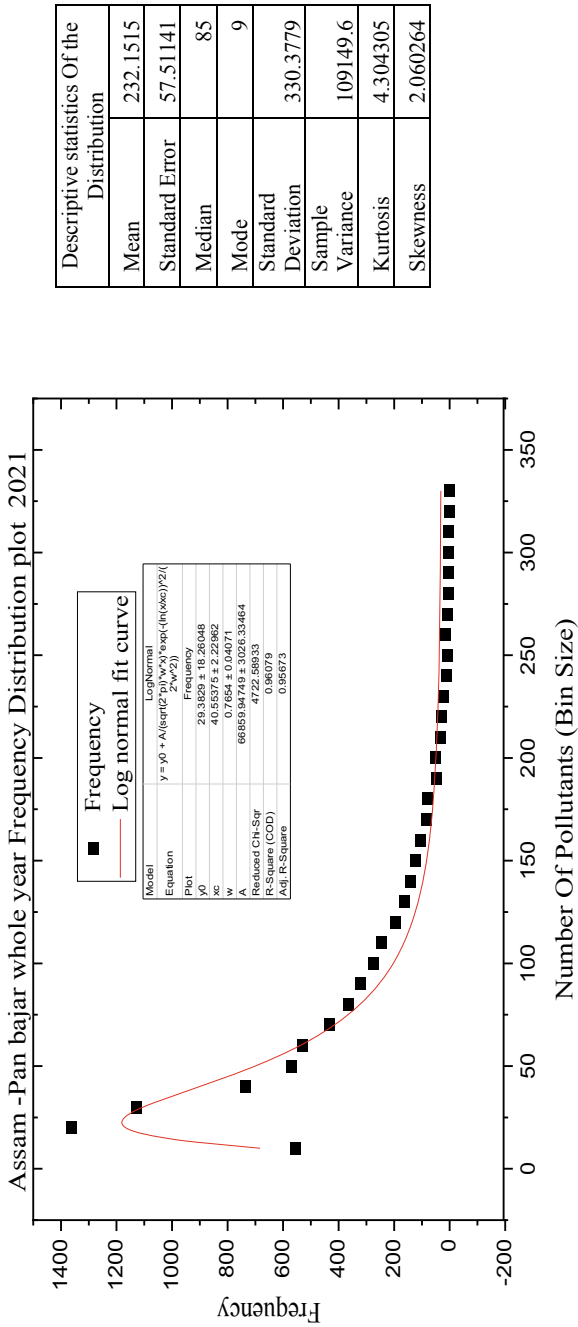
Descriptive statistics Of the Distribution	
Mean	232.1515
Standard Error	57.51141
Median	85
Mode	9
Standard Deviation	330.3779
Sample Variance	109149.6
Kurtosis	4.304305
Skewness	2.060264

Assam -Pan bajar whole year Frequency Distribution plot 2021

Model	LogNormal
Equation	y = y0 + A/(sqrt(2*pi)*w*x)*exp(-(ln(x/xc))^2/(2*w^2))
Plot	Frequency
y0	29.3829 ± 18.26048
xc	40.55375 ± 2.22962
w	0.7654 ± 0.04071
A	66859.94749 ± 3026.33464
Reduced Chi-Sqr	4722.58933
R-Square (COD)	0.96079
Adj. R-Square	0.95673

Fig. 7 Log-Normal distribution of Pan Bazar Assam

The above log-normal distribution can be verified by taking log of the number of pollutants and again if we plot the frequency distribution of that data, then we will get a Well fitted Gaussian curve, which verify the above distribution plot (Fig. 8).

4.2 Lumpyngngad-Meghalaya

We have every 1 h interval data of PM2.5. We will take those data to get the time series plot, from that we will also find the fluctuation of those particles in every 1 h (Figs. 9 and 10).

4.2.1 Frequency Distribution of Lumpyngngad-Meghalaya (PM2.5-2021)

We will do the binning of time series data for the whole year of 2021 to find the frequency distribution plot (Fig. 11).

The above log-normal distribution can be verified by taking log of the number of pollutants, and again if we plot the frequency distribution of that data, then we will get a well-fitted Gaussian curve, which verify the above distribution plot (Fig. 12).

5   To Determine the Type of Diffusion in North-East India

Procedure

'Central Pollution Control Board' of India published the data for number of pollutants like PM2.5, PM10, SO_2, CO_2 for every 1 h interval; we will take those data to calculate the type of diffusion.

As we have the theoretical concept that

$$\langle x^2 \rangle \propto t^\alpha$$

For $\alpha > 1$, it shows superdiffusion and $\alpha < 1$ shows subdiffusion, whereas $\alpha = 1$ shows normal diffusion.

For each distribution, there were some exact rules to calculate the α values, as we get all log-normal frequency distribution plots; we will use the cumulative addition rule to get the type of diffusion.

We have number of pollutants for each 1 h interval, and we will do the calculation for every month to get the α values. First we will cumulatively add the pollutants number with every previous hour data (x1, x1 + x2, x1 + x2 + x3, …. where x1, x2, x3 are number of pollutants with 1 h interval, respectively), then we will take the square of each term and take the average which will give $\langle x^2 \rangle$ which may be varied

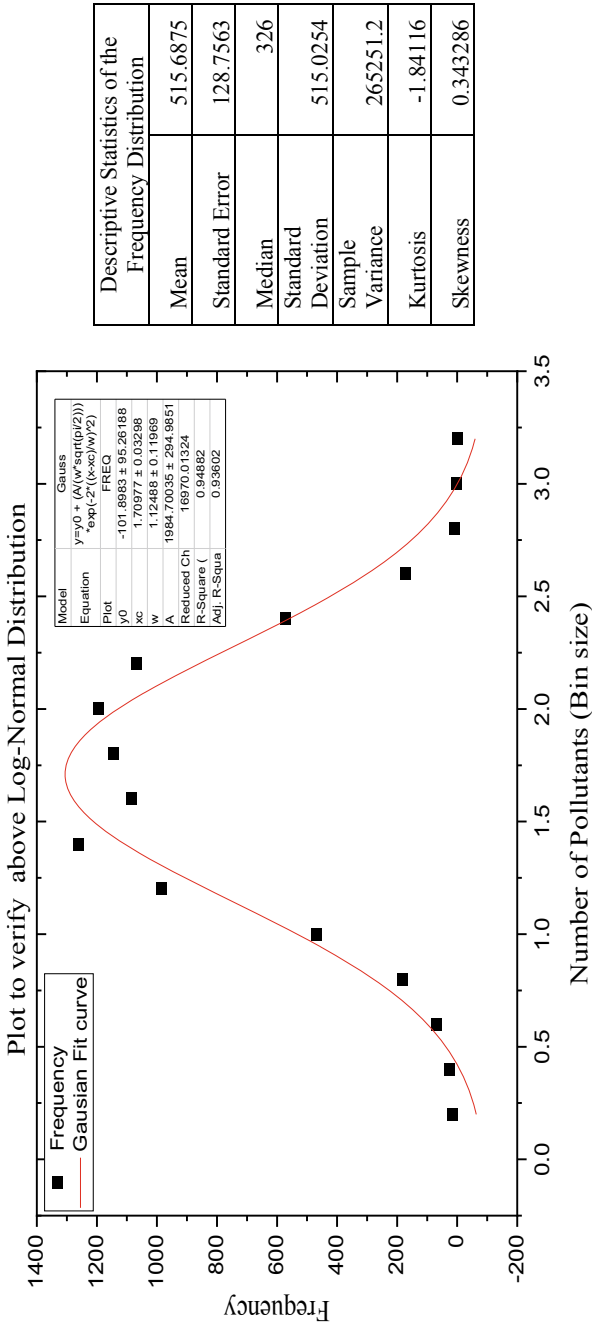| Descriptive statistics Of the Distribution	
Mean	547.8571
Standard Error	142.8421
Median	381.5
Standard Deviation	534.4664
Sample Variance	285654.3
Kurtosis	-1.85146
Skewness	0.318134
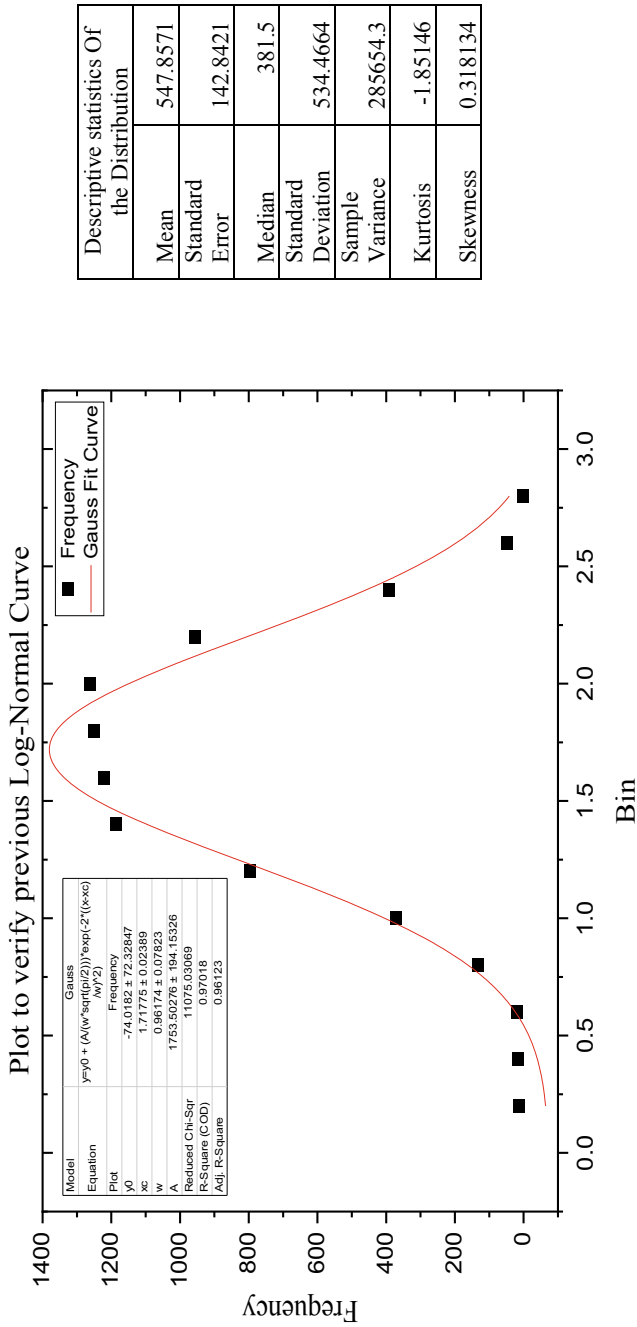
Fig. 8 Normal distribution of Pan Bazar Assam
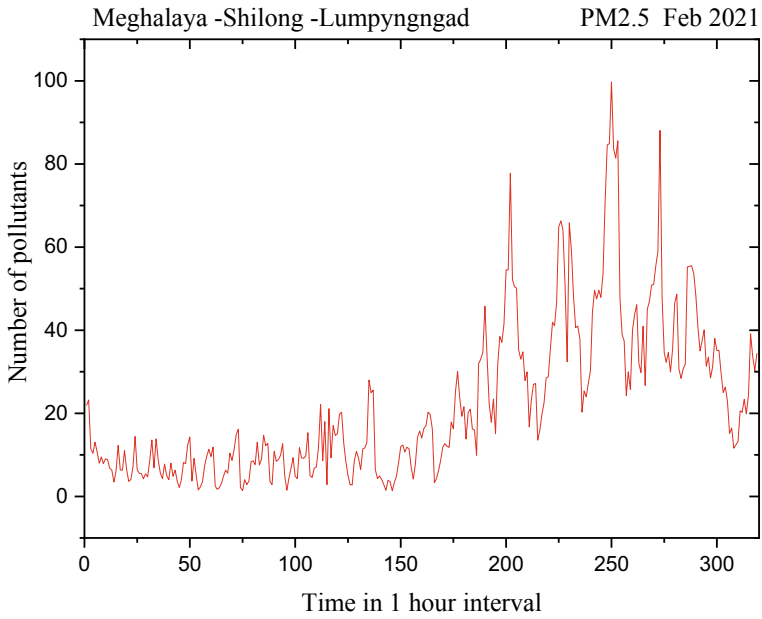
Fig. 9 Time series plot of pollutants

Fig. 10 Fluctuation of pollutants about mean position

Descriptive Statistics	
Mean	123.3824
Standard Error	55.55657
Median	3.5
Standard Deviation	323.9477
Sample Variance	104942.1
Kurtosis	11.39858
Skewness	3.371656

Meghalaya Log-Normal Distribution plot 2021   PM2.5

- ■ Frequency
- —— Log-Normal Distribution

Model	LogNormal
Equation	$y = y_0 + A/(\sqrt{2\pi} w x)\cdot\exp(-(\ln(x/x_c))^2/(2 w^2))$
Plot	freq
y0	3.31265 ± 2.08812
xc	9.69805 ± 0.07223
w	0.75848 ± 0.01129
A	$20683.61425 \pm 176.19202$
Reduced Chi-Sqr	106.98767
R-Square (COD)	0.99905
Adj. R-Square	0.99895

Number of Pollutants (Bin)

Frequency
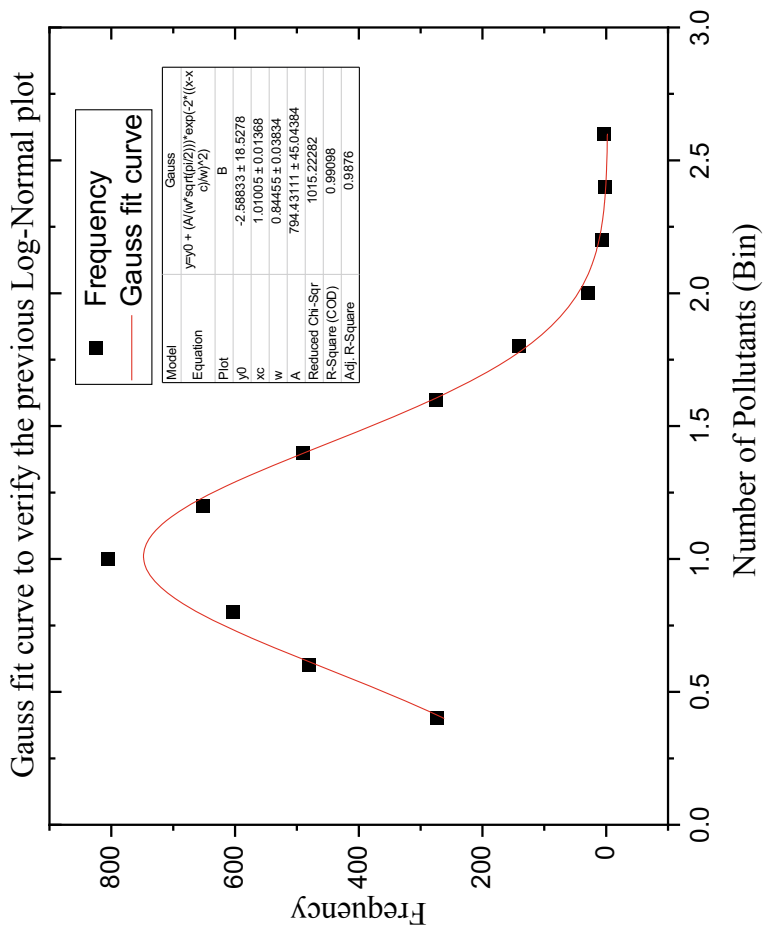
Fig. 11 Log-Normal distribution of Lumpyngngad-Meghalaya

Descriptive Statistics	
Mean	156.7917
Standard Error	28.72142
Median	137
Standard Deviation	140.7057
Sample Variance	19798.09
Kurtosis	-1.28127
Skewness	0.33881

Gauss fit curve to verify the previous Log-Normal plot

Fig. 12 Normal distribution of Lumpyngngad-Meghalaya

with t as $\langle x^2 \rangle \propto t^\alpha$, but it will be difficult to get the α by fitting $\langle x^2 \rangle$ vs. t plot. To avoid this problem, we will take $\log_{10}$ on both side and by fitting $\log\langle x^2 \rangle$ vs. $\log t$ we will get the α values.

We will do the same calculation for different stations of North-East region.

5.1 Railway Colony, Guwahati—APCB (State—Assam: 26.1796 °N, 91.7843 °E)

See the Fig. 13 and Tables 2, 3, 4.

… We have done the same calculation for whole month of January …

5.2 Pan Bazar, Guwahati (State—Assam: 28.1860 °N, 91.7454 °E)

See the Table 5.

5.3 Lumpyngngad, Shillong, (State—Meghalaya: 25.4670 °N, 91.3662 °E)

See the Tables 6 and 7.

5.4 PWD Junction, Kohima—NPCB, (State—Meghalaya: 25.6751 °N, 94.1086 °E)

See the Table 8.

6 To Calculate the Fractional Derivative Using Grunwald–Letnikov Operator

We will do this calculation for three nearest stations—Pan Bazar (Assam), Railway Station (Assam) and Lumpyngngad (Meghalaya). As the other stations are very far from each other, we will not do this calculation except these three stations, because there has no correlation between those stations which are far from each other.

To determine the value of α (January 2021) Assam Railway St 2021
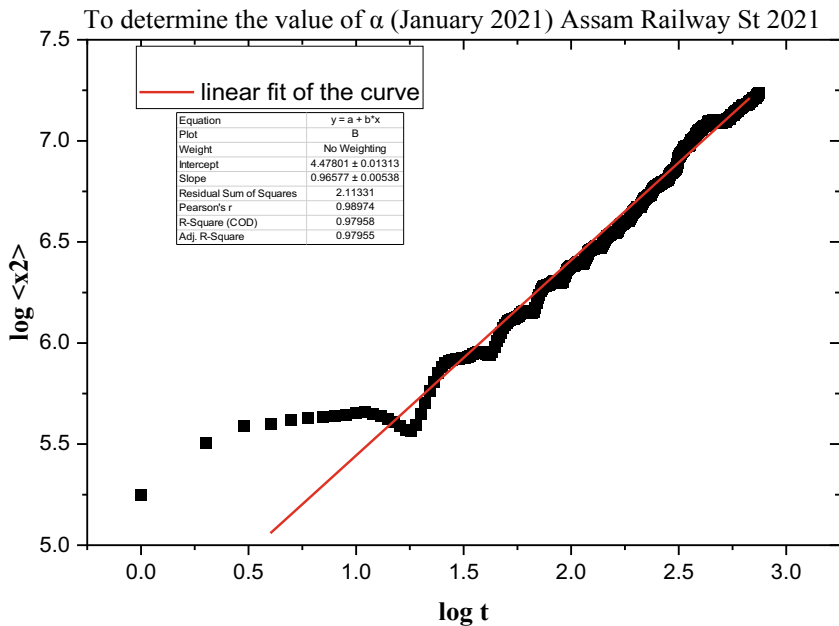
The slope of the above plot gives the value of α (0.96)

Fig. 13 Plot to determine the fractional parameters

6.1 Assam Railway Station (Year—2021)

To calculate the fractional derivative for whole year of 2021 for Assam Railway Station, as from Table 2 we can see that for Assam Railway Station subdiffusion part is dominant for whole year 2021, we will take the fractional parameter $\alpha = 0.5$, which denotes the subdiffusion.

From (4), we have

Table 2 To determine the value of α (January 2021)

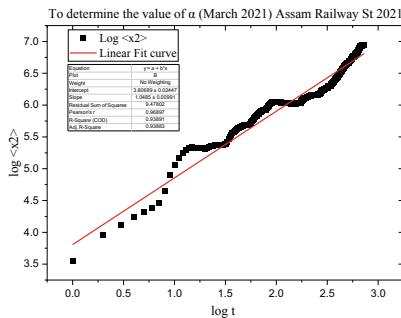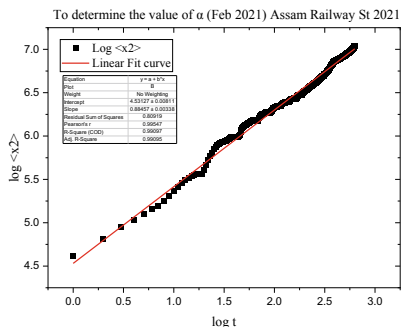| Time in 1 h interval	Number of Pollutants(x_i)	Cumulative Addition($x_i' = x_{i-1} + x_i$)	$x_i'^2$	Mean $x_i'^2/N$	log t	log $\left(\frac{x_i'^2}{N}\right)$
01–01–2021 01:00	420.48	420.48	176,803.4	176,803.4	0	5.247491
01–01–2021 02:00	381.69	802.17	643,476.7	321,738.4	0.30103	5.507503
01–01–2021 03:00	275.4	1077.57	1,161,157	387,052.4	0.477121	5.58777
01–01–2021 04:00	181.97	1259.54	1,586,441	396,610.3	0.60206	5.598364
01–01–2021 05:00	183.47	1443.01	2,082,278	416,455.6	0.69897	5.619569
01–01–2021 06:00	159.44	1602.45	2,567,846	427,974.3	0.778151	5.631418
01–01–2021 07:00	130.81	1733.26	3,004,190	429,170	0.845098	5.632629
01–01–2021 08:00	139.6	1872.86	3,507,605	438,450.6	0.90309	5.641921
01–01–2021 09:00	123.94	1996.8	3,987,210	443,023.4	0.954243	5.646427
01–01–2021 10:00	129.5	2126.3	4,521,152	452,115.2	1	5.655249
01–01–2021 11:00	113.58	2239.88	5,017,062	456,096.6	1.041393	5.659057
01–01–2021 12:00	80.75	2320.63	5,385,324	448,777	1.079181	5.652031
01–01–2021 13:00	62.45	2383.08	5,679,070	436,851.6	1.113943	5.640334
01–01–2021 14:00	50.89	2433.97	5,924,210	423,157.9	1.146128	5.626502
01–01–2021 15:00	31.2	2465.17	6,077,063	405,137.5	1.176091	5.607602
01–01–2021 16:00	29.94	2495.11	6,225,574	389,098.4	1.20412	5.590059
01–01–2021 17:00	24.23	2519.34	6,347,074	373,357.3	1.230449	5.572125
01–01–2021 18:00	58.53	2577.87	6,645,414	369,189.7	1.255273	5.56725
01–01–2021 19:00	151.18	2729.05	7,447,714	391,984.9	1.278754	5.593269
01–01–2021 20:00	263.61	2992.66	8,956,014	447,800.7	1.30103	5.651085
01–01–2021 21:00	271.6	3264.26	10,655,393	507,399.7	1.322219	5.70535
01–01–2021 22:00	296.33	3560.59	12,677,801	576,263.7	1.342423	5.760621

(continued)

Table 2 (continued)

Time in 1 h interval	Number of Pollutants(x_i)	Cumulative Addition$(x'_i = x_{i-1} + x_i)$	$x_i'^2$	Mean $x_i'^2/N$	log t	$\log\left(\frac{x_i'^2}{N}\right)$
01–01–2021 23:00	278.31	3838.9	14,737,153	640,745.8	1.361728	5.806686

Table 3 To determine the type of diffusion for 'Railway Colony, Guwahati—APCB' (PM2.5-Year 2021)

Month	Fitting equation	R^2 Value	α	Error in α	Type of diffusion
Jan-21	$Y = 0.9268X + 4.57$	0.97	0.92	0.0053	Subdiffusion
Feb-21	$Y = 0.8846X + 4.51$	0.99	0.88	0.0034	Subdiffusion
Mar-21	$Y = 1.0485X + 3.80$	0.94	1.04	0.001	Normal diffusion
Apr-21	$Y = 1.1606X + 3.50$	0.97	1.16	0.0039	Superdiffusion
May-21	$Y = 0.6203X + 3.87$	0.95	0.62	0.0056	Subdiffusion
Jun-21	$Y = 0.9340X + 3.67$	0.93	0.93	0.0078	Subdiffusion
Jul-21	$Y = 0.8416X + 3.05$	0.93	0.84	0.0098	Subdiffusion
Aug-21	$Y = 0.7809X + 3.56$	0.99	0.78	0.0023	Subdiffusion
Sep-21	$Y = 1.000X + 3.50$	0.95	1	0.0045	Normal diffusion
Oct-21	$Y = 0.9801X + 3.90$	0.9	0.98	0.0087	Subdiffusion
Nov-21	$Y = 1.1363X + 3.37$	0.93	1.13	0.0056	Superdiffusion
Dec-21	$Y = 1.123X + 3.56$	0.91	1.12	0.003	Superdiffusion

Table 4 To determine the type of diffusion for 'Railway Colony, Guwahati—APCB' (PM2.5-Year 2020)

Month	Fitting equation	R^2 Values	α	Error in α	Type of diffusion
Jan-20	$Y = 1.1255X + 3.91$	0.95	1.12	0.0067	Superdiffusion
Feb-20	$Y = 1.0436X + 4.11$	0.99	1.04	0.0087	Normal diffusion
Mar-20	$Y = 0.8815X + 4.11$	0.93	0.88	0.0056	Subdiffusion
Apr-20	$Y = 0.5508X + 4.91$	0.99	0.55	0.0066	Superdiffusion
May-20	$Y = 0.8907X + 4.01$	0.94	0.89	0.0034	Subdiffusion
Jun-20	$Y = 0.8931X + 2.88$	0.91	0.89	0.0043	Subdiffusion
Jul-20	$Y = 0.7232X + 3.16$	0.98	0.72	0.006	Subdiffusion
Aug-20	$Y = 0.7186X + 3.21$	0.96	0.71	0.0037	Subdiffusion
Sep-20	$Y = 0.9408X + 2.79$	0.95	0.94	0.0023	Subdiffusion
Oct-20	$Y = 0.9769X + 3.11$	0.97	0.98	0.0029	Subdiffusion
Nov-20	$Y = 1.2026X + 3.18$	0.98	1.2	0.0078	Superdiffusion
Dec-20	$Y = 1.2561X + 3.52$	0.89	1.25	0.0085	Superdiffusion

Table 5 To determine the type of diffusion for 'Pan Bazar, Guwahati' (PM2.5-Year 2021)

Month	Fitting equation	R^2 Values	α	Error in α	Type of diffusion
Jan-21	$Y = 0.8795X + 4.48$	0.9	0.87	0.0055	Subdiffusion
Feb-21	$Y = 0.8372 + 4.58$	0.94	0.83	0.0084	Subdiffusion
Mar-21	$Y = 1.457X + 3.50$	0.98	1.45	0.0045	Superdiffusion
Apr-21	$Y = 1.2335X + 2.99$	0.87	1.23	0.0078	Superdiffusion
May-21	$Y = 0.5479X + 4.087$	0.9	0.54	0.0054	Subdiffusion
Jun-21	$Y = 0.9348X + 2.73$	0.98	0.93	0.0023	Subdiffusion
Jul-21	$Y = 0.9098X + 2.78$	0.94	0.9	0.089	Subdiffusion
Aug-21	$Y = 0.8073X + 3.08$	0.93	0.8	0.0035	Subdiffusion
Sep-21	$Y = 1.009X + 2.71$	0.98	1	0.0022	Normal diffusion
Oct-21	$Y = 0.9140X + 3.76$	0.94	0.91	0.006	Subdiffusion
Nov-21	$Y = 1.061X + 3.49$	0.93	1.06	0.0051	Normal diffusion
Dec-21	$Y = 1.071X + 3.51$	0.97	1.07	0.0046	Normal diffusion

Table 6 To determine the type of diffusion for 'Lumpyngngad, Shillong' (PM2.5-Year 2020)

Month	Fitting equation	R^2 Value	α	Error in α	Type of diffusion
Jan-20	NA	NA	NA	NA	NA
Feb-20	$Y = 1.069X + 3.24$	0.96	1.07	0.0078	Superdiffusion
Mar-20	$Y = 1.219X + 2.44$	0.89	1.22	0.009	Superdiffusion
Apr-20	NA	NA	NA	NA	NA
May-20	$Y = 1.3074X + 1.63$	0.9	1.3	0.0056	Superdiffusion
Jun-20	$Y = 1.0709X + 2.36$	0.95	1.07	0.0078	Superdiffusion
Jul-20	$Y = 0.8037X + 2.54$	0.97	0.83	0.0066	Subdiffusion
Aug-20	NA	NA	NA	NA	NA
Sep-20	$Y = 0.8835X + 2.28$	0.94	0.88	0.0078	Subdiffusion
Oct-20	$Y = 1.015X + 2.25$	0.93	1.01	0.0087	Normal diffusion
Nov-20	$Y = 1.4932X + 1.31$	0.94	1.5	0.0045	Superdiffusion
Dec-20	NA	NA	NA	NA	NA

$$D^\alpha f(x) = \lim_{h \to 0} \frac{1}{h^\alpha} \sum_{m=0}^{\infty} (-1)^m \frac{\Gamma(\alpha + 1)}{\Gamma(m + 1)\Gamma(\alpha - m + 1)} f(x - mh)$$

we have 1 h interval data, so to calculate this we will take step function $h = 1$ (Table 9)

$$\text{So } \frac{d^{0.5}}{dt^{0.5}} f(x) = 103.03$$

Table 7 To determine the type of diffusion for 'Lumpyngngad, Shillong' (PM2.5-Year 2021)

Month	Fitting equation	R^2 Values	α	Error in α	Type of diffusion
Jan-21	NA	NA	NA	NA	NA
Feb-21	NA	NA	NA	NA	NA
Mar-21	$Y = 0.6918X + 2.68$	0.93	0.69	0.0074	Subdiffusion
Apr-21	NA	NA	NA	NA	NA
May-21	$Y = 0.6190X + 2.45$	0.94	0.62	0.0034	Subdiffusion
Jun-21	NA	NA	NA	NA	NA
Jul-21	NA	NA	NA	NA	NA
Aug-21	NA	NA	NA	NA	NA
Sep-21	NA	NA	NA	NA	NA
Oct-21	$Y = 1.2013X + 2.54$	0.95	1	0.0067	Normal diffusion
Nov-21	$Y = 0.7412X + 2.41$	0.92	0.74	0.0038	Subdiffusion
Dec-21	$Y = 1.4623X + 1.90$	0.93	1.46	0.0031	Superdiffusion

Table 8 To determine the type of diffusion for 'PWD Junction, Kohima—NPCB' (PM2.5-Year 2021)

Month	Fitting equation	R^2 Values	α	Error in α	Type of diffusion
Jan-21	$Y = 1.8673X + 1.14$	0.93	1.86	0.0056	Superdiffusion
Feb-21	$Y = 1.0275X + 3.37$	0.89	1.02	0.0067	Normal diffusion
Mar-21	$Y = 1.1781X + 3.12$	0.92	1.17	0.0063	Superdiffusion
Apr-21	$Y = 1.2337X + 2.754$	0.95	1.23	0.0083	Subdiffusion
May-21	$Y = 0.6606X + 3.995$	0.98	0.66	0.0034	Subdiffusion
Jun-21	$Y = 0.7470X + 3.01$	0.91	0.74	0.0084	Subdiffusion
Jul-21	$Y = 0.9149X + 2.49$	0.99	0.91	0.0067	Subdiffusion
Aug-21	$Y = 1.3984X + 1.40$	0.93	1.39	0.0065	Subdiffusion
Sep-21	$Y = 1.1268X + 1.94$	0.95	1.12	0.0034	Subdiffusion
Oct-21	$Y = 1.2588X + 1.76$	0.87	1.25	0.0046	Subdiffusion
Nov-21	$Y = 1.1312X + 2.41$	0.98	1.13	0.0078	Subdiffusion
Dec-21	$Y = 1.037X + 2.931$	0.94	1.03	0.0012	Subdiffusion

Table 9 To determine the fractional derivative for Railway Station, Assam (Jan 2021)

Time in 1 h interval	$f(x)$	α	m	$\frac{\Gamma(\alpha+1)}{\Gamma(m+1)\Gamma(\alpha-m+1)}$	Fractional derivative value (alpha = 0.5)
01–01–2021 21:00	271.6	0.5	0	1	271.6
01–01–2021 20:00	263.61	0.5	1	0.5	−131.805
01–01–2021 19:00	151.18	0.5	2	−0.125	−18.8975
01–01–2021 18:00	58.53	0.5	3	0.0625	−3.658125
01–01–2021 17:00	24.23	0.5	4	−0.0390625	−0.946484375
01–01–2021 16:00	29.94	0.5	5	0.02734375	−0.818671875
01–01–2021 15:00	31.2	0.5	6	−0.020507813	−0.63984375
01–01–2021 14:00	50.89	0.5	7	0.016113281	−0.820004883
01–01–2021 13:00	62.45	0.5	8	−0.013092041	−0.817597961
01–01–2021 12:00	80.75	0.5	9	0.010910034	−0.88098526
01–01–2021 11:00	113.58	0.5	10	−0.009273529	−1.05328743
01–01–2021 10:00	129.5	0.5	11	0.008008957	−1.03715992
01–01–2021 09:00	123.94	0.5	12	−0.007007837	−0.868551354
01–01–2021 08:00	139.6	0.5	13	0.006199241	−0.865414
01–01–2021 07:00	130.81	0.5	14	−0.005535036	−0.724038102
01–01–2021 06:00	159.44	0.5	15	0.004981533	−0.794255573
01–01–2021 05:00	183.47	0.5	16	−0.004514514	−0.828277884
01–01–2021 04:00	181.97	0.5	17	0.004116175	−0.74902028
01–01–2021 03:00	275.4	0.5	18	−0.00377316	−1.039128261
01–01–2021 02:00	381.69	0.5	19	0.003475279	−1.326479217
Sum = 103.03					
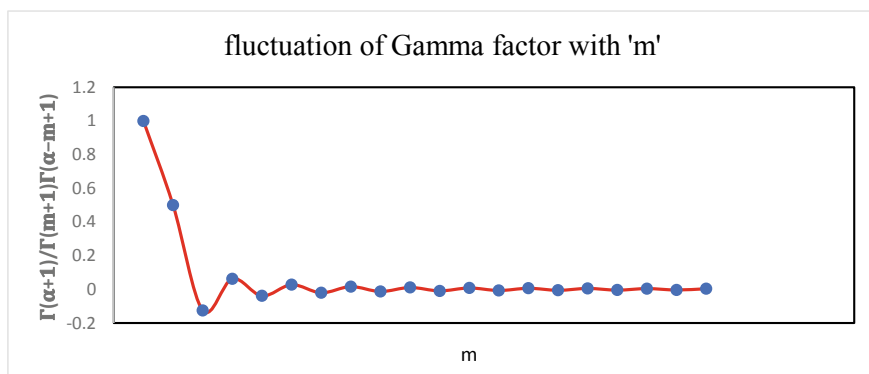
We will do this same calculation for several parts for the same month to get an average value of fractional derivative (Table 10).

Table 10 Fractional derivative value for the whole year (2021) of Assam Railway Station, Pan Bazar and Lumpyngngad (Meghalaya)

Month	Railway station (Assam)		Pan Bazar (Assam)		Lumpyngngad (Meghalaya)	
	α	Fractional derivative	α	Fractional derivative	α	Fractional derivative
Jan-21	0.5	21.67	0.5	8.57	NA	NA
Feb-21	0.5	20.95	0.5	14.18	0.94	2.67
Mar-21	0.5	16.95	0.5	10.94	0.94	0.9
Apr-21	0.5	12.07	0.5	10.72	0.94	0.4
May-21	0.5	2.172	0.5	10.05	0.94	NA
Jun-21	0.5	2.05	0.5	6.06	0.94	NA
Jul-21	0.5	1.84	0.5	4.04	0.94	NA
Aug-21	0.5	1.17	0.5	3.95	0.94	NA
Sep-21	0.5	1.01	0.5	3.54	0.94	0.3
Oct-21	0.5	0.95	0.5	3.5	0.94	0.35
Nov-21	0.5	0.9	0.5	3.45	0.94	0.28
Dec-21	0.5	1.2	0.5	2.78	0.94	0.18

7 Calculation of the Diffusion Coefficient

We have $\frac{\partial^\alpha N}{\partial t^\alpha} = D \frac{\partial^2 N}{\partial x^2}$.

Where N is the density of PM2.5, Δx is the distance between two nearest stations. ΔN is the difference in concentration between two nearest stations. (unit of N is given as $\mu g/m^3$).

We already calculated the fractional derivative part $\frac{\partial^\alpha N}{\partial t^\alpha}$ now to calculate $\frac{\partial^2 N}{\partial x^2}$ and we'll break the term like $\frac{\partial^2 N}{\partial x^2} = \frac{d}{dx}\left(\frac{\partial N}{\partial x}\right) = \frac{d}{dx}(F)$.

Distance between Railway Station and Pan Bazar is 0.5 km and average of $(\Delta N)_1$ between these two stations for the whole year 2021 is 4.98 $\mu g/m^3$.

$$\text{So } F_1 = \left(\frac{\partial N}{\partial x}\right)_1 = \frac{4.98}{0.5} = 9.96 \mu g/m^3/km$$

Distance between Pan Bazar and Lumpyngngad (Meghalaya) is 50 km and average of $(\Delta N)_2$ between these two stations for the whole year 2021 is 78.6 $\mu g/m^3$.

$$\text{So } F_2 = \left(\frac{\partial N}{\partial x}\right)_2 = \frac{78.6}{50} = 1.57 \mu g/m^3/km$$

Now $= \frac{\partial^2 N}{\partial x^2} = \frac{d}{dx}\left(\frac{\partial N}{\partial x}\right) = \frac{\Delta F}{\Delta x} = 0.17 \mu g/m^3/km^2$.
See the Fig. 14 and Table 11.

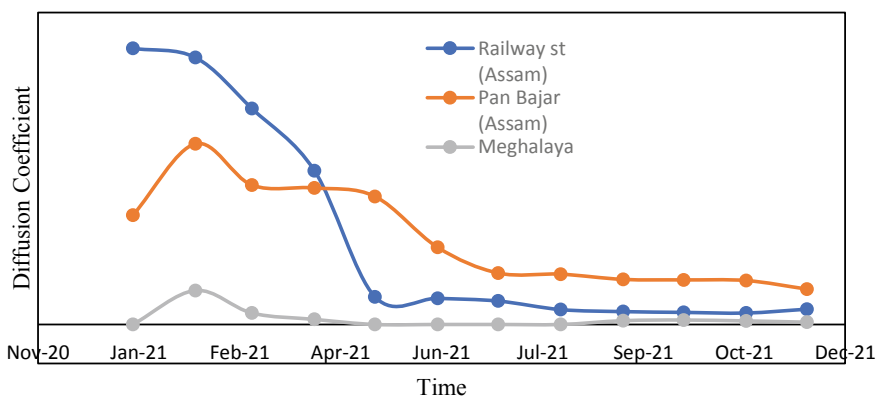## Variation of diffusion coefficient with time for the whole year 2021

Fig. 14 Variation of diffusion coefficient in different states of North-East India

Table 11 To determine the diffusion coefficient of Assam Railway Station, Pan Bazar and Lumpyngngad (Meghalaya) (PM2.5 2021)

Month	$\frac{\partial^2 N}{\partial x^2}$	Assam railway St		Pan Bazar (Assam)		Lumpyngngad (Meghalaya)	
		Fractional derivative $\left(\frac{\partial^{0.5} N}{\partial t^{0.5}}\right)$	Diffusion coefficient	Fractional derivative $\left(\frac{\partial^{0.5} N}{\partial t^{0.5}}\right)$	Diffusion coefficient	Fractional derivative $\left(\frac{\partial^{0.5} N}{\partial t^{0.5}}\right)$	Diffusion coefficient
Jan-21	0.17	21.67	0.0354085	8.57	0.014003268	NA	NA
Feb-21	0.17	20.95	0.03423203	14.18	0.023169935	2.67	0.004363
Mar-21	0.17	16.95	0.02769608	10.94	0.017875817	0.9	0.001471
Apr-21	0.17	12.07	0.01972222	10.72	0.01751634	0.4	0.000654
May-21	0.17	2.172	0.00354902	10.05	0.016421569	NA	NA
Jun-21	0.17	2.05	0.00334967	6.06	0.009901961	NA	NA
Jul-21	0.17	1.84	0.00300654	4.04	0.006601307	NA	NA
Aug-21	0.17	1.17	0.00191176	3.95	0.006454248	NA	NA
Sep-21	0.17	1.01	0.00165033	3.54	0.005784314	0.3	0.00049
Oct-21	0.17	0.95	0.00155229	3.5	0.005718954	0.35	0.000572
Nov-21	0.17	0.9	0.00147059	3.45	0.005637255	0.28	0.000458
Dec-21	0.17	1.2	0.00196078	2.78	0.004542484	0.18	0.000294

8 Conclusion

Since the beginning of the present work, the goal has been to offer several approaches to model anomalous diffusive processes covering a wide range of application. Anomalous diffusive processes are no longer confined in textbooks as analytical

methodologies. Rather with all the developments in fractional calculus and consequently in physics itself, the present decade has witnessed it to allow for the modelling of a variety of interesting physics problems, such as the diffusion equation with tempered fractional derivatives or 'integral of Brownian motions'. We cannot ignore that mathematical approaches help us immensely in studying different types of anomalous diffusions.

With the fast expansion of the economy and the ongoing improvement in human needs for a healthy living environment, study of air pollutants (particularly PM2.5) has garnered a lot of attention in India. Such pollutants cause foggy weather and acute health issues, thus being an urgent environmental issue to address. Therefore, it becomes vital to accurately calculate PM2.5 concentrations so as to minimise air pollution and enhance human living conditions. In this project, we analyse data corresponding to the most anomalous behaviour of air pollutant PM2.5.We also calculate the diffusion coefficient of different stations in North-East India. In future works, this project will serve as a Launchpad for weather forecasting and climate analysis.

References

1. Abe, S., Thurner, S.: Anomalous diffusion in view of Einstein's 1905 theory of Brownian motion. Physica A **356**(2–4), 403–407 (2005)
2. Oliveira, F.A., Ferreira, R.M.S., Lapas, L.C., Vainstein, M.H.: Anomalous diffusion: a basic mechanism for the evolution of inhomogeneous systems. Front. Phys. 7(FEB), 1–17 (2019)
3. Weisstein, E.W.: Mittag-leffler function. (2003). https://mathworld.wolfram.com, Last Accessed 2 March 2022
4. Glöckle, W.G., Nonnenmacher, T.F.: Fox function representation of non-debye relaxation processes. J. Stat. Phys. **71**(3–4), 741–757 (1993)
5. dos Santos, M.A.F.: Analytic approaches of the anomalous diffusion: a review. Chaos, Solitons Fractals **124**, 86–96 (2019)
6. Lutz, E.: Fractional Langevin equation. Phys. Rev. E Stat. Phys. Plasmas Fluids Relat Interdiscip. Topics **64**(5), 4 (2001)
7. Metzler, R., Klafter, J.: The random walk's guide to anomalous diffusion: a fractional dynamics approach. Physics Report. **339**(1), 1–77 (2000)

Environmental Issues: Problems and Sustainable Solutions

Material Recovery from Waste Printed Circuit Board Using Pyrolysis and Metal Extraction

Bibari Boro and Pankaj Tiwari

1 Introduction

With the advancement in technology, our day-to-day routine has become dependent on the use of electrical and electronic equipment (EEE). The lack of awareness and improper disposal management of E-Waste has led to the dumping of waste electrical and electronic equipment (WEEE) in the landfills. It has been reported that globally, 53.6 million metric tonnes (Mt) of E-Waste was generated in 2019, and it is increasing at an alarming rate of 2 (Mt) per annum [1]. India generated 3.23 Mt in 2019, making it the third-largest E-Waste producer country [2]. However, only 17.4% of the total generated E-Waste in 2019 is properly reported and recycled globally. E-Waste consists of a variety of EEE ranging from mobile phones, computers, air-conditioners, refrigerators, washing machines, lamps, etc. Thus, it is a heterogeneous mixture of metals, polymers, glass materials, etc. A total of 69 elements from the periodic table were found to be present in E-Waste [1]. The material composition of E-Waste is given in Fig. 1. It can be observed that 60% of the material composition is contributed by metals. Thus, E-Waste is also called secondary source of metals. The metals range from base metals like iron, aluminium, zinc, to heavy metals like lead, cadmium and mercury. Precious metals like gold, platinum, copper, silver, palladium are predominantly found in the printed circuit board (PCB) fraction of E-Waste. Thus, even though the PCBs contribute only 2% to the material composition of E-Waste, it carries the highest economic value. PCBs are also the indispensable component of any EEE. Considering these factors, PCB is chosen as the feed for study in this work. The composition and the design of PCB vary depending on the EEE it is being used. However, it has been reported that PCB consists of roughly 40% metals, 30%

B. Boro · P. Tiwari (✉)
Department of Chemical Engineering, Indian Institute of Technology, Guwahati, India
e-mail: pankaj.tiwari@iitg.ac.in

B. Boro
e-mail: b.bibari@iitg.ac.in

polymers and 30% ceramics. The most basic design of a PCB is that of a single layer PCB (Fig. 2). The layers of material found in a single layer PCB consists of a substrate, a layer of copper lining, solder mask and a silkscreen. The substrate provides the mechanical support, and it is commonly composed of glass fibre reinforced with epoxy resin; the copper lining is provided for the conductivity, solder mask is to protect the copper lining from the damage caused by the environment, and the silkscreen provides guide for placing the electronic components on the bare board.

The informal recyclers collect E-Waste and recover the valuable metals in a crude manner, such as direct burning, use of toxic chemicals like cyanide, which are disposed directly into the water bodies, or open land spaces. These activities adversely affect the environment and ultimately get into the food chain affecting the aquatic and the terrestrial organisms. Moreover, E-Waste itself consists of toxic materials like heavy metals and halogenated compounds [3]. Thus, development of proper recycling
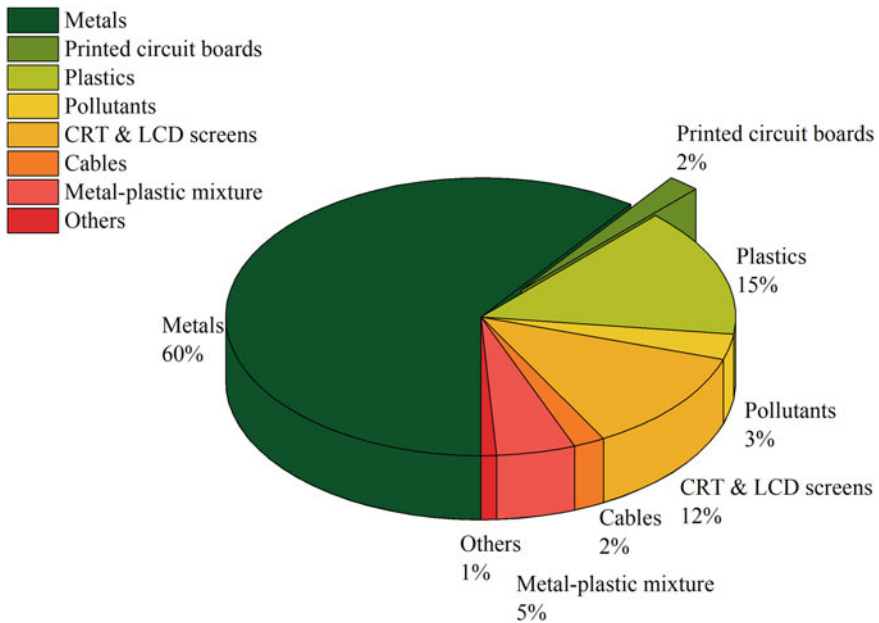

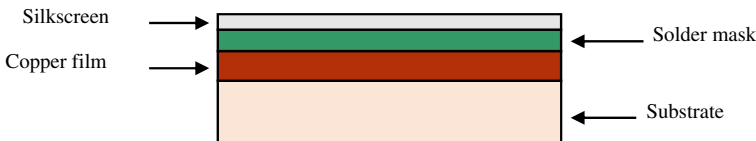**Fig. 1** Material composition of E-Waste [10]

Fig. 2 Typical layers of material in a single-sided printed circuit board

system is the need of the hour. Typical E-Waste processing methods include physical separation, pyrometallurgical, hydrometallurgical, pyrolysis and bio-metallurgical [4]. Physical separation method is the most widely used; however, this method only separates the metallic and the non-metallic fraction in a crude manner. The pyrometallurgical method includes thermal heating of the PCB at high temperature of around 1000 °C. Umicore smelting (Belgium), Noranda smelting (Canada) and Rönnskär smelter (Boliden) are well-known metal recovery processes from E-Waste using pyrometallurgy in a commercial scale [5, 6]. However, the burning produces toxic gases, which is again a threat to the environment. The hydrometallurgical method includes the reduction of metals into leachate using leaching agents such as cyanide, acid, thiourea and alkali. This method has higher selectivity towards metals. In the bio-metallurgical method, microbes are used for the recovery of metals. It is an environment-friendly approach; however, it is a time-consuming process and depends on the life of the microbes. Pyrolysis is a promising method for the conversion of organic materials into valuable fractions of liquid and gas [7, 8].

The aim of this study is to recover the most abundant and valuable metal, copper found in PCB (Table. 1). Most of the studies reported have performed acid leaching using ground samples of raw PCB. The leaching efficiency increases with the reduction in size of the feed because of the increase in surface area [9]. However, grinding of PCB produces dust, which causes pollution and loss of material occur at the very initial stage of the recycling process. Moreover, metals are embedded with the organic materials, and thus it is essential to delaminate the metal and the non-metallic fraction in the PCB. In this study, cut samples of computer PCB (CPCB) were used so that there is no generation of dust, and for the delamination of metallic and non-metallic components; the binding material, epoxy resin was thermally decomposed and removed by the process of pyrolysis. The epoxy resin was removed from the PCB in the form of liquid and gas products, which can be further used as chemical feedstock or energy generation. The remaining solid residue was then subjected to acid leaching for the recovery of the valuable metal, copper.

2 Materials and Methodology

2.1 Material

Waste computer printed circuit boards of different brands supplied by a local vendor were subjected to removing electronic components, such as capacitors, resistors, connectors and CPU fan. The bare boards were then cut into small pieces of approximately 5 mm × 5 mm size (Fig. 3). The cut pieces were cleaned using de-ionized water for the removal of impurities, followed by drying in a hot air oven overnight. The homogeneity of the sample was maintained by selecting the cut pieces containing copper as the dominant metal. The cut pieces containing solder and other metallic

Table 1 Material composition of printed circuit boards [11]

Metals (~40%)	Weight composition	Ceramics (~30%)	Weight %	Plastics (~30%)	Weight %
Copper	10–26.8%	SiO_2	15–30	Polyethylene	10–16
Iron	1.22–7.47%	Al_2O_3	6.0–9.4	Polypropylene	4.8
Tin	0–5.28%	Alkali-earthoxides	6.0	Polystyrene	4.8
Aluminium	0–4.78%	Titanates-micas	3.0	Epoxy	4.8
Lead	0–4.48%			Polyvinyl chloride	2.4
Nickel	0.28–3.32%			Polytetrafluoroethylene	2.4
Zinc	0–2.17%			Nylon	0.9
Antimony	0–1.82%				
Silver	0–3300 ppm				
Gold	80–1000 ppm				
Palladium	0–294 ppm				
Platinum	0–30 ppm				

Waste CPCB   Bare CPCB after the removal of electronic components   Cut bare CPCB of size 5mm by 5mm

Fig. 3 Steps for the preparation of sample

pieces were not considered throughout the experiment. The chemicals supplied by Merck Chemicals were of analytical grade and used as received.

2.2 Proximate Analysis

The proximate analysis was determined using the standard ASTM D-5142 method. The experiments were repeated, and the average value was reported. The moisture content, volatile matter and the ash content were directly obtained from the experiment. The fixed carbon content was obtained from the difference.

2.3 Thermogravimetric Analysis

The thermal degradation temperature window was determined using Thermogravi-metric Analyzer (TGA) of make: NETZSCH, model: TG 209 F1 *Libra*. Small pieces of the cut sample (~1 mm) weighing approximately 7 mg were subjected to controlled pyrolysis from 30 °C to 700 °C at the heating rate of 10 °C/min. Nitrogen gas (purity 99.995%) was used for creating the inert environment as purge gas (40 mL/min) and protective gas (20 mL/min).

2.4 Lab-Scale Pyrolysis

Semi-batch lab-scale pyrolysis experiments at varying temperatures of 450, 500 and 600 °C were conducted in a reactor of volume 1 L with 7.5 cm internal diameter. A tubular electrical furnace with PID controller (Dass & Co., India) was used for supplying the heat required for pyrolysis. The schematic diagram of the pyrolysis setup is shown in Fig. 4. Weighted sample of 30 g was placed inside the reactor, and N_2 gas (99.995% purity) was purged before the supply of heat for at least 10 min at the flow rate of 200 mL/min to ensure an inert environment was created throughout the line. A circulating chiller set at 4 °C was used to supply the condenser's cooling medium for obtaining the liquid product. The liquid products were collected in a collecting flask dipped in an ice bath, and the uncondensed gases were collected in tedlar bag. At the end of the experiment, the reactor was allowed to cool down to below 100 °C, and the residue was weighted for the solid yield. Since some amount of gas got condensed in the reactor outlet lining, dichloromethane was used to wash out the condensed gas. The liquid product was washed using 30 mL of dichloromethane and then removed by using rotary evaporator (Buchi, R-300). The reported liquid yield is the remaining product after solvent was removed using rotary evaporator. The gas yield was calculated considering no mass loss in the system.

2.5 Metal Extraction

After the removal of the organic material during the pyrolysis, the remaining residue, rich in inorganic material was subjected to acid leaching to recover valuable copper metal. 5 g of the pyrolysis residue was leached with sulfuric acid (H_2SO_4) along with an oxidant, hydrogen peroxide (H_2O_2). The experiment was conducted at room temperature with a mixing rate of 200 RPM for 4 h (Fig. 5). Sulfuric acid of 2 M concentration (50 mL) was used and followed by the addition of 7.5 mL of H_2O_2 after interval of 30 min. Since the process is exothermic, and to make sure there is no loss of water a condenser was fixed in the system. To ensure constant temperature condition, and uniform mixing, thermometer, and magnetic stirrer were used, respectively. At
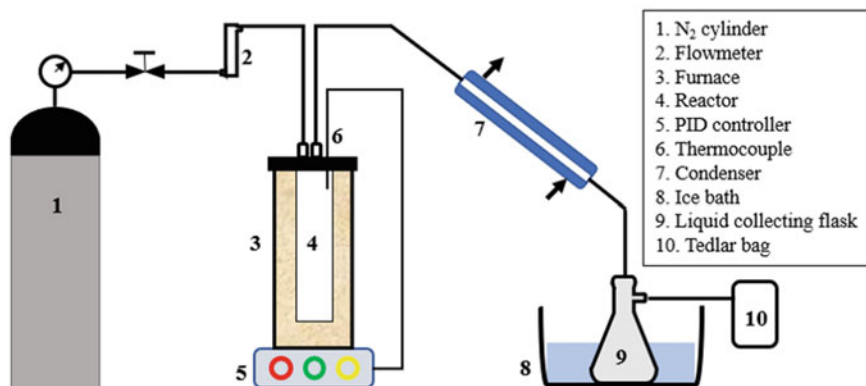
1. N₂ cylinder
2. Flowmeter
3. Furnace
4. Reactor
5. PID controller
6. Thermocouple
7. Condenser
8. Ice bath
9. Liquid collecting flask
10. Tedlar bag

Fig. 4 Lab-scale pyrolysis setup

4 h, the mixing was stopped, and the mixture was filtered immediately using a vacuum filtration unit, followed by drying the residue in the oven. The residue obtained was then subjected to XRD analysis.
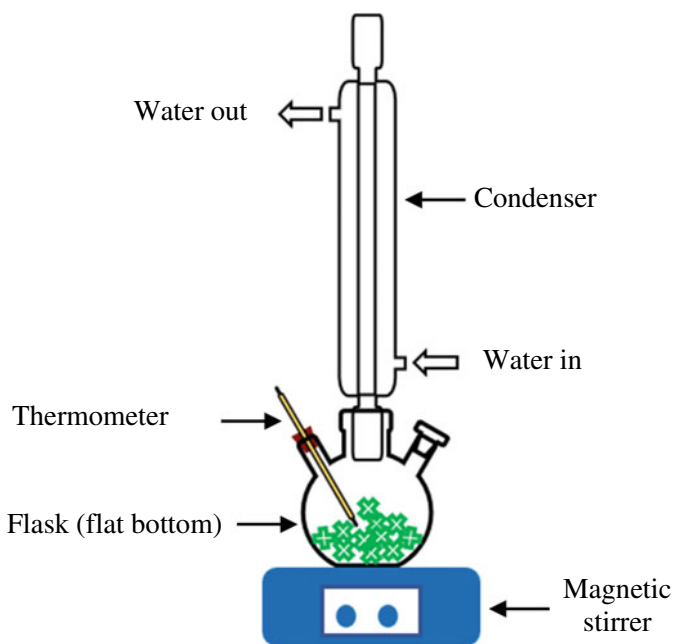

Fig. 5 Lab-scale metal extraction setup

2.6 FTIR Analysis

The liquid products obtained from pyrolysis at 600 °C were subjected to FTIR-ATR analysis for determining the functional groups. The analysis was carried out using Shimadzu, IRAffinity-1 in the wavelength range of 500–4000 cm^{-1} with total 30 scans.

2.7 XRD Analysis

The raw computer PCB and the residue remaining after acid leaching were analysed for the qualitative composition of copper using Powder XRD for macromolecules (Make: Rigaku Technologies, Japan, Model: SmartLab). This analysis also showed the leaching efficiency of the H_2SO_4 and H_2O_2 at room temperature. The analysis was carried out within the range of 5°–90° for two-theta, at the scan rate of 20° per minute. The XRD pattern obtained was analysed using the Match3! Software.

3 Results and Discussion

3.1 Proximate Analysis

The percentage composition of moisture, volatile matter, ash and fixed carbon of the raw computer PCB was found to be 1.17%, 28%, 69% and 1.83%, respectively. The results showed the presence of minimal amount of moisture and high amount of ash content in the sample. The high amount of ash content may be subjected to the presence of inorganic materials such as the metallic fraction, and the glass fibres present in the substrate [8].

3.2 Thermogravimetric Analysis

The thermal degradation stages of the computer PCB can be classified into three. Stage I (30–270 °C) showed no significant mass loss. Stage II (270–400 °C) showed major mass loss due to organic matter decomposition. This is clear from the DTG curve (Fig. 6), with maximum mass loss at 325 °C. At this stage, the epoxy resin underwent thermal degradation, which be condensed to liquid product [12]. During this stage, as the binding agent of the substrate, epoxy resin, is removed from the matrix, the separation of the metallic and the non-metallic components becomes easy. Further, there is no significant mass loss at stage III (400–700 °C).
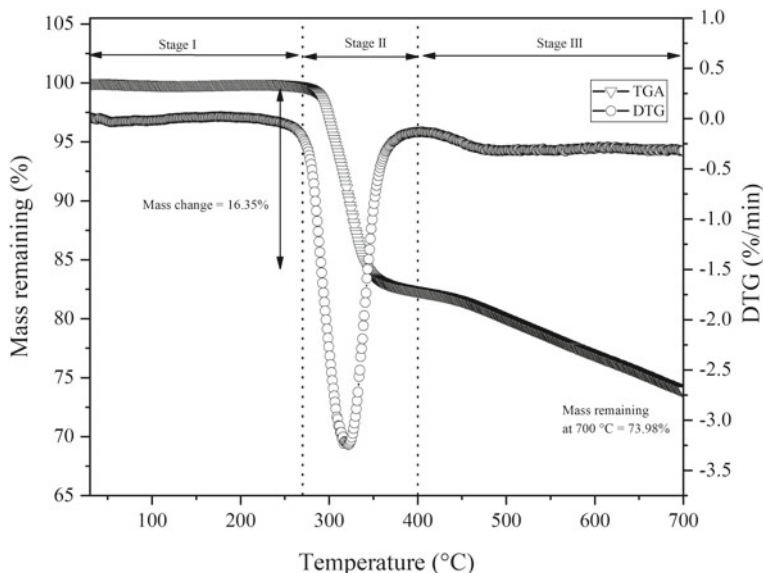
Fig. 6 TG-DTG curves of waste computer PCB from 30 to 700 °C at different heating rate of 10 °C/min

3.3 Lab-Scale Pyrolysis

The lab-scale pyrolysis experiments showed the organic decomposition increased from 21.34% at 450 °C to 24.45% at 600 °C [8]. Thus, 600 °C is the suitable pyrolysis temperature for maximum removal of the organic compounds. This will result into better separation of the metallic and the non-metallic fraction. The liquid product increased from 6.8% at 450 °C to 11.83% at 500 °C, but decreased to 3.84% at 600 °C [13]. The increase in gaseous fraction with pyrolysis temperature can be attributed to the production of lighter compounds at higher temperature as shown in Fig. 7 and Table 2.

3.4 FTIR

The FTIR spectra showed a wide range of functional groups (Fig. 8). The broad peak at 3332 cm^{-1} showed the presence of –OH group from phenol [14], peaks at 2975 and 2874 cm^{-1} can be attributed to stretching vibration of alkane [15]. The C=C vibration from aromatic compounds is represented by the peaks at 1596 and 1465 cm^{-1}. The peaks at 1227 and 1099 cm^{-1} can be attributed to the in-plane bending vibration of benzene ring, and the peaks at 827, 754 and 691 cm^{-1} can be attributed to the
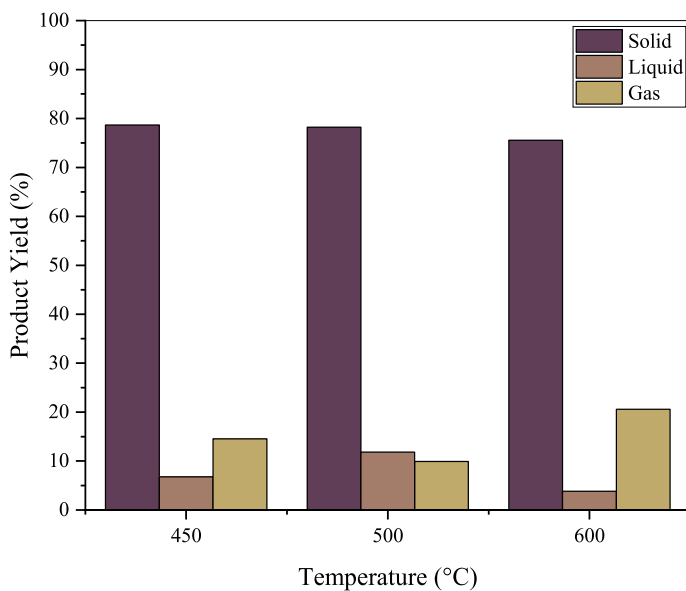
Fig. 7 Product distribution of pyrolysis at varying temperatures of 450, 500 and 600 °C

Table 2 Pyrolysis product distribution at varying temperatures of 450, 500 and 600 °C

Experiment no	Pyrolysis temperature (°C)	Organic mass loss (w/w%)	Solid (w/w%)	Liquid (w/w%)	Gas (w/w%)
Experiment 1	450	21.34	78.66	6.8	14.53
Experiment 2	500	21.77	78.23	11.83	9.94
Experiment 3	600	24.45	75.55	3.84	20.59

out-of-plane benzene ring vibration [15]. The presence of brominated compounds can be confirmed from the peak at 507 cm^{-1} representing C–Br stretch.
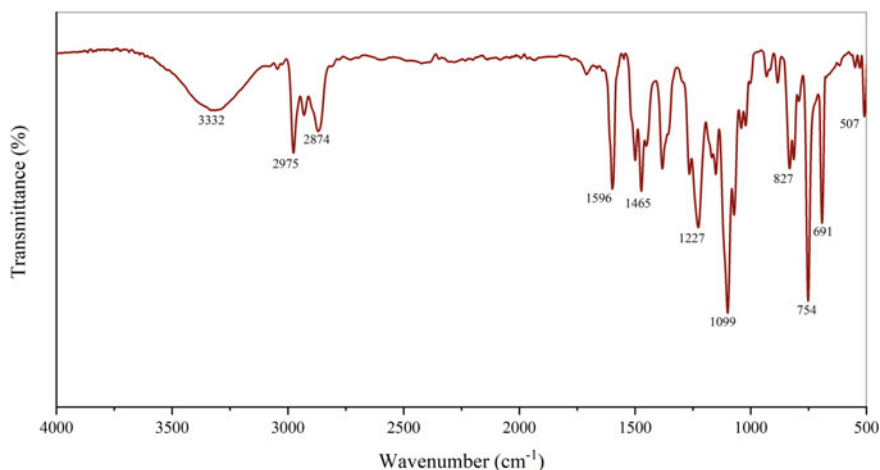
Fig. 8 FTIR spectra of liquid product obtained from pyrolysis of CPCB at 600 °C

3.5 *XRD Analysis*

The sharp peaks in the XRD spectra (Fig. 9) for the raw CPCB showed the presence of metallic copper, which got removed from the residue obtained from leaching of the pyrolyzed CPCB. The broad peaks near 20° showed the presence of amorphous SiO_2 from the glass fibres present in the substrate of the PCB [16, 17].

4 Conclusion

The waste CPCB pyrolysis experiments at varying temperatures showed that at 600 °C, the metallic and the non-metallic fractions get separated because of the removal of the epoxy resin. The liquid product obtained at pyrolysis temperature of 600 °C composed of phenolic compounds, aromatics, brominated compounds. Thus, the liquid product can be used as feedstock for production of chemicals or for energy generation. However, further treatment is required for the removal of the brominated compounds. The acid leaching of the pyrolysis residue effectively leached out the copper metal lining, which was confirmed by the XRD analysis of the residue remaining after acid leached.
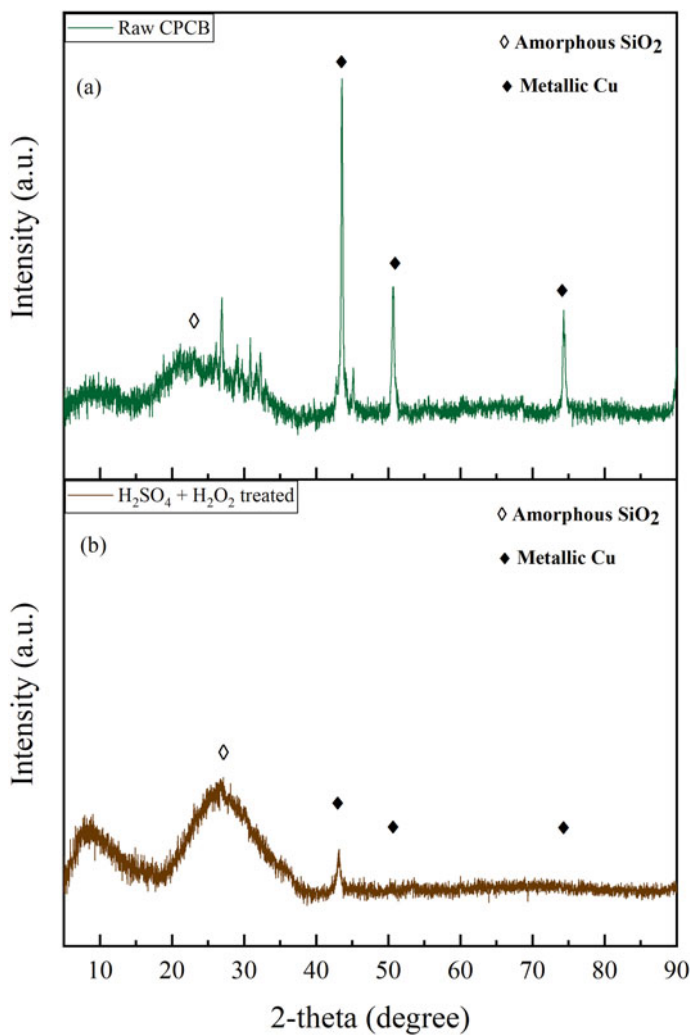
Fig. 9 XRD analysis for the (**a**) raw CPCB and (**b**) acid leached residue

References

1. Forti, V., Baldé, C.P., Kuehr, R., Bel, G.: The global E-waste monitor 2020: quantities, flows and the circular economy potential. United Nations University (UNU)/United Nations Institute for Training and Research (UNITAR)—co-hosted SCYCLE Programme, International Telecommunication Union (ITU) & International Solid Waste Association (ISWA), pp. 20–61, Bonn/Geneva/Rotterdam (2020)

2. Statista Homepage. https://www.statista.com/statistics/499952/ewaste-generation-worldwide-by-major-country/. Last Accessed 2 May 2022.

3. Das, P., Gabriel, J.P., Tay, C.Y., Lee, J.M.: Value-added products from thermochemical treatments of contaminated e-waste plastics. Chemosphere **269**, 129409 (2021)

4. Tipre, D.R., Khatri, B.R., Thacker, S.C., Dave, S.R.: The brighter side of e-waste-a rich secondary source of metal. Environ. Sci. Pollut. Res. **28**(9), 10503–10518 (2021)

5. Hasu, E., Barmak, K., West, A.C., Park, A.A.: Advancements in the treatment and processing of electronic waste with sustainability: a review of metal extraction and recovery technologies. Green Chem. **21**(5), 919–936 (2019)

6. Khaliq, A., Ramdhani, M.A., Brooks, G., Masood, S.: Metal extraction processes for electronic waste and existing industrial routes: a review and Australian perspective. Resources **3**(1), 152–179 (2014)

7. Sahle-demessie, E., Mezgebe, B., Dietrich, J., Shan, Y., Harmon, S., Lee, C.C.: Material recovery from electronic waste using pyrolysis: emissions measurements and risk assessment. J. Environ. Chem. Eng. **9**(1), 104943 (2020)

8. Chen, W., Chen, Y., Shu, Y., He, Y., Wei, J.: Characterization of solid, liquid and gaseous products from waste printed circuit board pyrolysis. J. Clean. Prod. **313**, 127881 (2021)

9. Yang, H., Liu, J., Yang, J.: Leaching copper from shredded particles of waste printed circuit boards. J. Hazard. Mater. **187**(1), 393–400 (2011)

10. Ongondo, F.O., Williams, I.D., Cherrett, T.J.: How are WEEE doing? A global review of the management of electrical and electronic wastes. Waste Manage. **31**(4), 714–730 (2011)

11. Zhang, Y., Liu, S., Xie, H., Zeng, X., Li, J.: Current status on leaching precious metals from waste printed circuit boards. Procedia Environ. Sci. **16**, 560–568 (2012)

12. Krishna, J.V.J., Damir, S.S., Vinu, R.: Pyrolysis of electronic waste and their mixtures: kinetic and pyrolysate composition studies. J. Environ. Chem. Eng. **9**(4), 105382 (2021)

13. Lin, K.-H., Chiang, H.-L.: liquid oil and residual characteristics of printed circuit board recycle by pyrolysis. J. Hazardous Mater. **271**, 258–265 (2014)

14. Das, P. P., & Purkait, M. K.: Treatment of cold rolling mill (CRM) effluent of steel industry. Sep. Purif. Technol. **274**, 119083 (2021)

15. Nie, C.-C., Wang, Y.-Y., Zhang, H., Zhang, Y.-K., Zhang, Y.-Q., Yan, Z.-Q., Li, B., Lyu, X.-J., Tao, Y.-J., Qiu, J., Li, L., Zhang, G.-W., Zhu, X.-N.: Cleaner utilization of non-metallic components in separation tailings of waste printed circuit board: pyrolysis oil, calorific value and building aggregate. J. Clean. Prod. **258**, 120976 (2020)

16. Panda, R., Jadhao, P.R., Pant, K.K., Naik, S.N., Bhaskar, T.: Eco-friendly recovery of metals from waste mobile printed circuit boards using low temperature roasting. J. Hazard. Mater. **395**, 122642 (2020)

17. Samanta, N. S., Das, P. P., Mondal, P., Bora, U., & Purkait, M. K.: Physico-chemical and adsorption study of hydrothermally treated zeolite A and FAU-type zeolite X prepared from LD (Linz–Donawitz) slag of the steel industry. J. Environ. Anal. Chem. **13**, 1–23 (2022)

A Study on Workability, Strength and Microstructure of Geopolymer Composites Made with Sustainable Materials

M. Leela Sai Rangarao , **Arup Kumar Mohapatra** , **and Bulu Pradhan**

1 Introduction

Around the world, the most widely utilized construction material for infrastructure development is concrete [1]. From the last few decades, the utilization of concrete has been increased enormously due to the rapid growth in the urbanization. Therefore, the utilization of ordinary Portland cement (OPC) as a basic binding material in concrete has been increased. However, the manufacturing of OPC emits 5–6% of carbon dioxide into the environment [2]. So, sustainable binding materials are required to replace OPC either partially or completely in the preparation of concrete. In this context, waste materials generated from industries like fly ash (FA), rice husk ash, copper slag and GGBFS can be utilized as alternative binding materials in combination with alkaline activators to replace the OPC partially or fully while producing the concrete.

The combined reaction of industrial wastes rich in aluminosilicates along with alkaline activators is known as a geopolymerization [3]. The fly ash-based geopolymers reaction is very slow at ambient temperature, so an elevated curing temperature is required for better geopolymerization reaction [4]. Few studies examined ways to improve the reactivity of FA, such as reducing the particle size of fly ash or adding calcium-based compounds [5]. Besides the aluminosilicate-based

M. Leela Sai Rangarao (✉) · A. K. Mohapatra
Department of Civil Engineering, Indian Institute of Technology Guwahati, Guwahati, Assam, India
e-mail: maradanileela@iitg.ac.in

A. K. Mohapatra
e-mail: arup_kumar@iitg.ac.in

B. Pradhan
Department of Civil Engineering, and Centre for Disaster Management and Research, Indian Institute of Technology Guwahati, Guwahati, Assam, India
e-mail: bulu@iitg.ac.in

geopolymer network, the addition of calcium oxide (CaO) leads in the evolution of calcium silicate hydrates [6]. The materials such as GGBFS, OPC, metakaolin, rice hush ash (RHA) and silica fume can be utilized as source materials along with fly ash for the preparation of GPc at ambient environment. There have been a few studies that compare GPc prepared with a mixture of FA and GGBFS, and FA and OPC. The current study examines the workability (slump value), early age compressive strength and XRD studies of geopolymer composites made with various proportions of FA-GGBFS and FA-OPC, as well as varied molarities of NaOH solution.

2 Experimental Program

2.1 Materials Utilized in Making of Geopolymer Composites

In the present research investigation, GGBFS or OPC was added with FA in the preparation of GPc mixes. OPC 43 grade cement confirming to ASTM C150/C150M-20 (Type I) [7] was used in the GPc mixes. The relative density of FA, GGBFS and OPC were 2.20, 2.67 and 3.10, respectively. The coarse aggregates utilized in preparation of GPc mixes were a combination of maximum size 25 mm and 12.5 mm having relative density of 2.64 and 2.66 respectively. Further, relative density of fine aggregate (river sand) was 2.70 and fineness modulus was 2.62. Alkaline solution utilized was a blend of sodium silicate (Na_2SiO_3) solution and sodium hydroxide (NaOH) solution.

2.2 Geopolymer Composite Proportions and Preparation

The proportions of geopolymer composites prepared with various replacement levels of GGBFS and OPC, and NaOH (SH) solution molarity are interpreted in Table 1. FA-GGBFS and FA-OPC based GPc were prepared by replacing fly ash with GGBFS and OPC, respectively, at 10% and 20% by mass of binder. The binder content and alkaline solution to binder content ratio were taken as 400 kg/m^3 and 0.6, respectively. The coarse aggregate was utilized at the proportion of 58% (25 mm aggregate) and 42% (12.5 mm aggregate) by mass of coarse aggregate. The SH solution was made at 6 M and 8 M concentrations. The SS and SH solutions were mixed at a mass ratio (SS/SH) of 1.2 for preparing the GPc mixes.

Before 48 h of GPc mix preparation, the SH pellets were mixed in tap water for the making of SH solution. Before 24 h of GPc mix preparation, the SS solution (commercially available) was added with SH solution to make the alkaline solution. The process followed for preparation of GPc mixes is as follows: Firstly, all the aggregates were introduced into the drum mixer and mixed thoroughly. Then, the binders, i.e. FA and GGBFS, or FA and OPC were mixed along with the aggregates.

Table 1 Mix proportions of geopolymer composites (quantities of ingredients of GPc in kg/m^3)

Type of GPc	Mix notation	Fly ash	GGBFS	OPC	SH solution molarity	Alkaline solution	Fine aggregate	Coarse aggregate
FA-GGBFS based geopolymer concrete (FA%:GGBFS%)	M1 (90%: 10%)	360	40	–	6 M	240	621.3	1013.7
	M2 (80%: 20%)	320	80	–				
	M3 (90%: 10%)	360	40	–	8 M			
	M4 (80%: 20%)	320	80	–				
FA-OPC based geopolymer concrete (FA%:OPC%)	M5 (90%: 10%)	360	–	40	6 M			
	M6 (80%: 20%)	320	–	80				
	M7 (90%: 10%)	360	–	40	8 M			
	M8 (80%: 20%)	320	–	80				

Once the binders and aggregates were thoroughly mixed, the alkaline solution was added, and further mixed to obtain a fresh geopolymer composite. Slump test was carried out on the freshly prepared concrete mix. Thereafter, the fresh GPc was filled in cube moulds (size: 150 mm) in three layers with proper compaction of each layer on the vibration table. The cube moulds with the specimens were then stored for 24 h after casting in the laboratory. The cube mould samples were then demolded and let to ambient condition until the testing date.

2.3 Tests on Geopolymer Concrete (GPc)

2.3.1 Workability and Compressive Strength Test on GPc

The workability of fresh GPc mix was determined by conducting the slump test on fresh GPc mix. The 7 days strength test was done on concrete cube (size: 150 mm)

specimens as per IS 516-2021 [8]. The mean value of 3 replicate 150 mm GPc cube samples was noted as the compressive strength value of a given geopolymer composite.

2.3.2 Microstructure Analysis

Following the completion of strength test, the broken cube pieces were grounded in a jaw crusher and the pulverized material was sieved through a sieve (with 75 micron meter square mesh). The passed geopolymer powder samples were collected in plastic zipper bags and stored in a desiccator. These powder samples were used for the microstructure study, i.e. through XRD analysis. The XRD analysis was performed on the GPc powder samples in Rigaku SmartLab X-ray diffractometer with a radiation of CuKα having a wavelength (λ) of 1.5405 Å. The GPc powder was scanned with in a range from 5° to 60° 2θ, with 0.03° 2θ as step size.

3 Results and Discussion

3.1 Workability of Geopolymer Composites

The slump test values of FA-GGBFS based and FA-OPC based geopolymer composites are depicted in Fig. 1. As noted from Fig. 1, among all the geopolymer composites, the highest slump value, i.e. 210 mm, was found in FA-GGBFS based GPc prepared with 10% GGBFS and 6 M NaOH solution. Similarly, FA-OPC (20%) based GPc with 8 M NaOH solution showed the lowest slump value of 145 mm. From Fig. 1, as the NaOH solution molarity was increased, the slump value was reduced. The viscosity of alkaline solution increased as NaOH solution molarity was increased [9], thereby reducing the slump of FA-GGBFS and FA-OPC based geopolymer composites.

Further, the slump value was reduced as the GGBFS or OPC content increased in geopolymer composites. This could be due to the presence of more angular-shaped particles of GGBFS, and OPC in the geopolymer composites [10, 11] that decreased the slump value of geopolymer composites. Further, irrespective of NaOH solution molarity and fly ash content, the FA-OPC based GPc showed a lower slump than FA-GGBFS based GPc as evident from Fig. 1. This is due to the influence of faster reactivity of OPC in the alkaline solution, which resulted in faster setting [12] of FA-OPC based GPc.
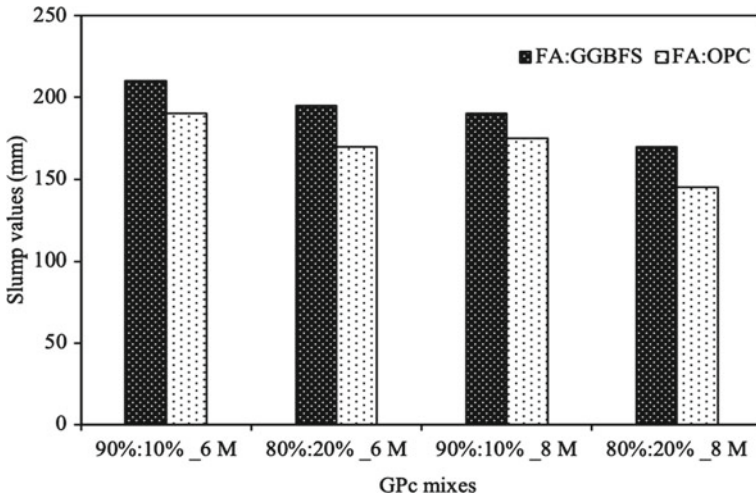
Fig. 1 Slump values of fresh geopolymer composites

3.2 Compressive Strength of Geopolymer Composites

The 7 days strength of FA-GGBFS and FA-OPC geopolymer composites is presented in Fig. 2.
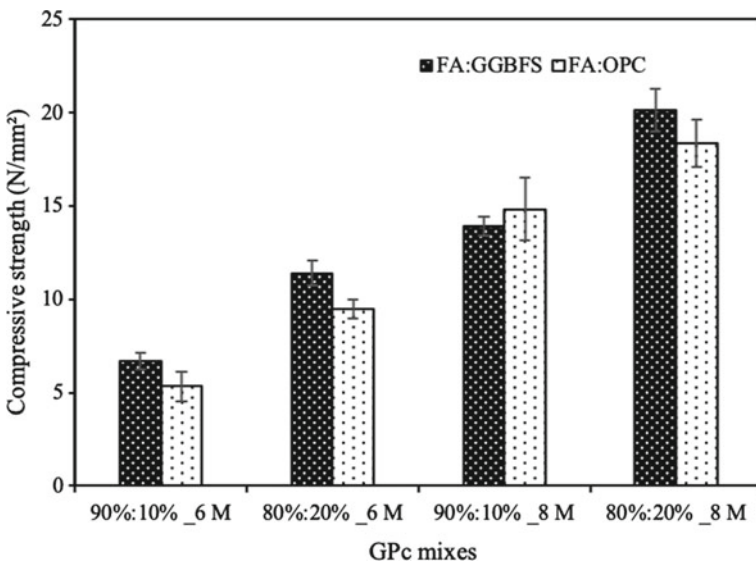

Fig. 2 Compressive strength of geopolymer composites

From Fig. 2, the strength (at 7 days age) of FA-GGBFS and FA-OPC based GPc mixes enhanced with increase in GGBFS and OPC content, respectively. The increase in GGBFS content led to more calcium content that resulted in the development of more amount of geopolymer gels leading to compact microstructure of FA-GGBFS based GPc mixes [10]. The higher OPC content led to more amount of calcium oxide (CaO) content in the GPc mixes, which reacted faster than other oxides in the presences of alkaline solution [12] and resulted in the development of higher amount of calcium-rich gels. From Fig. 2, as the concentration of NaOH (SH) solution increased, the strength of FA-GGBFS based and FA-OPC based GPc was increased. The higher SH solution molarity in FA-GGBFS and FA-OPC geopolymer composites resulted in dissolution of Si and Al from source materials to a comparatively larger extent, thereby resulting in improved polycondensation process in the mixes made with higher molarity of NaOH (SH) solution [13, 14]. From Fig. 2, it is inferred that the geopolymer composites made with FA and GGBFS mostly exhibited greater strength than GPc mixes made with FA and OPC, which could be due to the influence of comparatively greater extent of polymerization in FA-GGBFS geopolymer composites.

3.3 X-Ray Diffraction Analysis of GPc

Figures 3 and 4 represent the X-ray diffraction (XRD) plots of GPc mixes made with 6 M and 8 M SH solution, respectively. The obtained XRD plots of GPc showed the phases of muscovite (8.8° 2θ), albite (22.01° 2θ and 28.02° 2θ), anorthoclase (27.5° 2θ) and aragonite ($CaCO_3$) (45.8° 2θ) in all the GPc mixes. Similarly, the crystalline phases of quartz (SiO_2) and mullite ($Al_{4.75}Si_{1.25}O_{9.63}$) were also identified in all mixes. Nepheline ($NaAlSiO_4$) and C–S–H (calcium silicate hydrate) gel peaks were found at 27.1° 2θ and 29.5° 2θ, respectively, in XRD plots. The peaks corresponding to nepheline ($NaAlSiO_4$) were observed in all 8 M NaOH solution-GPc mixes and in fly ash-OPC (20%) based GPc mix with NaOH solution of 6 M. Further, the peak related to calcium silicate hydrate gel was observed in OPC (10% and 20%) based GPc mixes, and GPc mix with 20% GGBFS, activated with 8 M SH solution.

From Figs. 3 and 4, with increase in GGBFS content and NaOH solution concentration, albite and nepheline peaks were increased in FA-GGBFS based GPc. This indicates that more GGBFS content led to more amount of calcium that resulted in greater extent of geopolymerization reaction, thereby showing higher peak intensity of albite. In addition, greater dissolution of Al and Si from source materials with increase in concentration of NaOH (SH) solution resulted in higher peak intensity of albite and nepheline in FA-GGBFS based GPc mixes. From Figs. 3 and 4, as OPC replacement and concentration of NaOH (SH) solution increased, the albite peak intensity was increased in FA-OPC geopolymer composites. This indicates that increase in calcium oxide content at higher OPC content enhanced the polymerization process thus showing higher peaks related to albite. In addition, in fly ash-OPC
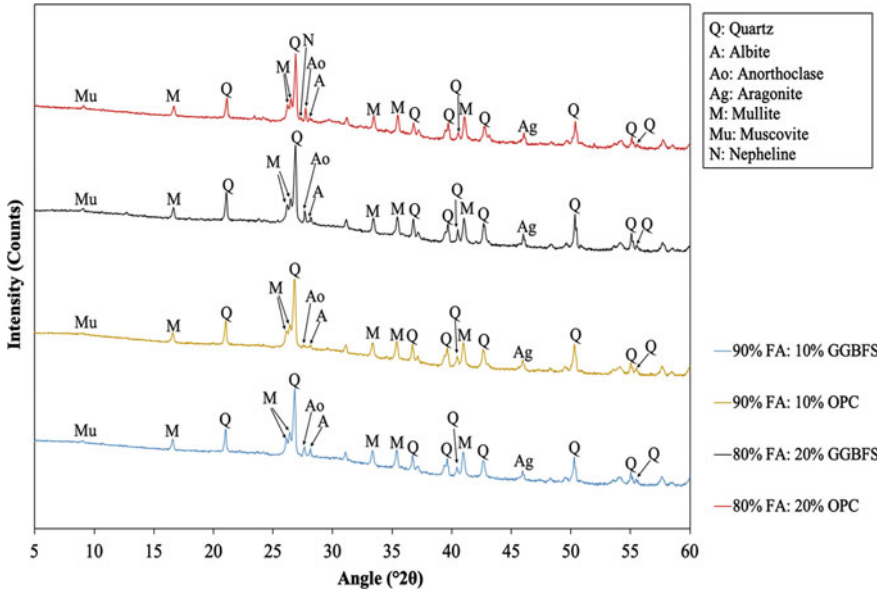
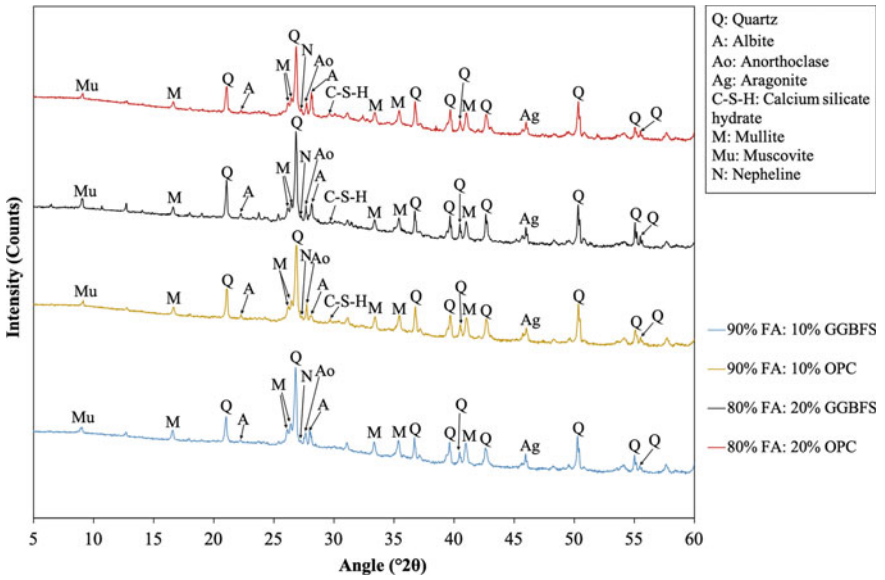**Fig. 3** XRD plots of GPc mixes with 6 M SH solution

Fig. 4 XRD plots of GPc mixes with 8 M SH solution

GPc mixes, the larger peak intensity of albite with increase in SH concentration led to larger dissolution of Si and Al from the precursor materials.

From Figs. 3 and 4, albite and anorthoclase peak intensities were higher in FA-GGBFS geopolymer composites than FA-OPC geopolymer composites. This is consistent with the variation in strength where FA-GGBFS mixes mostly showed higher strength than FA-OPC based GPc mixes (Fig. 2). Further, C–S–H gel peak was not identified in FA-GGBFS geopolymer composites with 10% GGBFS and 8 M SH solution. This might be the influencing factor for lower strength of FA-GGBFS (90%: 10%) based GPc mix than FA-OPC (90%: 10%) based GPc mix made with 8 M SH solution although the albite and anorthoclase peaks were higher in FA-GGBFS based GPc mix (90%: 10%) than FA-OPC based GPc mix (90%: 10%).

4 Conclusions

The outcomes of the current investigations were as follows:

- The slump values of FA-GGBFS and FA-OPC based GPc mixes reduced as the GGBFS or OPC content, and NaOH solution concentration increased.
- The slump values were greater in the geopolymer composites with GGBFS as compared to OPC, irrespective of GGBFS or OPC content, and NaOH solution concentration.
- The compressive strength was increased in FA-GGBFS and FA-OPC based geopolymer composites with increase in the GGBFS and OPC replacement, respectively. Similarly, the strength was also increased with molarity of NaOH solution.
- The FA-GGBFS geopolymer composites mostly exhibited greater strength as compared to FA-OPC geopolymer composites.
- The XRD analysis of GPc mixes with GGBFS showed higher peak intensity of albite and nepheline with increase in GGBFS content and NaOH (SH) solution concentration. Similarly, peaks related to albite increased with OPC content and concentration of NaOH (SH) solution in FA-OPC geopolymer composites. The increase in intensity of peak related to albite with concentration of NaOH (SH) solution is consistent with the variation in strength of all geopolymer composites.
- In comparison between FA-GGBFS based and FA-OPC based geopolymer composites, the intensity of peak related to albite and anorthoclase were greater in geopolymer composites with FA and GGBFS than geopolymer composites with FA and OPC. This corroborates the variation in strength where geopolymer composites with GGBFS mostly attained greater strength than geopolymer composites with OPC.

References

1. Luga, E., Atis, C.D.: Optimization of heat cured fly ash/slag blend geopolymer mortars designed by "Combined Design" method: Part 1. Constr. Build. Mater. **178**, 393–404 (2018)
2. Arıoğlu Akan, M.O., Dhavale, D.G., Sarkis, J.: Greenhouse gas emissions in the construction industry: an analysis and evaluation of a concrete supply chain. J. Clean. Prod. **167**, 1195–1207 (2017)
3. Almalkawi, A.T., Balchandra, A., Soroushian, P.: Potential of using industrial wastes for production of geopolymer binder as green construction materials. Constr. Build. Mater. **220**, 516–524 (2019)
4. Somna, K., Jaturapitakkul, C., Kajitvichyanukul, P., Chindaprasirt, P.: NaOH-activated ground fly ash geopolymer cured at ambient temperature. Fuel **90**(6), 2118–2124 (2011)
5. Changmai, M., Das, P. P., Mondal, P., Pasawan, M., Sinha, A., Biswas, P., ... & Purkait, M. K.: Hybrid electrocoagulation–microfiltration technique for treatment of nanofiltration rejected steel industry effluent. Int. J. Environ. Anal. Chem. **102**, 62–83 (2022)
6. Samanta, N. S., Das, P. P., Mondal, P., Bora, U., & Purkait, M. K.: Physico-chemical and adsorption study of hydrothermally treated zeolite A and FAU-type zeolite X prepared from LD (Linz–Donawitz) slag of the steel industry. Int. J. Environ. Anal. Chem. **13**, 1–23 (2022)
7. ASTM C150/C150M-20 (Type I), Standard specification for Portland cement. ASTM International, West Conshohocken, PA (2020)
8. IS 516: 2021 (Part 1/Sec 1), Method of tests for strength of concrete. Bureau of Indian Standard, Manak Bhavan, New Delhi (2021)
9. Chareerat, T., Chindaprasirt, P., Sirivivatnanon, V.: Workability and strength of coarse high calcium fly ash geopolymers. Cement Concr. Compos. **29**, 224–229 (2007)
10. Deb, P.S., Nath, P., Sarker, P.K.: The effects of ground granulated blast-furnace slag blending with fly ash and activator content on the workability and strength properties of geopolymer concrete cured at ambient temperature. Mater. Des. **62**, 32–39 (2014)
11. Jindal, B.B.: Investigations on the properties of geopolymer mortar and concrete with mineral admixtures: a review. Constr. Build. Mater. **227**, 116644 (2019)
12. Amer, I., Kohail, M., El-Feky, M.S., Rashad, A., Khalaf, M.A.: Characterization of alkali-activated hybrid slag/cement concrete. Ain Shams Eng. J. **12**(1), 135–144 (2021)
13. Chindaprasirt, P., Chalee, W.: Effect of sodium hydroxide concentration on chloride penetration and steel corrosion of fly ash-based geopolymer concrete under marine site. Constr. Build. Mater. **63**, 303–310 (2014)
14. Mohapatra, A.K., Pradhan, B.: A study on early age properties of hybrid alkali activated mortars cured under ambient condition. Mater. Today: Proc. **65**, 954–960 (2022)

Effect of Chemical Treatment on Decomposition Profiles of Carbon Fiber Reinforced Polymer Composites and Its Recycling

Eledathu Kuriachan Sachin, Pankaj Tiwari, and Nelson Muthu

1 Introduction

The composite industry is marked a global market size of USD 86.4 billion in 2021, and in the coming years (2021–2028), a 6.6% of compound annual growth is expected [1]. The growth is driven by its huge applicability in various industries like aerospace, construction, aviation, marine, wind energy, oil and gas, sporting goods, etc. [2, 3]. The remarkable material properties of composite materials like high strength-to-weight ratio, thermal and electrical properties, and corrosion resistance account for its thriving demand [4]. The fibrous composites, especially carbon fiber reinforced polymer (CFRP) composites, are one of the leading contributors to the growth considering their properties and applications. However, carbon fiber production is high energy demanding process achieved at high temperatures ranging from 1000 to 2000 °C [4]. On the other hand, the thriving nature of the CFRP composite industry in both production and consumption now leads to a large number of "End-of-Life" (EOL) materials that need to be recycled sustainably. It is estimated that 102. 4 Mt and 148.7 Mt CFRP waste materials will be accumulated from aviation and wind turbine, respectively, in the Asian region alone by 2050 [5, 6]. Therefore, the environmental problems related to the disposal of this composite waste and the cost of virgin

E. K. Sachin (✉) · P. Tiwari
Department of Chemical Engineering,
Indian Institute of Technology Guwahati, Guwahati, India
e-mail: sachinkuriachan@iitg.ac.in

P. Tiwari
e-mail: pankaj.tiwari@iitg.ac.in

N. Muthu
Department of Mechanical Engineering,
Indian Institute of Technology Guwahati, Guwahati, India
e-mail: nelsonm@iitg.ac.in

fibers demand that researchers find a sustainable recycling technique to recover the fibers from the EOL composites.

Mechanical, thermal, and chemical recycling are the major methods adopted to recycle CFRP composites. The mechanical recycling methods are limited, in that it does not recover the structure of the fiber; instead, the FRP composites are milled into small pieces called recyclate, which can be used as filling or aggregate replacement [2]. The chemical recycling methods ensure the recovery of fibers with better mechanical properties, but the disposal of the solvent and its impact on human health and the environment makes it challenging [2, 7]. In thermal recycling, pyrolysis stands out against incineration in end product usability. The gas and liquid coming out of the pyrolysis reactor can be used as chemical feedstock. However, the char formation on the surface of the recycled fibers and mechanical property deterioration at higher operating temperatures are the major limitations of the pyrolysis process [2, 3]. By understanding the advantages and drawbacks of each method, a complementary approach for recycling the CFRP can lead to a process with promising results. The present work examines the effect of chemical treatment before the thermal recycling method by pre-treating the CFRP composites with $ZnCl_2$-Ethanol solution.

2   Materials and Method

All the chemicals used in this study were reagent grade. The ethanol (99.5%) was supplied by Tedia company Inc., Fairfield, USA, and $ZnCl_2$ was by Merck Life Scientific Pvt. Ltd., Mumbai, India. The method followed for pre-treatment is shown in Fig. 1. The cured CFRP coupon was cut into 2 cm $\times$ 2 cm pieces. Different concentration (w/v) of $ZnCl_2$-Ethanol solution (5–40%) was prepared. The sized CFRP was treated with $ZnCl_2$-Ethanol solution in a stoppered flask under magnetic stirring at 80 °C for 2 h. The solid-to-solvent ratio was kept at 60. After the treatment, the CFRP pieces were filtered out from the solvent, washed, and dried. The samples were named CFRP_ZnXX, where XX represents the concentration of $ZnCl_2$ in an ethanol solution, i.e., CFRP_Zn10 represents the CFRP samples treated with 10% of $ZnCl_2$-Ethanol solution. The effect of chemical treatment on the decomposition of the matrix in the CFRP was analyzed using the thermogravimetric analyzer (TGA), TG 209 F1 Libra, M/s Netzsch, Germany. The samples were placed in a crucible, and TGA studies were conducted from room temperature to 1000 °C at a rate of 10 °C/min. Both TGA curve and derivative thermogravimetric (DTG) curves were obtained from the study. Further, the filtrate collected was characterized with Fourier transform infrared (FTIR) spectroscopy from 500 to 4000 cm^{-1} and compared with the fresh solvent before treatment.
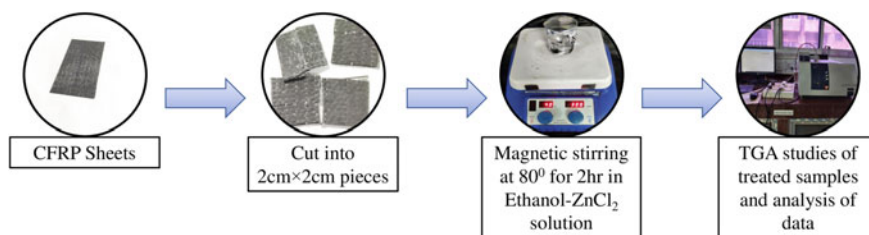
Fig. 1 Process flow diagram of the chemical treatment process of CFRP

3 Result and Discussions

The TGA curves of both raw and pre-treated CFRP composite were found to be similar and show only one sharp drop corresponding to the decomposition of the epoxy resin, as shown in Fig. 2. However, the range of temperature at which the mass loss happens varies with the concentration of $ZnCl_2$. Moreover, the peak of the DTG curve (Fig. 2) shifted to the left due to the effect of $ZnCl_2$, and the largest shift was at 10% $ZnCl_2$-Ethanol solution. The peak, onset, and end temperatures and maximum mass loss are shown in Table 1. At 10% of $ZnCl_2$, the peak temperature shifted to 32 °C left from 373.1 °C of the raw CFRP. The overall mass loss temperature range without pre-treatment was found to be between 336.8 and 442.7 °C, and that of 10% $ZnCl_2$ treatment is 307.6 and 355.7 °C. Therefore, the pyrolysis temperature of the CFRP composite can be reduced by 87 °C with the help of pre-treatment. The ethanol in the pre-treating solution acts as a swelling agent for epoxy resins and enables the penetration of the Zn^{2+} ion into it [8]. The penetrated Zn^{2+} ions then form organo-metallic bonds with the carbon–nitrogen bonds in epoxy resin and promote the catalytic decomposition of epoxy resins [9]. The C–N bonds in the epoxy resins are likely to break first during pyrolysis since it possesses lower bond energies throughout the cross-linked structure of epoxy resin [9]. The chemical action of Zn^{2+} ions accelerate the breakage of the C–N bond and lowers the temperature of the breakdown.

The peak temperature of decomposition of epoxy resins decreases first and reaches a minimum value (341.7 °C) at 10% $ZnCl_2$ solution and then increases with concentration (Table 1). The temperature range of mass loss also follows the same pattern. Initially, more Zn^{2+} ions are available for bond formation when the concentration increases from 5 to 10%. After 10%, the density and viscosity of the solution increase along with the increase in the number of Zn^{2+} ions. The higher density and viscosity of the solution decrease the swelling efficiency of ethanol and hence the penetration of Zn^{2+} ions [10].

The FTIR spectra of the 10% $ZnCl_2$-Ethanol solution before and after pre-treatment is shown in Fig. 3. Both samples gave a similar spectrum with a slight change in transmittance value, and it is comparable to one given in the literature [11]. The broad band (3598–3032 cm^{-1}) centered at 3302 cm^{-1} is assigned to the stretching vibration of the O–H bond in ethanol [11]. The stretching and bending
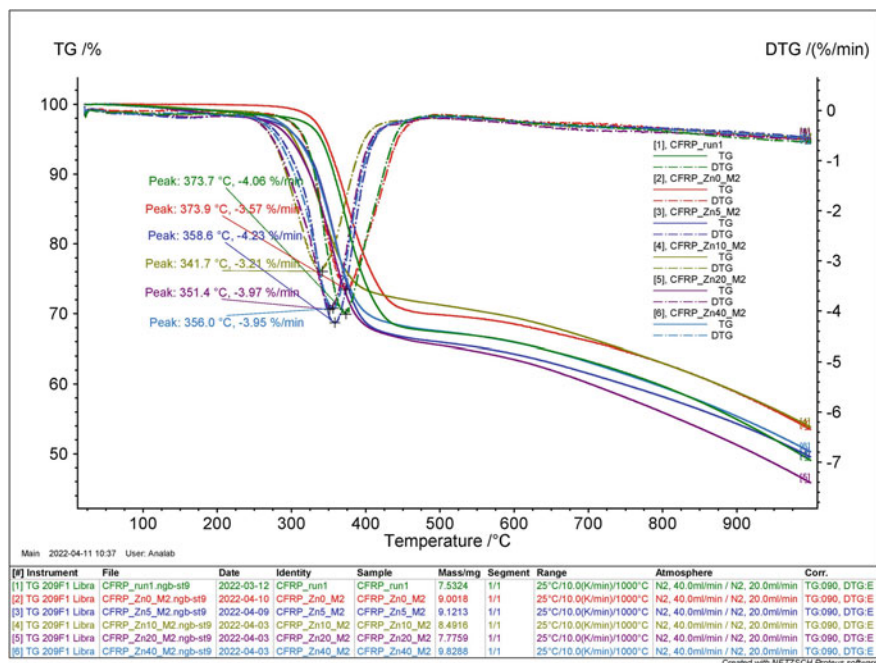
**Fig. 2** TGA and DTG curves of CFRP (raw and pre-treated)

Table 1 Temperature profile of resin decomposition zone

Sample	Concentration (%)	Resin decomposition zone		
		Onset Temp. (°C)	Max. Decomp. Temp. (°C)	Offset Temp. (°C)
CFRP	–	336.8	373.7	442.7
CFRP_Zn5	5	314.6	358.6	414.5
CFRP_Zn10	**10**	**307.6**	**341.7**	**355.7**
CFRP_Zn20	20	317.4	351.4	404.4
CFRP_Zn40	40	311.6	356.0	412.2

The best results of pre-treatment studies were obtained at 10% $ZnCl_2$-Ethanol solution and the particular values are given in 'bold'

vibrations of the –C–H bond of the –CH_3 group are shown by the peaks at 2974 cm^{-1} and 1383 cm^{-1}, respectively [12]. Compared to the peaks of pure, the peaks of $ZnCl_2$-Ethanol solution are shifted to the right due to the effect of $ZnCl_2$ in the ethanol [11]. Also, the peaks of the $ZnCl_2$-Ethanol solution collected after treatment show a slight shift due to the concentration difference compared to the freshly prepared solution. Furthermore, there are no new peaks identified after treatment which indicates that the ethanol only acts as a swelling agent rather than dissolving the epoxy material

Fig. 3 FTIR spectrum of pure and used $ZnCl_2$-Ethanol solution
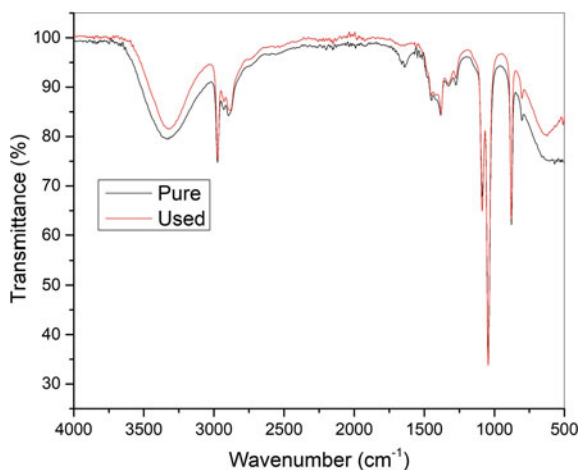
in the CFRP. Thus, the solution can be reused in the process effectively without any treatment.

4 Conclusions

The effect of Ethanol-$ZnCl_2$ solution on the decomposition of epoxy in CFRP was studied at different concentrations of the solution. It was found that both the swelling property of ethanol and the catalytic activity of Zn^{2+} ions help in reducing the decomposition temperature profile of the epoxy resin. A 10% of solution shows a higher effect with a reduction of 87 °C in the temperature range at which the major mass loss happens. The study can be extended to optimize the process parameters like temperature, time of the pre-treatment, and also the pyrolysis at the reduced temperature of CFRP to check the quality of recycled fibers.

References

1. Composites Market Size, Share & Trends Analysis Report by Product (Carbon, Glass), By Manufacturing Process (Layup, Filament, RTM), By End Use, By Region, And Segment Forecasts, 2021–2028. https://www.grandviewresearch.com/industry-analysis/composites-market. Last Accessed on 14 May 2022

2. Gopalraj, S.K., Karkl. T.: A review on the recycling of waste carbon fibre/glass fibre-reinforced composites: fibre recovery, properties and life-cycle analysis. SN Appl. Sci. **2**(433), 1–21 (2020)

3. Oliveux, G., Dandy, L.O., Leeke, G.A.: Current status of recycling of fibre reinforced polymers: review of technologies, reuse and resulting properties. Prog. Mater. Sci. **72**, 61–99 (2015)

4. Ghaedi, M., Shokrollahi, A., Tavallali, H., Shojaiepoor, F., Keshavarz, B., Hossainian, H., ... & Purkait, M. K.: Activated carbon and multiwalled carbon nanotubes as efficient adsorbents for removal of arsenazo (III) and methyl red from waste water. Toxicol. Environ. Chem. **93**, 438–449 (2011)

5. Lefeuvre, A., Garnier, S., Jacquemin, L., Pillain, B., Sonnemann, G.: Anticipating in-use stocks of carbon fiber reinforced polymers and related waste flows generated by the commercial aeronautical sector until 2050. Resour. Conserv. Recycl. **125**, 264–272 (2017)

6. Lefeuvre, A., Garnier, S., Jacquemin, L., Pillain, B., Sonnemann, G.: Anticipating in-use stocks of carbon fibre reinforced polymers and related waste generated by the wind power sector until 2050. Resour. Conserv. Recycl. **141**, 30–39 (2019)

7. Bhattacharjee, A., Purkait, M. K., & Gumma, S.: Loading and release of doxorubicin hydrochloride from iron (III) trimesate MOF and zinc oxide nanoparticle composites. Dalton Trans. **49**, 8755–8763 (2020)

8. Xing, M., Li, Z., Zheng, G., Du, Y., Chen, C., Wang, Y.: Recycling of carbon fibre-reinforced epoxy resins composite via a novel acetic acid swelling technology. Composite Part B **224**, 109230 (2021)

9. Wu, T., Zhang, W., Jin, X., Liang, X., Sui, G., Yang, X.: Efficient reclamation of carbon fibers from epoxy composite waste through catalytic pyrolysis in molten $ZnCl_2$. RSC Adv. **9**, 377–388 (2019)

10. Park, J., Kim, D.: Effect of polymer solution concentration on the swelling and mechanical properties of glycol chitosan super porous hydrogels. J. Appl. Polym. Sci. **115**(6), 3434–3441 (2009)

11. Kalhor, P., Wang, Y., Yu, Z.: The structures of $ZnCl_2$-ethanol mixtures, a spectroscopic and quantum chemical calculation study. Molecules **26**(9), 2498 (2021)

12. Sharma, M., Das, P. P., Sood, T., Chakraborty, A., & Purkait, M. K.: Ameliorated polyvinylidene fluoride based proton exchange membrane impregnated with graphene oxide, and cellulose acetate obtained from sugarcane bagasse for application in microbial fuel cell. J. Environ. Chem. Eng. **9**, 106681 (2021)

The Synergistic Effect of a Nickel Ion on the Corrosion Inhibition Efficiency of Purple Rice Bran Extract in Acidic Media

Abhradip Pal and Chandan Das

1 Introduction

A wide range of industries and their products are affected by corrosion globally. Corrosion results in the degradation of metal components and processing systems of any industry, and ultimately, the service life of manufacturing industries gets affected. The industrial sectors make extensive use of iron and it alloys. [1]. Those industries usually have many processes like acid pickling, acid descaling, and industrial cleaning at a regular interval. H_2SO_4, HCl, and H_3PO_4 are commonly used due to their aggressiveness and some chemical properties. Iron starts to corrode readily in such an acidic environment as the high concentration of protons excites the corrosion process [2].

Since this has been a severe problem in the industry, lots of preventive measurements are taken into consideration. There are various methods like up-gradation of metal alloy use of preventive inhibitors to prevent corrosion damages. Practically, the application of corrosion inhibitors is one of the efficient and economically viable approaches. In general, there are two types of corrosion inhibitors based on their source of synthesis: natural (organic) and synthetic. Natural inhibitors are more effective rather than synthetic inhibitors as they are economical and eco-friendly [3–5]. However, sometimes they are not so useful in reducing corrosion. To counter this problem for the last few decades, organic and inorganic inhibitors have been applied. Recently, green corrosion inhibitors have been employed, which are composed of organic components such as polysaccharides, amino acids, and polyphenols and are very much likely to contain S, N, O heteroatoms and other functional groups. The extracts of several biomasses have been implemented as natural inhibitors to mitigate corrosion. In this study, purple rice bran, a biodegradable agro by-product, was tested

A. Pal · C. Das (✉)

Department of Chemical Engineering, Indian Institute of Technology Guwahati, Guwahati, Assam 781039, India
e-mail: cdas@iitg.ac.in

227

as a green (natural) corrosion inhibitor. The simple, low-cost, and minimum energy-intensive extraction process for producing PRBE makes it a more commercially feasible material. In those cases, the effectiveness can be enhanced by synergism. The synergistic effect of cation over the organic inhibitor can be demonstrated by the interaction between the cation and the halide present in the electrolyte solution [6].

In the current study, we have used PRBE as natural corrosion inhibitors in acidic media to observe their efficiency on boiler quality (BQ) steel. The synergy between the nickel ion (Ni^{2+}) on corrosion inhibition of PRBE was also explored in the same condition.

2   Materials and Methodology

2.1   Steel Coupon Preparation

A BQ steel (ASTM A-537, Grade B) was cut to make a work piece (coupons). The coupons had 1 cm^2 of working area. After that, those coupons were grazed by sandpapers of grades 320, 600, 1000, 1200, and 1500 to get the mirror polish. The BQ steel composition is C: 0.24%; Cu: 0.38%; S: 0.025%; Si: 0.55%; P: 0.025%; Mn: 1.72%; and rest is Fe [7].

2.2   Inhibitor Preparation

The purple rice bran was macerated at 37.5 °C for 22.5 min in 43.74% (v/v) ethanol solution. After that, the filtrate was collected. Later, the freeze-drying process was employed to evaporate the solvent from the filtrate. The remaining crude extract was collected, stored, and used in all the experiments as an inhibitor [8].

2.3   Electrolyte Solution Preparation

1 M HCl solution was prepared to make thy acidic solution for the tests. 100 ppm of Ni^{2+} was used to observe the synergistic effect and was used with PRBE at the same condition of 1 M HCl.

2.4   Electrochemical Studies

The inhibition efficiency PRBE as natural corrosion inhibitors was tested using various electrochemical studies. Those studies were conducted in different conditions, like in the presence and absence of nickel ions, to observe the synergy of nickel ions.

Firstly, the average OCP was recorded for 60 min to attain the equilibrium. Then, potentiodynamic polarization (PDP) scan was achieved from -250 mV to $+250$ mV versus Ag/AgCl with respect to OCP. To perform the PDP tests, 1 mV/s scan rate was maintained. The charge transfer resistance (R_{ct}) was achieved by performing EIS tests. The tests were conducted at respective OCP maintaining a frequency range from 0.01 to 10,000 Hz and peak amplitude of 10 mV [9].

3   Results and Discussion

To understand the reaction mechanism and the electrochemical kinetics of the corrosion reactions, the electrochemical experiments are the most suitable way. The behavior of the species on BQ surface can be inferred by these experiments.

3.1   Effect of PRBE and PRBE + Ni^{2+}

3.1.1   Potentiodynamic Polarization

The impact of PRBE and Ni^{2+} is shown in Fig. 1. The PDP or Tafel polarization curves (Fig. 1) show the effect of PRBE and PRBE + Ni^{2+} at 1 M HCl on BQ steel. Figure 1 shows that the both cathodic and anodic currents are reduced by when PRBE was incorporated in the media. This shifting to the lower side in both anodic and cathodic current infer that both anodic and cathodic reaction is interrupted due to the presence of organic complexes in PRBE.

Furthermore, the presence of 100 ppm Ni^{2+} with the PRBE also shifts the anodic and cathodic current toward the lower side compared to the presence of only PRBE. The electro-kinetic parameters like corrosion potential (E_{corr}), anodic (b_a) and cathodic slope (b_c), corrosion rate (C_r), corrosion current (i_{corr}), and overpotential (η), were computed using the Tafel extrapolation method. These parameters are related to each other, which can be expressed by Butler Volmer equation (Eq. 1).

$$i = i_{corr}\left(e^{2.303\frac{\eta}{b_a}} - e^{2.303\frac{\eta}{b_c}}\right) \tag{1}$$
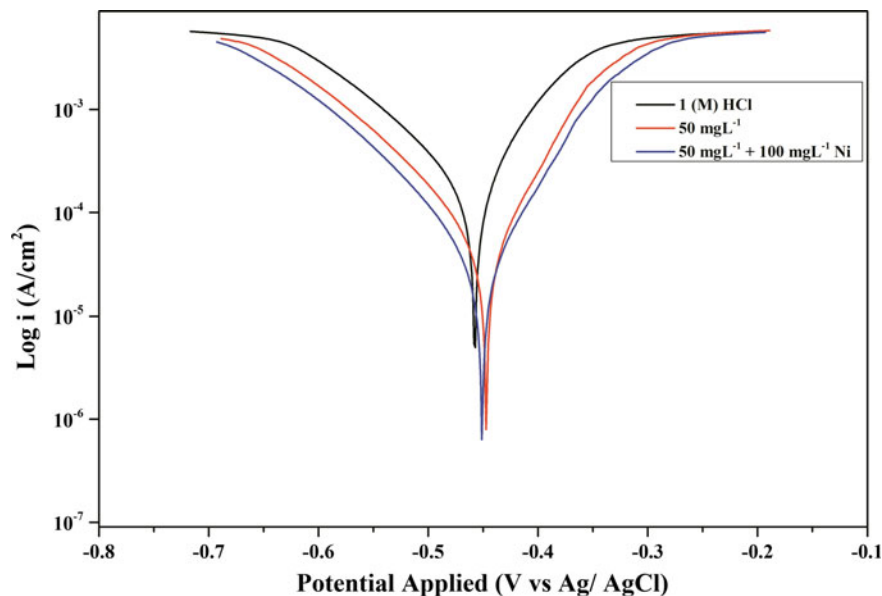
$$\eta = E - E_{corr} \tag{2}$$

Fig. 1 Tafel plots of BQ steel without and with addition of nickel ion with PRBE in 1 M HCl

The inhibition efficiency $(\mu_p\%)$ of OPE at different conditions was calculated using corrosion current density by the given equation

$$\mu_P\% = \frac{I^o_{corr} - I^i_{corr}}{I^o_{corr}} \times 100 \tag{3}$$

where and I^o_{corr} and I^i_{corr} are corrosion current density without and with applying the inhibitors.

The results are summarized in Table 1. The PRBE decreases the i_{corr}, and the presence of Ni cations decreases the i_{corr} furthermore. The results of the PDP tests indicate the mixed-type behavior of PRBE. The Ni cations enhanced efficiency of PRBE to reduce the corrosion on BQ steel [10–12].

3.1.2 Electrochemical Impedance Spectroscopy (EIS)

The EIS study is represented by a Nyquist plots (Fig. 2) and Bode plots (Fig. 3). The experiments were conducted under the same conditions as potentiodynamic polarization was done. The plots are semicircle, which satisfies the theory of EIS. The depressed semicircle is seen in the absence of PRBE in 1 M HCl on BQ steel and in other conditions also, which is determined by charge transfer resistance (R_{ct}). The depression in the semicircle is observed due to the heterogeneity of the surface. There are other parameters like solution resistance (R_s) and constant phase element (CPE)

Table 1 Parameters of Tafel polarization for BQ steel without and with addition of nickel ion with PRBE in 1 M HCl

Conc. (mg L^{-1})	b_a (mVdec^{-1})	$-b_c$ (mVdec^{-1})	E_{corr} (mV vs. AgCl)	i_{corr} (μAcm^{-2})	CR × 10^2 (mm year^{-1})	R_P (Ωcm^{-2})	(μ_P%)
0 (Blank) 1(M)HCl	110.98	66.84	−457.12	179.06	208.07	101.17	0.00
50	87.00	64.68	−443.97	47.92	55.68	336.23	73.24
50 + Ni (100)	80.43	65.69	−451.40	30.75	35.73	510.65	82.83

were found from the electrochemical circuit fit. The larger diameter of semicircles shows that the surface exhibits strong corrosion prevention. It is observed from the plots that the incorporation of PRBE in the 1 M HCl increases the diameter of a semicircle, hence controlling the corrosion. The diameter is increased more after the addition of 100 ppm Ni^{2+} with PRBE of the same concentration. The Bode plots indicate that the phase angle is not ideally 90° [7, 8]. Hence, the surface does not behave like an ideal capacitor. From Table 2, we can see that the R_{ct} value is increased after the addition of Ni^{2+}. This increase in the resistance is resultant of a protective layer of BQ steel surface. The polyphenolic compounds of PRBE help to form this protective film on the. The phenolic compounds become protonated in the HCl media and make a complex with Ni^{2+} and adsorbed on the steel surface [10, 12, 13].

A charge transfer resistance-based expression was also used to calculate the inhibition efficiency by the given expression

$$\mu_{R_{ct}}\% = \frac{R_{ct}^i - R_{ct}^0}{R_{ct}^i} \times 100 \tag{4}$$

where R_{ct}^0 and R_{ct}^i represent charge transfer resistance without and with applying inhibitor.
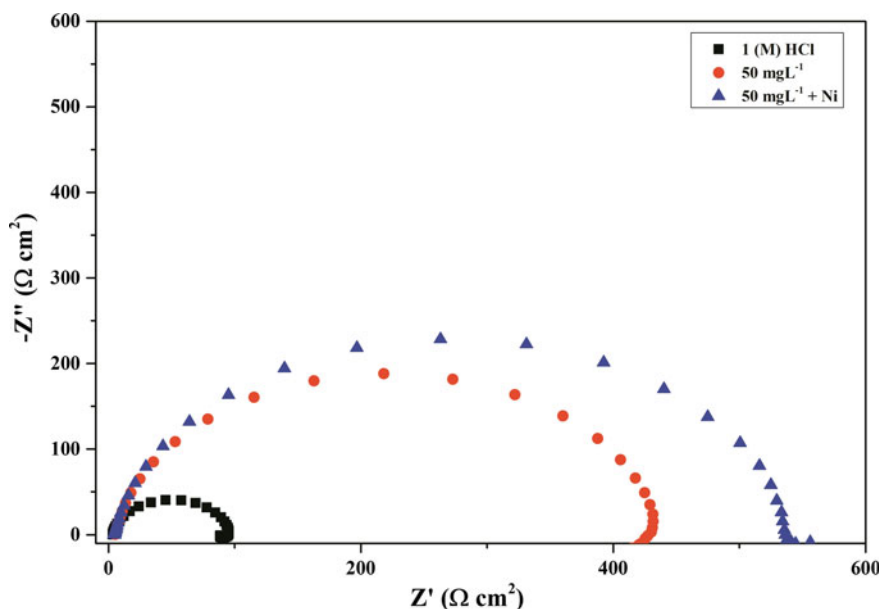

Fig. 2 Nyquist plots of BQ steel without and with addition of nickel ion along with PRBE in 1 M HCl
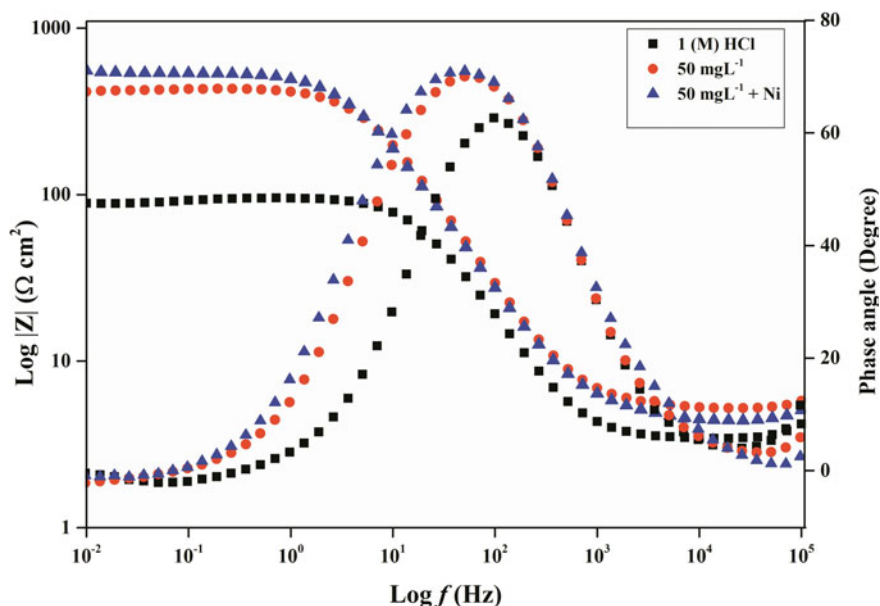
Fig. 3 Nyquist plots of BQ steel without and with the addition of nickel ion and PRBE in 1 M HCl

Table 2 EIS parameters of BQ steel without and with the addition of nickel ion and PRBE in 1 M HCl

Conc. (mg L^{-1})	R_S (Ω cm^2)	R_{ct} (Ω cm^2)	CPE parameters		C_{dl} (μF cm^{-2})	$\mu_{R_{ct}}$ %
			n	Y_o (μMho cm^{-2})		
0 (Blank) 1 (M) HCl	3.49	89.72	0.93	137.01	97.3	0.00
50	5.3102	425.82	0.89	117.39	84.5	78.93
50 + Ni (100)	4.5531	538.58	0.91	98.41	72.2	83.34

3.1.3 Mechanism of Corrosion

The presence of Ni^{2+} enhances the alkalinity of the media. The nickel cation is easily reduced and hinders the cathodic reaction. Moreover, it reacts with Cl$^-$ present on the surface (Fig. 4). It competes with protonated phenolic compounds also to be reduced by electrons. Hence, the cathodic reaction to form the H$_2$ gas is obstructed. If the cathodic zone is blocked, then the anodic region will be less oxidized [6].
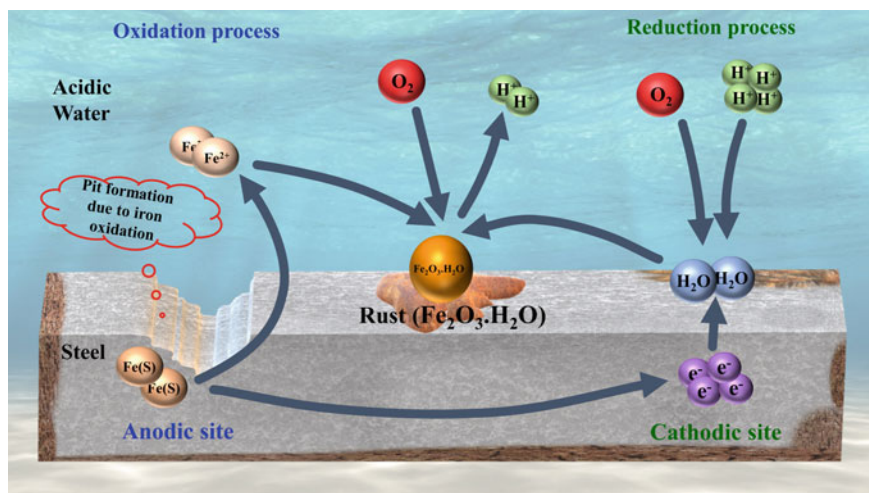
Fig. 4 Corrosion mechanism in acidic water

4 Conclusion

This current study has led to the following conclusions:

1. PRBE is an economical, eco-friendly, and mixed-type inhibitor to control corrosion in acidic media.
2. Adsorbed Ni cations improve the efficiency of PRBE in reducing the corrosion rate on BQ surface.

References

1. Ganash, A.A.: Theoretical and experimental studies of dried marjoram leaves extract as green inhibitor for corrosion protection of steel substrate in acidic solution. Chem. Eng. Commun. **205**, 350–362 (2018)
2. Parthipan, P., Elumalai, P., Narenkumar, J., Machuca, L.L., Murugan, K., Karthikeyan, O.P., Rajasekar, A.: Allium sativum (garlic extract) as a green corrosion inhibitor with biocidal properties for the control of MIC in carbon steel and stainless steel in oilfield environments. Int. Biodeterior. Biodegrad. **132**, 66–73 (2018)
3. Srivastava, V., Chauhan, D.S., Joshi, P.G., Maruthapandian, V., Sorour, A.A., Quraishi, M.A.: PEG-functionalized chitosan: a biological macromolecule as a novel corrosion inhibitor. ChemistrySelect **3**, 1990–1998 (2018)

4. Ali Asaad, M., Sarbini, N.N., Sulaiman, A., Ismail, M., Huseien, G.F., Abdul Majid, Z., Bothi Raja, P.: Improved corrosion resistance of mild steel against acid activation: impact of novel Elaeis guineensis and silver nanoparticles. J. Ind. Eng. Chem. **63**, 139–148 (2018)
5. Verma, C., Quraishi, M.A., Ebenso, E.E., Bahadur, I.: A green and sustainable approach for mild steel acidic corrosion inhibition using leaves extract: experimental and DFT studies. J. Bio- Tribo-Corrosion. **4** (2018)
6. Changmai, M., Das, P. P., Mondal, P., Pasawan, M., Sinha, A., Biswas, P., ... & Purkait, M. K.: Hybrid electrocoagulation–microfiltration technique for treatment of nanofiltration rejected steel industry effluent. Int. J. Environ. Anal. Chem. **102**, 62–83 (2022)
7. Pal, A., Das, C.: A novel use of solid waste extract from tea factory as corrosion inhibitor in acidic media on boiler quality steel (2020)
8. Pal, A., Das, C.: New eco-friendly anti-corrosion inhibitor of purple rice bran extract for boiler quality steel: experimental and theoretical investigations. J. Mol. Struct. **1251**, 131988 (2022)
9. M'hiri, N., Veys-Renaux, D., Rocca, E., Ioannou, I., Boudhrioua, N.M., Ghoul, M.: Corrosion inhibition of carbon steel in acidic medium by orange peel extract and its main antioxidant compounds. Corros. Sci. **102**, 55–62 (2016)
10. Thirion, G., Saxena, A., Hulhoven, X., Markine-Goriaynoff, D., Van Snick, J., Coutelier, J.P.: Modulation of the host microenvironment by a common non-oncolytic mouse virus leads to inhibition of plasmacytoma development through NK cell activation. J. Gen. Virol. **95**, 1504–1509 (2014)
11. Ji, G., Anjum, S., Sundaram, S., Prakash, R.: Musa paradisica peel extract as green corrosion inhibitor for mild steel in HCl solution. Corros. Sci. **90**, 107–117 (2015)
12. Mourya, P., Banerjee, S., Singh, M.M.: Corrosion inhibition of mild steel in acidic solution by Tagetes erecta (Marigold flower) extract as a green inhibitor. Corros. Sci. **85**, 352–363 (2014)
13. Das, P. P., & Purkait, M. K.: Treatment of cold rolling mill (CRM) effluent of steel industry. Sep. Purif. Technol. **274**, 119083 (2021)

Performance of Granular Bentonite Under the Influence of Chemical and Mechanical Loadings

Himanshu Yadav, Ajeet Sharma, and T. V. Bharat

1 Introduction

Solid waste disposal facilities are an important component of the integrated solid waste management system. Leachate generated from the MSW can migrate and contaminate the groundwater and surface water sources [7, 10–12, 16, 17]. Engineered landfills are the most economical and effective way of disposal of MSW. The landfill contains liners to prevent the flow of contaminants to the groundwater. The liner consists of bentonite compacted at a certain field density also known as compacted clay liner achieve low hydraulic conductivity ($< 10^{-9}$ m/sec). Diffusion is the dominant contaminant transport mechanism under such low advective flow [3, 9, 14, 18]. The compacted clay liners with 1–2 m thickness have been completely replaced by GCLs due to their ease in transportation, installation, and handling. The GCL generally consists of a granular form of bentonite but sometimes it also contains powdered bentonite [1]. The granular bentonite particles swell and fill the larger voids present in the compacted sample upon hydration. The sealing, hydraulic, sorption, and diffusion performance are the desirable qualities for any material to act as a barrier. Bentonite has all these properties which makes bentonite is a suitable liner material. Generally, most of the GCLs contain sodium dominant bentonites [9, 15].

Leachate contains a high amount of inorganic salt solutions (i.e. Na^+, K^+, and Ca^{2+}) [5]. The presence of salt solution or cations influences the diffused double layer thickness, which further influences the hydraulic conductivity of bentonite. The liner system experiences overburden stresses due to the weight of the waste in the

H. Yadav (✉) · A. Sharma · T. V. Bharat
Department of Civil Engineering, Indian Institute of Technology Guwahati, Guwahati, India
e-mail: yadav18b@iitg.ac.in

A. Sharma
e-mail: ajeetsharma@iitg.ac.in

T. V. Bharat
e-mail: tvb@iitg.ac.in

landfill [9, 13, 20]. However, the many studies have not incorporate the loading from the weight of the landfill waste. Behaviour of GCL for hydraulic and mechanical stability is important under mechanical and chemical loading environments. The present study evaluates the influence of salt concentration on hydraulic and volume change performance under chemo-mechanical loading conditions. To evaluate the influence of cation type (i.e. Na^+, K^+, and Ca^{2+}) on the hydraulic and normalized thickness of compacted GB, three salts with different cations were used in the study.

In this study, the GB exhumed from commercially available GCL was used. The hydraulic and volume change performance was evaluated under 50 kPa mechanical load with DW, 0.1 M, and 0.5 M concentration of KCl, NaCl, and $CaCl_2$ salt environment. The hydraulic performance of GB was not found to be satisfactory under a high concentration of salt solutions.

2   Materials and Methodology

2.1   Granular Bentonite

The granular bentonite (GB) used in the study was taken out from GCL. The basic geotechnical properties of GB were performed by standard procedure and are shown in Table 1 from earlier works of author [19]. Atterberg's limit was performed after maturation of GB slurry for eight days in a closed environment at saturated vapour pressure to ensure proper distribution of moisture [2]. The MB sorption was performed for specific surface area for GB at 4 pH [6].

The potassium, sodium, and calcium chlorides were used to make the required concentration of various salt solutions at 0.1 M and 0.5 M concentrations.

Table 1 Basic geotechnical characteristics of GB

Properties	Values
Specific gravity (G_s)	2.78
Liquid limit (w_{LL})	658
Plastic limit (w_{PL})	48
Specific surface area, S_{sa}, (m^2/g)	648
Cation exchange capacity, CEC (meq/100 g)	152.67
Na^+	86.1
K^+	0.87
Ca^{2+}	42.2
Mg^{2+}	23.5

2.2 Methodology

The hydro-mechanical behaviour of GB was studied using a modified odometer setup (Figure 1). The hydraulic infiltration and volume change were evaluated for GB under the influence of loading conditions with salt solutions. The consolidation cells were fabricated using a Perspex rod with 53 mm internal diameter. The bentonite was compacted for 10 mm thickness at a compacted density of 1.2 Mg/m^3. A filter paper was placed in between the GB sample and porous stone to prevent the clogging of the pores of the porous stone on either end. The compacted GB sample was placed on loading assembly, a burette with desired pore fluid was connected, and movement of fluid was maintained towards upward direction. A mechanical load of 50 kPa was applied to simulate the landfill weight. The burette with the pore fluid was opened to allow the permeation of pore fluid. The test was continued until the hydraulic infiltration rates and volume change readings were found to be constant for 24 h. The hydraulic conductivity lower than 1×10^{-9} m/sec represents the complete sealing of larger voids of GB.
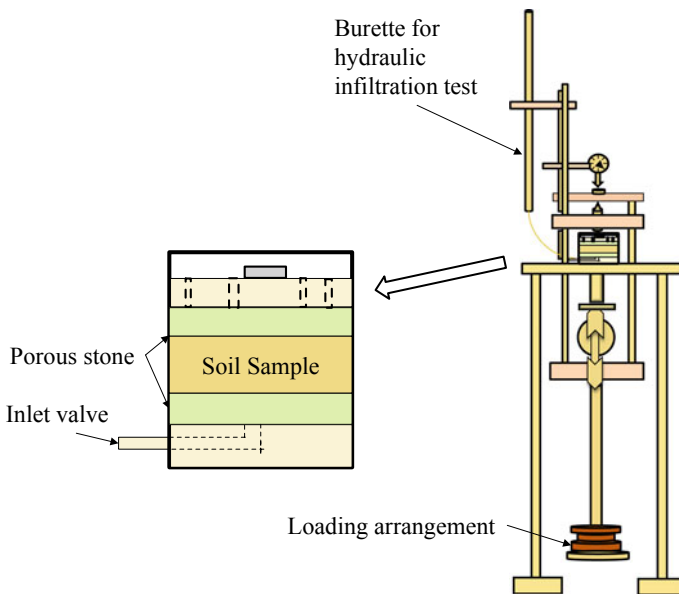

Fig. 1 Experimental set up for hydro-mechanical behaviour of GB

3   Results and Discussion

The temporal variations of hydraulic infiltration rates were plotted and shown in Fig. 2. The effect of NaCl on hydraulic infiltration rates was plotted in Fig. 2a. The final hydraulic infiltration rates increase with the concentration of NaCl. The sealing time (ST) also increases with the concentration of NaCl. The 0.5 M concentration of NaCl does not achieve sealing. Temporal variations of hydraulic infiltration with different concentrations of KCl were plotted in Fig. 2b. Both the concentrations of 0.1 M and 0.5 M KCl do not achieve the sealing. Hydraulic conductivity rates increase with the concentration of KCl. The temporal variations of hydraulic infiltration rates were plotted with different concentrations of $CaCl_2$ as shown in Fig. 2c. The hydraulic infiltration rates increase with the increase in the concentration of $CaCl_2$. Sealing time also increases with the concentration of $CaCl_2$ salt solution. At a high concentration of $CaCl_2$, the GB was not able to seal.

Temporal variations of normalized thickness (h/h_0) for 50 kPa mechanical load with 0.1 and 0.5 M concentrations of different pore fluids were presented in Fig. 3. The temporal variations of normalized thickness with different concentrations of NaCl and its comparison with distilled water are plotted in Fig. 3a. The compacted GB sample showed an initial collapse of 1–3% from distilled water to 0.5 M NaCl at 15 s after the start of the test. The magnitude of initial collapse increases with the concentration of NaCl. Equilibrium normalized thickness of GB decreases with the concentration of NaCl.

The temporal variations of normalized thickness with different concentrations of KCl under 50 kPa mechanical loading were plotted in Fig. 3b. The amount of initial collapse was found to be highest (i.e. 9%) in the case of 0.5 M KCl after 15 s of starting the experiment. The equilibrium normalized thickness decreases with the concentration of KCl.

The temporal variations of normalized thickness with different concentrations of $CaCl_2$ were plotted in Fig. 3c. A slight initial collapse of 2–4% was observed with $CaCl_2$ salt solutions. The equilibrium normalized thickness also decreases with the concentration of $CaCl_2$.

Specific surface area, gradation, plasticity, and cation exchange capacity of bentonites are the governing parameters for surface forces as well as the hydraulic performance of bentonites under chemo-mechanical loadings. Permeation of distilled water through GB leads to the generation of osmotic pressure among hydrated clay particles. The repulsive osmotic pressure leads to the disintegration of granules of GB into individual particles. Hydrated clay particles restrict the voids present in the compacted sample which leads to the hydraulic conductivity lesser than 10^{-9} m/sec. With a higher concentration of salt solution, the thickness of diffused double layer decreases, and the granules of GB were not able to break into individual particles. With a higher concentration of each salt, the granules lose their capacity to break into individual particles. Due to this, its hydraulic conductivity increases several folds. The application of mechanical loads supports the disintegration of granules

Fig. 2 Temporal variations of hydro-mechanical behaviour of GB under 50 kPa mechanical loading with different concentrations of **a** NaCl; **b** KCl; and **c** CaCl$_2$ salt environment

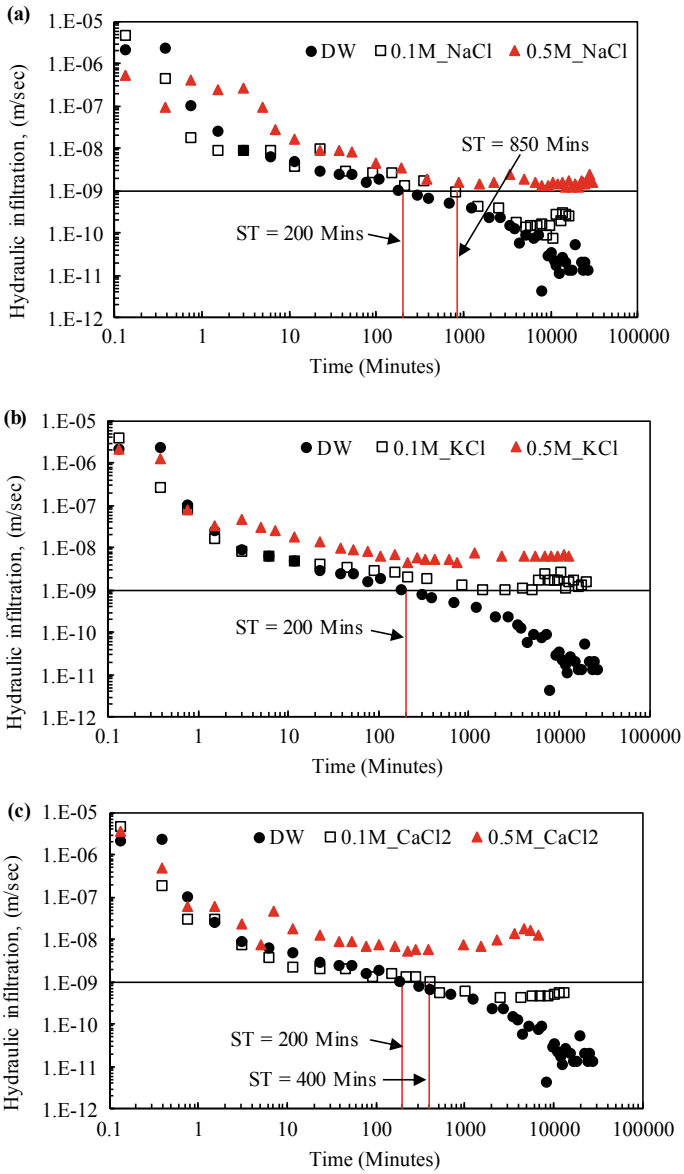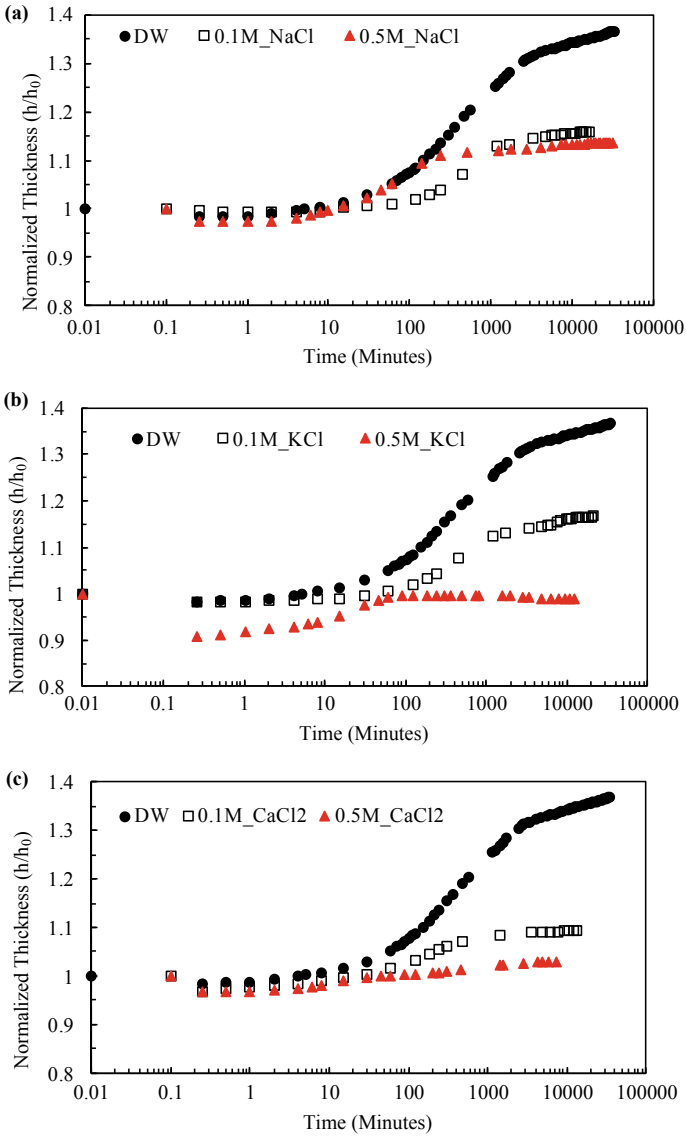**Fig. 3** Temporal variations of normalized thickness of GB under 50 kPa mechanical loading with different concentrations of **a** NaCl; **b** KCl; and **c** CaCl$_2$ salt environment

into individual particles. The decrease in equilibrium normalized thickness with the concentration of pore fluids is due to the decrease in DDL thickness.

4 Conclusions

The following points were concluded from chemo-mechanical study of GB:

- The GB swells and seals the macro-voids present in it upon hydration with distilled water or with low concentration pore fluid. A significantly high normalized thickness shows high swelling of GB in distilled water and low concentration pore fluids.
- The granules of GB do not break into individual particles upon hydration with a high concentration of salt solutions. The normalized thicknesses also reduce with high ionic salt solutions, which represents lower swelling or collapse of GB under high concentration pore fluid.
- Hydraulic performance of GB under a high concentration of studied salts (i.e. Na^+, K^+, and Ca^{2+}) was not found to be satisfactory. GB-based GCLs must not be used in landfills containing harsh leachates.
- The application of such GCLs containing granular bentonite in the field is questionable. GB-based GCLs do not perform well in tested conditions in terms of hydraulic performance.

References

1. Acikel, A.S., Gates, W.P., Singh, R.M., Bouazza, A., Rowe, R.K.: Insufficient initial hydration of GCLs from some subgrades: factors and causes. Geotext. Geomembr. **46**, 770–781 (2018)
2. Bharat, T.V., Yadav, H., Mahaur, J.P., Kushwaha, S.: Effect of aging time on consistency limits of bentonites. Geotech. Geol. Eng. **38**, 3737–3749 (2020). https://doi.org/10.1007/s10706-020-01251-3
3. Bouazza, A., Van, I.WF.: Liner design for waste disposal sites. Environ. Geol. **35**(1), 41–5 (1998)
4. Chapman, H.D.: Cation-exchange capacity. In: Black, C.A. (ed.) Methods of Soil Analysis—chemical and microbiological properties. Agronomy, vol. 9, pp. 891–901 (1965)
5. Christensen, T.H., Kjeldsen, P.: Basic biochemical processes in landfills. In: Sanitary Landfilling: Process, Technology, and Environmental Impact, pp. 29–49. Academic Press, New York (1989)
6. Das, D.S., Tadikonda, B.V.: Specific surface area of plastic clays from equilibrium sediment volume under salt environment. Geotech. Test. J. (2021). https://doi.org/10.1520/GTJ20200190
7. Fatta, D., Papadopoulos, A., Loizidou, M.: A study on the landfill leachate and its impact on groundwater quality of the greater area. Environ. Geochem. Health **21**, 175–190 (1999)
8. IS 2720-3.: Methods of Test for Soils, Part 3: Determination of Specific Gravity. Bureau of Indian Standards, New Delhi (1980)
9. Lee, J.M., Shackelford, C.D.: Impact of bentonite quality on hydraulic conductivity of geosynthetic clay liners. J. Geotech. Geoenviron. Eng. ASCE **131**(1), 64–77 (2005)
10. Maiti, S.K., De, S., Hazra, T., Debsarkar, A., Dutta, A.: Characterization of Leachate and its impact on surface and groundwater quality of a closed dumpsite—a case study at Dhapa, Kolkata, India. Procedia Environ. Sci. **35**, 391–399 (2016)
11. Papadopoulou, M.P., Karatzas, G.P., Bougiokou, G.G.: Numerical modelling of the environmental impact of landfill leachate leakage on groundwater quality—a field application. Environ. Model Assess. **12**, 43–54 (2007). https://doi.org/10.1007/s10666-006-9050-x

12. Pastor, J., Hernandez, A.J.: Heavy metals, salts and organic residues in old solid urban waste landfills and surface waters in their discharge area: determinants for restoring their impact. J. Environ. Manage. **95**, S42–S49 (2012). https://doi.org/10.1016/j.jenvman.2011.06.048
13. Setz, M.C., Tian, K., Benson, C.H., Bradshaw, S.L.: Effect of ammonium on the hydraulic conductivity of geosynthetic clay liners. Geotext. Geomembr. **45**(6), 655–673 (2017)
14. Jana, S., Purkait, M. K., & Mohanty, K.: Clay supported polyvinyl acetate coated composite membrane by modified dip coating method: Application for the purification of lysozyme from chicken egg white. J. Membr. Sci. **382**, 243–251 (2011)
15. Shackelford, C.D., Benson, C.H., Katsumi, T., Edil, T.B., Lin, L.: Evaluation the hydraulic conductivity of GCLs permeated with non-standard liquids. Geotext. Geomembr. **18**, 133–161 (2000)
16. Yadav, H., Kumar, P., Singh, V.P.: Hazards from the municipal solid waste dumpsites: a review. In: International Conference on Sustainable Waste Management through Design, pp. 336–342. Springer, Cham (2018)
17. Yadav, H., Singh, V.P.: Risk assessment due to municipal solid waste dumpsites and geo-environmental measures for closure. Int. J. Environ. Waste Manage. **26**(2), 190–211 (2020)
18. Yadav, H., Bharat, T.V.: Bentonite based barriers for protecting offshore monuments from salt-water intrusion. In: Proceedings of 3rd International Symposium on Geotechnical Engineering for Protection of Monuments and Historic Sites at Napoli, Italy (2022a)
19. Yadav, H., Bharat, T.V.: The influence of mechanical granulation process and granular bentonite plasticity on self-sealing and volume change behavior. J. Hazardous, Toxic, Radioactive Waste **26**(2), 04022003 (2022b)
20. Yadav, H., Bharat, T.V.: Sealing and volume change behaviour of polymer-amended granular bentonite under extreme chemical loading. Geo-Congress 2022. Geotechnical Special Publication, GSP—335. ASCE, pp. 199–208 (2022c). https://doi.org/10.1061/9780784484050.021

Flow Hydrodynamics Influences Due to Flood Plain Sand Mining in a Meandering Channel

O. P. Maurya, K. K. Nandi, S. Modalavalasa, and S. Dutta

1   Introduction

River hydrodynamics study is important to sustainable development for river health. River health is damaged due to a lot of human interventions like sand mining, damming, pollution [1], and so on. River irregularities like bend formation, mining activities, instream vegetation, hydraulic structures, and sediment transport are the main cause of energy loss [2–5] in the river system. Sand mining is necessary for river management, but it should follow the proposed guidelines [6, 7] in terms of the location of sand mining, size, and shape sand mining. Many researchers have proposed guidelines about sand mining activity through experimental, numerical, and field-based studies [8, 9], most of the proposed sand mining guidelines use experimental instream sand mining, but sand mining activity is also going on a floodplain. During the monsoon, season sediment gets deposited on a floodplain, and extraction of newly deposited sand is necessary because of the sustainability of the river, so the calculation of annual sediment deposition is required. When people do not follow the guidelines, this makes the river unhealthy in terms of river migration, river width increase, etc., and as a result, may chance to damage the agriculture field [10, 11]. A sudden change in the river's width can result in a drop in the specific energy of flow, which can have a number of adverse consequences in the downstream region, including effects on vegetation, agriculture, social economy, and water table [12, 13]. Sand mining affects the hydrodynamics of river systems like secondary current,

O. P. Maurya (✉) · K. K. Nandi · S. Modalavalasa · S. Dutta
Department of Civil Engineering, Indian Institute of Technology Guwahati, Guwahati, Assam, India
e-mail: om1996@iitg.ac.in

K. K. Nandi
e-mail: ketan18@iitg.ac.in

S. Dutta
e-mail: subashisa@iitg.ac.in

streamwise velocity, turbulence kinetic energy, and so on [14–16]. In this study, a rectangular sand mining pit is considered on the flood plain of sand mining and investigate the effect of sand mining on the hydrodynamics of the main channel, using a numerical software Flow-3D.

2 Material and Method

In this study, there are two software are used:

(1) CAD modeling Solidworks,
(2) Flow-3D hydro.

Channel setup is built in Solidworks software, and simulation is done in Flow-3D hydro software. It solves fluid equations of motion using highly advanced numerical techniques (finite volume method). The benefits of numerical models are that they can save time and money while also allowing researchers to work at any scale and provide all the necessary information.

2.1 Governing Equations

There are two governing equations of flow: continuity and momentum conservation.

Continuity equation

$$\frac{\partial}{\partial x}(uA_x) + \frac{\partial}{\partial y}(vA_y) + \frac{\partial}{\partial z}(wA_z) = \frac{R_{SOR}}{\rho} \tag{1}$$

where ρ is the fluid density, A_x, A_y, and A_z are the fractional area that is open to flow in the x, y, and z-direction, respectively, (u, v, w) are the velocity components in the coordinate directions (x, y, z), R_{SOR} is a mass source.

Momentum Equations

The Navier–Stokes equation with additional terms for the fluid velocity components $(u, v,$ and $w)$ is used to calculate fluid motion in the three coordinate directions.

$$\frac{\partial u_i}{\partial t} + \frac{1}{V_F}\left(u_j A_j \frac{\partial u_i}{\partial x_j}\right) = -\frac{\partial P}{\partial x_i} + g_i + f_i \tag{2}$$

where V_F is the fractional volume that is open to flow, f_i is viscous acceleration, and g_i is body acceleration.

2.2 Numerical Setup

The CAD modeling of numerical setups is built using Solidworks software. All the geometric parameters are considered as per the IIT Guwahati Fluvial hydro-ecological laboratory with dimensions of 18 m long, 1 m wide, and 0.3 m deep. The following Table 1 and Fig. 1 show the channel configurations and details:

2.3 Physical and Turbulence Model

In this study, a non-mobile bed channel is considered with a roughness height of 0.0016 m, and its sidewalls are smooth with zero roughness. And a slope of 1 in 1000 is assumed for the channel. We assumed clean water at 20 °C was flowing into the channel. Based on the physical conditions of the numerical setups, there are two physical models required.

(1) Turbulence and viscosity model.
(2) Gravity model.

There are several turbulence models present in flow-3D. Here, we have used the RNG $k - \varepsilon$ model because it is almost compatible with the experiment [17]. The gravity model will evaluate the slope effect on fluid flow.

Table 1 Detail of geometrical parameters of numerical setup

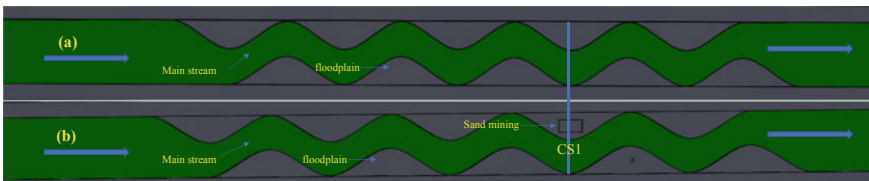| Channel dimension	18 m × 1 m × 0.3 m
Sinuosity index	1.25
Main channel width	0.53 m
Flood plain height	0.08 m
Sand mining size	0.4 m × 0.2 m × 0.06 m
Slope	1:1000

Fig. 1 CAD modeling sinuous channel setup, **a** sinuous channel and **b** sinuous channel with floodplain sand mining pit

Table 2 Initial conditions

Initial velocity (x, y, and z-direction)	0.11 m/s, 0.0
Fluid friction	0
Pressure	Hydrostatic
Flow depth (H)	0.14 m
Discharge	0.01536 m^3/s
TKE	0.0000605 J/Kg
Bed roughness	0.0016 m

2.4 Boundary and Initial Condition

Boundary conditions are depending on the physical condition of channel setups, for this study, all the boundary conditions are selected based on the laboratory condition of IIT Guwahati. There are five boundary conditions considered wall, no-slip, free-surface, volume flow rate, and outflow. Initial conditions are based on flume lab setup, which are tabulated in Table 2.

3 Result and Discussion

In this section, there are various flow characteristics are discussed at CS1, like streamwise velocity, secondary current, and turbulence kinetic energy (TKE). Figure 2 represents the contour plots of streamwise velocity, secondary current, and turbulent kinetic energy at CS1. Left-side plots are for the sinuous channel and right-side sinuous channel with sand mining pit. Figure 2a represents the comparison streamwise velocity, and the maximum zone of streamwise velocity shifted toward the outer bank and maximum magnitude of streamwise velocity decreases by 10% due to mining pit. Maximum zone of streamwise velocity concentrated in the mid of main channel and a shear layer separates the low velocity zone and high velocity zone [18, 19].

Figure 2b represents the secondary current comparison, secondary current domination at the outer bank increases as a result of the mining pit, and it also dominates in the mining pit [20] therefore, scour or erosion at the outer bank more, and river migrates laterally. Figure 3 represents the cross-sectional view of CS1 of both channel setups and also shows the domination of secondary current. Figure 4 represents a field photograph of river outer bank migration. Figure 2c represents the comparison of turbulent kinetic energy (TKE), which is domination in the mining pit and near the inner bank. The TKE indirectly represents the shear stress [21–24] of the flow. The further increase of TKE than the critical shear stress, the bed material and bank material will be in motion.
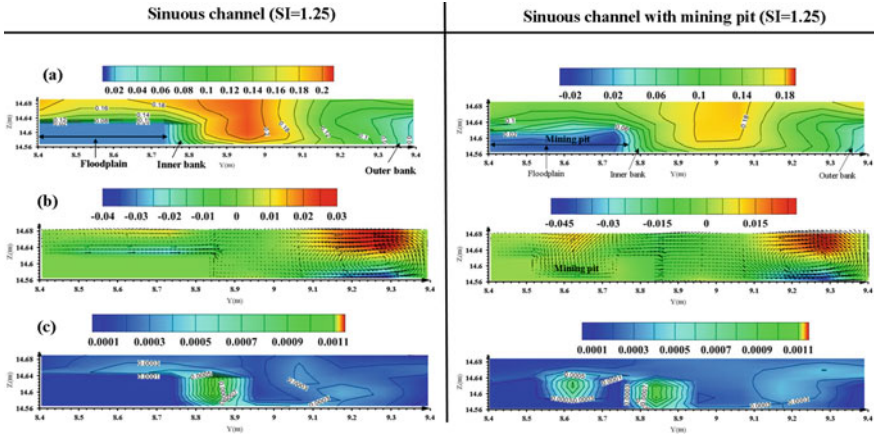
Fig. 2 Comparison of flow characteristics (at CS 1), **a** streamwise velocity, **b** secondary velocity, **c** turbulence kinetic energy
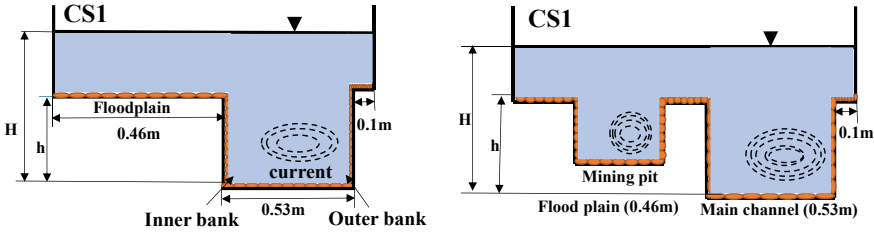

Fig. 3 Cross-sectional view of secondary current at CS1

Fig. 4 River outer bank migration due to outer bank secondary current

4   Conclusion

The findings of this study are as follows:

- Due to the mining pit, the maximum zone of streamwise velocity is shifted in the main channel, and the magnitude of maximum velocity decreases. Therefore, the shear layer zone shifts from the inner bank to the main channel, possibly promoting sedimentation, and aquatic life shifts. As the streamwise velocity decreases, stream power will decrease and may be a cause of sediment deposition near the inner bank, but at the outer bank, the secondary current is dominant; therefore, deposition is not possible.
- Secondary current is domination at the river's outer bank and may be the cause of scouring or erosion; the river's outer bank migrates, and the fertile or culturable field is lost. In the mining pit, the secondary current is also dominated. There may be a chance of increasing the width of the river at that location and a decrease in specific energy flow. In the lean period, the low volume of water flows in the downstream causes riparian vegetation wilting, water table effect, fish population effect, and also socio-economic effect.
- TKE is more dominant near the inner bank as well as in the mining pit. If it exceeds the critical limit, it may have an impact on the river armoring.

References

1. Best, J.: Anthropogenic stresses on the world's big rivers. Nat. Geosci. **12**(1), 7–21 (2019)
2. Bagnold, R.A.: Some Aspects of the Shape of River Meanders. US Government Printing Office (1960)
3. Kondolf, G.M.: Freshwater Gravel Mining and Dredging Issues: White Paper. Washington Department of Fish and Wildlife (2002)
4. Molnár, P., Ramírez, J.A.: Energy dissipation theories and optimal channel characteristics of river networks. Water Resour. Res. **34**(7), 1809–1818 (1998)
5. Padmalal, D., Maya, K.: Sand Mining: Environmental Impacts and Selected Case Studies. Springer (2014)
6. Hübler, M., Pothen, F.: Can smart policies solve the sand mining problem? PLoS ONE **16**(4), e0248882 (2021)
7. Khan, S., Sugie, A.: Sand mining and its social impacts on local society in rural Bangladesh: a case study of a village in Tangail district. J. Urban Reg. Stud. Contemp. India **2**(1), 1–11 (2015)
8. Daneshfaraz, R. et al.: The experimental study of the effects of river mining holes on the bridge piers. Iranian J. Soil Water Res. **50**(7), 1619–1633 (2019)
9. Hackney, C. R., Darby, S. E., Parsons, D. R., Leyland, J., Best, J. L., Aalto, R., ... & Houseago, R. C.: River bank instability from unsustainable sand mining in the lower Mekong River. Nat. Sustain. **3**(3), 217–225 (2020)
10. Callander, R.A.: River meandering. Annu. Rev. Fluid Mech. **10**(1), 129–158 (1978)
11. Koehnken, L., Rintoul, M.: Impacts of sand mining on ecosystem structure, process and biodiversity in rivers. World Wildlife Fund International (2018)
12. Gavriletea, M.D.: Environmental impacts of sand exploitation. Analysis of sand market. Sustainability **9**(7), 1118 (2017)

13. Koehnken, L., et al.: Impacts of riverine sand mining on freshwater ecosystems: a review of the scientific evidence and guidance for future research. River Res. Appl. **36**(3), 362–370 (2020)
14. Myers, W.R.C.: Momentum transfer in a compound channel. J. Hydraul. Res. **16**(2), 139–150 (1978)
15. Rajaratnam, N., Ahmadi, R.M.: Interaction between main channel and flood-plain flows. J. Hydraul. Div. **105**(5), 573–588 (1979)
16. Sellin, R.H.J.: A laboratory investigation into the interaction between the flow in the channel of a river and that over its flood plain. La Houille Blanche **7**, 793–802 (1964)
17. Karami, H., et al.: Verification of numerical study of scour around spur dikes using experimental data. Water Environ. J. **28**(1), 124–134 (2014)
18. Bathurst, J.C., et al.: Overbank sediment deposition patterns for straight and meandering flume channels. Earth Surf. Proc. Land. **27**(6), 659–665 (2002)
19. Xu, D., Bai, Y.: Experimental study on the bed topography evolution in alluvial meandering rivers with various sinuousnesses. J. Hydro-Environ. Res. **7**(2), 92–102 (2013)
20. Priego-Hernández, G.A., Rivera-Trejo, F.: Secondary currents: measurement and analysis. Atmósfera **29**(1), 23–34 (2016)
21. Alshamani, K.M.M.: Correlations among turbulent shear stress, turbulent kinetic energy, and axial turbulence intensity. AIAA J. **16**(8), 859–861 (1978)
22. Biron, P.M., et al.: Comparing different methods of bed shear stress estimates in simple and complex flow fields. Earth Surface Process. Landforms: J. British Geomorphol. Res. Group **29**(11), 1403–1415 (2004)
23. Clark, L.A., Theresa, M.W.: Boundary Shear Stress Along Vegetated Streambanks (2007)
24. Kim, S.-C., et al.: Estimating bottom stress in tidal boundary layer from acoustic Doppler velocimeter data. J. Hydraul. Eng. **126**(6), 399–406 (2000)

Microalgal Growth in Low-Cost Media for Biodiesel Production

Bikram Chakraborty ⓘ**, Velentina Das** ⓘ**, and Dhanapati Deka** ⓘ

1 Introduction

The growing world population increases the need for alternative fuels from renewable sources, but the conversion technologies are still in the developing phase. Therefore, the difference in fuel price is a major issue regarding the non-commercialization of alternative fuels in many countries. Despite that, biomass conversion fuels are grabbing a large market in many developed countries due to the huge availability of feedstocks. Also, these fuels are carbon neutral and thus reduce the emission of greenhouse gases (GHGs) which helps in decreasing the effect of global warming. The most commercialized biofuels are bioethanol, which is derived from corn or sugarcane and biodiesel, which is derived from edible feedstock like soybean, rapeseed oil, canola oil, etc., thus, it creates a large crisis in meeting the needs of the people for feeding purposes. Therefore, to solve this problem, waste biomass and non-edible or waste cooking oil are used to produce biofuels, which are termed the second-generation feedstock. But, it also affects the agricultural land and creates a major concern to moving to the third generation of feedstock, i.e., microalgae. Oil extraction from microalgae is more as compared to second-generation feedstock, and efficiency is also high. Microalgal biomass produces a high number of triglycerides (TGs), proteins, and carbohydrates, and through the bio-refinery approach, many chemical products related to bio-fertilizer and pharmaceutical products are developed.

Different organic nitrogen sources such as cow dung, cow or human urine, poultry waste, and agricultural waste can be used for the cultivation of algae, which enhances the growth and lipid accumulation. Among these, cow urine seems to be the most

B. Chakraborty (✉) · V. Das · D. Deka
Department of Energy, Tezpur University, Tezpur, Assam, India
e-mail: chakraborty.bikram92@gmail.com

D. Deka
e-mail: dhanapati@tezu.ernet.in

promising source as it contains nearly 17% nitrogen, which is the highest as compared to other feedstocks viz. human urine (8%), cow dung (0.7%), and poultry waste (1%) [1]. Substituting readily available commercialized chemical nutrients with organic natural nutrients helps in decreasing the price of the final product, i.e., biofuel. Urine contains not only a high amount of NPK but a trace number of elements such as Cu, Mo, B, Mn, Zn, etc., which are also present and help in high growth and lipid accumulation by algae [2, 3]. Cattle urine contains mainly 95% water, 2.5% of mineral salts, hormones, enzymes, and 69% of nitrogen, sulfur, and magnesium [4]. Cattle urine has a high amount of nitrogen ranging from 5.5 to 21.6 g/L where 69% are present in the form of urea [5]. Adamsson 2000 reported that microalgae *Scenedesmus acuminatus* show a biomass production of 0.16 g/L in 2% human urine. Sharma and Rai, 2015, also reported that microalgae *Chlorella pyrenoidosa* shows the highest biomass production of 1.93 g/L in 7.5% of cattle urine and the lowest of 0.6 g/L in 12.5% of cattle urine. On the other end, Suresh et al. 2019 show *Chlorella sp.* contains high biomass of 2.6 g/L in 10% of cattle urine and the lowest biomass content was observed in *Oscillatoria sp.,* (CWA) of 0.3 g/L in 1% cattle urine. Therefore, from the earlier research, it was clear that cattle urine acts as a great medium for culturing microalgae.

Biodiesel from microalgae is encouraging because of environmentally friendly and restricts the emission of GHGs. The majority of micro and macroalgae are highly oil-rich and can be transformed into biodiesel using a variety of modern technologies [6, 7]. Proper optimization in the mixing of alcohol and acid or base catalyst is the main in obtaining a higher yield of biodiesel from algal biomass [8–10]. Sometimes high or low reaction time also helps in the high yield of biodiesel depending on the use of algal species.

In this study, the application of low-cost media (cow urine) in different concentrations was analyzed for growing microalgae *Chlorella vulgaris*. Lipid content was investigated which was used further for biodiesel production. The characterization of produced biodiesel is done with NMR spectroscopy.

2 Materials and Methods

2.1 Collection and Physicochemical Analysis of Cow Urine

Eight liters of cow urine (from various breeds of the cow) were collected from a cow shelter in the Napaam region, Tezpur. Filtration of the collected urine was performed using Whatman filter paper to clean the unwanted substances like debris, precipitated material, etc., and was stored at 4 °C. The physicochemical properties of mixed cow urine were analyzed partly at the Sophisticated Analytical Instrumentation Centre (SAIC), Tezpur University, and partly at the North Eastern Regional Institute of Water and Land Management (NERIWALM), Tezpur.

2.2 Preliminary Method—Strain Selection and Optimization of Culture Media

Two algal strains *Scenedesmus obliquus* and *Chlorella vulgaris* were procured from the Department of Biotechnology, Guwahati University, India, and cultured at Biomass Conversion Laboratory, Department of Energy, Tezpur University, India. Two culture media was prepared by mixing BG11 with diluted and non-diluted urine in different concentrations, and growth was analyzed by UV–vis spectrometer at 750 nm for 6 days continuously. *Chlorella species* show the highest growth as compared to *Scenedesmus species* in non-diluted urine. So, further, experiment was carried out with *Chlorella species* in non-diluted urine media.

2.3 Media Preparation and Growth Condition

Ten different concentrations of cow urine (CU) ranging from 10, 20, 30, 40, 50, 60, 70, 80, 90, and 100 v/v % were prepared by mixing with autoclaved BG11 medium containing 300 ml of sample in 500 ml Erlenmeyer flasks for growing freshwater alga *Chlorella vulgaris*. BG11 medium consists of (g/L) $NaNO_3$, 1.5; Na_2CO_3, 0.02; K_2HPO_4, 0.04; $MgSO_4.7H_2O$, 0.075; citric acid, 0.006; ferric ammonium citrate, 0.006; Na_2EDTA, 0.001; $CaCl_2.2H_2O$, 0.036; and 1 mL of a microelement solution consisting of (g/L) H_3BO_3, 2.86; $Na_2MoO_4.2H_2O$, 0.39; $ZnSO_4.7H_2O$, 0.22; $CuSO_4.5H_2O$, 0.08; $Co (NO_3)_2.6H_2O$, 0.05; and $MnCl_2.4H_2O$, 1.81. Sterilization of media was done before inoculating with fresh cells by autoclaving at 121 °C for 15 min. The pH of the same was maintained at seven. The culture was incubated for 18 days under 24 h cool-white fluorescent tube light with constant feeding of 2% CO_2 at 25 °C (Fig. 1).

Fig. 1 Set up of ten different concentrations of cow urine in laboratory condition

Fig. 2 Growth of algae in concentrations 10, 20, 30% cow urine, and Bg11 after 14 days

2.4 Algal Biomass Estimation

The cell growth was analyzed minutely from lag phase to stationary phase during the cultivations by the optical density measurement at 750 nm (i.e., OD_{750}), using UV–vis spectrophotometer. OD was taken daily at a regular interval of 24 h (Fig. 2).

2.5 Harvesting of Algae

The microalgae *Chlorella vulgaris* was harvested from the culture medium using normal sedimentation followed by centrifugation. Initially, the grown-up cells after 18 days of culture were allowed to settle down by gravity. To determine the cell dry weight, 50 ml from the aliquots culture was separated for centrifugation at 5000 rpm for 5 min. The algal cells were concentrated at the bottom of the centrifuge tube as pellets and the liquid was separated in the upper layer as supernatant. The pellets were then rinsed twice with double distilled water to clean the salts that had become adhered to the cell surface. The cells were then moved to a pre-weighed tube and dried at 105 °C until the weight remained consistent. An analytical balance (Sartorius CPA225D, Germany) was used to find out the dry weight of the cell. Thus, the actual cell dry weight was computed by lessening the weight of the tube with microalgae and the empty tube. Therefore, the biomass productivity can be determined as follows:

$$\text{Biomass productivity(mg/L/day)} = (CDW_2 - CDW_1)/T_2 - T_1 \qquad (1)$$

where CDW_1 and CDW_2 represent cell dry weight (mg/L) at the beginning of the culture at times (T_1) and finish of the experiment at times (T_2), respectively.
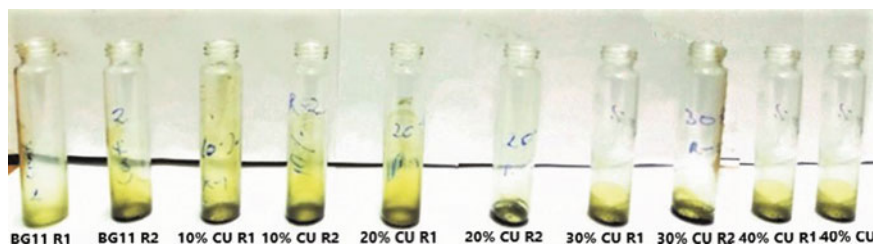
Fig. 3 Lipid content of different concentrations of urine

2.6 *Lipid Extraction*

To extract lipid from the algal biomass of four concentrations of 10, 20, 30, and 40% of urine, and BG11, the modified Bligh and Dyer method was implemented. Methanol and chloroform were mixed in a 2:1 ratio with algal biomass, and the lipid extracted was gravimetrically measured. The lipid content and productivity were determined by the below equations [11, 12] (Fig. 3).

$$\text{Lipid content}(\%) = \text{Total lipids(g)/Dry biomass(g)} \tag{2}$$

$$\text{Lipid productivity(mg/L/day)} = \text{Biomass productivity} \times \text{Lipid content}(\%)/100 \tag{3}$$

2.7 *Biodiesel Production*

Based on the lipid content and growth analysis, 30% cow urine media was selected for further growth of algae to produce biodiesel. Then, algae were grown in 20 L photobioreactor (PBR) for 18 days.

Photo bioreactor system

A polyethylene terephthalate transparent bottle of 20 L was used as a photobioreactor for the cultivation of algae. An inoculum size of 0.12 g L−1was used to inoculate the photobioreactor with fresh cells of microalgae. The photobioreactor was operated at a surrounding temperature of 25 °C and pH of seven. No additional outside carbon dioxide was introduced to the photobioreactor, and four white fluorescent tube lights (14 W) were used to give constant illumination on both sides of the device. An air pump was used to aerate and mix the media culture [13]. After attaining the stationary phase (after 18 days), the dry cell biomass and lipid content of the sample was evaluated with proper procedure (Fig. 4).
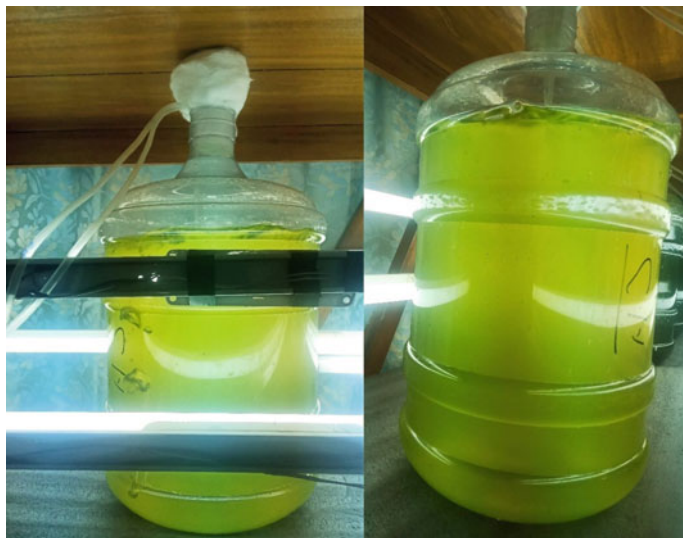
Fig. 4 Photobioreactor for 30% cow urine concentration inside the laboratory

Harvesting of algae

Microalgal cell harvesting was done after 18 days of culture by the flocculation method. Flocculating agent, ferric chloride ($FeCl_3$) was used to aggregate the cells of microalgae [14].

Lipid Extraction by Soxhlet Apparatus

For 20 L bottle PBR, the lipid was extracted by the Soxhlet extraction method. The extraction process was carried out at 60 °C using 450 ml of methanol and chloroform in the ratio of (2:1) as a solvent for 12 h. The oil extracted was weighed and marked as lipid content (%) w/w (Fig. 5).

Transesterification reaction

Transesterification reaction was carried out by mixing the total extracted lipid with methanol and sulfuric acid to produce fatty acid methyl ester (FAME). A 250 ml round-bottom flask containing lipid that was placed in a water bath with 0.6 ml of sulfuric acid and 4.4 ml of methanol in it was heated on the hot plate of a magnetic stirrer for three hours. Following completion of the reaction, the sample was cool down for 30 min at room temperature. Then, hexane and water were mixed in the ratio (2:1; v/v) for washing and separating of layer formation, respectively, and left undisturbed for 24 h. The upper layer containing FAME and hexane was collected by a gas-tight syringe to a glass vial and kept inside the oven for a few minutes to remove the solvent. Thus, the FAMEs were collected and analyzed with a [+]HNMR and ^{13}CNMR spectrometer (Oxford, AS400, China) for confirming the formation of biodiesel. Determine the conversion efficiency of the biodiesel formed, [+]HNMR is

Fig. 5 Lipid extraction by
Soxhlet apparatus

taken into consideration by analyzing the peaks of methoxy protons of the methyl ester at 3.6 ppm and α-methylene protons at 2.3 ppm. Therefore, the conversion efficiency can be calculated by the following equation [15, 16].

$$C(\%) = \frac{2 \times A}{3 \times B} \times 100 \tag{4}$$

where

C = conversion percentage of triglycerides to methyl esters.
A = integration value of methoxy methyl ester peak at 3.6 ppm.
B = integration value of α-methylene at 2.3 ppm of $^{+}$HNMR spectra.

3 Results and Discussions

3.1 *Physicochemical Characterization of Cow Urine*

The physicochemical characteristics of cow urine were analyzed to determine the micro and macronutrient present in it which helps in the growth of microalgae. Table 1 depicts a few parameters of cow urine, which contains a total dissolved solid of 16.26 g/l with an electrical conductivity of 29.93 mS/cm, which indicates a large amount of dissolved mineral present in it. The pH of urine was found to be 7.2. Dissolve oxygen and salinity were found at 2.46 ppm and 16.43 g/L, respectively. Urine contains 1.9 g/L of Na followed by Ca and Mg as 0.5 g/L and 0.024 g/L, respectively. Mo (3.27 mg/L), Al (2.11 mg/L), and Fe (1.59 mg/L) were also observed in urine. Few traces number of elements were also found in urine like Zn (0.091 mg/L), Mn (0.08 mg/L), and Cu (0.01). The importance of NPK in the growth of microalgae is noticeable. A high value of total nitrogen (5.9 g/L), potassium (6.24 g/L), and phosphorous (0.1 g/L) were noticed which is near about similar to the data recorded in New Zealand [17]. Thus, the high value of NPK and other nutrients in urine supports the growth of microalgae.

Table 1 Physicochemical characterization of cow urine

pH	7.2
Electrical conductivity	29.93 mS/cm
DO	2.46 ppm
TDS	16,260 mg/L
Turbidity	43.33 mg/L
Salinity	16,430 mg/L
TN	5900 mg/L
P	111.4 mg/L
K	6240 mg/L
Na	1960 mg/L
Ca	526 mg/L
Mg	24 mg/L
Mo	3.27 mg/L
Al	2.11 mg/L
Fe	1.59 mg/L
Zn	0.091 mg/L
Mn	0.08 mg/L
Cu	0.01 mg/L

3.2 Effect of Cow Urine (CU) Media on Growth and Biomass Productivity of Chlorella Vulgaris

The availability of nutrients in the media is critical to the growth of microalgae. So, to provide the requisite nutrients from outside, the cost of final products increases. Thus, cow urine acts as the sole nutrient source for the growth of algae, which in turn reduces the use of commercially available nutrients [18]. Therefore, in this study, cow urine was considered a nutrient for maturing selected microalgae and expected to increase the biomass and lipid content simultaneously. In this experiment, ten different concentrations (from 10 to 100%) of cow urine with BG11 were prepared for analyzing the growth of microalgae *Chlorella vulgaris* for 18 days. The growth curve of *Chlorella vulgaris* was plotted for BG11 as control and different concentration of urine was shown in Fig. 6. The curve shows a longer lag phase for BG11 as compared to concentration of urine below 30%. OD_{750} ranges from 0.135 to 0.988 for BG11 media. Whereas, it ranges from 0.128 to 1.573 (in 10% cow urine) which seems to be the highest value among other concentrations of cow urine. For 20% of cow urine, it ranges from 0.134 to 1.391, and for 30% of cow urine, it was 0.115 to 1.255. From the curve, it was observed that the growth of algae is more prominent in cow urine supplemented media below 30% than in the BG11 media. This was due to the presents of more nutrients in cow urine as compared to artificially prepared BG11 media. 5.9 g/L of nitrogen and 6.6 g/L of potassium were present in cow urine, which was way higher than the amount of nitrogen (1.5 g/L) and potassium (0.04 g/L) present in BG11 media. Also, the 30% curve shows an uneven growth with a long exponential phase because of raise in the concentration of cow urine. It can be observed that there was a gradual fall in OD_{750} value with the rise in the concentration of cow urine. Thus, it can be inferred that the growth or biomass content also decreases from 10 to 40%. So, 40% of cow urine shows an OD_{750} value ranging from 0.105 to 0.529, which was less than the value noted down for BG11. Similarly, for 50% cow urine, the OD_{750} value ranges from 0.103 to 0.379 up to ten days of culture, then the growth was slower and decreasing. A similar trend was noticed from 60% cow urine to 100% cow urine where the OD_{750} value increases speedily for the first 5 days due to the introduction to a new environment. This rapid initial increase in the growth of algae is due to the absorbance of ammonia, which converts it into organic molecules [19]. After exhaustion of the nutrients, a gradual decrease in values was noted. This was the reason that growth inhibition occurred because of the high concentration of ammonia presents in urine as depicted earlier by another researcher [20, 21]. After a certain amount of nitrogen intake, the cell loses the capacity to take more nitrogen for its growth, thus leading to the death of cells. Also, other external factors or selected algal strain itself might be the reason for decreasing growth with increasing concentration of cow urine. From Fig. 9(b), it was seen that the color of samples above 50% turned brownies, which reflects the death of cells. Therefore, concentrations above 50% were discarded and not taken forward for further study.
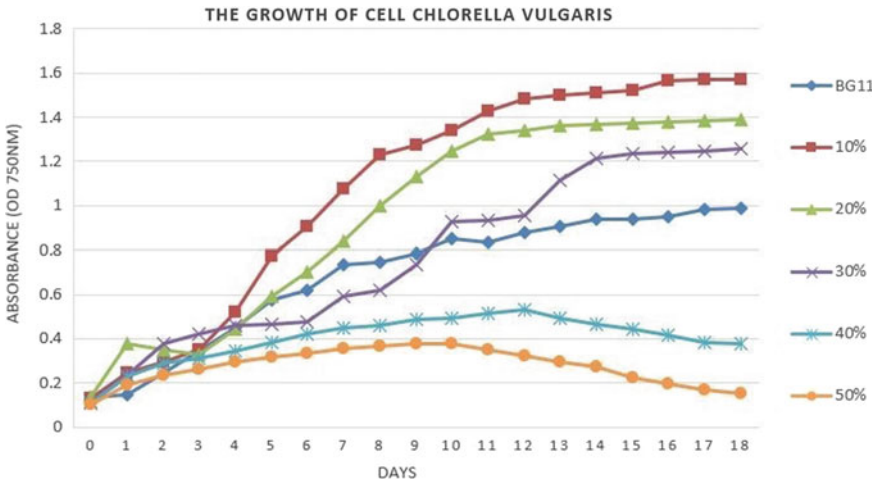
Fig. 6 Growth curve of *Chlorella vulgaris* in cow urine and BG11

From Fig. 7a, the microscopic image of *Chlorella vulgaris* in 10% CU shows cleavage of cells which indicates reaching to exponential phase on the third day of culture and Fig. 7b depicts the fully grown-up cells with the formation of the colony on last day of culture. It shows 10% concentration of CU gives good growth and biomass at the end of 18 days of culture.

From Fig. 8, it was found that growth curve results run following the values of biomass productivity i.e., 10% cow urine shows the highest biomass productivity of 90.21 mg/L/day followed by 20% cow urine containing 63.42 mg/L/day of biomass. 30% and 40% of cow urine show a value of 44.14 mg/L/day and 18.42 mg/L/day, respectively, which was much less than the value of 10% of cow urine. Whereas,

Fig. 7 Microscopic image of Chlorella vulgaris in 10% cow urine (40 × resolution), **a** seen on the third day of culture, **b** seen on the 18th day of culture

BG11 recorded 34.78 mg/L/day of biomass productivity which was less than the values of different concentrations of urine. Thus, it proves that cow urine supports the growth of microalgae even better than the growth in artificial media. Algal cells 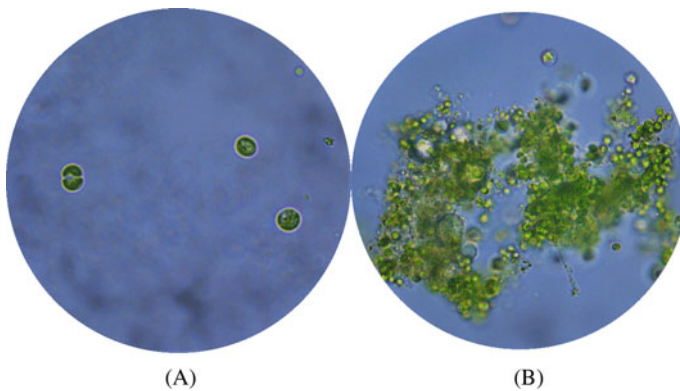when grown in nitrogen stress possess' starch and increase the lipid content. But, in a nitrogen-rich environment, microalgae utilize the nutrients to enhance biomass growth and side-by-side increase the protein and carbohydrate content [22, 23]. Jaatinen, 2015, worked with *Chlorella vulgaris* in diluted human urine and found biomass productivity of 0.73 g VSS/L [24]. Adamsson, 2000, and Lun and Cheng, 2006, investigated 2% and 0.6% human urine, respectively, and found that above that concentration microalgae were unable to grow which is opposite to the result obtained in this study. Similar results were shown by Sharma and Rai, 2015, where concentration above 7.5% leads to reducing the growth of microalgae [25, 26]. In this study, concentration below 10% cow urine was not tried but a 10% concentration of cow urine shows a significantly high growth as compared to 20% and 30% cow urine. So, these results were contradictory to the previous studies conducted on the same media. The difference in results might be because of use of different algal strains (*Chlorella vulgaris*) and other environmental factors like temperature, light intensity, etc., influenced the growth in a higher concentration of urine. In this study, it was found that 10% of cow urine has more growth, which is following the previous work done with the same media [27]. But, the new finding was that 20%, 30%, and 40% of cow urine media were capable of growing algae and converting it to lipid for further utilization (Fig. 9).
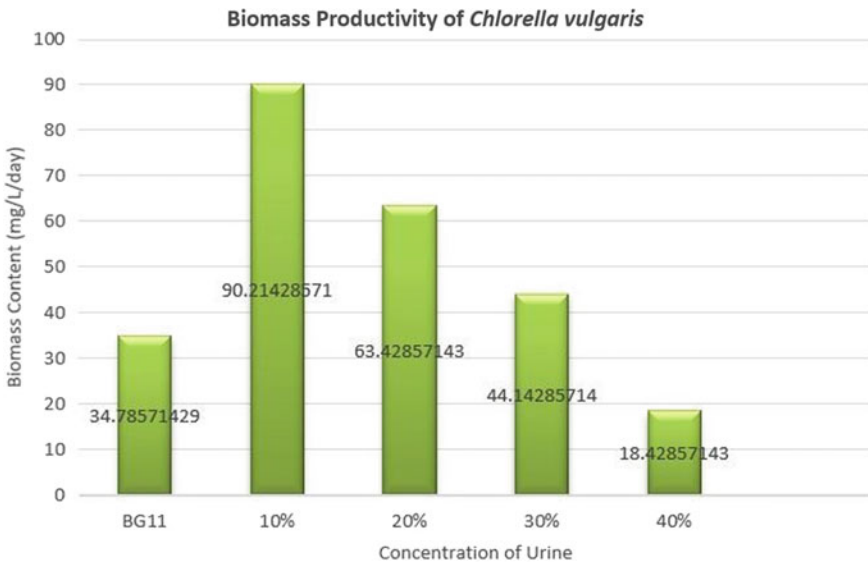
Fig. 8 Biomass productivity of *Chlorella vulgaris* in different concentrations of cow urine
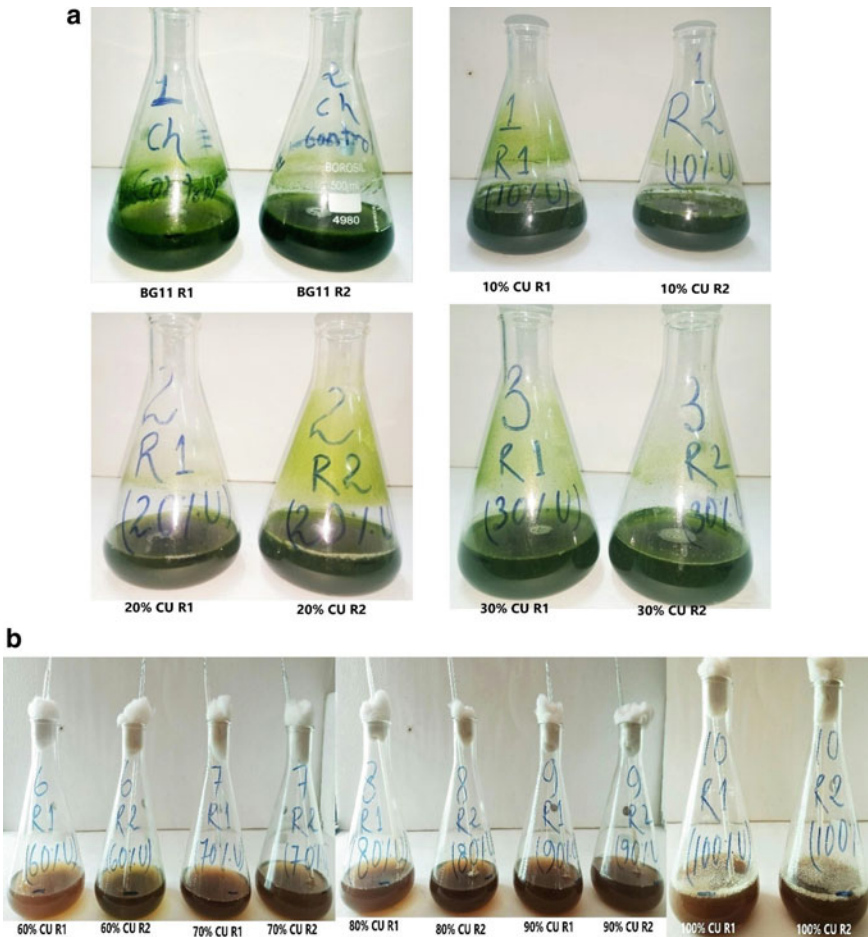
Fig. 9 a Growth of algae after 18 days, b cells died in a concentration above 50%

3.3 Lipid Production

The trend of lipid content in numerous concentrations of cow urine was opposite to the biomass content of the same concentration. The maximum lipid content was found in 30% of cow urine at 25.23%, whereas the biomass content was very low in 30% of cow urine. The lipid content of 10% of cow urine was 18.13% followed by 20% of cow urine containing 20.9% of lipid. A gradual increase in lipid content was noticed from 10 to 30% of cow urine, and then a drastic drop in value was observed in 40% of cow urine containing 12.4% of lipid. Whereas BG11 shows a quite high lipid content of 23.26% which was higher than all the concentrations of cow urine except 30% of cow urine (shown in Fig. 10). Earlier studies by Sharma and Rai, 2015, show a high lipid content of 33% in 10% urine and 23% in 7.5% cattle urine

by Chlorella sp., which was diverse from the values obtained in this study. The result of this study was different from the previous work because of the use of different algal strains (*Chlorella vulgaris*) from earlier work, and also growth condition has a great impact on enhancing lipid in a higher concentration of urine. A gradual increase in lipid content from 10% to 30% was noticed because of the increasing amount of NPK supply to the microalgae. But, a drastic decline in biomass and lipid content was shown at 40% because as the concentration increases, the amount of nutrient percentage also increases thus forming an excessive amount of ammonia, which inhibits the algal growth and leads to a decrease in lipid content [21]. The effect of ammonia inhibition can be minimized by adding organic carbon sources from outside in the early phase of culturing microalgae [28].

Our study is the first conducted experiment where cow urine is utilized as a culture medium to increase biomass and lipid production of *Chlorella vulgaris* and then further move to biodiesel production. Therefore, it will lower the cost of producing biodiesel as the cost of culture media is very low compared to synthetic media (Table 2).
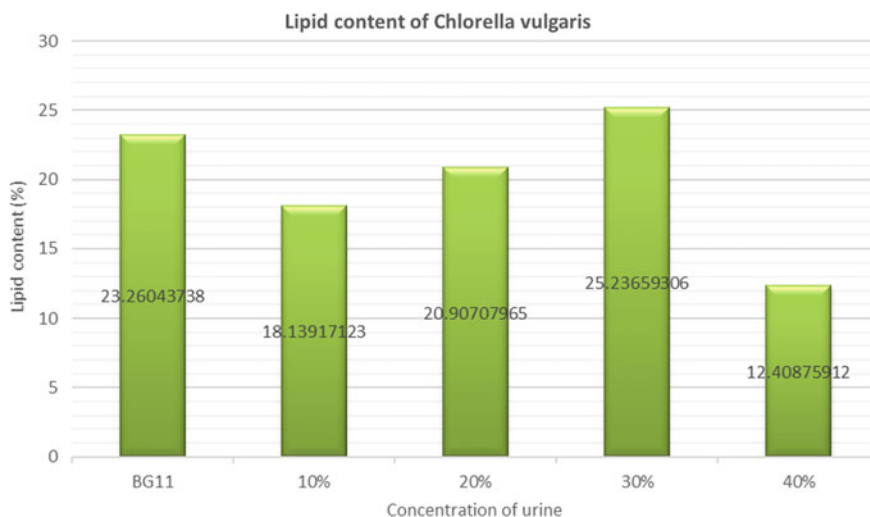
Fig. 10 Lipid content of *Chlorella vulgaris* in different concentrations of cow urine

Table 2 Comparison of lipid and biomass content

SAMPLE	Biomass content (g/L)	Lipid content (%) w/w
BG11	0.503	23.26
10% cow urine	1.279	18.13
20% cow urine	0.904	20.90
30% cow urine	0.634	25.23
40% cow urine	0.274	12.40

3.4 NMR Spectroscopy of Produced Biodiesel

After the transesterification reaction, the biodiesel was produced which was further analyzed with NMR spectroscopy to understand the characteristics and quality of produced biodiesel.

¹HNMR spectra

The algal biodiesel produced from the cow urine-grown cells were characterized using ^{1}HNMR techniques. To confirm the formation of biodiesel, the characteristic peak of the singlet was observed at 3.6 ppm corresponding to the methoxy group, also a triple peak related to α—CH$_2$ protons are observed near 2.3 ppm. The presence of multiple peaks nearby 1.6 ppm indicates—carbonyl methylene protons. The peak observed at 2.81 ppm is due to—Linolenic ester and peaks nearby 5.3 ppm appeared because of olefinic hydrogen [29, 30]. To identify the efficiency of conversion, ^{1}HNMR is used. Therefore, the conversion efficiency of triglycerides to methyl esters was found to be 87% (Fig. 11).
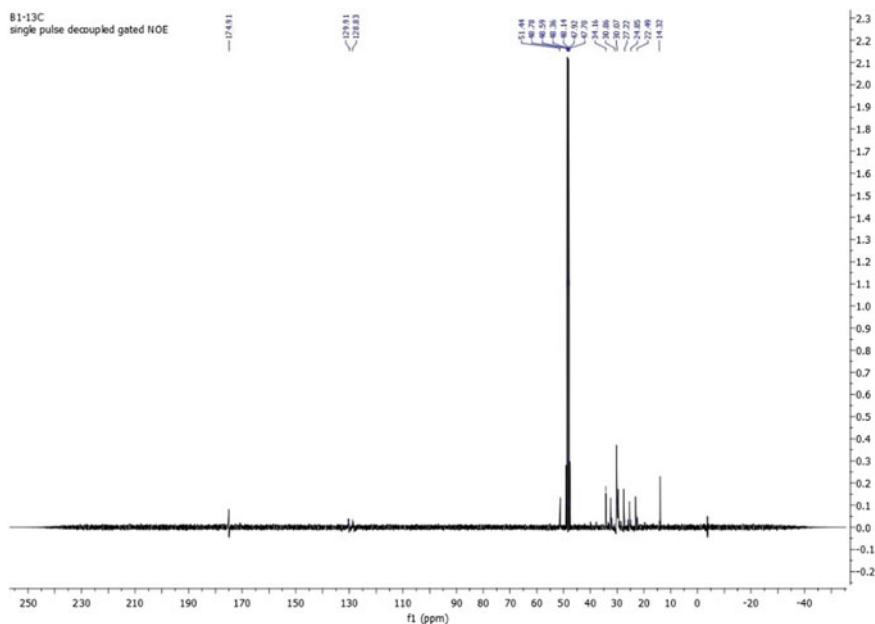
Fig. 11 ^{1}HNMR for biodiesel produced from cow urine-grown cell
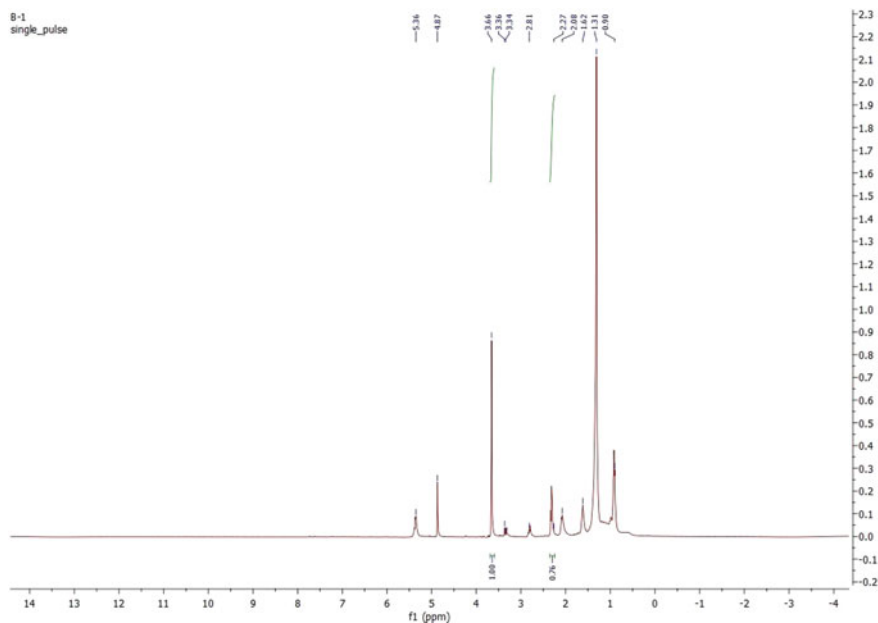
Fig. 12 ^{13}CNMR for biodiesel produced from cow urine-grown cells

^{13}CNMR spectra

^{13}CNMR spectrum was used to analysed the quality of algal biodiesel. The presence of a peak at 51.44 ppm corresponds to –OCH3 and shows that methyl ester is produced. The signal around 129.91 and 128.83 ppm is an indication that unsaturated fatty acid is present. The peak at 174.91 ppm is due to ester carbonyl. The presence of the CH_2–CH_2 group of FAME is confirmed by the signals appearing at 22–34 ppm (Fig. 12).

4 Conclusion

This study shows a great potential of cow urine to grow microalgae solely since it is a great source of organic nitrogen. Along with the huge amount of NPK, the micro- and macronutrients present in cow urine enhanced the growth of microalgae. From the numerous concentrations of cow urine, 10% CU shows maximum growth in the growth curve and also the highest value in biomass productivity of 90.21 mg/L/day among all other concentrations, whereas the lipid content value was different from the biomass values. The lipid content was increased with an increase in concentration up to 30% CU and then again decreases to 40% CU concentration. The maximum lipid content of 27.44% was observed in 30% CU. With the highest extracted lipid,

biodiesel was produced by the transesterification process and the characterization was done by NMR spectroscopy. Finally, the conversion efficiency of triglycerides to methyl esters was found to be 87%. The high biomass and lipid content of microalgae *Chlorella vulgaris* grew in cow urine media shows its potential to grow on a large scale for commercial purposes. Thus, it can be concluded that cow urine alone can support the growth of microalgae and hence produce a good amount of biomass and lipid. Further, research is needed in optimization in downstream processing of algal biomass and obtaining some value-added products.

References

1. Kumar, V., Kumar, A., Nanda, M.: Pretreated animal, and human waste as a substantial nutrient source for cultivation of microalgae for biodiesel production. Environ. Sci. Pollut. Res. **25**(22), 22052–22059 (2018)
2. Godia, F., Albiol, J., Montesinos, J.L., Pérez, J., Creus, N., Cabello, F., Lasseur, C.: MELISSA: a loop of interconnected bioreactors to develop life support in space. J. Biotechnol. **99**(3), 319–330 (2002)
3. Duarah, P., Haldar, D., Patel, A. K., Dong, C. D., Singhania, R. R., & Purkait, M. K.: A review on global perspectives of sustainable development in bioenergy generation. Bioresour. Technol. **348**, 126791 (2022)
4. Dodd, M.C., Zuleeg, S., Gunten, U.V., Pronk, W.: Ozonation of source-separated urine for resource recovery and waste minimization: process modelling, reaction chemistry, and operational considerations. Environ. Sci. Technol. **42**(24), 9329–9337 (2008)
5. Guschina, I.A., Harwood, J.L.: Lipids and lipid metabolism in eukaryotic algae. Prog. Lipid Res. **45**(2), 160–186 (2006)
6. Scott, S.A., Davey, M.P., Dennis, J.S., Horst, I., Howe, C.J., Lea-Smith, D.J., Smith, A.G.: Biodiesel from algae: challenges and prospects. Curr. Opin. Biotechnol. **21**(3), 277–286 (2010)
7. Chisti, Y.: Biodiesel from microalgae. Biotechnol. Adv. **25**(3), 294–306 (2007)
8. Haldar, D., & Purkait, M. K.: Micro and nanocrystalline cellulose derivatives of lignocellulosic biomass: A review on synthesis, applications and advancements. Carbohydr. Polym. **250**, 116937 (2020)
9. Haldar, D., & Purkait, M. K.: A review on the environment-friendly emerging techniques for pretreatment of lignocellulosic biomass: Mechanistic insight and advancements. Chemosphere, **264**, 128523 (2021)
10. Volli, V., & Purkait, M. K.: Selective preparation of zeolite X and A from flyash and its use as catalyst for biodiesel production. J. Hazard. Mater. **297**, 101–111 (2015)
11. Axelsson, M., Gentili, F.: A single-step method for rapid extraction of total lipids from green microalgae. PLoS ONE **9**(2), e89643 (2014)
12. Bligh, E.G., Dyer, W.J.: A rapid method of total lipid extraction and purification. Can. J. Biochem. Physiol. **37**(8), 911–917 (1959)
13. Gohain, M., Hasin, M., Eldiehy, K.S., Bardhan, P., Laskar, K., Phukon, H., Deka, D.: Bio-ethanol production: a route to sustainability of fuels using bio-based heterogeneous catalyst derived from waste. Process Saf. Environ. Prot. **146**, 190–200 (2021)

14. De Godos, I., Guzman, H.O., Soto, R., García-Encina, P.A., Becares, E., Muñoz, R., Vargas, V.A.: Coagulation/flocculation-based removal of algal–bacterial biomass from piggery wastewater treatment. Biores. Technol. **102**(2), 923–927 (2011)
15. Hu, Q., Sommerfeld, M., Jarvis, E., Ghirardi, M., Posewitz, M., Seibert, M., Darzins, A.: Microalgal triacylglycerols as feedstocks for biofuel production: perspectives and advances. Plant J. **54**(4), 621–639 (2008)
16. Das, V., Tripathi, A.M., Borah, M.J., Dunford, N.T., Deka, D.: Cobalt-doped CaO catalyst synthesized and applied for algal biodiesel production. Renewable Energy **161**, 1110–1119 (2020)
17. Saunders, W.H.M.: Effects of cow urine and its major constituents on pasture properties. N. Z. J. Agric. Res. **25**(1), 61–68 (1982)
18. Suresh, A., Mahalakshmi, R., Suriyapriya, S., Harini, K., Sevanthi, H.V., Deepan Guna, R., Sharmila, D.: Phycoremediation of Cooum wastewater as nutrient source for microalgal biomass production. J. Algal Biomass Utilization **9**(4), 42–47 (2018)
19. Syrett, P.J.: Nitrogen metabolism of microalgae. Can. Bull. Fish. Aquat. Sci. **210**, 182–210 (1981)
20. Belkin, S., Boussiba, S.: High internal pH conveys ammonia resistance in Spirulina platensis. Biores. Technol. **38**(2–3), 167–169 (1991)
21. Adamsson, M.: Potential use of human urine by greenhouse culturing of microalgae (Scenedesmus acuminatus), zooplankton (Daphnia magna) and tomatoes (Lycopersicon). Ecol. Eng. **16**(2), 243–254 (2000)
22. Li, Y., Horsman, M., Wang, B., Wu, N., Lan, C.Q.: Effects of nitrogen sources on cell growth and lipid accumulation of green alga Neochloris oleoabundans. Appl. Microbiol. Biotechnol. **81**(4), 629–636 (2008)
23. Li, Y., Chen, Y.F., Chen, P., Min, M., Zhou, W., Martinez, B., Ruan, R.: Characterization of a microalga Chlorella sp. well adapted to highly concentrated municipal wastewater for nutrient removal and biodiesel production. Bioresour. Technol. **102**(8), 5138–5144 (2011)
24. Jaatinen, S., Lakaniemi, A.M., Rintala, J.: Use of diluted urine for cultivation of Chlorella vulgaris. Environ. Technol. **37**(9), 1159–1170 (2016)
25. Feng, D.L., Wu, Z.C.: Culture of Spirulina platensis in human urine for biomass production and O$_2$ evolution. J. Zhejiang Univ. Sci. B **7**(1), 34–37 (2006)
26. Sharma, N., Rai, M.P.: Cattle urine increases lipid content in Chlorella pyrenoidosa: a low-cost medium for bioenergy application. Iranica J. Energy Environ. **6**(4), 334–339 (2015)
27. Suresh, A., Tamilvanan, S., Harini, K., Seventhi, H.V., Deepan Guna, R., Mahalakshmi, R., Thenmozhi, M.: Feasibility of cattle urine as nutrient medium for the microalgal biomass production. Global J. Environ. Sci. Manage. **5**(4), 441–448 (2019)
28. Chang, Y., Wu, Z., Bian, L., Feng, D., Leung, D.Y.: Cultivation of Spirulina platensis for biomass production and nutrient removal from synthetic human urine. Appl. Energy **102**, 427–431 (2013)
29. Sarpal, A.S., Costa, I.C., Teixeira, C.M.L.L., Filocomo, D., Candido, R., Silva, P.R., Daroda, R.J.: Investigation of biodiesel potential of biomasses of microalgaes chlorella, spirulina and tetraselmis by NMR and GC-MS techniques. J. Biotechnol. Biomater. **6**(220), 2 (2016)
30. Mello, V.M., Oliveira, F.C., Fraga, W.G., do Nascimento, C.J., Suarez, P.A.: Determination of the content of fatty acid methyl esters (FAME) in biodiesel samples obtained by esterification using ^{1}H-NMR spectroscopy. Magnet. Resonance Chem. **46**(11), 1051–1054 (2008)

Propensity for Segregation of Household Municipal Solid Waste: An Empirical Study

Sinmoy Goswami

1 Introduction

Massive industrialization in different parts of the world has resulted in development of the standard of living of people. This has resulted in changes in the lifestyle of these people [1]. Because of these changes, there has also been a noticeable increase in improper habits among such people. One such issue is related to the swelling unscientific disposal of various types of wastes including household municipal solid waste (HMSW) [2]. This fact coupled with rapid increase in global population has become a huge problem for many nations including India. This fact has been supported by other scholars [3, 4]. In this regard, appropriate segregation of such wastes is one of the scientifically proven befitting steps towards proper disposal of HMSW [1]. Another study indicated that inadequate awareness and technical knowhow, insufficient funding, and ineffective execution of laws and policies lead towards improper management of municipal solid waste (MSW) which also includes HMSW [5]. In addition, studies have shown that pitiable collection and improper transportation have led to accumulation of garbage especially HMSW in every part of towns and cities in India [6–10].

2 Literature Review

Solid waste comprises of unusable non-liquid and nongaseous products as a result of various activities undertaken by humans [11]. Municipal solid waste (MSW) comprises of wastes generated from commercial firms and households within any

S. Goswami (✉)
Assam Institute of Management (AIM), Bigyan Path, Paschim Boragaon (Opposite IASST), Guwahati, Assam 781035, India
e-mail: sinmoy.goswami@gmail.com

municipal or notified area. Such wastes can be in the form of solids or semisolids. This is as per Municipal Solid Waste (MSW) Rules [12]. This, however, excludes industrial hazardous wastes but includes treated biomedical wastes. Other scholars have defined MSW as a specific type of waste originating from households [13]. According to Solid Waste Management Rules (SWM), 2016, the above definition of MSW has been extended to include areas outside municipal areas. The latter includes urban clusters, towns, industrial townships, areas under the control of Indian Railways, airports, special economic zones, places of religious and historical importance, and State and Central Government organizations [14].

2.1 Significance of Management of HMSW Through Proper Segregation

Globally, around 2.01 billion tonnes of municipal solid waste are generated every year [15]. One third of such wastes are not disposed in an environmentally safe manner. The average amount of waste generated per person per day ranges from 0.11 to 4.54 kg [15]. It has also been reported that approximately 2 billion tonnes municipal solid waste (MSW) were generated from households worldwide in the year 2016 [16]. The same study has also emphasized on the significance of household municipal solid waste (HMSW) as they pose severe health risks because of their proximity to the inhabitants of households. Other studies have also highlighted other points of significance of HMSW [13, 16, 17]. Other scholars have mentioned the following negative effects arising from generated HMSW [18–20].

 (i) Plastic waste generated as a part of HMSW takes long periods to biodegrade. Also, these wastes on being consumed by various organisms, moves to the food chain with terrible consequences for humans,
 (ii) Significant proportion of greenhouse gases (GHGs) occurs due to emissions from various treatments of generated HMSW, *and*
 (iii) Emission of harmful air pollutants due to open burning of HMSW. These have long-term negative impact on the health of living organisms including humans.

Keeping in view the above points, management of HMSW is highly important for both the environment and the economy of a region or country [21]. This is evident from the example of Sweden, which utilizes heat generated from incineration of such wastes for electricity generation and for heating purpose in most homes [22, 23]. As a matter of fact, appropriate waste management involves proper collection, transportation, incineration, composting, recycling, and disposal of wastes [24, 25]. This can immensely help in controlling pollution in any nation or region.

Studies have established that management of HMSW involves all processes and activities related to their "generation", "storage", "collection", "transfer", and "transport" [1]. The same study also established that the above-mentioned management of HMSW primarily includes four activities, namely "generation", "collection", "transportation", and "disposal" in countries like India. It has been noticed that food items,

papers, metals, glass, wood, yard trimmings, etc., as major components of municipal solid waste in the United States of America (USA) [26]. In most Indian cities, urban garbage mainly constitutes paper and card, metals, glass, textiles, plastics, leather, rubber, etc. [27]. The above-mentioned four activities namely "generation", "collection", "transportation", and "disposal" of HMSW are optimally possible through appropriate segregation of such wastes [28–30]. A study stated that any type of generated domestic wastes should be segregated into three suitable bins, one each for biodegradable, non-biodegradable, and hazardous waste [14]. One of the most promising means for proper disposal of HMSW is through segregation of above type of waste into the following four categories [4, 29]:

(i) *Compostable organic wastes:* These include fruit and vegetable peels, food waste, etc.,
(ii) *Recyclable wastes:* These include paper, plastics, glass, metals, etc.,
(iii) *Toxic wastes:* These include paints, pesticides, used batteries, medicines, etc., *and*
(iv) *Soiled wastes:* These include blood-stained cottons, sanitary napkins, baby diapers, adult diapers, disposable syringes, etc.

Based on the definition for municipal solid waste (MSW) in the section, *Literature Review*, it is prudent to categorize HMSW into a fifth category [12]. This category comprises *wet waste* concerning semisolid waste.

3 Need for the Study

The above explanations indicate the significance of proper segregation of household municipal solid waste (HMSW) as the most important means for its scientific disposal. This is in line with the observations in a study that stated that HMSW should be segregated as biodegradable and non-biodegradable wastes [31]. In this regard, it should be noted that household food wastes, which form an integral component of HMSW, should be appropriately segregated at the sources. This can play a major role in their management [32]. Another study has emphasized on the importance of segregation of HMSW particularly in urban dwellings [33]. In this regard, various waste reduction processes like composting, recycling, and incineration as noted earlier have also been emphasized in this study. The latter study has also stated that such segregation of these wastes is essential owing to disadvantages caused by landfills reaching maximum capacity with consequent negative environmental effects. These effects are mainly in the form of methane (CH_4) production as well as permeation of leachates into the topsoil. Considering these points, proper segregation of HMSW seems to be a good option [33, 34]. Therefore, this present study is an attempt to observe the tendency of people to carry out similar segregation of such wastes.

In the case of Guwahati city in the state (province) of Assam in North East India, there is a noticeable lack of proper waste management [35]. The latter scholar has mentioned about the disturbing issue of residents of this city throwing household

garbage in roads. Also, the same scholar has highlighted the problem of the same residents burning accumulated garbage in their homes. This creates severe civic and environment related problem in this city. This corroborates with the findings of another study [36]. Here, the issue of uncontrolled urbanization and consequent environmental degradation of Guwahati city has been highlighted. As mentioned earlier, one visible negative occurrence of these activities is unscientific disposal of wastes including household municipal solid waste (HMSW). Ever increasing accumulation of such wastes is clearly visible in various dumping grounds in and around the above city. This has led to many problems like degradation of water quality and high air pollution, resulting in serious health implications in the aforementioned city. In this regard, the process of accumulation of HMSW in the garbage dump located at Boragaon in Guwahati city is shown in Fig. 1 in the Annexure. It is to be noted that this garbage dump was closed on August 2021. Another similar study revealed the impact of improper disposal of solid wastes (which includes HMSW) in dumping grounds in and around the Silchar town of Assam in soil and groundwater contamination [37]. It is to be noted in this regard that certain pollutants like cadmium (Cd), mercury (Hg), arsenic (As), chromium (Cr), nickel (Ni), dioxins, polychlorinated biphenyls ($C_{12}H_{10-x}Cl_x$), polycyclic aromatic hydrocarbon (PAH), particulate matter (PM), and sulphur dioxide (SO_2) can result in serious health problems for humans [38–40]. This may lead to the following diseases among people [40–44].

(i)   Squamous metaplasia,
(ii) Dysplasia of bronchial epithelial cells,
(iii) Congenital anomalies,
(iv) Cardiac anomalies,
(v)   Obstructive uropathies, *and*
(vi) Various skin anomalies.

Other studies have also supported the above views [45, 46]. It has been found that for every surge of 10 $\mu g/m^3$ in particulate matter PM_{10}, the lung cancer rate increases by 22%. In this regard, it is worth mentioning that particulate matter $PM_{2.5}$ was particularly harmful due to its high potential to penetrate lungs [47].

In the year 2017, around 62 million tonnes of waste were generated annually in India. Of these, 5.6 million tonnes constituted plastic waste, 0.17 million tonnes constituted biomedical waste, 7.90 million tonnes constituted hazardous waste, and 1.5 million tonnes comprised of e-waste [48, 49]. As per government records, around 65 million tonnes of waste were generated annually in India [50]. Of these, around 62 million tonnes comprise of municipal solid waste (MSW) that comprises of organic waste, recyclables like paper, plastic, wood, glass, etc. Of these, around 75–80% of municipal waste generated gets collected. Again, only 22–28% of such wastes is processed and treated and the rest is disposed in garbage dumps [48–50]. In the year 2012, the average MSW generation rate was 0.7 kg/capita/day in Guwahati city [51]. The latter study also mentioned about the generation of electric power from these wastes. The aforementioned discussion highlights the importance of implementing appropriate techniques for management of all types of wastes including HMSW. In this regard, it is to be noted that Guwahati city has been ranked as one of the dirtiest

cities of India within the category of cities having 1 lakh to 10 lakh population in the country, according to Swachh Survekshan 2021 [52]. Also, in general, the present status of waste management in the entire state of Assam (which includes Guwahati city and many other towns including Jorhat, Silchar, etc.) is not satisfactory and, therefore, there is a requirement of more constructive effort in this regard [51, 52]. This implies that there is an urgent requirement of steps aimed towards cleanliness concerning this state including proper management of generated wastes including HMSW. For this purpose, there is a need of appropriate and authentic data of various types of wastes generated in entire Assam in general. However, it is noticed that there is a noticeable lack of accurate data generated wastes including HMSW for whole of the above-mentioned state. This can seriously jeopardize any attempts to undertake proper plans for management of HMSW keeping in view the significance of its segregation as mentioned earlier for the state of Assam. This presents an enormous gap considering the study of this issue for the aforementioned state. This gap indicates an exclusive prospect for carrying out suitable research on this subject. Hence, this present study is a step towards plugging this gap. Also, the above discussion further justifies the need for this study aimed at identifying the tendency of resident citizens (people) in Assam to carry out segregation of HMSW.

4   Objectives of This Study

The objective of this study is to examine the propensity for segregation of household municipal solid waste (HMSW).

5   Methodology

This study was carried out to achieve the objectives stated above. It involves both exploratory and descriptive research design. The needed data for this study has been obtained through primary and secondary data sources. Of these, secondary data was obtained from books, websites, articles in journals, periodicals, etc. Primary data was collected through a survey involving a structured questionnaire for respondents (resident citizens (people)) in individual households spread all over Assam. It is to be noted that the aforesaid respondents were the head of these households. Appropriate care was taken to identify such heads of these households. Initially, a draft questionnaire was prepared and circulated in a pilot survey involving 50 such respondents. Based on their suggestions, required modifications were carried out and a final questionnaire was prepared. Such questionnaires were administered among 1500 such respondents in the above-mentioned households spread all over the above-mentioned state. As there was no authentic sampling frame or defined population, non-probability sampling technique was employed to select the aforesaid sample households from

the study population comprising all households in the above state. Based on applicability, snowball sampling technique was employed to select the above respondents. Around 1018 fully filled questionnaires with all required responses were collected. Hence, the total sample size of this study was 1018 respondents. This study was carried out within a time period of nine (9) months (from 1 May 2021 to 31 January 2022).

In the beginning, the process of identification of the main types of household municipal solid wastes (HMSW) generated in households of Assam was carried out. This was conducted with the help of the following:

(i)   Study of secondary data (as mentioned earlier),
(ii) Structured and unstructured observations in the above-mentioned selected households, *and*
(iii) Personal interviews of members of the above-mentioned respondents with the help of the aforementioned questionnaire.

Based on the above activities, the following types of HMSW have been found to be generated in the respondent households as shown in Table 1. Also, on the basis of the above processes, it was observed that the above HMSW could be classified as recyclable wastes, toxic wastes, compostable organic wastes, soiled wastes, and wet wastes (comprising semisolid waste). This is as explained in the sub-section, *significance of management of HMSW through proper segregation*. These findings are in line with those of other studies [4, 28, 29].

Thereafter, it was tried to find out the different processes of handling various types of generated HMSW in households. It was seen that these processes include disposal, decomposition, selling as scrap for recycling, and other processes including reuse of such wastes. Here, it was attempted to find out the processes of handling various types of generated HMSW, which was employed by majority of the respondents. Next, it was attempted to identify the nature of storage of different types of generated HMSW in households. A thorough observation of the respondents revealed that such types of storage include storage in closed container(s), in open container(s), in plastic bag(s),

Table 1 Various types of generated HMSW in households

Compostable organic wastes	Fruit and vegetable peels	Soiled wastes	Blood-stained cottons
	Other food wastes		Sanitary napkins
Recyclable wastes	Paper		Baby diapers
	Plastic		Adult diapers
	Glass		Disposable syringes
	Metals	Mix of all the above	
Toxic/hazardous wastes	Paints	Others	
	Pesticides	Wet wastes (comprising semisolid waste)	
	Used batteries		
	Medicines		

and by accumulating in the backyard. Here, it was tried to measure respondents' perception in each of such types of storage with the help of a dichotomous scale, i.e. "*done*", and "*not done*". Then, the propensity of respondents for segregation of different types of generated HMSW in households in the following forms was studied:

(i)   As dry and wet wastes,
(ii) As recyclable waste, toxic/hazardous waste, compostable waste, soiled waste, and wet wastes (comprising semisolid waste), *and*
(iii) In any other form.

In this regard, it was attempted to measure respondents' propensity to carry out each of above types of segregation with the help of a three-point scale, i.e. "*always done*", "*sometimes done*", and "*not done*".

This was followed by measuring the degree of relationship between different processes of handling various types of generated HMSW and propensity for segregation of such wastes. This was done using Pearson's product moment correlation. The above relationship was tested by calculating the correlation coefficient (r) using SPSS software. This coefficient was also used in other studies [53–55]. According to these studies, whenever "r" is greater than or equal to 0.7, it indicates stronger correlation, i.e. strong relationship. This viewpoint has been supported by other scholars [55–65]. Also, whenever, the aforementioned value of "r" is greater than or equal to 0.5, it indicates moderate (satisfactory) correlation, i.e. moderate (satisfactory) relationship [64, 66]. It is to be noted that the above relationship between different processes of handling various types of generated HMSW and propensity for segregation of such wastes was planned to be additionally tested using discriminant analysis and logistic regression. However, discriminant analysis could not be used due to the fact that the dependent variable, propensity of respondents for segregation of different types of generated HMSW in households was measured in three levels (three-point scale) as noted earlier and hence is not categorical [57, 67–69]. In this regard, it may be noted that any action to convert this dependent variable into a categorical variable would make it meaningless in this research endeavour. This would prove to be a major obstacle while using discriminant analysis in the above regard. In addition, logistic regression could not be used for testing the above relationship. This was because the aforementioned dependent variable was not binary as per requirements for using this analytical tool [57, 67–69]. In addition, any means to convert this dependent variable into a binary variable would render it futile for this study.

6 Findings

It was observed that the idea regarding segregation of household municipal solid wastes (HMSW) was found to be present as per the perception of most of the respondents (74.95%). This is depicted in Table 2.

Table 2 Perception regarding having idea for segregation of generated HMSW

	Frequency	Percent
No idea present	255	25.05
Idea present	*763*	*74.95*
Total	1018	100.00

Values in italics indicate maximum value(s) and percentage(s) (as applicable)

The findings of this study also revealed that most of the respondents in Assam disposed compostable organic wastes in dustbins or any other suitable place or mode of disposal. Such wastes include fruit and vegetable peels and other food wastes (refer to Table 3 in the Annexure). It is to be noted that significant number of these respondents undertook decomposition activities with regard to these types of wastes. It has also been seen that few of these respondents reported that they sold leftovers of certain food items, which included paper filters, loose-leaf tea, and paper tea bags. This corroborates with the report of the Agency of Natural Resources, Department of Environmental Conservation, State of Vermont, USA [70]. Also, few respondents reported selling fruit and vegetable peels as scrap, which would be later used for producing compost. As per the above report, food scraps comprise of valuable nutrients. These nutrients are good for the soil in the form of compost. The latter can be used in gardens, farms, and landscaping [70]. Again, various studies have also indicated the use of fruit and vegetable peels for making various products. For example, huge amounts of peels, seeds/kernels, and bagasse are obtained through processing of mango in food-based industries [71, 72]. It is to be noted that bagasse contains bioactive compounds and nutrients. Usually, such wastes are converted into powders and flours and used as functional ingredients of various food items. Also, it has been found that raw and defatted flours from mango seed kernels are used as wheat flour substituent while making bread [72, 73]. It has also been noticed that the above-mentioned fruit and vegetable peels are rich in bioactive compounds (including carotenoids, enzymes, polyphenols, vitamins, etc.). These bioactive compounds show their application in various industries such as food industries to develop edible films, probiotics, etc. [74]. In addition, the aforementioned bioactive compounds are used to produce nanoparticles, carbon dots, microbial media, biochar, and biosorbents [74]. These views have also been supported by other studies [75, 76]. It has also been noticed that among recyclable wastes, paper, and plastic are disposed of by most of the respondents. However, majority of the respondents mostly scrapped waste glass and metals. It has been also seen that most of the respondents mostly disposed of toxic/hazardous wastes (like paints, pesticides, used batteries, and medicines) and soiled wastes (like blood-stained cottons, sanitary napkins, baby diapers, adult diapers, and disposable syringes). These findings are shown in Table 3 in the Annexure. It was also found that majority of the respondents disposed HMSW (in the form of wet wastes (comprising semisolid waste)) in drains. None of them handled such HMSW (as wet wastes) by any other means like decomposition, selling as scrap or involving other processes including reuse. In this regard, around few respondents reported that such HMSW

(as wet semisolid wastes) were not generated in their respective households. As such, data obtained regarding such wastes were not subjected to further analysis. This is because it is meaningless to do so [57, 67–69].

The nature of storage of different types of generated HMSW in households has been depicted in Table 4 in the Annexure. It was seen that most respondents stored the aforementioned wastes in closed containers and plastic bags.

Also, in case of most of the respondents, household municipal solid wastes (HMSW) are sometimes segregated as dry and wet wastes. Besides, as per majority of such respondents, HMSW has not been found to be segregated as recyclable waste, toxic/hazardous waste, compostable waste, soiled waste, and wet wastes (comprising semisolid waste). This finding presents the cornerstone of this study. These findings also highlight a major problem that will effect responsible management of such wastes as far as Assam and India in general are concerned. However, it was observed that segregation of the above-mentioned wastes in any other form was sometimes carried out by most of these respondents (and households in general). These findings are shown in Table 5 in the Annexure.

As noted in the section, *Methodology*, Pearson's product moment correlation was carried out between different processes of handling various types of generated HMSW and propensity for segregation of such wastes. The results are shown in Table 6 in the Annexure in the form of values of coefficient of the aforementioned correlation (r). It has been noticed that satisfactory positive correlation existed between the above two variables in case of wastes in the form of fruit and vegetable peels, and plastic (wastes) considering the propensity of segregation of HMSW as recyclable, toxic/hazardous, compostable organic, soiled waste, and wet wastes (comprising semisolid waste). It is to be noted that in both these two cases, the coefficient of correlation (r) between the above two variables was found to be above 0.500 indicating satisfactory correlation. From Table 1, it is seen that among majority of the respondents, wastes in the form of fruit and vegetable peels (under compostable organic wastes), and plastic (under recyclable wastes) were disposed in dustbins or any other place or container for disposal. This implies that those households wherein there is relatively high emphasis and interest in dealing with these two wastes as a part of generated HMSW, there lies greater tendency to segregate such solid wastes involving five separate bins one each for the earlier mentioned five categories of HMSW. In a way, it can be inferred that there is a significant tendency to properly handle these two forms of wastes considering their respective volumes generated in the households in Assam. From Table 6, it has also been observed that satisfactory correlation existed between different processes of handling generated HMSW in the form of pesticides (under toxic/hazardous wastes), and propensity for segregation of such wastes as dry waste and wet waste in two separate bins. Here, the coefficient of correlation (r) between the above two variables was found to be above 0.500 indicating satisfactory positive correlation. This infers that those households wherein there is relatively high emphasis and interest in dealing with pesticides as a part of generated HMSW, there is a greater tendency to segregate such solid wastes as dry and wet wastes. This is in contrast to segregation process of such wastes as toxic/hazardous wastes (as a part of segregation process into five types, namely recyclable, toxic/hazardous, compostable

organic, soiled waste, and wet wastes (comprising semisolid waste)). In other words, this finding highlights the need for creating appropriate awareness to properly handle pesticide (wastes) considering their harmful effects through the segregation process involving five separate bins for each of the aforementioned five types of HMSW in the households in Assam. It was also noticed that the aforesaid coefficient of correlation (r) between different processes of handling other various types of generated HMSW, and propensity for segregation of such wastes was less than 0.500 (refer to Table 6). This indicates non-satisfactory relationship between these two variables. This infers that there is a greater need for generating awareness to properly segregate other types of generated HMSW in the above-mentioned households. In fact, there should be more emphasis to segregate such wastes involving five separate bins one each for the previously mentioned five types of HMSW.

The above discussion revealed that most respondent individuals in households had the idea regarding segregation of HMSW. It was noticed that there were differences in aforementioned respondents' propensity to segregate such wastes through various means. It has been noticed that majority of these respondents sometimes had the tendency to segregate such wastes into separate bins comprising dry and wet waste, respectively. Similarly, maximum of them sometimes had the tendency to segregate such wastes into any other form. However, regarding segregation of HMSW as recyclable waste, toxic/hazardous waste, compostable organic waste, soiled waste, and wet wastes (comprising semisolid waste) in five separate bins (or any other suitable mode of storage), it was seen that most of respondents never carried out such activities. It is to be noted that the above segregation of HMSW should be carried out involving five separate bins one each for recyclable waste, toxic/hazardous waste, compostable organic waste, soiled waste, and wet wastes (comprising semisolid waste). The above findings throw light upon the significance for increasing awareness and knowledge for proper execution of the segregation process for HMSW as mentioned above through five separate suitable bins. These processes can result in cleaner surroundings. In the end, this will be beneficial for the environment in general and human health in particular.

7 Conclusion

Household municipal solid waste (HMSW) generated in our households need to properly disposed. Actually, management of disposal of such wastes is highly important. It has been noticed that if management of disposal techniques of HMSW is not done properly, it will result in ever-increasing accumulation of such wastes into gigantic proportions in the coming future. This has become an ugly reality in most parts of the world including various parts of India. This situation raises a concern regarding possible pollution, increasing communicable and non-communicable diseases, and degradation of our environment. As explained elsewhere in this study, right segregation of HMSW is an important step towards handling of this problem of accumulation of such wastes. In short, this will help in reduction of such accumulation of these

wastes in and around our localities, and in dumping grounds and landfills. Also, the above-mentioned segregation of HMSW will also result in recycling of recyclable items present. These will lead towards sustainable development all over the world benefitting everyone including the human race.

Annexure

See the Tables 3, 4, 5, 6 and Fig. 1.

Table 3 Different processes of handling various types of generated HMSW in households

Types of wastes		Disposal	Decomposition	Selling as scrap for recycling	Other processes including reuse	Non-generation	Total
Compostable organic wastes	Fruit and vegetable peels	633	351	5	0	29	1018
	Other food wastes	606	273	75	0	64	1018
Recyclable wastes	Paper	560	90	308	21	39	1018
	Plastic	581	3	280	115	39	1018
	Glass	243	42	263	95	375	1018
	Metals	18	0	573	27	400	1018
Toxic/hazardous wastes	Paints	313	21	84	176	424	1018
	Pesticides	408	93	36	27	454	1018
	Used batteries	403	9	186	2	418	1018
	Medicines	514	82	12	1	409	1018
Soiled wastes	Blood-stained cottons	541	44	12	1	420	1018
	Sanitary napkins	854	10	12	0	142	1018
	Baby diapers	387	6	12	1	612	1018

(continued)

Table 3 (continued)

Types of wastes		Disposal	Decomposition	Selling as scrap for recycling	Other processes including reuse	Non-generation	Total
	Adult diapers	*465*	6	12	1	534	1018
	Disposable syringes	*460*	11	12	1	534	1018
	Mix of all the above	*411*	11	12	1	583	1018
	Others	*704*	6	16	17	275	1018
Wet wastes (comprising semisolid waste)		*826*	0	0	0	182	1018

Values in italics indicate maximum value(s) and percentage(s) (as applicable)

Table 4 Nature of storage of different types of generated HMSW in households

Types of wastes	Done	Not done	Total
In closed container(s)	*933*	85	1018
In open container(s)	136	*882*	1018
In plastic bag(s)	*515*	503	1018
By accumulating in the backyard	112	*906*	1018

Values in italics indicate maximum value(s) and percentage(s) (as applicable)

Table 5 Propensity for segregation of different types of generated HMSW in households

Nature of segregation of wastes	Always done	Sometimes done	Not done	Total
As dry and wet wastes	211	*791*	16	1018
As recyclable waste, toxic/hazardous waste, compostable waste, soiled waste, and wet wastes (comprising semisolid waste)	102	237	*679*	1018
In any other form	444	*542*	32	1018

Values in italics indicate maximum value(s) and percentage(s) (as applicable)

Table 6 Results of correlation—different processes of handling various types of generated HMSW and propensity for segregation of such wastes

Types of wastes		Propensity for segregation of HMSW as dry waste and wet waste in two separate bins	Propensity for segregation of HMSW as recyclable, toxic/hazardous, compostable organic, soiled waste, and wet wastes (comprising semisolid waste) in five separate bins	Propensity for segregation of HMSW in any other form
Compostable organic wastes	Fruit and vegetable peels	0.205	*0.660*	0.152
	Other food wastes	0.098	0.334	0.004
Recyclable wastes	Paper	0.047	0.203	0.091
	Plastic	0.162	*0.508*	0.101
	Glass	0.095	−0.469	−0.204
	Metals	−0.123	−0.209	−0.261
Toxic/hazardous wastes	Paints	0.301	−0.134	−0.092
	Pesticides	*0.529*	−0.04	0.091
	Used batteries	0.428	0.064	−0.07
	Medicines	0.46	0.128	−0.075
Soiled wastes	Blood-stained cottons	0.078	−0.084	−0.152
	Sanitary napkins	0.131	0.127	0.12
	Baby diapers	0.205	0.152	−0.048
	Adult diapers	0.119	0.099	−0.052
	Disposable syringes	0.097	0.071	−0.07
	Mix of all the above	0.095	0.044	−0.078
	Others	0.316	0.032	−0.018

Note Majority of the respondents disposed HMSW (in the form of wet wastes (comprising semisolid waste)) in drains. Hence, data obtained regarding such wastes were not subjected to further analysis
Values in italics indicate maximum value(s) and percentage(s) (as applicable)

Fig. 1 Process of accumulation of household municipal solid waste (HMSW) in garbage dump located at Boragaon in Guwahati City

References

1. Sharholy, M., Ahmad, K., Mahmood, G., Trivedi, R.C.: Municipal solid waste management in Indian cities—a review. Waste Manage. **28**, 459–467 (2008). https://doi.org/10.1016/j.wasman.2007.02.008

2. Rathi, S.: Alternative approaches for better municipal solid waste management in Mumbai, India. J. Waste Manage. **26**(10), 1192–1200 (2006). https://doi.org/10.1016/j.wasman.2005.09.006

3. Ray, M.R., Roychoudhury, S., Mukherjee, G., Roy, S., Lahiri, T.: Respiratory and general health impairments of workers employed in a municipal solid waste disposal at open landfill site in Delhi. Int. J. Hyg. Environ. Health **108**(4), 255–262 (2005). https://doi.org/10.1016/j.ijheh.2005.02.001

4. Das, P. P., Sharma, M., & Purkait, M. K.: Recent progress on electrocoagulation process for wastewater treatment: A review. Sep. Purif. Technol. **292**, 121058 (2022). https://doi.org/10.1016/j.seppur.2022.121058

5. Joshi, R., Ahmed, S.: Status and challenges of municipal solid waste management in India: a review. Cogent Environ. Sci. **2**, 1–18 (2016). https://doi.org/10.1080/23311843.2016.1139434

6. Kansal, A., Prasad, R.K., Gupta, S.: Delhi municipal solid waste and environment—an appraisal. Indian J. Environ. Prot. **18**(2), 123–128 (1998)

7. Kansal, A.: Solid waste management strategies for India. Indian J. Environ. Prot. **22**(4), 444–448 (2002)

8. Gupta, S., Krishna, M., Prasad, R.K., Gupta, S., Kansal, A.: Solid waste management in India: options and opportunities. Resource, Conserv. Recycl. **24**, 137–154 (1998)

9. Sharholy, M., Ahmad, K., Mahmood, G., Trivedi, R.C.: Analysis of municipal solid waste management systems in Delhi—a review. In: Book of Proceedings for the Second International Congress of Chemistry and Environment, pp. 773–777. Indore, India (2005)

10. Singh, S.: Solid waste management in urban India: imperatives for improvement. In: Observer Research Foundation (ORF) Occasional Paper No. 283, pp. 5–43. Observer Research Foundation, New Delhi (2020)

11. Babayemi, J.O., Dauda, K.T.: Evaluation of solid waste generation, categories and disposal options in developing countries: a case study of Nigeria. J. Appl. Sci. Environ. Manage. **13**(3), 83–88 (2009). https://doi.org/10.4314/jasem.v13i3.55370

12. Toolkit for Solid Waste Management, http://jnnurm.nic.in/wp/content/uploads/2012/11/SWM-toolkit.pdf. Last Accessed 12 Dec 2021

13. Wilson, D.C., Velis, C.A.: Waste management—still a global challenge in the 21st century: an evidence-based call for action. Waste Manage. Res. **33**, 1049–1051 (2015). https://doi.org/10.1177/0734242X15616055

14. Ministry of Environment, Forest and Climate Change (MEFCC): Notification dated 8th April, 2016. The Gazette of India: Extraordinary [Part II-Sec.3(ii)]. 51–55 (2016)

15. The World Bank, https://datatopics.worldbank.org/what-a-waste/trends_in_solid_waste_management.html#:~:text=The%20world%20generates%202.01%20billion, from%200.11%20to%204.54%20kilograms. Last Accessed 27 Oct 2021

16. Chen, D.M., Bodirsky, B.L., Krueger, T., Mishra, A., Popp, A.: The world's growing municipal solid waste: trends and impacts. Environ. Res. Lett. **15**, 074021 (2020). https://doi.org/10.1088/1748-9326/ab8659

17. Monni, S., Pipatti, R., Lehtilä, A., Savolainen, I., Syri, S.: Global Climate Change Mitigation Scenarios for Solid Waste Management, p. 603. ESPOO VTT publications (2006)

18. Thompson, R.C., Moore, C.J., vom Saal, F.S., Swan, S.H.: Plastics, the environment and human health: current consensus and future trends. Philos. Trans. Royal Soc. B **364**(1526), 2153–2166 (2009). https://doi.org/10.1098/rstb.2009.0053

19. Lambert, S., Wagner, M.: Microplastics are contaminants of emerging concern in freshwater environments: an overview. In: Wagner, M., Lambert, S. (eds.) Freshwater Microplastics: Emerging Environmental Contaminants?, pp.1–24. Springer, Berlin (2018). https://doi.org/10.1007/978-3-319-61615-5_1

20. Wiedinmyer, C., Yokelson, R.J., Gullett, B.K.: Global emissions of trace gases, particulate matter, and hazardous air pollutants from open burning of domestic waste. Environ. Sci. Technol. **48**, 9523–9530 (2014). https://doi.org/10.1021/es502250z

21. Finnveden, G., Björklund, A., Reich, M.C., Eriksson, O., Sörbom, A.: Flexible and robust strategies for waste management in Sweden. Waste Manage. **27**, S1–S8 (2007). https://doi.org/10.1016/j.wasman.2007.02.017

22. Eriksson, O., Reich, M.C., Frostell, B., Björklund, A., Assefa, G., Sundqvist, J.-O., Granath, J., Baky, A., Thyselius, L.: Municipal solid waste management from a systems perspective. J. Clean. Prod. **13**, 241–252 (2005). https://doi.org/10.1016/j.jclepro.2004.02.018

23. Visit Sweden, https://visitsweden.com/about-sweden/weather-and-climate/#:~:text=Winter%20and%20summer%20temperature%20differences,thanks%20to%20the%20Gulf%20Stream.&text=Above%20the%20Arctic%20Circle%2C%20winter,regularly%20hit%20%2B20°C. Last Accessed 27 Oct 2021

24. Amemba, C.S., Nyaboke, P.G., Osoro, A., Mburu, N.: Elements of green supply management. Eur. J. Bus. Manage. **5**(12), 51–61 (2013)

25. Gungor, A., Gupta, S.M.: Issues in environmentally conscious manufacturing and product recovery: a survey. Comput. Ind. Eng. **36**, 811–853 (1999)
26. Abdel-Shafy, H.I., Mansour, M.S.M.: Solid waste issue: sources, composition, disposal, recycling, and valorization. Egypt. J. Pet. **27**, 1275–1290 (2018). https://doi.org/10.1016/j.ejpe.2018.07.003
27. Jain, A.P.: Solid waste management in India. In: 20th WEDC Conference on Affordable Water Supply and Sanitation, pp. 177–182. Colombo, Sri Lanka (1994)
28. Khan, R.R.: Environmental management of municipal solid wastes. Indian J. Environ. Prot. **14**(1), 26–30 (1994)
29. Reddy, S., Galab, S.: An Integrated Economic and Environmental Assessment of Solid Waste Management in India—The Case of Hyderabad. Environmental Science, India (1998)
30. United Nations Economic and Social Commission for Asia and Pacific (UNESCAP), https://www.unescap.org/sites/default/files/CH08. PDF. Last Accessed 20 Aug 2021
31. Banga, M.: Household knowledge, attitudes and practices in solid waste segregation and recycling: the case of Urban Kampala. Zambia Soc. Sci. J. 1(2), 27–39 (2011), http://scholarship.law.cornell.edu/zssj/vol2/iss1/4
32. Bernstad, A.: Household food waste separation behavior and the importance of convenience. Waste Manage. **34**(7), 1317–1323 (2014). https://doi.org/10.1016/j.wasman.2014.03.013
33. Malik, N.K.A., Abdullah, S.H., Manaf, L.A.: Community participation on solid waste segregation through recycling programmes in Putrajaya. Procedia Environ. Sci. **30**, 10–14 (2015). https://doi.org/10.1016/j.proenv.2015.10.002
34. Burntley, S.J.: A review of municipal solid waste composition in the United Kingdom. J. Waste Manage. **27**(10), 1274–1285 (2007). https://doi.org/10.1016/j.wasman.2006.06.018
35. Gogoi, L.: Municipal solid waste disposal: a case study in Guwahati city to mitigate the man made disaster. IOSR J. Humanit. Soc. Sci. **9**(3), 55–60 (2013)
36. Sultana, M.: The effect of urbanisation on environment: with special reference to the city of Guwahati, Assam. Palarch's J. Archaeol. Egypt/Egyptol. **17**(9), 228–235 (2020)
37. Choudhury, M., Jyethi, D.S., Dutta, J., Purkayastha, S.P., Deb, D., Das, R., Roy, G., Sen, T., Bhattacharyya, K.G.: Investigation of groundwater and soil quality near to a municipal waste disposal site in Silchar, Assam, India. Int. J. Energy Water Resour. **6**, 37–47 (2022). https://doi.org/10.1007/s42108-021-00117-5
38. Ministry of Environment, Forest and Climate Change (MEFCC), http://www.moef.gov.in/sites/default/files/SWM%202016.pdf. Last Accessed 21 May 2021
39. Das, P. P., & Purkait, M. K.: Treatment of cold rolling mill (CRM) effluent of steel industry. Sep. Purif. Technol. **274**, 119083 (2021). https://doi.org/10.1016/j.seppur.2021.119083
40. Singh, A., Raj, P.: Segregation of waste at source reduces the environmental hazards of municipal solid waste in Patna, India. Arch. Environ. Prot. **44**(4), 96–110 (2018). https://doi.org/10.24425/122306
41. Cordier, S., Chevrier, C., Robert-Gnansia, E., Lorente, C., Brula, P., Hours, M.: Risk of congenital anomalies in the vicinity of municipal solid waste incinerators. Occup. Environ. Med. **61**, 8–l5 (2004)
42. Elliott, P., Briggs, D., Morris, S., Hoogh, C., Hurt, C., Jensen, T.K.: Risk of adverse birth outcomes in populations living near landfill sites. British Med. J. (BMJ) **323**, 363–368 (2001). https://doi.org/10.1136/bmj.323.7309.363
43. Ray, M.R., Mukherjee, G., Roychowdhury, S., Lahiri, T.: Respiratory and general health impairments of ragpickers in India: a study in Delhi. Int. Arch. Occup. Environ. Health **77**, 595–598 (2004). https://doi.org/10.1007/s00420-004-0564-8
44. Tian, H., Gao, J., Hao, J., Lu, L., Zhu, C., Qiu, P.: Atmospheric pollution problems and control proposals associated with solid waste management in China: a review. J. Hazard. Mater. **252–253**, 142–154 (2013). https://doi.org/10.1016/j.jhazmat.2013.02.013
45. Floret, N., Mauny, F., Challier, B., Arveux, P., Cahn, J.Y., Viel, J.F.: Dioxin emissions from a solid waste incinerator and risk of non-hodgkin lymphoma. Epidemiology **14**, 392–398 (2003). https://doi.org/10.1097/01.ede.0000072107.90304.01

46. Rushton, L.: Health hazards and waste management. Br. Med. Bull. **68**, 183–197 (2003). https://doi.org/10.1093/bmb/ldg034
47. Raaschou-Nielsen, O., Andersen, Z.J., Beelen, R., Samoli, E., Stafoggia, M., Weinmayr, G., et al.: Air pollution and lung cancer incidence in 17 European cohorts: prospective analyses from the European Study of Cohorts for Air Pollution Effects (ESCAPE). Lancet Oncol. **14**(9), 813–822 (2013). https://doi.org/10.1016/S1470-2045(13)70279-1
48. Civilsdaily, https://www.civilsdaily.com/solid-waste-management-rules-2016/. Last Accessed 13 June 2021
49. Down to Earth, https://www.downtoearth.org.in/news/waste/solid-waste-management-rules-2016-53443. Last Accessed 6 Sept 2021
50. Pabithra, K.M., https://factly.in/review-municipal-solid-waste-generated-in-india-set-to-increase-7-times-in-the-next-30-years/. Last Accessed 17 July 2021
51. Pradhan, P.K., Mohanty, C.R., Swar, A.K., Mohapatra, P.: Urban solid waste management of Guwahati city in North-East India. J. Urban Environ. Eng. **6**(2), 67–73 (2012). https://doi.org/10.4090/juee.2012.v6n2.067073
52. The Times of India, http://timesofindia.indiatimes.com/articleshow/87822440.cms?utm_source=contentofinterest&utm_medium=text&utm_campaign=cppst. Last Accessed 17 Aug 2021
53. Hemphill, J.F.: Interpreting the magnitudes of correlation coefficients. Am. Psychol. **58**(1), 78–80 (2003). https://doi.org/10.1037/0003-066x.58.1.78
54. Das, P. P., Mondal, P., Sinha, A., Biswas, P., Sarkar, S., & Purkait, M. K.: Treatment of steel plant generated biological oxidation treated (BOT) wastewater by hybrid process. Sep. Purif. Technol. **258**, 118013 (2021). https://doi.org/10.1016/j.seppur.2020.118013
55. Mukaka, M.M.: Statistics corner: a guide to appropriate use of correlation coefficient in medical research. Malawi Med. J. **24**(3), 69–71 (2012)
56. Asuero, A.G., Sayago, A., González, A.G.: The correlation coefficient: an overview. Crit. Rev. Anal. Chem. **36**, 41–59 (2006). https://doi.org/10.1080/10408340500526766
57. Cooper, D.R., Schindler, P.S., Sharma, J.K.: Business Research Methods, 12th edn. McGraw Hill Education, New Delhi (2019)
58. Dallal, G.E.: Correlation Coefficient. Tufts University (2003). http://www.tufts.edu/~gdallal/corr.htm
59. Lawson, J., Erjavec, J.: Modern Statistics for Engineering and Quality Improvement. Brooks Cole, New York (2000)
60. Meyer, G.J., Finn, S.E., Eyde, L.D., Kay, G.G., Moreland, K.L., Dies, R.R., Eisman, E.J., Kubiszyn, T.W., Reed, G.M.: Psychological testing and psychological assessment: a review of evidence and issues. Am. Psychol. **56**, 128–165 (2001)
61. Mishra, P.: Business Research Methods. Oxford University Press, New Delhi (2015)
62. Phillippe, J.: LesM´ethodes Statistiques en Pharmacie et en Chimie. Masson, Paris (1967)
63. Rosenthal, R.: Meta-Analytic Procedures for Social Research. Sage, Newbury Park, CA (1991)
64. Rumsey, D.J.: Statistics for Dummies. Wiley Publishing, Indianapolis, Indiana (2011)
65. Zady, M.F.: Correlation and Simple Least Squares Regression. Westgard QC. http://www.westgard.com/lesson44.htm
66. Bohannon, R.W.: Comfortable and maximum walking speed of adults aged 20–79 years: reference values and determinants. Age Aging **26**, 15–19 (1997). https://doi.org/10.1093/ageing/26.1.15
67. Aaker, D.A., Kumar, V., Leone, R.P., Day, G.S.: Marketing Research, 11th edn. Wiley India (P) Limited, New Delhi (2016)
68. Chawla, D., Sondhi, N.: Research Methodology, 1st edn. Vikas Publishing House Private Limited, Noida (2011)
69. Malhotra, N.K., Dash, S.: Marketing Research: An Applied Orientation, 7th Revised edn. Pearson Education, New Delhi (2019)
70. Agency of Natural Resources, Department of Environmental Conservation, State of Vermont, USA, https://dec.vermont.gov/waste-management/solid/materials-mgmt/organic-materials. Last Accessed 14 Nov 2021

71. Campos-Vega, R., Oomah, B.D., Vergara-Castañeda, H.A.: Food Wastes and By-Products: Nutraceutical and Health Potential. John Wiley & Sons Ltd., Hoboken, NJ, USA (2020)
72. Melini, V., Melini, F., Luziatelli, F., Ruzzi. M.: Functional Ingredients from agri-food waste: effect of inclusion thereof on phenolic compound content and bioaccessibility in bakery products. Antioxidants. **9**, 1216–1244 (2020). https://doi.org/10.3390/antiox9121216
73. Amin, K., Akhtar, S., Ismail, T.: Nutritional and organoleptic evaluation of functional bread prepared from raw and processed defatted mango kernel flour. J. Food Process. Preserv. **42**(4), e13570 (2018). https://doi.org/10.1111/jfpp.13570
74. Kumar, H., Bhardwaj, K., Sharma, R., Nepovimova, E., Kuča, K., Dhanjal, D.S., Verma, R., Bhardwaj, P., Sharma, S., Kumar, D.: Fruit and vegetable peels: utilization of high value horticultural waste in novel industrial applications. Molecules **25**, 2812–2832 (2020). https://doi.org/10.3390/molecules25122812
75. Akhtar, M.S., Panwar, J., Yun, Y.S.: Biogenic synthesis of metallic nanoparticles by plant extracts. ACS Sustain. Chem. Eng. **1**, 591–602 (2013). https://doi.org/10.1021/sc300118u
76. Ghosh, P.R., Fawcett, D., Sharma, S.B., Poinern, G.E.J.: Production of high-value nanoparticles via biogenic processes using aquacultural and horticultural food waste. Materials **10**, 852 (2017). https://doi.org/10.3390/ma10080852